

2011

Thermal Integrity Profiling Instrumentation Development

Byron Keith Anderson

University of South Florida, byrona@seiflorida.com

Follow this and additional works at: <http://scholarcommons.usf.edu/etd>

 Part of the [American Studies Commons](#), and the [Civil Engineering Commons](#)

Scholar Commons Citation

Anderson, Byron Keith, "Thermal Integrity Profiling Instrumentation Development" (2011). *Graduate Theses and Dissertations*.
<http://scholarcommons.usf.edu/etd/2987>

This Thesis is brought to you for free and open access by the Graduate School at Scholar Commons. It has been accepted for inclusion in Graduate Theses and Dissertations by an authorized administrator of Scholar Commons. For more information, please contact scholarcommons@usf.edu.

Thermal Integrity Profiling Instrumentation Development

by

Byron Keith Anderson

A thesis submitted in partial fulfillment
of the requirements for the degree of
Master of Science in Civil Engineering
Department of Civil and Environmental Engineering
College of Engineering
University of South Florida

Major Professor: A. Gray Mullins, Ph.D.
Rajan Sen, Ph.D.
Michael Stokes, Ph.D.

Date of Approval:
September 16, 2011

Keywords: Concrete Temperature, Drilled Shaft, Infrared, Thermocouple, Cross-Hole
Sonic Logging, Gamma Gamma Testing, Concrete Heat of Hydration, Geotechnical
Testing, Structural Failure

Copyright © 2011, Byron Keith Anderson

Acknowledgements

This thesis and related research are the result of many years of work that has resulted in a mass concrete integrity testing methodology that is helping to make constructed foundations not only less expensive, but also safer. The culmination of this work would not have been possible without contributions from the following:

- ✧ Department of Civil and Environmental Engineering, University of South Florida
- ✧ Austin Gray Mullins, PhD, PE - major professor
- ✧ Rajan Sen, PhD, PE - committee member
- ✧ Michael Stokes, PhD, PE - committee member
- ✧ Stanley C. Kranc, PhD, PE - retired committee member
- ✧ Danny Winters, MSCE - research associate
- ✧ Robert Van Wagner, PE - research associate
- ✧ Nestor Sotelo, PE - research associate
- ✧ George Onorato, PE - research associate
- ✧ Thomas Miller, PE
- ✧ Cheryl Martin, PE
- ✧ The employees at Structural Engineering and Inspections, Inc.
- ✧ Nancy, Ethan, Abigail and Lyla Anderson – the family
- ✧ Billy Joe Anderson – my father

Table of Contents

List of Tables	iii
List of Figures	iv
List of Symbols and Abbreviations.....	xiv
Abstract	xv
Chapter 1 - Introduction.....	1
1.1 Background.....	1
1.2 Organization of Thesis	5
Chapter 2 - The State of Drilled Shaft Integrity Testing	7
2.1 Introduction.....	7
2.2 Cross-Hole Sonic Logging.....	9
2.3 Crosshole Tomography	22
2.4 Single Hole Sonic Logging.....	23
2.5 Sonic Echo Test	26
2.6 Impulse Response Test	36
2.7 Gamma-Gamma Testing (GGT) or Gamma Density Logging (GDL) or Gamma-Gamma Logging (GGL)	39
2.8 Concreteoscopy.....	46
2.9 Parallel Seismic Integrity Testing.....	46
2.10 Conclusion	50
Chapter 3 - History of the Basic Theories of Deep Thermal Infrared Instrumentation	51
3.1 Introduction.....	51
3.2 Thermal Integrity Profiling Instrumentation.....	52
3.3 Temperature Measurement	52
3.4 Temperature - Thermocouple	56
3.5 Temperature – Radiation (Infrared)	60
Chapter 4 - Basic Instrumentation and Lab Scale Tests	65
4.1 Introduction.....	65
4.2 Basic Instrumentation Version 1.0.....	65
4.3 Lab Scale Test #1 – Feasibility Study.....	67
4.4 Lab Scale Test #2.....	69
4.5 Depth Measurements	71

4.6 Field Trial #1.....	72
4.7 Basic Instrumentation – Version 2.0.....	90
4.8 Field Trial #2.....	98
4.9 Basic Instrumentation – Version 2.1 and Software Development.....	107
Chapter 5 - Full Scale Testing – Auburn, AL.....	110
5.1 Introduction.....	110
5.2 Test Site Set-Up.....	111
5.3 Rebar Cage Preparation Auburn Test Site.....	117
5.4 Drilled Shaft Excavation and Cage Placement.....	119
5.5 Mix Specifications.....	122
5.6 Quality Assurance.....	124
5.7 Cross-Hole Sonic Logging Auburn Test Shafts.....	125
5.8 Shaft Integrity Testing Auburn Test Shafts.....	130
5.9 Thermal Integrity Profiling – Auburn Test Shafts.....	133
5.10 Post Grout– Auburn Test Site.....	139
5.11 Additional Testing – Auburn Test Site.....	141
5.12 Lessons Learned from Thermal Integrity Profiling - Auburn Test Site.....	145
Chapter 6 - Summary and Conclusions.....	148
6.1 Overview.....	148
6.2 Present Practice.....	149
List of References.....	151
Appendices.....	156
Appendix A - Additional Information from Field Trial #1.....	157
Appendix B - Additional Information from Field Trial #2.....	162
Appendix C - Additional Information Auburn Test Site.....	180

List of Tables

Table 1.1 - Resistance factors for driven piles and drilled shafts (AASHTO, 2010)	4
Table 2.1 - P-wave velocities in different mediums	11
Table 2.2 - Minimum number of CSL tubes per shaft based on diameter (ADOT, 2001)	12
Table 2.3 - Approximate time window for acquiring optimal CSL data	14
Table 2.4 - WSDOT general rating criteria for CSL results (WSDOT, 2009)	19
Table 2.5 - Compression wave velocity in concrete	30
Table 3.1 - Thermocouple types and temperature ranges (Omega-5)	59
Table 4.1 - Signal voltage for trial #1	68
Table 5.1 - Detailed summary of concrete mixes	124

List of Figures

Figure 1.1 - Drilled shaft with absent concrete.....	3
Figure 1.2 - Concrete failure at top of drilled shaft during load test (Left), concrete failure at top of drilled shaft during load test (Right) (Stokes, 2007).....	3
Figure 2.1 - Data presentation from a CSL test	21
Figure 2.2 - Limited sampling area for CSL.....	22
Figure 2.3 - A Velocity tomogram on a drilled shaft of a highway bridge showing an anomalous zone between 31 and 33 feet.....	23
Figure 2.4 - Single hole sonic logging test set-up (left), example test results from SSL showing possible anomaly (right) (FHWA, 2007).....	25
Figure 2.5 - Typical SET test set up / theory (left), sample of data (right) (FHWA, 2009)	31
Figure 2.6 - GGT indicating necking of a drilled shaft.....	42
Figure 2.7 - Statistical distribution “bell” curve used for interoperation of gamma-gamma data	43
Figure 2.8 - GGT Testing Equipment and Sample Test Results, equipment (top), sample GGT test showing anomaly in shaft (bottom), (Rucker & Verquer).....	45
Figure 3.1 - Herschel's infrared discovery (OMEGA-H2).....	62
Figure 3.2 - Wavelengths and infrared rays (Suite 101).....	62
Figure 3.3 - IR thermocouple signal (OMEGA-2).....	64
Figure 4.1 - OS36-RA and TX901 wiring diagram	66
Figure 4.2 - Lab scale test #1 set up.....	67
Figure 4.3 - Lab scale test 1 results.....	68

Figure 4.4 - Set up configuration for trial #2	70
Figure 4.5 - Cement paste temperature vs. time	70
Figure 4.6 - Depth measuring device	72
Figure 4.7 - IR sensor mount for field test #1	74
Figure 4.8 - Top view field trial #1	74
Figure 4.9 - Field trial #1 side view	75
Figure 4.10 - Field trial #1 test set-up, A - location of test shaft, B -securing access tubes to #3 circular ties	76
Figure 4.11 - Placing anomalies for field trial #1, A - inserting and securing access tubes and ties, B - example of anomaly sand box, C - inside of Sonotube showing anomalies, access tubes and ties, D - end or bottom view of replica shaft showing access tubes and anomaly	77
Figure 4.12 - Excavation and erection of test shafts for field trial #1, A - auger attached to skid steer, B - completed hole, C - setting Sonotube into hole, D - final erection of Sonotube	78
Figure 4.13 - Field trial #1 erected test shaft, A - top view of erected Sonotube, B - work platform and bags of type I cement	79
Figure 4.14 - Mixing and Placing Cement for field trial #1, A - double cement mixers, B - transferring paste from mixer into grout chute, C - Placing paste into replica shaft, D - nearing completion of paste placement, E - completion of paste placement	80
Figure 4.15 - Installing thermocouples in test shaft for field trial #1, A - inserting rubber tube into drilled shaft utilizing a welding rod, B - inserting two-wire thermocouples into capillary tube, C - removing capillary tube, leaving thermocouple in place	81
Figure 4.16 - Running tests field trial #1, A - instrumentation check, B - running tests inside of access tubes, C - running tests in access tubes close-up	83
Figure 4.17 - Delamination of PVC access tubes, A - bleed water boiling, B - bleed water boiling and thermal crack, C - delamination of access tube starting, D - full delamination of access tube	85
Figure 4.18 - Temperature vs. depth, outside of replica shaft field trial #1	86

Figure 4.19 - Temperature traces from access tube #3 field trial #1	87
Figure 4.20 - Thermocouple data from replica shaft field trial #1	88
Figure 4.21 - Drawings and specifications for version 2.0 instrumentation, A - assembled version 2.0 instrumentation including housing, B - enlarged view of assembled device, C - sample sections of device.....	91
Figure 4.22 - Manufacturing and assembly of version 2.0 instrumentation, A - housing manufacturing, B - completed pieces, C - housing pieces for down hole signal conditioning, D - IR thermocouple housing pieces, E - complete device disassembled, F - IR thermocouple section assembled.....	92
Figure 4.23 - 4-20 milliamp voltage to current loop converter.....	93
Figure 4.24 - Current to voltage conversion	94
Figure 4.25 - Complete wiring diagram.....	95
Figure 4.26 - Version 2.0 wiring, A - Voltage to current loop circuits, B - Terminal block to DAQCard, C - current loop to voltage conversion overall, D - current loop to voltage circuitry close up	95
Figure 4.27- Version 2.0 depth measuring device, A –overall view of depth wheel, B - digital encoder and coupling to wheel shaft, C - Umbilical cord, depth wheel and tripod.....	97
Figure 4.28 - Test set-up for field trial #2, A - side view control shaft, B - side view test shaft, C - top view control shaft, D - top view test shaft	100
Figure 4.29 - Tying rebar cages for field trial #2, A - inclinometer casing and #3 ties, B - inclinometer casing and rebar cage for second shaft.....	101
Figure 4.30 - Field trial #2 test set-up, A - sand box anomaly, B - anomaly and cage inside of Sonotube, C - erected control shaft top view, D - erected control shaft elevation view	102
Figure 4.31 - Installing thermocouples for field trial #2, A - insertion of 2-wire thermocouples, B - data logger for thermocouples	103
Figure 4.32 - Field Trial #2 Testing, A - field trial #2 data collection overall, B - field test #2 data collection close-up.....	104
Figure 4.33 - Field trial #2 thermocouple data	105

Figure 4.34 - Sample data from field trial #2 - tube E-2.....	106
Figure 4.35 - Sand box anomaly found adjacent to tube E-2.....	106
Figure 4.36 - Thermal integrity profiling system setup	108
Figure 4.37 - Screen shot from TIP data post processing worksheet.....	109
Figure 5.1 - Auburn University's NGES Test Site, Opelika, Alabama (Google Maps)	112
Figure 5.2 - Alabama site soil testing, A - CPT soundings in test area, B - subsurface exploration using the USF mini-CPT rig.....	113
Figure 5.3 - TS-1 mini CPT sounding	113
Figure 5.4 - TS-2 mini CPT sounding	114
Figure 5.5 - TS-3 mini CPT sounding	114
Figure 5.6 - TS-4 mini CPT sounding	115
Figure 5.7 - TS-5 mini CPT sounding	115
Figure 5.8 - Test shaft layout	116
Figure 5.9 - Auburn test shafts set-up, A - example of sand bag anomaly attached to rebar cage, B - overall picture of rebar cage, C - close up view of toe of TS-1 (a. post grout cell, b. sister bar), D - inside of rebar cage (a. grout tube, b. CSL / thermal access tube).....	119
Figure 5.10 – Excavation and erection for Auburn test shafts, A - truck mounted drill rig, B - close up of double flight rotary auger, C - completed excavation being inspected with bore scope, D - centralizer.....	121
Figure 5.11 - Flow tests for SCC mixes, A - “L”-box flow test device used for measuring the flow of SCC mixes, B - material flows through lower gate and drop height is recorded	123
Figure 5.12 - CSL velocity and energy plots for test shaft TS-3 - all tube pairs	126
Figure 5.13 - Sand bag anomaly centered on tube B (2) for TS-3 Auburn test site	127
Figure 5.14 - Control shaft TS-4 and the CSL test results for TS-4 Auburn test site.....	128
Figure 5.15 - TS-1 CSL data and toe anomaly Auburn test site	129

Figure 5.16 - SET test set-up for Auburn test site	130
Figure 5.17 - SET data for TS-1 before grouting (top) and after load testing (bottom).....	131
Figure 5.18 - SET data for TS-2 before grouting (top) and after load testing (bottom).....	131
Figure 5.19 - SET data for TS-3 before grouting (top) and after load testing (bottom).....	132
Figure 5.20 - SET data for TS-4 before grouting (top) and after load testing (bottom).....	132
Figure 5.21 - SET data for TS-5 before grouting (top) and after load testing (bottom).....	133
Figure 5.22 - TIP testing at Auburn test site, A - tripod, depth wheel, tripod and down hole sensor, B - driver motor and pulleys, signal conditioning and portable computer, C - overall test setup, D - screen shot showing real time thermal sensors	134
Figure 5.23 - Temperature traces vs. depth for test shaft TS-2 Auburn test site	136
Figure 5.24 - Fourier analysis of inward-facing sensor temperature data for shaft TS-3 (tube A) Auburn test site.....	137
Figure 5.25 - Low-passed (“rebar-filtered”) temperature traces and one unfiltered trace of the inward-facing channel from shaft TS-3 (tube A) Auburn test site	139
Figure 5.26 - Post Grouting at Auburn test site, A - grout pump and mixing of grout, B - injection of grout into top of shaft, C - string potentiometers used to measure vertical displacement of shaft.....	140
Figure 5.27 - 4MN statnamic load test setup Auburn test site.....	142
Figure 5.28 - Sample of rapid load test results on Auburn test shafts	143
Figure 5.29 - Exhuming, coring and dissecting the test shafts at the Auburn test site	144
Figure A1 - TIP data from field trial #1 all tubes	157
Figure A2 - TIP data from field trial #1 tube 1	158

Figure A3 - TIP data from field trial #1 tube 2.....	159
Figure A4 - TIP data from field trial #1 tube 3.....	160
Figure A5 - TIP data from field trial #1 outside of shaft.....	161
Figure B1 - Concrete mix design for field trial #2.....	162
Figure B2 - Ready mix delivery ticket for concrete used in Field Trial #2.....	164
Figure B3 - Field trial #2 TIP test #1 rebar shaft tube 1.....	165
Figure B4 - Field trial #2 TIP test #1 rebar shaft tube 2.....	166
Figure B5 - Field trial #2 TIP test #1 rebar shaft tube 3.....	167
Figure B6 - Field trial #2 TIP test #1 control shaft tube 1.....	168
Figure B7 - Field trial #2 TIP test #1 control shaft tube 2.....	169
Figure B8 - Field trial #2 TIP test #1 control shaft tube 3.....	170
Figure B9 - Field trial #2 TIP test #2 rebar shaft tube 1.....	171
Figure B10 - Field trial #2 TIP test #2 rebar shaft tube 2.....	172
Figure B11 - Field trial #2 TIP test #2 rebar shaft tube 3.....	173
Figure B12 - Field trial #2 TIP test #2 control shaft tube 1.....	174
Figure B13 - Field trial #2 TIP test #2 control shaft tube 2.....	175
Figure B14 - Field trial #2 TIP test #2 control shaft tube 3.....	176
Figure B15 - Field trial #2 TIP test #3 rebar shaft tube 1.....	177
Figure B16 - Field trial #2 TIP test #3 rebar shaft tube 2.....	178
Figure B17 - Field trial #2 TIP test #3 rebar shaft tube 3.....	179
Figure C1 - Explanation of thermocouple data from Auburn test site.....	180
Figure C2 - Auburn test site thermocouple data from foam coolers.....	180
Figure C3 - Auburn test site thermocouple data normalized.....	181

Figure C4 - Auburn test site thermocouple data from adiabatic box #1	181
Figure C5 - Auburn test site thermocouple data from adiabatic box #2	182
Figure C6 - Auburn test site thermocouple data from first four mixes.....	182
Figure C7 - Auburn test site thermocouple data for three different volumes of the same mix (M1).....	183
Figure C8 - Auburn test site normalized thermocouple data for three different volumes of mix M1	183
Figure C9 - Auburn test site TIP test results TS1 tube A Test 1	184
Figure C10 - Auburn test site TIP test results TS1 tube B Test 1.....	185
Figure C11 - Auburn test site TIP test results TS1 tube C Test 1.....	186
Figure C12 - Auburn test site TIP test results TS2 tube A Test 1	187
Figure C13 - Auburn test site TIP test results TS2 Tube B Test 1	188
Figure C14 - Auburn test site TIP test results TS2 Tube C Test 1	189
Figure C15 - Auburn test site TIP test results TS3 Tube A Test 1	190
Figure C16 - Auburn test site TIP test results TS4 Tube A Test 1	191
Figure C17 - Auburn test site TIP test results TS4 Tube B Test 1	192
Figure C18 - Auburn test site TIP test results TS4 Tube C Test 1	193
Figure C19 - Auburn test site TIP test results TS5 Tube A Test 1	194
Figure C20 - Auburn test site TIP test results TS5 Tube B Test 1	195
Figure C21 - Auburn test site TIP test results TS5 Tube C Test 1	196
Figure C22 - Auburn test site TIP test results TS1 Tube A Test 2	197
Figure C23 - Auburn test site TIP test results TS1 Tube B Test 2	198
Figure C24 - Auburn test site TIP test results TS1 Tube C Test 2	199
Figure C25 - Auburn test site TIP test results TS2 Tube A Test 2	200

Figure C26 - Auburn test site TIP test results TS2 Tube B Test 2	201
Figure C27 - Auburn test site TIP test results TS2 Tube C Test 2	202
Figure C28 - Auburn test site TIP test results TS3 Tube A Test 2	203
Figure C29 - Auburn test site TIP test results TS3 Tube B Test 2	204
Figure C30 - Auburn test site TIP test results TS3 Tube C Test 2	205
Figure C31 - Auburn test site TIP test results TS4 Tube A Test 2	206
Figure C32 - Auburn test site TIP test results TS4 Tube B Test 2	207
Figure C33 - Auburn test site TIP test results TS4 Tube C Test 2	208
Figure C34 - Auburn test site TIP test results TS5 Tube A Test 2	209
Figure C35 - Auburn test site TIP test results TS5 Tube B Test 2	210
Figure C36 - Auburn test site TIP test results TS5 Tube C Test 2	211
Figure C37 - Auburn test site TIP test results TS1 Tube A Test 3	212
Figure C38 - Auburn test site TIP test results TS1 Tube B Test 3	213
Figure C39 - Auburn test site TIP test results TS1 Tube C Test 3	214
Figure C40 - Auburn test site TIP test results TS2 Tube A Test 3	215
Figure C41 - Auburn test site TIP test results TS2 Tube B Test 3	216
Figure C42 - Auburn test site TIP test results TS2 Tube C Test 3	217
Figure C43 - Auburn test site TIP test results TS3 Tube A Test 3	218
Figure C44 - Auburn test site TIP test results TS3 Tube B Test 3	219
Figure C45 - Auburn test site TIP test results TS3 Tube C Test 3	220
Figure C46 - Auburn test site TIP test results TS4 Tube A Test 3	221
Figure C47 - Auburn test site TIP test results TS4 Tube B Test 3	222
Figure C48 - Auburn test site TIP test results TS4 Tube C Test 3	223

Figure C49 - Auburn test site TIP test results TS5 Tube A Test 3	224
Figure C50 - Auburn test site TIP test results TS5 Tube B Test 3	225
Figure C51 - Auburn test site TIP test results TS5 Tube C Test 3	226
Figure C52 - Auburn test site TIP test results TS1 Tube A Test 4	227
Figure C53 - Auburn test site TIP test results TS1 Tube B Test 4	228
Figure C54 - Auburn test site TIP test results TS1 Tube C Test 4	229
Figure C55 - Auburn test site TIP test results TS2 Tube A Test 4	230
Figure C56 - Auburn test site TIP test results TS2 Tube B Test 4	231
Figure C57 - Auburn test site TIP test results TS2 Tube C Test 4	232
Figure C58 - Auburn test site TIP test results TS3 Tube A Test 4	233
Figure C59 - Auburn test site TIP test results TS3 Tube B Test 4	234
Figure C60 - Auburn test site TIP test results TS3 Tube C Test 4	235
Figure C61 - Auburn test site TIP test results TS4 Tube A Test 4	236
Figure C62 - Auburn test site TIP test results TS4 Tube B Test 4	237
Figure C63 - Auburn test site TIP test results TS4 Tube C Test 4	238
Figure C64 - Auburn test site TIP test results TS5 Tube A Test 4	239
Figure C65 - Auburn test site TIP test results TS5 Tube B Test 4	240
Figure C66 - Auburn test site TIP test results TS5 Tube C Test 4	241
Figure C67 - Auburn test site TIP test results TS1 Tube A Test 5	242
Figure C68 - Auburn test site TIP test results TS1 Tube B Test 5	243
Figure C69 - Auburn test site TIP test results TS1 Tube C Test 5	244
Figure C70 - Auburn test site TIP test results TS2 Tube B Test 5	245
Figure C71 - Auburn test site TIP test results TS2 Tube C Test 5	246

Figure C72 - Auburn test site TIP test results TS3 Tube A Test 5	247
Figure C73 - Auburn test site TIP test results TS3 Tube B Test 5	248
Figure C74 - Auburn test site TIP test results TS3 Tube C Test 5	249

List of Symbols and Abbreviations

ρ	dry density (g/cm^3)
γ	unit weight (lb/ft^3) and (N/m^3)
Q	heat flow (W/m)
λ	thermal conductivity ($\text{W}/\text{m}\cdot\text{K}$)
c	specific heat ($\text{kJ}/\text{g}\cdot\text{K}$)
C	Heat Capacity ($\text{J}/\text{cm}^3\cdot\text{K}$)
k	diffusivity (m^2/s)
T	temperature ($^{\circ}\text{C}$)
t	time (s)

Abstract

This thesis has shown that the development of the instrumentation necessary to provide in-situ thermal imaging for the determination of homogeneity of concrete is theoretically sound.

Drilled shafts are large diameter underground cast-in-place columns that necessarily rely on sound integrity to properly withstand imposed loadings. As a by-product of the most common construction techniques, the entire process is often completely blind whereby the excavation and concreting processes are conducted beneath the surface of the water table (or slurry level). This results in an inability to inspect the final product and in many cases allows anomalous inclusions (soil cave-ins, slurry pockets, etc) to go undetected especially when they are formed outside the steel reinforcing cage.

In an effort to gain verification of the as-built, below ground structure, numerous non-destructive test methods have been devised. Each of these methods have merits and drawbacks with regards to the full extent of the tested concrete volume. To further this cause, a new methodology was developed that uses the energy from hydrating concrete to assess the presence or absence of an intact concrete. Therein, the temperature generated

by the curing concrete can be measured and correlated to the probable dimensions of the drilled shaft.

This thesis outlines the development of the instrumentation capable of making in-situ temperature measurement of drilled shafts to assure the homogeneity of concrete is acceptable. To that end, several configurations of instrumentation approach were tested on varying scales from small lab specimens to full-size field constructed drilled shafts. The bulk of this work was conducted several years before the completion of the thesis and has the benefit of noting later developments. For instance, this study was used to seed future research and led to subsequent FDOT and WSDOT (Washington State DOT) funded research for the express purpose of identifying capabilities of thermal testing in those states. Likewise, present day practice and use of the approach has also been documented.

Chapter 1 - Introduction

Drilled shafts are large diameter concrete foundations that are preferable in many applications over driven pile foundations due to their enormous axial and lateral (moment) capacities. In fact, they are the preferred foundation for bridges due to their large capacities. Bridge foundations must be designed and constructed to resist extreme event loads such as ship or barge impact. For example, it can be shown that six (6) 7'-0" diameter drilled shafts have an equivalent lateral capacity to 50 – 80 driven prestressed piles. However, the disadvantages of drilled shafts over driven foundations include the inability to visually inspect the final structural product and a reduction in redundancy. Both of these disadvantages have led the author to investigate new technology which utilizes the inherent heat production in mass concrete elements to scan newly completed drilled shafts for defects and determine their integrity thus improving the overall safety and eventually reducing the overall costs of drilled shaft foundations.

1.1 Background

Resistance factors, typically referred to as Φ factors, are used in the design of structural and foundation elements to account for as-constructed unknown factors. These factors may include: variability in constructed dimensions, material strengths and

properties, and soil conditions. Drilled shafts are governed by geotechnical and structural capacity as well as the associated resistance factors as shown in the following equations:

$$P_U \leq \Phi_{geo} P_{N_{geo}}$$

OR

$$P_U \leq \Phi_{str} P_{N_{str}}$$

Therein, $P_{U_{geo}}$ and $P_{U_{str}}$ are computed from two different failure modes but both must be satisfied. A problem arises, however, when $\Phi_{str} P_{N_{str}}$ represents the capacity below ground where visual inspection cannot be provided. Presently, both above and below ground structures receive the same structural considerations and the same resistance factor is used for both. This assumption may in fact lead to an over estimation of the foundation integrity / capacity, leading to a catastrophic failure of the foundation system.

The resistance factors applied to the structure of a drilled shaft is based on the Φ factors for a column which are 0.85 compression and 0.90 for bending (ACI, AASHTO 2010). These Φ factors are assuming adequate quality control which cannot be achieved in the “Blind Construction” of a drilled shaft. Figure 1.1 is an example of a drilled shaft which shows a significant defect near the surface where the need for structural capacity is at the highest.



Figure 1.1 - Drilled shaft with absent concrete

Even where the entire section is in place, it has been shown that load test failures may in some cases be the result of structural failure (Figure 1.2).



Figure 1.2 - Concrete failure at top of drilled shaft during load test (Left), concrete failure at top of drilled shaft during load test (Right) (Stokes, 2007)

As shown in Table 1.1, current AASHTO Standards set resistance factors based on geotechnical testing and type of construction (AASHTO, 2010).

Table 1.1 - Resistance factors for driven piles and drilled shafts (AASHTO, 2010)

Type of Foundation	Resistance Factor Range
Driven Piles	0.10 – 0.90
Drilled Shafts	0.35 – 0.7

Although these factors also address unknowns in geotechnical materials, the disparity between above and below ground conditions should be reflected by a change in the resistance factor or the quality assurance should be assured below ground. Currently accepted methods for evaluating the integrity of drilled shafts have been shown to be ineffective in providing a full picture of the actual as-built condition of the shaft. Some testing methods are effective at evaluating the core of the shaft while others are limited to only the proximity of access tubes, which are used to insert test equipment. This thesis focuses on an alternative means to provide increased inspection for drilled shafts (id est underground concrete columns).

1.2 Organization of Thesis

This thesis is organized into five chapters describing the background, testing, results, and finally applications of the thesis findings with conclusions.

Chapter two outlines the current state of drilled shaft and mass concrete integrity testing and includes in depth discussions about the currently most used testing methods. The chapter also discusses the pros and cons of each of the testing methods. The chapter concludes with the shortcomings of the current technology and emphasizes the need to develop a better testing method.

Chapter three focuses on the history of basic theories utilized in the development of a deep thermal infrared instrument. These include but are not limited to the genesis of the idea of using temperature as a means to determine the integrity of mass concrete elements and the history of temperature measurement and infrared technology. This chapter concludes with discussions about why infrared was chosen as the preferred method to measure the temperature of deep mass concrete.

Chapter four provides an overview and examines several different variations or generations of the thermal profiling instrumentation set-up and sample lab scale tests associated with each. Chapter four also contains discussions about the pros and cons of each instrumentation set-up and what improvements should be made for the ensuing generation. The chapter concludes with descriptions of an acceptable instrumentation

configuration and software development that can be utilized on a production basis in full scale operations.

Chapter five discusses a series of full scale tests that were completed on test drilled shafts in conjunction with Auburn University close to the Auburn campus in Alabama. This chapter concludes with discussions of the successes and shortcomings of the full scale tests in Auburn and makes recommendation on future improvements that could be made to the instrumentation and the process.

Chapter six concludes the thesis by summarizing the results and discussing some of the lessons learned through failed tests. This chapter concludes with information on the current state of Thermal Integrity Profiling Instrumentation.

Chapter 2 - The State of Drilled Shaft Integrity Testing

This chapter discusses the current state of drilled shaft and mass concrete integrity testing and includes in depth discussions about the most currently used testing methods. The chapter also discusses the pros and cons of each of the testing methods. The chapter concludes with the shortcomings of the current technology and emphasizes the need to develop a better testing method.

2.1 Introduction

The design of structural elements, including mass foundations, assures that the resistance of a specific structural element exceeds the Ultimate, Serviceability, and Specific limit states with an acceptable factor of safety. The magnitude of the factor of safety applied to a structural system has a direct correlation to the ability of the designer to verify the resistances from structural and geotechnical components. It is then verified that these resistances exceed the direct load effects. The factor of safety also has a direct effect on the overall size and cost of any structural system.

In the case of super structure members such as bridge girders, the inspection process can be straightforward, since the structural elements are easily inspected during manufacturing, shipping and installation, yielding an efficient system that accomplishes

the required task with little waste. However, substructure elements, such as drilled concrete shaft foundations, do not have the same liberties of inspection as the aforementioned superstructure counterparts. Therefore, several methods have been developed in an effort to determine the integrity of a completed drilled shaft. The most widely accepted methods are described herein along with a synopsis of the underlying physical principles or science that these tests are founded on, along with a discussion of the pros and cons for each test.

In general design procedures, it must be verified that the resistances from structural components exceed the applied load effects. Load effects are independent of the structural component and include, bending moment, shear, axial forces, torque, deflection and vibration. The ability of a structural component to resist these effects is considered resistance. Strength Reduction Factors, Φ , which are less than one and Load Factors, α , which are greater than one, are introduced to account for the fact that the resistance may be less and the loads may be higher than anticipated (MacGregor 1996). The resistance of structural members will most likely vary from the calculated strength because of variability in material strengths, differences in as-built dimensions from calculated dimensions, and effects of simplifying mathematical assumptions made during resistance calculations.

Although drilled shaft capacity is closely linked to soil type, it has been long understood that construction practice can drastically affect anticipated capacity (Garbin 2001). Of particular concern is the loss of concrete cover around the steel reinforcement

which will result in corrosion of the reinforcement and a loss of strength. Some inclusions or anomalies may be so severe that the foundation is considered unusable.

Consider a drilled shaft that is constructed with bentonite slurry. With current technology, it is not possible to determine exactly how well a drilled shaft has been constructed. Foundations contribute a major part of the overall cost in most bridges, buildings and other structures that require mass concrete foundations to resist the applied loads. Clearly, an increase in the ability to determine the integrity of a mass concrete foundation results in a direct reduction in the overall budget. Many years of research and development have resulted in multiple different methods to determine the in-situ condition of drilled shafts or piles.

This chapter will investigate the current state of integrity testing and conclude by identifying the present need for more robust capabilities. Methods can be categorized as either destructive or nondestructive and include: concrete coring, seismic echo, impulse response, cross-hole sonic logging, and density testing by downhole gamma-gamma logging.

2.2 Cross-Hole Sonic Logging

Cross-Hole Sonic Logging (CSL) is perhaps the most widely accepted and used integrity testing method. CSL evaluates the uniformity and continuity of concrete by recording the velocity of signals between preset tubes or pipes (Lew et al., 2002). In fact,

Alabama Department of Transportation's *Specifications for Drilled Shaft Construction*, Section 506 states in 506.10(a)1, "The nondestructive testing method called Crosshole Sonic Logging (CSL) shall be used on all production and trial drilled shafts (a) when constructed with the placement of concrete under water or through slurry, (b) when required by special note on the plans, (c) when full length temporary casing is used to prevent water from entering the shaft, or (d) when determined to be necessary by the Engineer" (ADOT 2001). In short, whenever there is a high probability of the existence of drilled shaft inclusions or a problem, Alabama requires CSL testing be performed. Alabama does not recognize or accept any other testing methods in their state specifications.

State of California Department of Transportation Engineering Service Center Division of Structures, *California Foundation Manual* and New York State Department of Transportation's *Drilled Shaft Inspector's Guidelines* have similar requirements to Alabama, but also allow the use of several different testing methods included in this chapter.

The primary reason that CSL is so widely accepted is because it is an accurate, cost-effective, and nondestructive means of investigating the integrity of concrete in drilled shaft foundations (Branagan & Associates, Inc., 2002). Furthermore, CSL determines the integrity and homogeneity of concrete in a deep foundation and identifies voids or soil intrusions within the structure.

The CSL Test includes placing a signal generator in one access tube and a signal receiver in another access tube. The basic theory of the CSL test is that the arrival time of the compression wave signal from the generator to the receiver has a direct correlation to the density of the concrete. The ultrasonic compression-wave (or p-wave) arrival time from a signal source in one tube is measured to a receiver in another tube. The test is normally run from the bottom to the top with both the receiver and the generator at the same vertical elevation. Knowing the tube separation distance, the p-wave velocity is calculated for each depth. The results are plotted as velocity with respect to depth (Branagan & Associates, Inc., 2002).

P-wave velocities for sound concrete free of defects are typically around 3,700 m/sec (12,000 ft/sec). Decreases in sonic-velocity from the local velocity average, accompanied by decreases in signal energy, indicate a departure from uniform concrete quality. Soil intrusion, poor concrete mix quality, voids, or other non-cemented intrusive materials can cause a decrease in p-wave velocity (Branagan & Associates, Inc., 2002). Table 2.1 indicates the p-wave velocity in different mediums.

Table 2.1 - P-wave velocities in different mediums

Material	Velocity (ft/sec)	Velocity (km/sec)
Sound Concrete	12,000	3.7
Water	4,800	1.5
Air	1,100	0.3

The equipment set up for the CSL test includes placing either steel or PVC access tubes around the perimeter of the reinforcement cage that is to be installed in the drilled shafts to be tested. The number of tubes to be installed will depend on the diameter of the shaft and requirements of the state drilled shaft construction specifications where the shaft is being installed. The general guide, however, is to install one access tube per foot of shaft diameter (or one tube per 0.25 to 0.30 meters of shaft diameter) (Branagan & Associates, Inc., 2002). Alabama requires that 1.5 inch to 2.0 inch {40 mm to 50 mm} inside diameter schedule 40 steel pipe be used in quantities specified in Table 2.2.

Table 2.2 - Minimum number of CSL tubes per shaft based on diameter (ADOT, 2001)

Shaft Diameter D	Minimum Number of Tubes
$D \leq 4.5$ feet {1372 mm}	4
4.5 feet {1372 mm} < $D \leq 5.5$ feet {1676 mm}	5
5.5 feet {1676 mm} < $D \leq 6.5$ feet {1981 mm}	6
6.5 feet {1981 mm} < $D \leq 7.5$ feet {2286 mm}	7
7.5 feet {2286 mm} < $D \leq 8.5$ feet {2591 mm}	8
8.5 feet {2591 mm} < $D \leq 9.0$ feet {2743 mm}	9
9.0 feet {2743 mm} < $D \leq 10.0$ feet {3048 mm}	10
10.0 feet {3048 mm} < $D \leq 11.0$ feet {3353 mm}	11
11.0 feet {3353 mm} < $D \leq 12.0$ feet {3658 mm}	12

Whether steel or PVC access tubes are used, the tubes must have end caps and couplers that are watertight. The tube inside diameter must allow for the top-to-bottom free and unobstructed passage probes having dimensions of 1.41 inches diameter and 4

inches in length. Prior to CSL testing, tubes should have removable caps at the surface to prevent foreign material which could obstruct the tube (Branagan & Associates, Inc., 2002). The access tubes are filled with potable water prior to testing. The water provides a medium from which the p-wave signal can be transmitted and received inside the access tube.

Another consideration for assuring the accuracy and reliability of the test is de-bonding. De-bonding occurs when the concrete loses bond with the surface of the access tube. This loss of bonding means that an air space has developed between the surface of the pipe and the concrete. This space will produce false and attenuated signals. To help curb this problem, the tube surface shall be clean and free from contamination and the test should be completed with the specified time after concrete placement. Shrinkage of concrete increases with time and is a major cause of de-bonding. PVC tubes cost less than steel but tend to de-bond more rapidly from concrete than steel tubes. Therefore, when PVC tubes are used they shall be roughened by abrasion prior to installation (Branagan & Associates, Inc., 2002). Table 2.3 indicates the approximate time window for acquiring optimal CSL data.

Table 2.3 - Approximate time window for acquiring optimal CSL data

Tube Composition	Tube ID (inches)	Approximate Time Window for Acquiring Optimal CSL Data
Schedule 40 Black Steel	1.5 to 2.0	24 hours up to 45 days
Schedule 40 PVC	1.5 to 2.0	24 hours up to 10 days

The installation of access tubes shall in general terms follow the following procedures:

1. Consult with the project engineer and project specifications to verify: the type of tubes to be used, the quantity to be installed per shaft, required tube dimensions, and the method of tube installation (Branagan & Associates, Inc., 2002). For example, Alabama specifications require that, “The tubes shall be installed in each shaft in a regular, symmetric pattern such that each tube is equally spaced from the others around the perimeter of the cage. The Contractor shall submit to the testing organization his selection of tube size, along with his proposed method to install the tubes, prior to construction.” (ADOT, 2001)
2. Watertight caps shall be placed on the bottom and the top of the tubes. In addition, any couple used to make full-length tubes shall be watertight. Butt welding of steel tube couplings and the use of tape to wrap pipes is not permitted.

In addition, if PVC pipe is used, couplers shall be threaded or glued (Branagan & Associates, Inc., 2002).

3. Access tubes shall be attached to the interior of the reinforcing cage with wire ties at regular intervals along the length of the shaft, for example every three feet. Tubes shall be secured to maintain vertical and parallel alignment during cage lifting, lowering and concrete placement. Tubes that are not vertical and parallel can adversely affect the outcome of a CSL test (Branagan & Associates, Inc., 2002). In addition, care shall be taken during reinforcement installation operations in the drilled shaft hole so as to not damage the tubes (ADOT, 2001).

4. In order to include the toe of the shaft in the testing, the access tubes shall be installed such that their bottoms are close to the bottom of drilled shaft. Generally, tubes are placed within six inches of the toe of the shaft. Tubes are also extended two to three feet above what will be the top of the concrete shaft (Branagan & Associates, Inc., 2002).

5. The tubes must be filled with clean water as soon as possible after the reinforcement cage is set; in no case shall the tubes remain dry for more than one hour after concrete placement. The addition of the water to the tubes helps prevent the tubes from de-bonding. The tubes shall be capped or plugged immediately after being filled with water to prevent debris from entering into the tubes (Branagan & Associates, Inc., 2002).

6. Alabama Specifications require, “The pipe caps or plugs shall not be removed until the concrete in the shaft has set. Care shall be exercised in the removal of caps or plugs from the pipes after installation so as not to apply excess torque, hammering, or other stresses which could break the bond between the tubes and the concrete.”(ADOT 2001).

7. Normally, after the CSL test is completed, the access holes are evacuated and filled with an approved grout mix.

When determining how soon after concrete placement a CSL Test can be completed, consideration must be given to how much the concrete has cured. In no case shall a test be considered accurate if completed within twenty-four hours after concrete placement. This time may need to be extended for larger diameter shafts or if mix designs that retard concrete setting is used (Branagan & Associates, Inc., 2002). In the interest of correcting any problems found in a timely manner and before the concrete is fully cured, the shaft should be tested as soon as possible after it has adequately cured.

The procedure for completing a CSL test includes the following:

1. The top and bottom elevations for the shaft being tested, or the shaft length, are recorded. The concrete placement date is recorded along with any other pertinent data regarding unusual observations or events that occurred during construction of the concrete shaft (Branagan & Associates, Inc., 2002).

2. A sketch of the shaft under consideration is made and the access tubes are assigned a reference number. This reference number is recorded on the sketch along with precise distance measurement between all of the tube pairs and the tube stick-ups above the concrete surface. Since the theory behind the CSL Test is based on the p-wave arrival time, exact determination of the distance between tube pairs is necessary to accurately analyze a test (Branagan & Associates, Inc., 2002).

3. A tripod with the depth wheel is set up over top of the foundation to be tested and cabling is spooled from the computer, over the depth wheel to each of the source and receiver probes (Branagan & Associates, Inc., 2002). The cabling along with a cable from the depth wheel runs back to the microprocessor based data acquisition unit. These cables provide both excitation and signal return for the hydrophone, receiver, and depth encoder.

The data from a CSL test is typically presented to the client in the form of a written report which in addition to general descriptive information, includes the following specific information. Conclusions are based on transit times and signal strength between each tube pair tested.

1. Interpretation of velocity profile logs with regard to the integrity of the concrete.

2. Identification of the depth interval and tube pair that includes a sonic anomaly.

3. Profiles of the initial acoustic pulse arrival time versus depth and pulse energy / amplitude versus depth (Branagan & Associates, Inc., 2002).

Acceptance criteria vary by state. For example, Florida Department of Transportation (FDOT) guidelines define acceptance solely on a 30% velocity reduction threshold. (FDOT, 2010)

Washington State Department of Transportation (WSDOT) defines their use and interpolation with more detail:

“If it is determined, from CSL Testing that a drilled shaft contains an anomaly, several methods may be used to try and isolate the location of the anomaly. Ultimately, however, the drilled shaft will likely need to be cored to determine whether or not if the shaft is acceptable.

CROSSHOLE SONIC LOGGING (CSL) CONDITION RATING CRITERIA

This CSL rating criteria categorizes abrupt increases in the signal arrival times that correspond to decreases in the average signal velocity of the material between the test probes. These abrupt changes are a result of one or more of the following conditions: (1) increased signal path length as the signal travels around the flaw; (2) a decrease in the signal velocity as it travels through a lower velocity material such as weaker concrete, honeycomb, or contaminated concrete; and (3) deterioration of the bond between the access tube and the concrete. Of the three conditions that cause increased signal arrival times, the deterioration of the tube-concrete bond is the least common and is typically identified only in the upper portions of shafts and in shafts with PVC access tubes.

This CSL rating criteria is based on the percentage reduction of the signal velocity through the flawed area versus the signal velocity through sound material immediately adjacent to the flaw. This ensures that the signal arrival times used to calculate the signal velocities are measured through the same amount of material, which is very important if a tube pair is not

evenly spaced from shaft top to bottom. This CSL criteria is in large part based on experience with ultrasonic pulse velocity measurements of structural concrete, which uses signal velocities to determine material integrity. However, the calculated signal velocities in the CSL testing are reduced by inherent delays due to the slower water, and PVC tube materials. This signal delay yields artificially lower signal velocity for path lengths of 24 inches or less. In contrast, the percentage change in signal velocity between good and flawed material is unaffected by inherent signal delays.” (WSDOT, 2009)

Additionally, as shown in Table 2.4, WSDOT publishes the following general rating criteria for CSL results.

Table 2.4 - WSDOT general rating criteria for CSL results (WSDOT, 2009)

<i>Rating NDT Results indicative of Drilled Shaft Concrete Condition Good (G)</i>	<i>No signal distortion and decrease in signal velocity of 10% or less is indicative of good quality concrete.</i>
<i>Questionable (Q)</i>	<i>Minor signal distortion and a lower signal amplitude with a decrease in signal velocity between 10% and 20%. Results indicative of minor contamination or intrusion and/or questionable quality concrete. Investigation of anomalies with 10% to 15% reductions in velocity have identified sound concrete at some sites and flawed concrete at others.</i>
<i>Poor/Defect (P/D)</i>	<i>Severe signal distortion and much lower signal amplitude with a decrease in signal velocity of 20% or more. Results indicative of water slurry contamination or soil intrusion and/or poor quality concrete.</i>

Table 2.4 Continued

<i>No Signal (NS)</i>	<i>No signal was received. Highly probable that a soil intrusion or other severe defect has absorbed the signal (assumes good bonding of the tube-concrete interface). If PVC tubes are used or if measurement is from near the shaft top the tube-concrete bonding is more suspect.</i>
<i>Water (W)</i>	<i>A measured signal velocity of nominally $V = 4,800$ to $5,000$ fps. This is indicative of a water intrusion or of a water filled gravel intrusion with few or no fines present.</i>

As shown in Figure 2.1, typical data presentation for CSL includes first arrival time (FAT) plot (left), velocity plot (center) and waterfall plot (right). The CSL test indicates the presence of poor concrete at the top of the shaft.

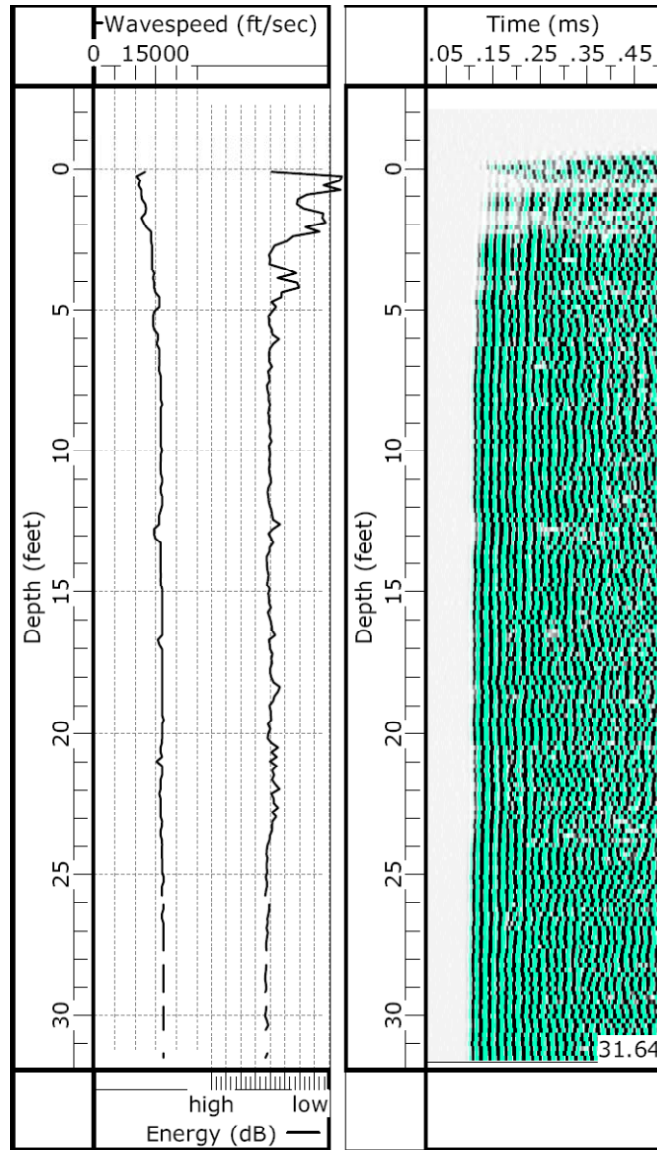


Figure 2.1 - Data presentation from a CSL test

The biggest limitation to CSL is that, as shown in Figure 2.2, CSL only has the ability to sample material velocities between pairs of access tubes. Therefore, it will only detect a shaft defect if it is within the rebar cage. It cannot detect defects outside of the rebar cage, which due to the need to protect the reinforcement and being the areas of highest stress are most critical to the structural performance of the drilled shaft.

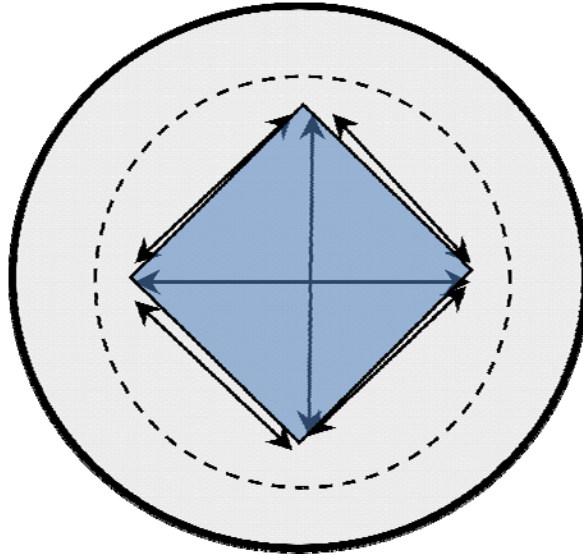


Figure 2.2 - Limited sampling area for CSL

2.3 Crosshole Tomography

Several variations of the CSL test have been developed using the same instrumentation as the CSL. These tests are typically employed after CSL has determined the high probability of an anomaly in a given area and are applied to improve location accuracy and to further characterize the feature. The additional information is utilized to reduce the uncertainty in coring and remediating the defective area (Branagan & Associates, Inc., 2002). One of the most popular of these variations is Crosshole Tomography.

A Crosshole Tomography test is completed by leaving the receiver in a fixed position and raising the hydrophone while the hydrophone is producing sonic pulses. As in the CSL Test, the arrival times from the hydrophone to the receiver are recorded. This

procedure produces ray-paths that allow for three dimensional modeling of the suspect shaft. Figure 2.3 shows a velocity tomogram on a drilled shaft of a highway bridge. The anomalous zone in Figure 2.3 is the slow-velocity area which lies in between 31 and 33 feet below the top of the concrete near tube one. Note that the center of the shaft is sound (Olson, 2003).

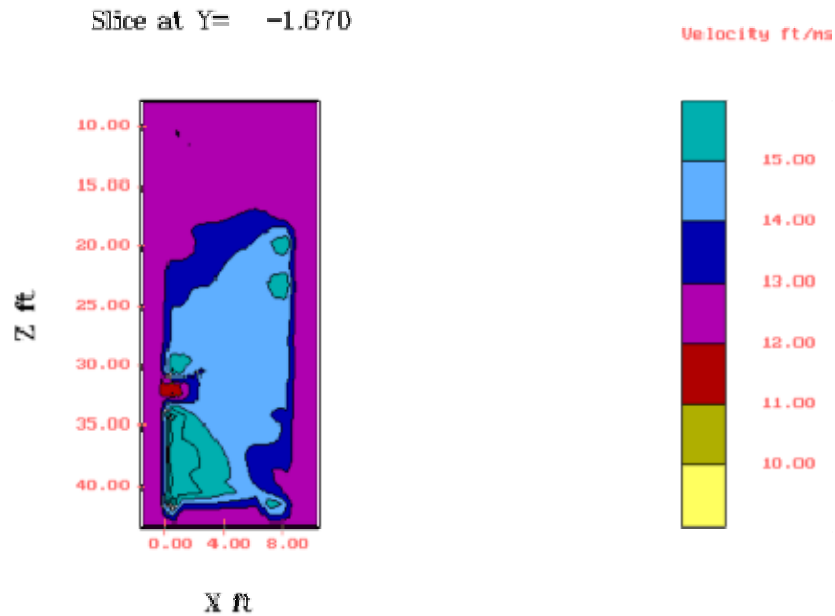


Figure 2.3 - A Velocity tomogram on a drilled shaft of a highway bridge showing an anomalous zone between 31 and 33 feet

2.4 Single Hole Sonic Logging

Another variant of CSL testing is Single Hole Sonic Logging (SSL) which has some capabilities of assessing concrete quality outside of the reinforcing cage. As the name implies, both the source and the receiver are placed in a single access hole and travel in a vertical direction, as shown in Figure 2.2. The disadvantage of SSL as

compared to CSL is that the method is limited to only detecting defects directly adjacent to the tube; the advantage is that unlike CSL, it may have the ability to detect a defect that is outside of the rebar cage (Paikowsky et al, 2000). Another advantage of SSL is due to the necessity for only one access tube to be utilized during the SSL test and the high cost of concrete coring, it is often the preferred method utilized when coring of a shaft is necessary to further investigate a suspected defect or anomaly. SSL is also utilized in smaller diameter shafts and augercast piles (~24" diameter) in which the insertion of multiple access tubes for CSL testing is not practical.

As with CSL, a strong signal and an arrival time that is comparable to the wave speed of good concrete is indicative of locally sound concrete, free of defects. Alternatively, a slow arrival time is indication that a defect may be present in the area of the access tube. Figure 2.4, right side represents a sample test utilizing SSL testing in which the dark lines shown on the time record represent arrivals of signal energy plotted on a vertical scale of depth vs. time on the horizontal axis. The absence of lines in the 5 to 6 m depth interval are delayed arrival times and a weak signal which may be indicators of a defect in the pile. (FHWA, 2007)

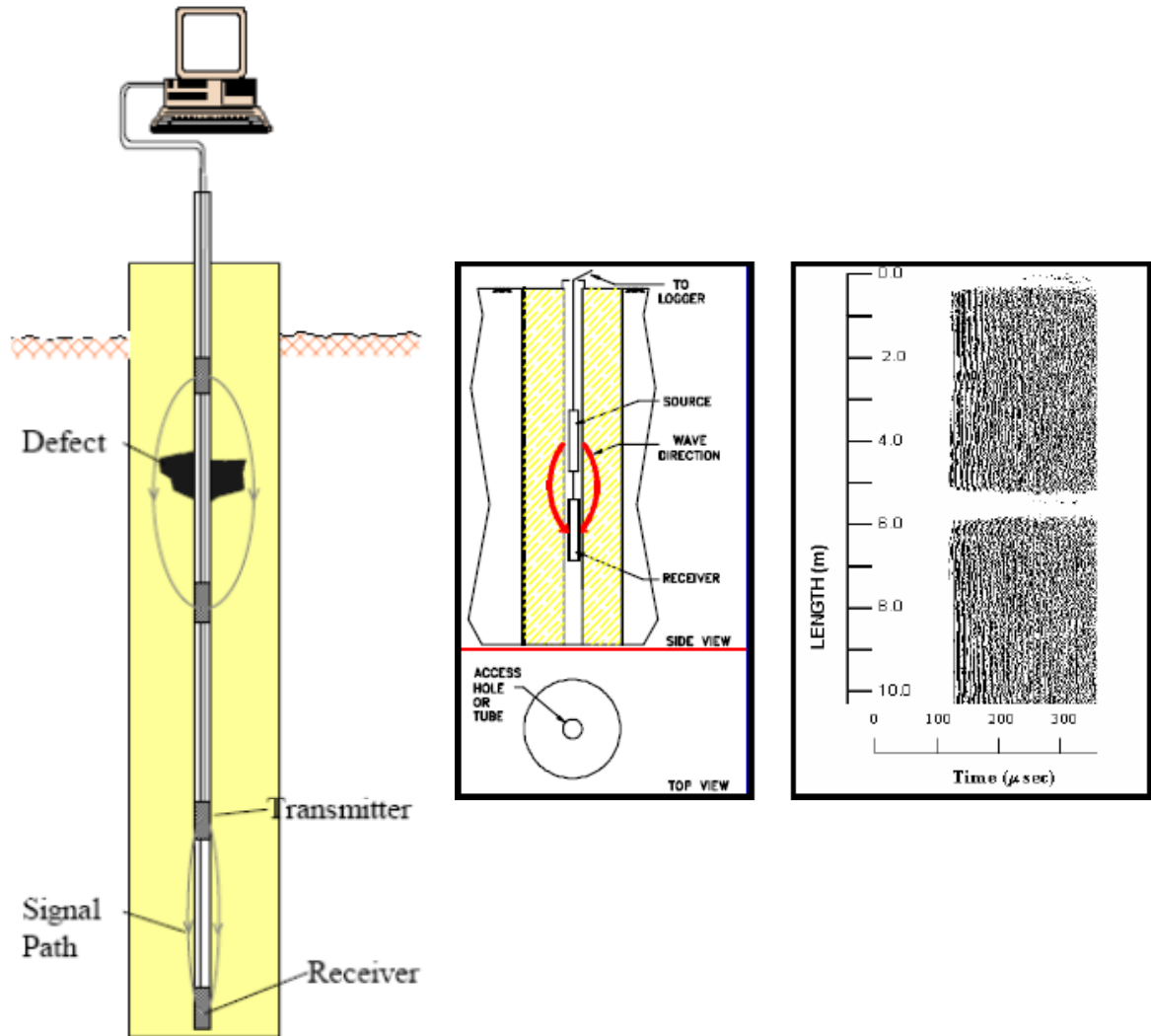


Figure 2.4 - Single hole sonic logging test set-up (left), example test results from SSL showing possible anomaly (right) (FHWA, 2007)

As will be discussed later, similar to gamma-gamma logging, SSL has a limited cross sectional area in which it can detect defects. By placing the transmitter and the receiver close together, the resolution is improved; however the detectible cross sectional area is diminished. Conversely, by spreading the transmitter and receiver apart, the detectible cross sectional area is increased, but the resolution is diminished. It has been shown that if a defect is not directly adjacent to the access tube, it may need to be in

excess of 25% of the cross sectional area before being detected by SSL. All applications involving SSL are only qualitative and cannot define physical meaning to an anomaly.

2.5 Sonic Echo Test

Sonic Echo Tests (SET) are probably the most un-intrusive and economical of any of the integrity tests and do not require any access holes in the drilled shaft being inspected. The SET is based on stress wave theory and is part of a family of tests referred to as surface reflection methods.

In surface reflection tests, a stress wave is introduced into the structure by a hammer impact. The hammer generates stress waves which cause physical distortion to the media in which the impact occurred. Four types of waves of concern are generated in the medium due to the impact (Finno & Prommer, 1994):

1. Compression waves which are also referred to as primary, “bar”, or longitudinal waves.
2. Shear waves which are also referred to as secondary or transverse waves.
3. Surfaces waves or Rayleigh waves.
4. Stoneley waves or tube wave.

The basis behind integrity tests that are developed from stress wave theory is that the time that it takes for a compressional stress wave to be generated at the surface, reflected off the toe, and return to the surface is based on the velocity of the wave and the length of the shaft. Any variation from the expected arrival time may be indicative of a problem.

The compression wave is the primary concern for SET and is the fastest wave traveling 13,100 ft/s (4,000 m/s) in solid high quality concrete. The compression wave causes the material being tested to alternate compressional and tensile stresses by the wave (Blitz 1971). At the point of the hammer impact, a compression zone is produced which results in the formation of a compressional stress wave. The compressional wave travels down the shaft at a velocity (v_c) with a force (F). Shaft impedance (Z) is a ratio of v_c and F. It is also a function of the elastic modulus, E, cross-sectional area, A, and compression wave velocity (v_c) of the shaft (Finno & Prommer, 1994).

A change in the cross-sectional area of the drilled shaft and/or a change in the density of the medium (concrete) will cause a change in impedance. Part of the stress wave reflects back up the shaft whenever the wave encounters a change in impedance. The remainder of the stress wave continues on down the length of the shaft. A compression or negative wave is reflected back up the shaft whenever an increase in cross-section or density occurs. A tensile or positive wave is reflected back up the shaft with a reduction in cross-sectional area or concrete density. In the absence of changes in

impedance, the stress wave travels until it is reflected off the pile toe (Finno & Prommer, 1994).

Part of the impact energy is radiated into the soil (Paquet, 1968). Attenuation of the stress waves are continually occurring as they travel down the shaft as a function of the concrete quality, soil conditions surrounding the shaft, and the shaft cross-sectional area. Stress wave attenuation will be greater for shafts placed in stiff soil than for those placed in loose soil. In addition, wave attenuation will be less for shafts with larger cross-sectional areas than for those with smaller cross-sectional areas. “In general, scattering of the signal occurs due to changes in the material the wave is propagating through, especially at boundaries where there are abrupt changes in the impedance between two materials.” (Finno & Prommer, 1994)

The Dutch first used the Sonic Echo Test in the 1970’s as a means to provide quality control for driven precast concrete piles. The SET uses a compression wave generated at the surface and propagating down the shaft until it reflects off the toe of the shaft. As stated above, if the shaft contains irregularities in the concrete, such as cracks, a change in cross sectional area, or poor concrete quality, reflections will occur which indicate the presence of an irregularity. Discontinuities can be severe enough to prevent the stress wave from reaching the toe altogether (Finno & Prommer, 1994).

Test Equipment for the SET includes a hammer with a triggering device combined with a vertical geophone attached to a laptop or portable computer. Geophones

are low frequency transducers that can measure frequencies below 2 kHz. As an alternate, accelerometers may be used in lieu of the geophone. However, since the system measures arrival times, additional signal processing must be performed to convert to velocity or using wave speed of the “known” material, the location of reflective boundaries can be determined. The laptop typically contains a data acquisition card in combination with a signal conditioning unit.

In order to perform a SET, two areas on the top of the concrete shaft being tested are cleaned and ground to a smooth surface. Surface shall be free of loose debris and even. One area is cleaned close to the center of the shaft. This location is the impact point for the hammer. The second location shall be near the perimeter, but within the rebar cage. The geophone is fixed to the concrete surface with a coupling agent. Next, the shaft being tested is struck with the hammer at the area close to the center of the shaft. Once the hammer impacts the top of the shaft, the portable computer is triggered and records the response of the top of the shaft via the geophone or the accelerometer. Background noise can be eliminated by performing the test several times and comparing and averaging the results (Finno & Prommer, 1994).

The results of the SET indicating a sound shaft show compression wave reflection planes at the concrete-soil interface at the toe and the concrete-air interface at the top. Almost all of the energy is reflected back down the shaft for the top interface, while some of the energy is lost at the toe of soil to concrete interface. Defects in the shaft will also cause the waves to reflect. The waves will continue to reflect back and forth between the

reflection points until full attenuation has occurred. The depth of the reflector is determined by the following equation:

$$Z=V_b\Delta t/2$$

where z is the depth to the reflector, either a defect or the toe of the shaft, V_b is the longitudinal wave velocity in concrete, and Δt is the travel time of the reflected wave. A (2) is placed in the numerator of the equation since Δt is the time it takes for the compression wave to travel from the surface to the reflector and back to the surface. Since the velocity of the compression wave varies with concrete quality, it is preferable to determine V_b based on concrete samples that are representative of the in-situ concrete in the drilled shaft being tested. As a less accurate method it is reasonable to use the values indicated in Table 2.5. These values differ from source to source. Therefore, the values indicated are based on ultrasonic pulse velocity measurements represented by an infinite concrete medium as reported by Hearne et al. (1981). These values are reduced 5%, assuming a Poisson's ratio 0.2 for concrete since Hearne et al's experiments were based on an infinite concrete medium.

Table 2.5 - Compression wave velocity in concrete

Compression wave velocity, feet per second (meters per second)	General concrete quality
Above 14,200 (4,300)	Excellent
11,400 – 14,200 (3,500 – 4,300)	Good
9,500 – 11,400 (2,900 – 3,500)	Questionable
6,700 – 9,500 (2,000 – 2,900)	Poor
Below 6,700 (2,000)	Very Poor

Figure 2.5 shows the typical test set-up and sample test results from a SET test.

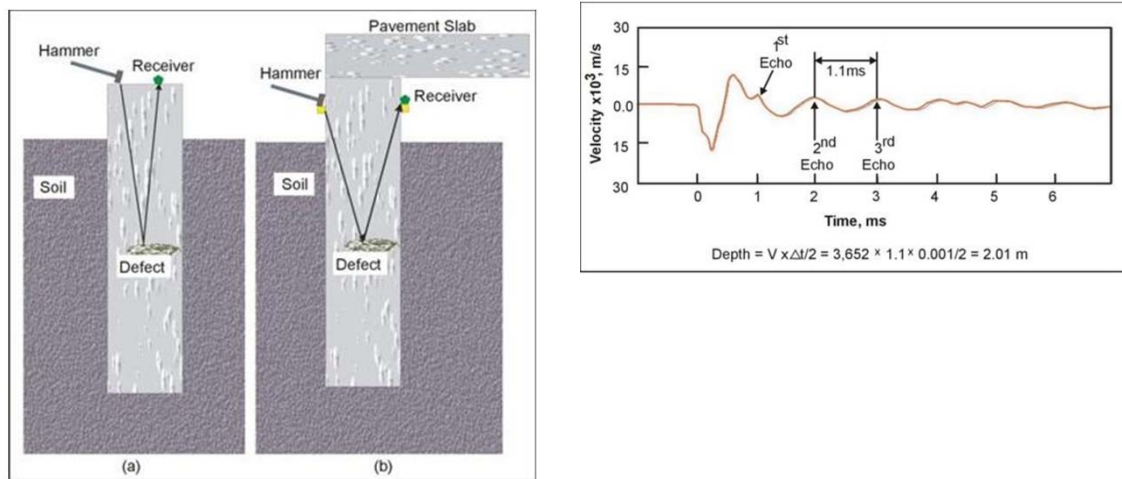


Figure 2.5 - Typical SET test set up / theory (left), sample of data (right) (FHWA, 2009)

According to a report published by the FHWA (Baker et al. 1993), concrete with a compressive strength of approximately 4,300 to 5,100 psi (30 to 35 N/mm²) has a V_c between 12,500 and 13,100 ft/s (Finno & Prommer, 1994).

In order to interpret a SET both the concrete quality and the shaft length must be known or assumed. Given these parameters, it will be easy to determine if a reflection in the signal is either the toe or an anomaly present in the shaft (Finno & Prommer, 1994).

Exponential amplification is used to progressively increase the amplitude of the reflected signal in a similar manner to its attenuation. This amplification process is required because the impact at the top of the shaft produces small strains relative to those required to mobilize the shaft capacity. However, it is important to verify that the reflection is being amplified and not just background noise (Finno & Prommer, 1994).

There is a limiting length / diameter (L/D) ratio beyond which all wave energy is dissipated and no toe response can be detected (Baker et al., 1993) The limiting L/D ratio varies depending on the dampening and signal loss into adjacent soils. With soft soil deposits such as silts, good results can be obtained for L/D ratios of 50:1 (Davis and Robertson, 1976). For stiff clays, this ratio is reduced to 30:1 (Hearne et al, 1981). In cases where the L/D ratio is exceeded, the only useful information that can be obtained from a SET test is the presence or absence of anomalies in the upper portion of the shaft (Finno & Prommer, 1994).

As with the CSL Test, several variations of the SET have been developed in which a receiver is embedded along the shaft or at the shaft toe. The additional points allow direct measurement of the compression wave arrival time and permit more accurate velocity calculations. This method also allows for shafts that exceed the L/D ratio to be tested with a higher level of confidence. However, this method drastically increases the cost of the SET since care must be given to the installation of the embedded receivers and the receivers are not able to be retrieved and used again. They become a permanent part of the shaft (Finno & Prommer, 1994).

The sonic echo test is only useful for determining the linear continuity of a shaft. Its limitations include but are not limited to (Finno & Prommer, 1994):

1. SET provides no quantifiable information about the shaft's cross-sectional area or behavior of the shaft under load.

2. Unless the test utilizes embedded receivers, only the uppermost defect can be readily detected. Any defects occurring below the initial defect may not receive adequate signal to return a reflection that will not be masked out by noise.
3. The hammer impact generates Rayleigh waves which propagate along the shaft surface and cause a noisy environment. This problem is especially troublesome in the top 10 feet of a shaft.
4. Defects located near the toe of the shaft can be difficult to identify since reflections from anomalies close to the toe may easily be misinterpreted as the toe and not an anomaly.
5. Since a reduction in concrete shaft cross sectional area, or necking, and poor concrete quality both produce reductions in impedance, it is not possible to determine them apart. In addition, a gradual decrease in cross sectional area may not generate a reflection at all.
6. A layer of stiff soil may cause reflections similar to those of increases in impedance, increasing the uncertainty of the shaft integrity.
7. An increase in cross sectional area will actually increase the shaft capacity and is generally not viewed as a problem. However, the reflection from the bulb will be similar to that of a defective shaft.

8. Utilizing higher frequency waves would improve the accuracy of the test.

However the wavelength used for the SET cannot decrease much less than the diameter of the shaft. If shorter wavelengths are used, the shaft will behave as an elastic medium where compression waves will occur from all shaft boundaries and not like a rod type structure.

9. In stiff soils, wave attenuation can be a problem. The more similarity between the toe bearing material and the concrete, the lower the amplitude toe reflection.

Therefore, shaft with end bearing in rock have very poor toe reflections.

10. Anomalies located below other anomalies may not be detectable.

It has been summarized in Finno & Prommer, 1994 that, “The method (SET) is best suited for checking precast and permanently cased piles due to the straight-sided shafts these structures provide. It is not as suitable for drilled shafts due to variations in cross-section that often exist causing multiple reflections.”

Several case studies of SET are discussed in (Finno & Prommer, 1994). They are summarized below as supporting documentation to the information contained here within:

1. SET tests were performed on 1.6 ft (0.5 m) diameter augur cast friction piles with lengths ranging from 20 to 59 ft (6 to 18m) and founded in stiff and very stiff clay

layers. As expected, the piles with a L/D ratio of 32:1 and 36:1 did not produce a toe reflection. Since the length of the piles were known, allowing for the determination of the compression wave velocity, it was also possible to determine that one pile had poor or questionable concrete quality. Specifically, the compression wave velocity in this pile was $V_c = 11,200$ ft/s (3,400 m/s). The remaining piles had V_c ranging from 11,500 to 13,100 ft/s.

2. As part of a FHWA test program for evaluating drilled shafts for bridge foundations, a test section was constructed at Texas A & M University with nine shafts. These shafts varied in length from 34 to 79 feet with 3 feet of stick-up above the ground level. All of the shafts were constructed with a 36 inch diameter cross section (L/D ratio from 11:1 to 26:1). The integrity tests performed on the piles included the Impulse Response, Sonic Logging, and Sonic Echo. In this study, several shafts were constructed with both planned and unplanned defects. In conclusion of this test, SET was able to determine some areas where defects occurred. However, the results also showed the limits of the sonic echo test and in one case, "...One could have been deceived into thinking that the reflection at 31 ft (9.4m) was the toe, if it was unknown that the shaft was 79 ft (24.1 m) long" (Briaud et al, 2002).

Clearly the SET method of integrity testing method can return some questionable results that may lead an engineer to falsely accept or deny the integrity of a test.

2.6 Impulse Response Test

Another method that is based on the measurement of compression wave reflections is the Impulse Response Test (IRT). This test is an extension of the vibration test, which was found to provide more information than the SET, particularly with the irregular profiles of drilled shafts. In the IRT the head of the shaft is impacted with a hammer that induces transient vibrations with frequencies as high as 2,000 Hz. The shafts response to these vibrations is measured in the time domain and the signal is digitally converted to the frequency domain for analysis (Finno & Prommer, 1994).

The equipment set up for IRT is similar to SET except the impact hammer has a load cell that measures the impact force with time. The hammer has the ability to generate transient vibrations up to 2,000 Hz. A vertical geophone is triggered upon hammer impact and records the vibrations at the shaft head. Both the hammer and the geophone are connected to a portable PC which is used for acquiring, analyzing and storing the data (Finno & Prommer, 1994).

The testing procedure for IRT is identical to the SET. However, it is critical that the hammer strikes the shaft head squarely to ensure proper force measurement (Finno & Prommer, 1994).

Unlike SET, IRT provides a determination of the homogeneity of concrete in the shaft and measure of the shaft's performance (Higgs and Robertson, 1979). IRT provides a stiffness value of the shaft which has a direct correlation to the shaft's performance. In

addition, the length of the shafts may be determined from the IRT (Finno & Prommer, 1994).

Analysis of the results obtained from an IRT includes performing Fast Fourier Transform (FFT) on the force and velocity signals to convert them from the time to frequency domain. Next, a plot of mobility versus frequency is obtained by dividing the velocity spectrum by the force spectrum. The length of the shaft is calculated by measuring the frequency change between resonant peaks (Finno & Prommer, 1994).

The low-strain dynamic stiffness (K') can be calculated and correlated to the static stiffness. At low frequencies, the lack of internal effects causes the shaft/soil system to behave as a spring. This behavior appears as a linear increase in amplitude of mobility from zero to the onset of resonance (Baer et al., 1993). The commonly accepted dynamic stiffness value (K) provides a good indication of the low-strain, soil-foundation interaction. For a rigid base, a high stiffness value will be calculated. For a compressible base, a low stiffness value will be calculated. By comparing stiffness values for similar sized shafts, it can be determined which ones should be considered questionable. Shafts founded in loose soil and shafts that have soil inclusions, necks, and breaks will have lower stiffness values than sound shafts founded in solid soils (Finno & Prommer, 1994).

An evaluation of the shaft performance is made by calculating the K_{\min} and K_{\max} or the theoretical limiting values for dynamic stiffness and comparing them with the actual stiffness value. In addition, the IRT provides a calculation of the theoretical mass

of the shaft which can be checked against field logs for a cross check on the amount of concrete used in the shaft (Finno & Prommer, 1994).

It is easier to determine if a bulb or a neck has occurred with IRT than with SET. Stiffness values are lower than normal for necked shafts and higher than normal for shafts with bulbs. In all, this method proves to be better for testing the integrity of drilled shafts than SET with some of the same limitations such as:

1. This is a surface reflection method that relies on measuring reflected responses.
2. There is a limiting L/D ratio based on the soil conditions.
3. As the L/D ratio is approached, the curve will flatten out to where resonant peaks are not discernible.
4. This method is subject to the problems associated with surface waves and there is a limit on the size of defects that can be detected.
5. Only the top defect in a shaft can be detected, even if multiple defects exist.
6. In order to interpret the results from a test either the concrete compression wave velocity or the shaft length must be known.

2.7 Gamma-Gamma Testing (GGT) or Gamma Density Logging (GDL) or Gamma-Gamma Logging (GGL)

Gamma-Gamma Testing (GGT) is an integrity testing method that is widely used and accepted by the California Department of Transportation (Caltrans). It should be noted that this testing method is also referred to as Gamma Density Logging (GDL) or Gamma-Gamma Logging (GGL). In GGT testing, a source of ionizing radiation (typically Cesium 137) and a Sodium Iodide crystal-photomultiplier detector are lowered down an access tube similar to CSL. The probe that emits the radiation also contains but is separated by a shield from a gamma-ray detector. The basic theory behind GGT is that the number of gamma-ray photons per unit of time that are reflected from the nuclei of the molecule of the material surrounding the tube, and return at a given energy level to the detector is related to the density of the material surrounding the tube. The remaining electrons either lose their energy or change direction in a manner called Compton scattering. The number of these interactions is directly related to the number of electrons in the surrounding material (Rucker & Verquer). In short, GGT can detect significant reductions in localized density of the shaft concrete which would be indicative of a void or imperfection in the shaft (O'Neill & Reese 1999). GGT has an advantage over CSL in that it can detect reductions in concrete density outside of the reinforcement cage.

The access tubes for GGT should be made of a material such as PVC that will allow the photons to pass through and reflect back through the wall of the tube. Steel will cause a reduction zone for the GGT in that photons will be scattered at a greater rate by the dense steel tube as compared to the lower density of the PVC. In general GGT will

not detect changes in density of the concrete outside of about a 3 to 4 1/2 inch radius from center of access tube when PVC is used and as stated, this detection zone is diminished when steel access tubes are used. In order to accurately determine the density of the entire shaft, access tubes would need to be placed at 8 inches (200 mm) on center. Since this is not possible, an engineer must be content with having intermittent sampling of the concrete density around the perimeter of the cage (O'Neill & Reese 1999). Caltrans recommends that one access tube be used per foot of pile diameter (Lew et al 2002). This leaves a tube spacing of about 2.75 feet around the circumference of the cage.

It is further recommended that the access tubes be placed at least 3 inches (76 mm) away from any vertical reinforcement. Since the vertical steel reinforcement is about 3 times denser than concrete, having the reinforcement too close the access tubes or varying the distance between the tubes and the reinforcement will cause false readings in the bulk density readings. Furthermore, if the access tubes around the perimeter of the cage are not placed so that they have the same influence from the reinforcement, different tubes within the shaft cannot be compared (Speer, 1997).

Due to the length of the gamma-gamma probe, vertical alignment of the access tubes must be maintained so that a 2 foot (0.6 m) long by 1.9 inch (48 mm) diameter rigid cylinder, called a dummy probe, be allowed to pass from the top to bottom of the tube (Speer, 1997). Since radiation sources are subject to Nuclear Regulatory Commission (NCR) regulations which require special training and licensing for the handling and

transporting of the device, abandoning a lodged device and grouting it in place is not an option. During one well documented GGT, the ion transmitting probe was wedged in the inspection tube. It took two weeks to remove the probe using special drilling and finishing tools (Lew et al 2002). Access tubes that do not allow the dummy probe to pass must be core drilled to gain the necessary vertical alignment (Speer, 1997). In addition, the process can be time consuming compared to other testing methods. A typical 7 foot (2.1 m) diameter shaft with seven inspection tubes that is 60 feet (18 m) long will take eight hours to test.

The standard GGT has a 1.87 inch (47 mm) diameter gamma-gamma probe with either a 10 or 100 millicurie Cs 137 source. The probe is lowered down the access tube with a cable. The probes are configured for the determination of density by backscatter. This method allows for the use of less powerful radioactive source. Radiation is emitted from the source at the bottom of the probe. The radiation is simultaneously absorbed and scattered by the concrete and reinforcement surrounding the inspection tube. The receiver at the top of the tube counts the reflected gamma rays over a time interval. More gamma rays are counted in less dense material than in dense material (Speer, 1997).

GGT data is processed by first plotting the gamma count rate versus time. Next, this data is compared to all of the data for shafts in the same vicinity, using the same probe. The data sets are reviewed and data that is insignificant and redundant is discarded. The mean, mean minus two standard deviations and the mean minus three

standard deviations are plotted on the same graph. Figure 2.6 shows the result of GGT that shows the effect of a necking defect (Speer, 1997).

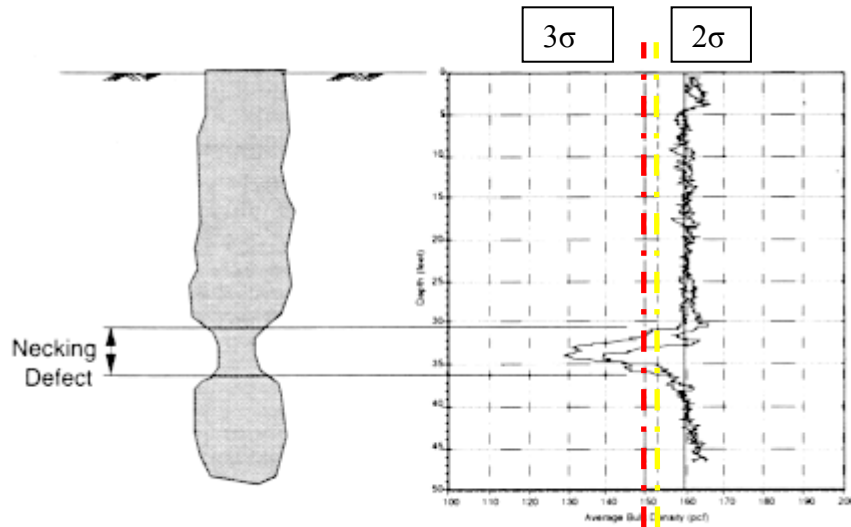


Figure 2.6 - GGT indicating necking of a drilled shaft

Caltrans is typically considered to be the leading department of transportation in the development of testing methods and specifications related to GGT or in Caltrans case, GGL.

Interpretation of the test results rely equally on experience, engineering judgment, and statistical analysis (Speer, 1997). In any shaft, there is normally some variation in the density of normal concrete from different points in the shaft. In general, if the bulk density of the concrete appears to drop below the mean minus three standard deviations line, these values are typically associated with an anomaly (O'Neill & Reese, 1999, Caltrans, 2006). A standard statistical distribution curve showing the divisions of the standard deviations is shown in Figure 2.7. There are several shortcomings associated with this approach:

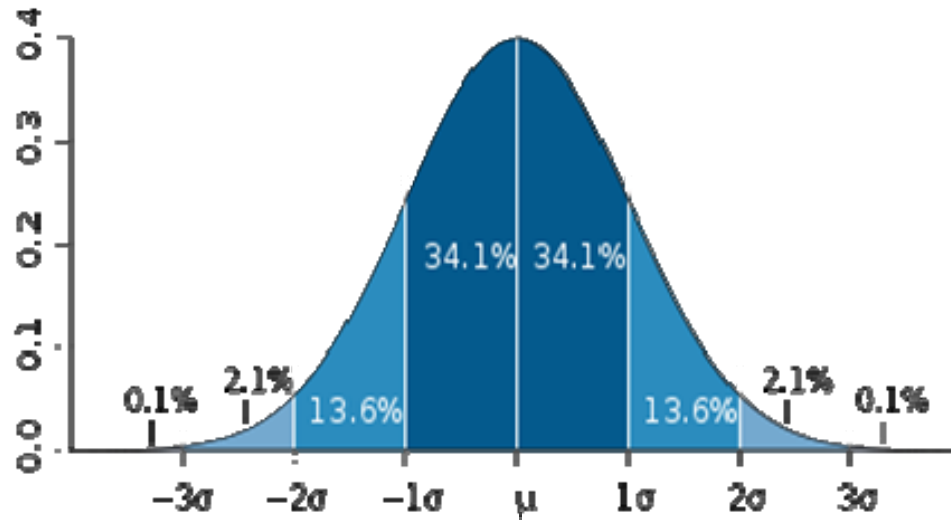


Figure 2.7 - Statistical distribution “bell” curve used for interoperation of gamma-gamma data

1. By basing the decision on whether an anomaly exists on statistical data, the presence of a large void may skew these results. The presence of the void will cause the statistical mean and the standard deviation to be altered. Caltrans and others attempt to correct for this shortcoming by utilizing 55 gallon drums filled with concrete of known density. These drums are then utilized to calibrate between the interpreted concrete density and the recorded data (Caltrans, 2006). Again though, variations of reinforcement steel placement from the access tubes may provide improper results.

2. Due to the limited cross sectional area of a drilled shaft that is actually covered by a GGT, extreme bulges, or inclusions on the center of the shaft may be missed. Specifically, only about 15% of coverage is provided on a 36 inch diameter shaft. This number drops to about 5% on a 10 foot diameter shaft.

3. As with most, if not all of the integrity testing methods, it is difficult, if not impossible, to determine the exact nature and full extent of potential anomalies without extracting the shaft.

Figure 2.8 shows a sample of the equipment and test results from a GGL test. As the data is often reviewed on the basis of statistics, it is possible for an entire tube to be surrounded by poor concrete and still be within the range of the statistical norm. The data shown are side by side plots from the shaft tubes shown. One could assume an average for the first tube and visually assess the quality of the concrete that is assumed to be good. The limits established by Caltrans are essential for proper evaluation.

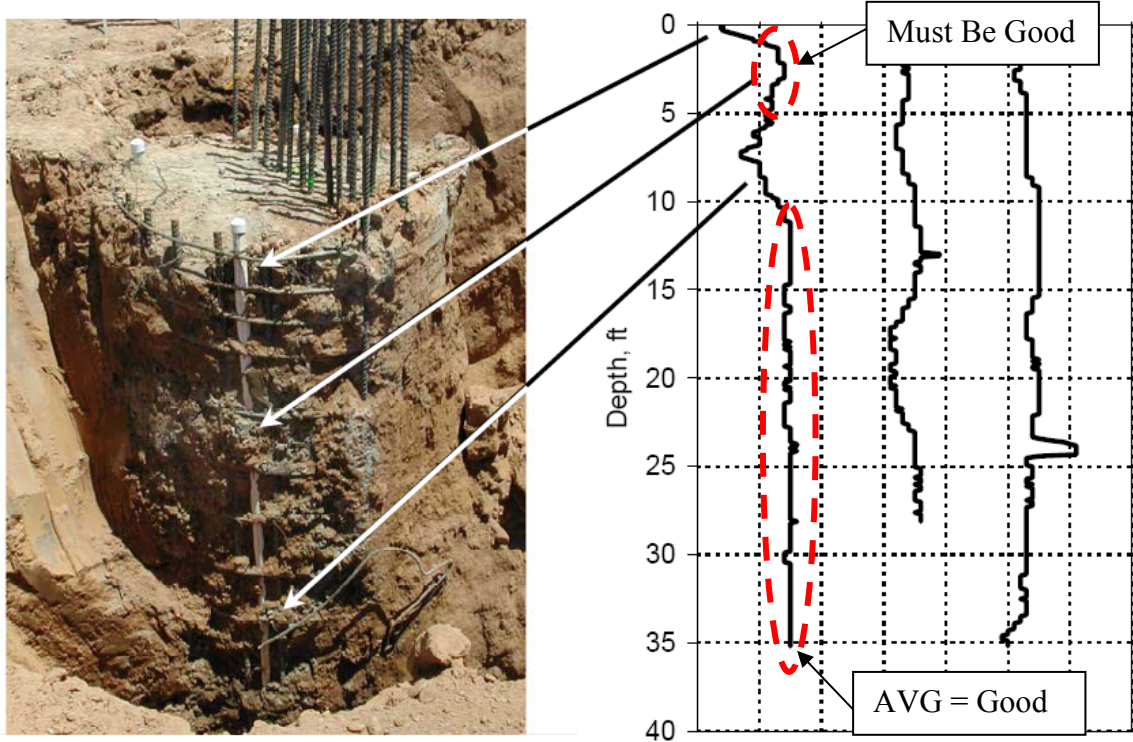


Figure 2.8 - GGT Testing Equipment and Sample Test Results, equipment (top), sample GGT test showing anomaly in shaft (bottom), (Rucker & Verquer)

2.8 Concreteoscopy

Concreteoscopy is a relatively new testing method that allows the integrity of the shaft to be checked real time. In this testing method, clear, ½ inch diameter (12.7 mm) clear plastic tubes are attached to the rebar cage. As the concrete is placed, a miniature television camera on a fiber-optic cable is used to view the concrete from within the tubes. This test is similar to the GGT except that the results provide visual confirmation as to the soundness of the concrete instead of relying on density monitoring. As with GGT, Concreteoscopy is able to view only the material directly adjacent to the access tubes (O'Neill & Reese 1999).

2.9 Parallel Seismic Integrity Testing

Parallel Seismic Integrity Testing was developed in France in the 1970's to evaluate the conditions of piles and drilled shafts under existing structures (Davis and Hertlein, 1993). Clearly, if Parallel Seismic Integrity Testing can be utilized to determine the length and soundness of a drilled shaft, it can be used to determine the state of a freshly placed drilled shaft.

The general procedure for the Parallel Seismic Integrity Test (PSIT) is that after the shaft construction is complete, a bore hole is drilled adjacent to and slightly deeper than the shaft being tested. Stress wave energy is generated on the surface of the structure by impacting it with a hammer and the arrival time of the compression wave is monitored

in the bore hole by means of a transducer known as a hydrophone. The tests are typically completed in increments of approximately 20 inches (50 cm) (Stain, 1987). A profile of signals is built up for the entire length of the shaft. Under good conditions, transmission distances up to 130 ft (40 m) are possible (Davis and Hertlein, 1993).

As in the CSL test, the access tubes are filled with water. As discussed in earlier testing methods, the stress waves generated on the surface due to the impact have a velocity that is directly proportional to the density of the medium in which they are propagating. Therefore, the arrival times of the stress waves are proportional to the depth of the hydrophone. A difference in the rate of the arrival time velocity with respect to depth indicates a change in the medium or the base of the shaft being tested (Finno & Prommer, 1994).

The test equipment required for a PSIT includes an impulse hammer, a hydrophone receiver, and a data acquisition system that allows high speed sampling of the hydrophone. In a typical arrangement, the data acquisition system is triggered when the impulse hammer strikes the pile or the shaft. The hydrophone then records the arrival of the generated stress waves. The hydrophone receiver must be capable of withstanding the hydrostatic pressure generated due to the head of the water column above. This pressure can exceed 43 psi (196 kPa) at depth (Finno & Prommer, 1994). The data is collected by the acquisitions system, which typically consists of a data acquisition card in a portable computer, and may be analyzed on site.

The borehole should be made in the ground adjacent to the foundation being tested and slightly deeper. To assure the correctness of the test, the boreholes must be parallel to and within 3 feet of the shaft wall. If the shortest distance between the shaft and the borehole is not relatively constant, variations in arrival time will occur leading to false readings. In addition, if the borehole is greater than three feet from the shaft wall, the signal will be affected due to attenuation and the non-homogeneity of the different soil layers. Since compression waves are able to travel through fluids, water is added to the tubes to act as a coupling medium for the hydrophone receiver (Finno & Prommer, 1994).

This method of testing can also be accomplished by coring a hole in the suspect structure, filling with water, and performing the test as outlined above. This test method is referred to as the downhole seismic method. The arrival of the compression wave is critically refracted along the core hole wall at the propagation wave velocity of concrete (Davis and Hertlein, 1993).

The test results and integrity are dependent on the ability to measure the direct arrival time of stress waves. An anomaly in a drilled shaft will appear as an increase in the arrival time of the wave at the depth in which the anomaly occurs. A test result for a continuous shaft without defects should contain a linear increase in arrival time with depth. The toe of the shaft will also cause an increase in the wave arrival time, giving a clear indication of the location of the shaft toe. (Finno & Prommer, 1994).

The downhole seismic test records a second wave in addition to the compression wave. This second wave is known as the tube, hydro, or Stoneley wave. The tube wave velocity is a function of tube diameter, roughness and the permeability of the material surrounding the hole. The velocity of the tube wave is approximately 5,000 ft/s (1,500 m/s) in cored concrete and its amplitude is much greater than that of the concrete compression wave (Davis and Hertlein, 1993).

Tube waves are reflected from the ends of the core hole. They are refracted at locations where the bulk elastic modulus of concrete and the diameter of the core hole change. The shape and the spectral content of the tube waves have a higher frequency and a shorter duration than the first direct waves. Vertical receivers are generally used for recording Tube waves (Galperin, 1985). Little has been studied about obtaining information from the tube wave, which theoretically should be able to yield information on the concrete quality (Finno & Prommer, 1994).

All that can be determined from reviewing the results from either a parallel seismic or downhole test is that arrival time of the compression wave or tube wave has increased as a result of lower wave propagation velocity. These changes can be caused by several factors including changes in concrete quality, cracks, soil inclusions and the toe of the shaft. Therefore, it is difficult to determine the type of defect, if any exists, that has caused the change in the slope of the arrival time line. This may lead to inconclusive results. Another major disadvantage of the tests is the cost of coring and installing the access hole (Finno & Prommer, 1994).

In review of a case study as reported by (Finno & Prommer, 1994), two test piles were constructed at a research site in France by the CEBTP (Centre Expérimental d'Études du Bâtiment et des Traveux Publics). They were both 46 ft (14 m) long and 26 inches (65 cm) in diameter. One was continuous and the other had a break at 24.6 ft (7.5 m). Access tubes were installed adjacent to the shafts to a depth of 66 ft (20 m) to facilitate parallel seismic testing. The sound shaft had a signal transmission time that increased linearly with depth down to the toe, proving continuity over the full length. The broken pile was linear down to 24.6 ft (7.5 m), but the arrival time increased significantly below this point. For this shaft, it was known that the pile extended to 46 ft and had a break at 24.6 ft, but the test was unable to differentiate whether the break was in fact a defect or whether it was the pile toe (Stain, 1982).

2.10 Conclusion

When combining proper geotechnical monitoring and observation of the shaft installation with an integrity method, confirmation of the adequacy of a deep foundation system can be estimated (Lew et al., 2002). However, each of the aforementioned testing methods contains an unacceptable level of uncertainty in their results. In order to truly be effective, a new form of testing should be developed that allows for determination of the presence of anomalies as soon as possible after the concrete is placed in the shaft. This thesis focuses on the feasibility of a new methodology that uses the hydration energy of curing concrete to assess the presence or absence of intact concrete.

Chapter 3 - History of the Basic Theories of Deep Thermal Infrared Instrumentation

3.1 Introduction

Circa 1970 – 1980 researchers at the University of South Florida, Department of Civil and Environmental Engineering, Tampa, FL, proposed the idea of measuring the soil temperature adjacent to a drilled shaft to determine the integrity of the shafts. The theory was that temperature probes could be inserted adjacent to a newly placed drilled shaft to determine the effect of the cement heat of hydration on the surrounding soil. A variation in the temperature in the surrounding soil may be evidence of a section of the shaft that is not uniform and therefore producing a variation in the thermal trace. This initial theory was shelved because it was determined that it is not feasible to insert a thermal probe on the exterior and in the vicinity of a drilled shaft, mostly due to the drilled shafts being socketed into rock or other impenetrable bearing material.

Circa 1990 inclinometer casing started to be installed in the cross section of the drilled shaft and by about 1996 cross-hole sonic logging started to become not only recognized, but the standard for drilled shaft integrity testing. The advent and acceptance of CSL led researchers at USF to revamp earlier theories of and start investigations into the viability of using thermal measurements from within the boundaries of the drilled shaft as a determination of shaft integrity.

Circa 2000, Kranc, Mullins, the author and other research fellows started extensive studies on the heat of hydration of concrete, thermal transmission into various soils, mathematical modeling of the thermal image of a drilled shaft and the development of instrumentation to measure temperature of a drilled shaft foundation (Mullins and Kranc, 2004).

3.2 Thermal Integrity Profiling Instrumentation

After the development of the concept of testing the integrity of drilled shafts using thermal imaging, the focus turned to developing reliable instrumentation that could be used to measure and record the temperature of the shafts. It was determined that the instrumentation and testing methods should utilize existing technologies and testing procedures as much as possible. In this chapter, some of the basic theories utilized in Thermal Integrity Profiling are discussed along with the inherent complications in later chapters. Further, a look at some of the different instrument configurations and trial tests associated with each is presented.

3.3 Temperature Measurement

There are only four fundamental quantities in the International Measuring System: Length, Time, Mass and Temperature. Of these quantities, temperature is the only one that is not additive. For example, if two objects are combined that have the same length and mass, these quantities will double. Similarly, if two time intervals are combined, the

resulting time interval will be the sum of the two original times. However, if two objects that have the same temperature are combined, the resulting temperature will remain the same (Doebelin, 2004).

Statistical mechanics relates temperature to the mean kinetic energies of molecules. This molecular kinetic energy which is dependent on mass, length and time for their description are currently not measurable, resulting in the need for an independent temperature standard (Doebelin, 2004).

The zeroth law of thermodynamics states: For two bodies in contact to be said to have the same temperature, they must be in thermal equilibrium; that is, when thermal communication is possible between them, no change in the thermodynamic coordinates of either occurs. When two bodies are each in thermal equilibrium with a third body, they are in thermal equilibrium with each other and all bodies are the same temperature. This provides the ability to calibrate a thermometer or other temperature reading device to a standard and then use it to determine unknown temperatures (Doebelin, 2004).

The problem of repeating a fixed temperature for the purposes of calibration is difficult at best. Ordinarily, the triple point of water which is defined as the state at which solid, liquid and vapor phases are present is considered the most reproducible state known. The number assigned to this point is 273.16 K, making the difference between the ice point and the steam point of water equal to 100K (Doebelin, 2004).

The Thermodynamic Temperature Scale proposed by Lord Kelvin in 1848 provides a theoretical base for a temperature scale independent of any material property based on the Carnot Cycle. The Carnot Cycle assumes an ability to perfectly transfer heat without a loss of energy. Since it is not possible to transfer heat without a loss of energy, the Kelvin Thermodynamic Temperature Scale remains theoretical only.

The International Practical Temperature Scale (IPTS) conforms closely to the thermodynamic scale. This scale uses the triple point of water along with five other primary fixed points: The boiling point of liquid oxygen (-182.962°C); the boiling point of water (100 °C); and the freezing points of zinc (419.58 °C), silver (961.93 °C) and gold (1064.43 °C). Additionally, other secondary points are established with the highest being the boiling point of gold (1064.43 °C) and the lowest being the triple point of hydrogen (-259.34 °C). The IPTS also establishes different instruments, equations and procedures to be used to interpolate between the fixed points, the idea being that no one equation, instrument or procedure will be applicable over the entire range (Doebelin, 2004).

Considering that 273.16 is the triple point of pure water at one atmosphere of pressure, calibration of instrumentation using this reference is difficult for the following reasons:

- ✧ Changing of pressure due to elevation and / or changes in weather patterns will change the triple point.

✧ Any impurities in the water will change the triple point.

✧ Temperature variations may exist across the calibrating medium.

There are currently many different instruments employed to measure temperature.

These include but are not limited to:

✧ *Bimetallic Thermometers* – Bimetallic thermometers are constructed by bonding together two different metals, each with a different thermal expansion coefficient. As the metals expand or contract differently, the differing change in length causes a deflection of the combined material.

✧ *Liquid-in-Glass Thermometers* – These thermometers use a liquid, typically mercury, in combination with a gas sealed inside of a glass tube. As the liquid is heated, it expands, compressing the gas. A scale is typically placed in the glass tube to allow the height of the liquid column to be measured.

✧ *Pressure Thermometers* – Pressure thermometers utilize a bulb that is sensitive to pressure and a capillary tube that is connected to a pressure measuring device. The bulb and the tube are filled with either a liquid or a gas and the temperature is measured by either the compressibility of the liquid or the pressure change of the gas.

- ✧ *Electrical Resistance Sensors* – Electrical resistance thermometers rely on the fact that for certain materials, the electrical resistance changes in a reproducible manner in relation to the material's temperature. These materials are configured into an electrical resistor and then incorporated into one of several different electrical circuit configurations that record the change in the voltage as a result of the change in the temperature of the resistor.

- ✧ *Junction Semiconductor Sensors* – Diodes and transistors exhibit temperature sensitivities. These temperature sensitivities are reproducible, linear and maintain good sensitivity within a given range (-55 to +200 °C).

A few additional methods of recording temperature that deserve additional attention and consideration will now be discussed:

3.4 Temperature - Thermocouple

At first, several different ideas were discussed regarding the measurement of the temperature of a drilled shaft. The standard and most widely used method for measuring temperature is to utilize a thermocouple.

In 1821 T. J. Seebeck discovered the thermoelectric effect. The thermoelectric effect occurs when two lengths of dissimilar metal wires (such as Iron and Constantan) are connected at both ends to form a complete electric circuit and one junction of the two

wires is at a different temperature than the other junction and an electromagnetic field (emf) forms. The developed emf (actually a small millivoltage) is dependent upon two conditions:

1. The difference in temperature between the hot junction and the cold junction.

Note that any change in either junction temperature can affect the emf value.

2. The metallurgical composition of the two wires (OMEGA-1).



A thermocouple is usually thought of as two wires joined at one end and open on the other. However, this is not a true thermocouple unless the other ends of the wires are also connected. As we will discuss later, it is important to remember “‘Where there is a hot junction there is always a cold or reference junction’ (even though it may seem hidden inside an instrument 1,000 feet away from the hot junction)” (OMEGA-3).

The net emf of a thermocouple circuit is the combined effects of the Peltier effect and the Thomson effect. In 1834, Jean Peltier discovered that there is an emf produced solely from the contact of the two dissimilar wires. Later in 1851, William Thomson, a.k.a. Lord Kelvin, discovered that an emf is produced by a temperature gradient along a metal conductor. Given that there are two points of contact and two different metals or alloys in a thermocouple circuit, there are two Peltier and Thomson effects in any thermocouple circuit (OMEGA-3).

Given that the net emf is primarily a function of the temperature difference between the two junctions and the kinds of materials used, if the temperature of the cold junction is compensated for or maintained constant, the net change in the emf will be a function of the hot junction temperature. This change in the emf can be measured by a potentiometer connected to the circuit. However, it is typically not practical to maintain a constant temperature at the cold junction (OMEGA-3).

There are many different types of thermocouples. Each type has a different combination of metals and corresponding unique properties and useable range. Table 3.1 describes properties of some of the most commonly used thermocouple types. Within the tolerance columns, T represents the temperature of the hot junction, in degrees Celsius. For example, a thermocouple with a tolerance of $\pm 0.0025 \times T$ would have a tolerance of ± 2.5 °C at 1000 °C (Omega-5).

Table 3.1 - Thermocouple types and temperature ranges (Omega-5)

ANSI Code	Alloy Combination		Thermocouple Color Coding		Maximum Temperature Useful Range	EMF (mV) Over Max. Temperature Range	Limits of Error** (Whichever is Greater)	
	+Lead	-Lead	Thermocouple Grade	Extension Grade			Standard	Special
J	±IRON Fe (magnetic)	CONSTANTAN COPPER-NICKEL Cu-Ni			0 to 750°C (32 to 1382°F) Therm. Grade 0 to 200°C (32 to 392°F) Ext. Grade	-8.095 to 69.553	0 to 750°C (32 to 1382°F)	2.2° C or 0.75% 1.1° C or 0.4%
K	CHROME-GA NICKEL-CHROMIUM Ni-Cr	ALOMEGA NICKEL-ALUMINIUM Ni-Al (magnetic)			-200 to 1250°C (-328 to 2282°F) Therm. Grade 0 to 200°C (32 to 392°F) Ext. Grade	-6.458 to 54.886	-200 to 1250°C (-328 to 2282°F)	2.2°C or 0.75% Above 0°C 2.2°C or 2.0% Below 0°C 1.1°C or 0.4%
V*	COPPER Cu	CONSTANTAN COPPER-NICKEL Cu-Ni	NONE ESTABLISHED	NONE ESTABLISHED	0 to 80°C (32 to 176°F) Ext. Grade			
T	COPPER Cu	CONSTANTAN COPPER-NICKEL Cu-Ni			-200 to 350°C (-328 to 662°F) Therm. Grade -60 to 100°C (-76 to 212°F) Ext. Grade	-6.528 to 20.872	-200 to 350°C (-328 to 662°F)	1.0°C or 0.75% Above 0°C 1.0°C or 1.5% Below 0°C 0.5°C or 0.4%
E	CHROME-GA NICKEL-CHROMIUM Ni-Cr	CONSTANTAN COPPER-NICKEL Cu-Ni			-200 to 900°C (-328 to 1652°F) Therm. Grade 0 to 200°C (32 to 392°F) Ext. Grade	-9.835 to 76.373	-200 to 900°C (-328 to 1652°F)	1.7°C or 0.5% Above 0°C 1.7°C or 1.0% Below 0°C 1.0°C or 0.4%
N	OMEGA-P NICROSIL Ni-Cr-Si	OMEGA-N NISIL Ni-Si-Mg			-270 to 1300°C (-450 to 2372°F) Therm. Grade 0 to 200°C (32 to 392°F) Ext. Grade	-4.345 to 47.513		2.2°C or 0.75% Above 0°C 2.2°C or 2.0% Below 0°C 1.1°C or 0.4%
R	PLATINUM 13% RHODIUM Pt-13% Rh	PLATINUM PT	NONE ESTABLISHED		0 to 1450°C (32 to 2642°F) Therm. Grade 0 to 150°C (32 to 300°F) Ext. Grade	-0.226 to 21.101	0 to 1450°C (32 to 2642°F)	1.5°C or 0.25% 0.6°C or 0.1%
S	PLATINUM 10% RHODIUM Pt-10% Rh	PLATINUM PT	NONE ESTABLISHED		0 to 1450°C (32 to 2642°F) Therm. Grade 0 to 150°C (32 to 300°F) Ext. Grade	-0.236 to 18.693	0 to 1450°C (32 to 2642°F)	1.5°C or 0.25% 0.6°C or 0.1%

After due consideration, it was decided that permanently embedding thermocouples into a drilled shaft was not practical for several reasons. First, the delicate nature of thermocouples and the thermocouple wiring is not conducive to drilled shaft construction. Consider, for example, that it is impossible to replace a malfunctioning thermocouple after the shaft has been constructed. Second, the cost associated with using sacrificial thermocouples was prohibitive.

3.5 Temperature – Radiation (Infrared)

For the purposes of measuring the temperature of a drilled shaft, radiation or infrared measuring methods were investigated. It was determined that the infrared methods offered several distinct advantages over the other temperature measuring methods. Specifically, these methods do not require that the instrument be in direct physical contact with the surface and is commonly utilized in production applications to scan the surface of an object. Currently utilized applications for infrared technology include, manufacturing quality control, night vision, missile guidance and infrared spectroscopy (Doebelin, 2004). Additionally, an advantage of the infrared thermocouple is that it could be configured to utilize the same access tubes as CSL testing, thereby meeting one of the stated goals of utilizing existing technology as much as possible.

A historical perspective on the theories of infrared temperature measurement should begin with the scientists that made the original contributions. First, Galileo Galilei (1564 – 1642) invented the thermometer in Italy. This was about 100 years before

Sir Isaac Newton (1642 – 1727) discovered that by passing white light through a prism, it could be divided into a range of colors. In Newton's 1704 publication, *Opticks*, he showed that the least bent portion of the white light was red followed in order by orange, yellow, green, blue, indigo and finally violet (OMEGA-H2).

In 1800, scientist and astronomer Fredrick William Herschel (1738-1822) while experimenting with sunlight discovered that different colored eye glasses produced a different heat sensation. Accordingly, as shown in Figure 3.1, Herschel devised an experiment in which he utilized a prism to divide sunlight into the distinctive color regions. He then used a thermometer to measure the surface temperature of each of the distinctive color regions. What he found was that the temperature rose as he advanced from the violet to the red region. Then wanting to know the dissipation of the temperature past the red region, he placed a thermometer just beyond the red region. What he found surprised him in that the temperature beyond the red region was actually higher. This region "below the red" was referred to as the infrared region. It was not understood until some half century later that infrared radiation had all of the properties of light waves except they did not affect the retina in the eye in a way to produce light (OMEGA-H2).

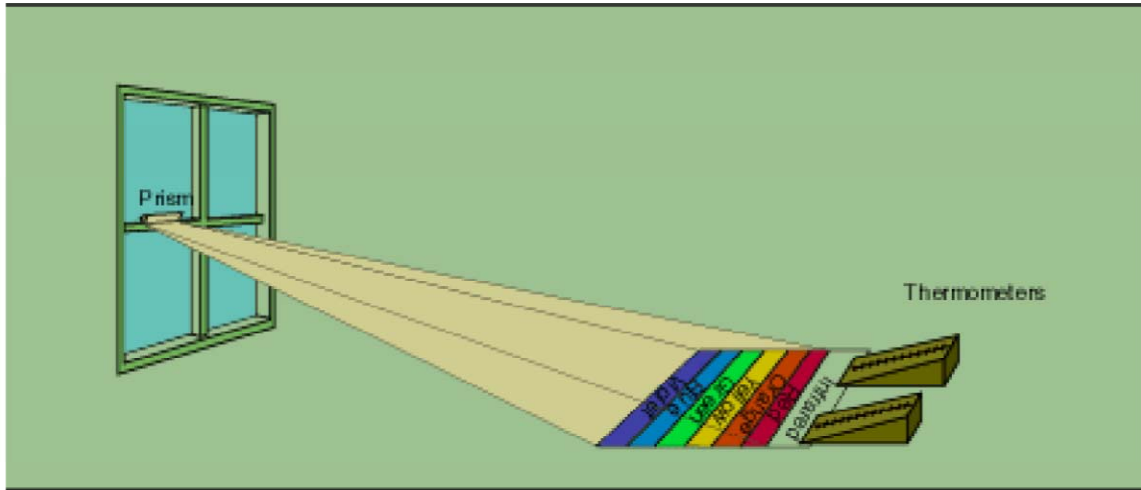


Figure 3.1 - Herschel's infrared discovery (OMEGA-H2)

In fact, visible infrared temperature measurement has unknowingly been used for thousands of years. Craftsmen have long used the color of heated metal or glass as a way to determine if the material is the correct temperature to “work” (OMEGA-H1).

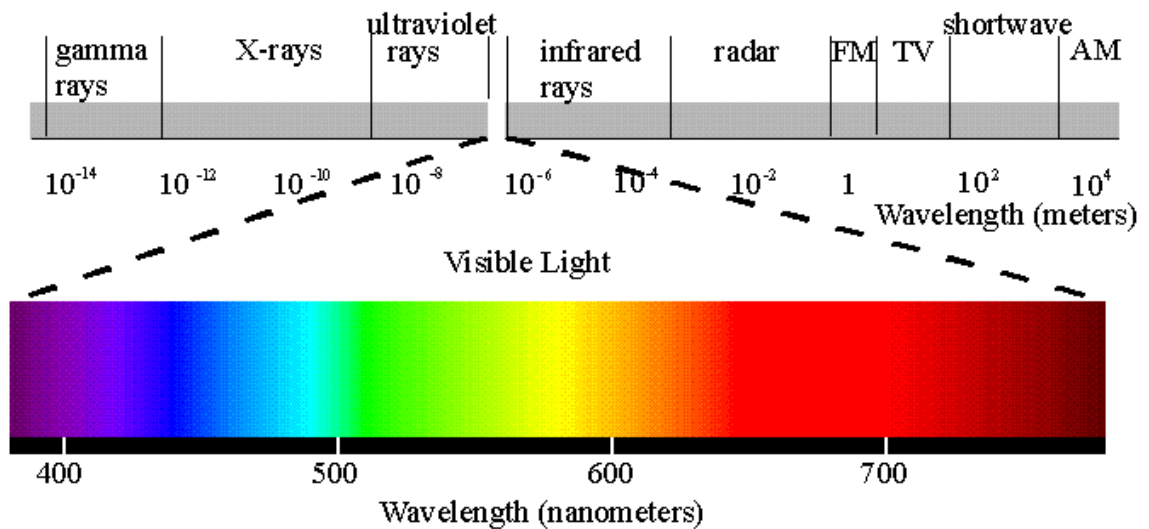


Figure 3.2 - Wavelengths and infrared rays (Suite 101)

Infrared thermocouples operate in a similar fashion as a standard thermocouple; however, they do not require contact with the surface to measure the temperature. Therefore, the idea was developed to utilize infrared thermocouples inside of access tubes similar to those used in Cross-hole Sonic Logging (CSL).

The past several decades have seen a tremendous development in small infrared thermocouples. Many of the developments have been necessitated by the various applications in which infrared thermocouples are currently being utilized. Although from the exterior, current infrared thermocouples may seem simplistic, they are actually quite sophisticated and include a complex optical system and electronic circuitry (OMEGA-2).

The specific design of most infrared thermocouples is proprietary; however, the basic concept is that they utilize a lens or a set of lenses to focus the infrared signal from the target area onto a thermopile. A thermopile is a group of several thermocouples typically connected in series, which generate an emf relative to their temperature. In fact, given the correct configuration, the infrared thermocouple will develop enough emf to be connected directly to conventional thermocouple measuring and recording systems. (OMEGA-2).

Infrared thermocouples utilize the incoming infrared radiation to produce a millivolt output signal. The signal which is produced through thermoelectric effects follows the rules of radiation thermal physics and its output is similar to the curve shown in Figure 3.3. As shown in part two of the figure, it can be shown that over a narrow temperature range, the output curve is sufficiently linear to be considered a millivolt

output range matched to the millivolt output of a given thermocouple. The instrument, once properly selected and calibrated, will produce a smooth curve over the operating range with about a 1% error (OMEGA-2).

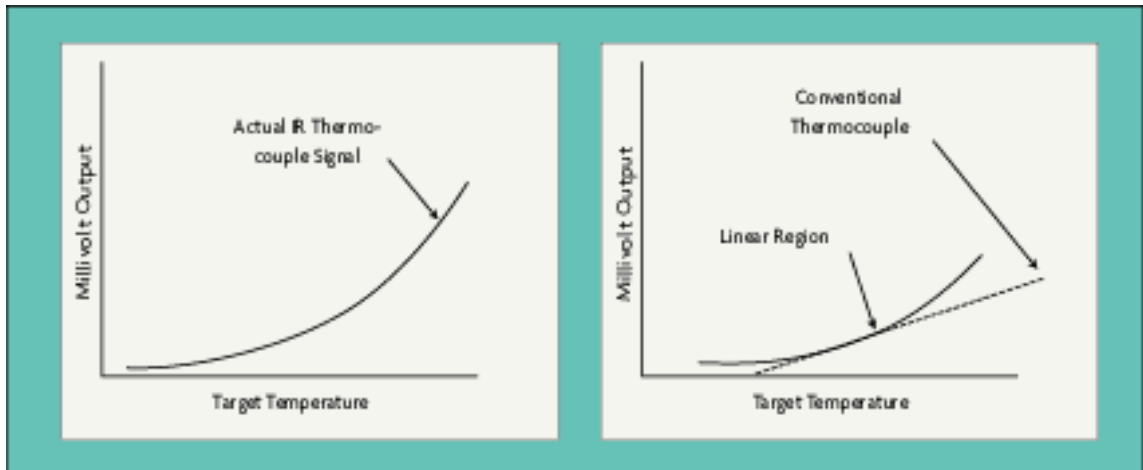


Figure 3.3 - IR thermocouple signal (OMEGA-2)

Modern infrared thermocouples are solid, hermetically-sealed and fully potted. This is done to allow the instrument to be used in severe use environments without causing either a mechanical or metallurgical change in the instrument. In contrast to traditional thermocouples, modern infrared thermocouples are well protected inside of a stainless steel body. Due to their construction, modern infrared thermocouples do not experience the drift problems associated with conventional thermocouples.

Based on the aforementioned benefits, infrared was chosen as the primary means of measuring temperature with verification by embedding sacrificial thermocouples into the concrete.

Chapter 4 - Basic Instrumentation and Lab Scale Tests

4.1 Introduction

After thoroughly investigating the state of current drilled shaft integrity testing techniques and the modern state of temperature measurement, focus was redirected towards how to develop an instrumentation system which would be rugged enough to be used on construction sites and as much as possible, use existing drilled shaft testing methodologies. However, there were several distinct obstacles to overcome.

4.2 Basic Instrumentation Version 1.0

Once it was decided that the infrared thermocouple was the appropriate instrument to utilize, a search was completed of the commercially available infrared thermocouples. Initially, the Omega OS36-RA was the best choice. The OS36-RA has a 90° viewing window and a sensing range of -50° to 1200°F (-45° to 650°C). By using the Type E-140, the usable temperature range with a 2% accuracy is 80° to 180 °F (25 ° to 80 °C)

As drilled shafts may be in excess of one-hundred feet deep, long lead wires would be required. Given that output from an infrared thermocouple is a millivolt or low

voltage signal, impedance, noise and signal loss associated with these long lead wires was a concern. Accordingly, the millivolt output signal from the infrared thermocouple was transformed into a current loop, whereby the current loop would not be subjected to the same signal problems of low voltage sources.

Again, a search was conducted for readily available transmitter devices that would allow the millivolt signal from the infrared thermocouple to be transformed into a current loop. The Omega TX901 transmitter was chosen. The transmitter accepts thermocouple sensor types J, K, T, E, R or S and produces a 4-20 mA output signal proportional to the output millivolt signal of the thermocouple. Therein, the 4 mA was at the low end of the temperature sensing range and 20 mA was at the high end (OMEGA-4).

The TX901 transmitter requires an unregulated power supply of at least +7V, but no more than +35Vdc. It was also necessary to have a standard voltmeter or data acquisition system to measure the change in voltage across a shunt resistor in the circuit line. See Figure 4.1 for a schematic and wiring diagram for the OS36 and TX901.

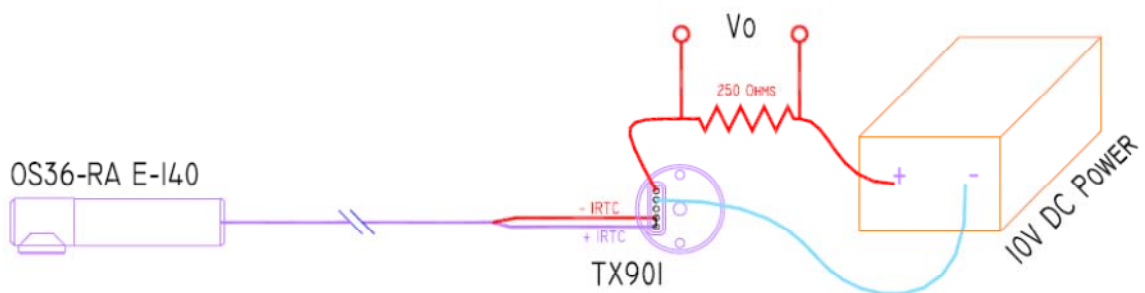


Figure 4.1 - OS36-RA and TX901 wiring diagram

4.3 Lab Scale Test #1 – Feasibility Study

After researching the different systems available to measure temperature, it was decided that it was prudent to conduct a lab scale test to determine the viability of the measuring the heat of hydration of a concrete sample. Accordingly, a lab scale test was devised in which two standard 6 inch diameter x 12 inch tall concrete cylinders were utilized. One cylinder had an access tube placed in the center of the cylinder while the other specimen had the access tube placed towards the edge of the cylinder. After filling the cylinders with concrete, the temperatures were recorded at each of the four radial directions and at the top, bottom, middle and quarter points as well as the ambient temperature. See Figure 4.2 for a diagram of the test setup. Table 4.1 shows a sample of the data that was collected for a given time.

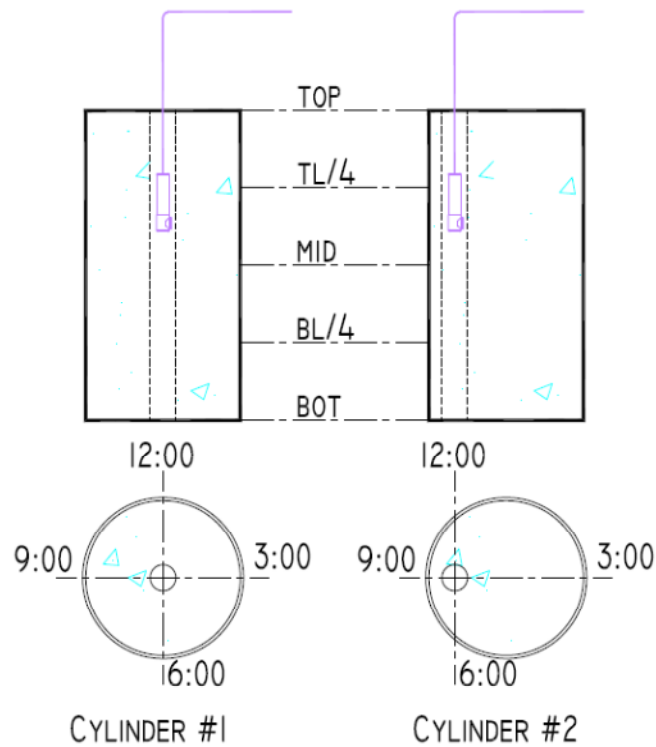


Figure 4.2 - Lab scale test #1 set up

Table 4.1 - Signal voltage for trial #1

Date	7/24/2000	Time	7:39		
			PM		
Offset Specimen					Ambient
	12:00	3:00	6:00	9:00	1.91
Top	1.98	1.984	1.986	1.986	
TL/4	1.996	1.999	2.005	2.001	
Mid	2.006	2.009	2.015	2.013	
BL/4	2.007	2.01	2.017	2.013	
Bot	1.984	1.986	1.999	1.994	
Center Specimen					
	12:00	3:00	6:00	9:00	
Top	1.969	2.005	2.002	2.002	
TL/4	2.004	2.019	2.018	2.02	
Mid	2.023	2.015	2.014	2.016	
BL/4	2.021	2.018	2.018	2.019	
Bot	1.998	1.994	1.995	1.998	

Test Cylinder Sample Temperature Signals

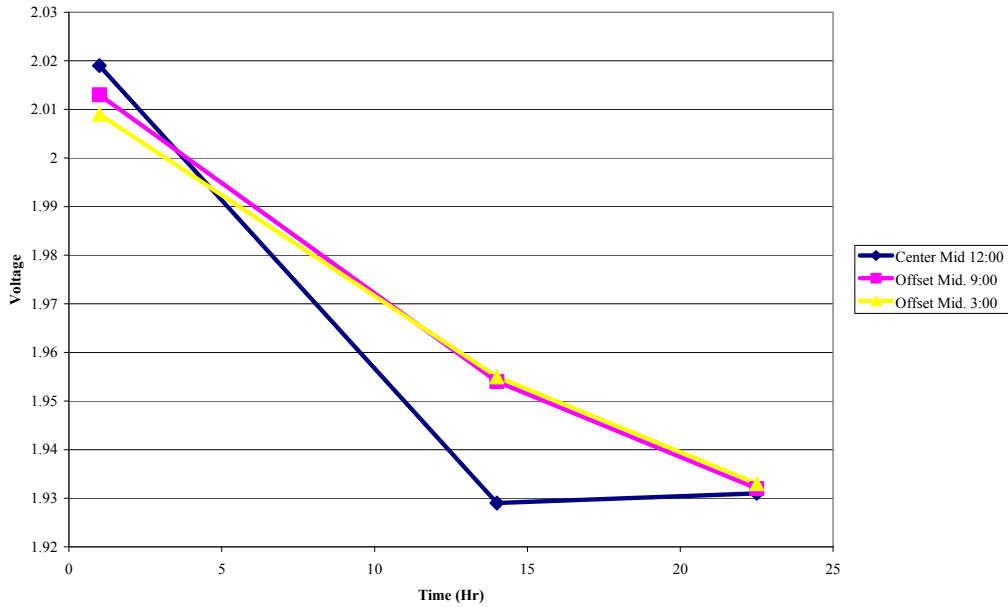


Figure 4.3 - Lab scale test 1 results

After reviewing the data, several problems became apparent. First, the time interval for collecting the data missed the peak temperature for this particular concrete

mix and conditions. Second, it did not appear that the heat generated was enough to determine a spatial difference.

4.4 Lab Scale Test #2

In order to overcome the shortcomings of the original test, it was decided to utilize a data acquisition system in combination with a laptop computer to monitor and record the output voltages at regular intervals, thereby capturing the rise and fall of the concrete temperature. The Optim Electronics Corporation Megadac 3415AC attached to a standard laptop was chosen for the data acquisition and data recording.

A second lab test was devised to not only check the viability of the testing equipment but to also determine the conditions under which a cement paste sample produces a temperature trace. Accordingly, a laboratory scale test was set up in which 40lb of type I portland cement was mixed with 16 lb of water to produce a mix with a water to cement ratio of 0.4. This cement water paste was then placed into a Styrofoam cooler with a capped 1" diameter schedule 80 PVC access tube. The IR temperature sensing probe was then placed inside of the access tube and the lid was placed on top of the Styrofoam cooler. The data acquisition system was then set up to record data every ten minutes and the test ran for a total of 63 hours. The diagram for the set-up is shown in Figure 4.4 with the results shown in Figure 4.5.

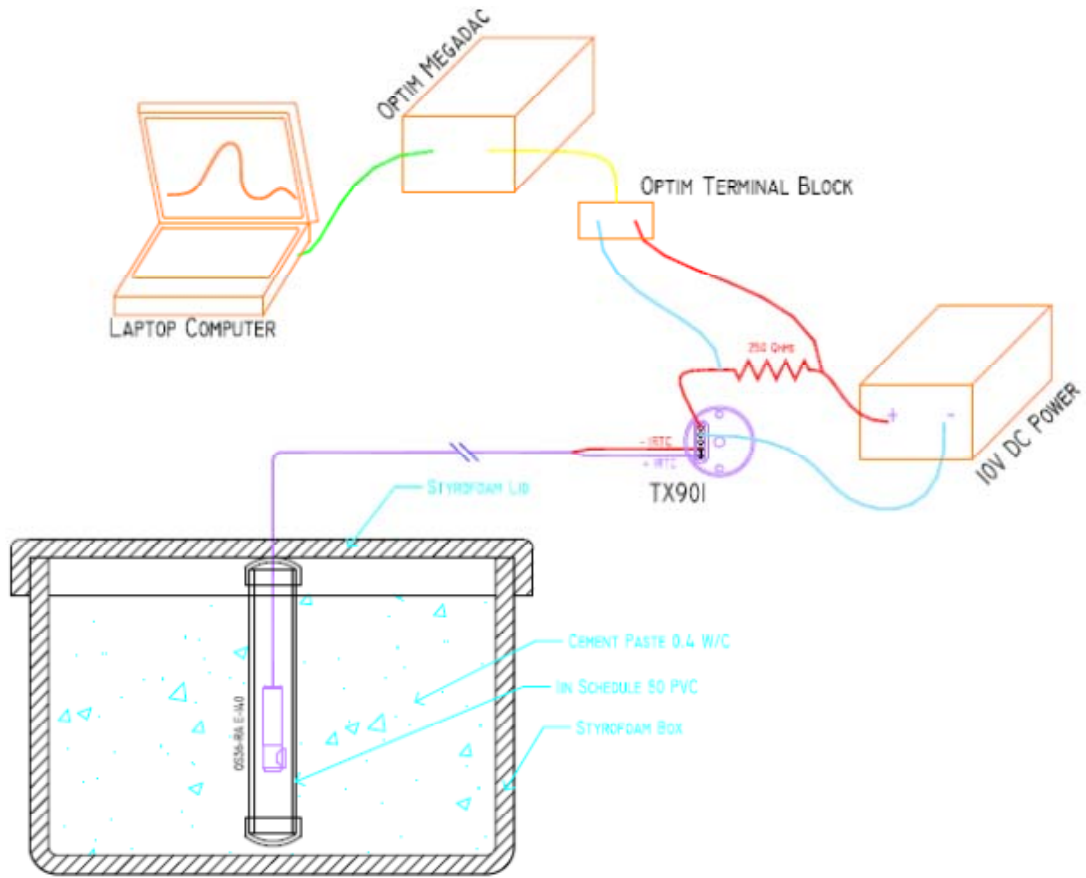


Figure 4.4 - Set up configuration for trial #2

Cement Heat of Hydration Trial 2

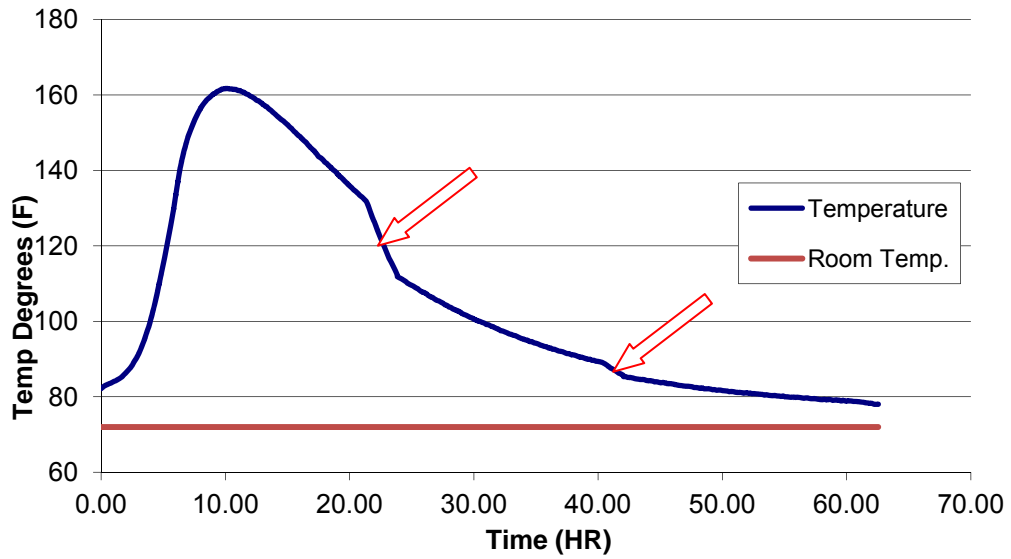


Figure 4.5 - Cement paste temperature vs. time

The results of the test showed that the cement paste temperature appeared to rise steadily for about 10.33 hours. At that point, the temperature peaked and began to decrease steadily. There are two regions of particular interest with this graph. These areas as highlighted with the arrows show an apparent increase in the cooling rate of the cement paste mixture. It is believed, however, that this change in slope of the graph is a result of the computer resetting the time at 24 hour intervals. It is also important to note that since calibration of the instrument had not yet been completed, the temperature data was presented in Volts and not an actual temperature. Given that there was time associated with mixing the paste, placing it in the Styrofoam box and setting up the instrumentation, the slightly elevated temperature at the beginning of the test appears reasonable.

4.5 Depth Measurements

The concept is to be able to measure and record temperature measurements throughout the length of a drilled shaft and to be able to relate a given temperature to a given depth. Having seemingly developed a viable option for measuring and recording the temperature, focus turned towards depth measurement. In order to continue feasibility testing, a depth measuring device was assembled utilizing equipment on hand.

As shown in Figure 4.6, this length measuring device utilized a string type multi-turn variable resistor (called an industrial string potentiometer) to record the position of a bolt on a threaded rod. The bolt was allowed to move laterally, but not rotate as the

threaded rod turned. A primary pulley was attached to the end of the threaded rod and an idler pulley was utilized to ensure good contact between the umbilical PVC pipe and the primary pulley. As the PVC pipe, on which the IR thermocouple would be mounted was moved vertically, the threaded rod would turn, causing the bolt on which the end of the string for the string potentiometer was attached to move. This system allowed the vertical displacement of the PVC to be measured and recorded utilizing the string potentiometer and the Megadac 3415AC attached to a standard laptop.

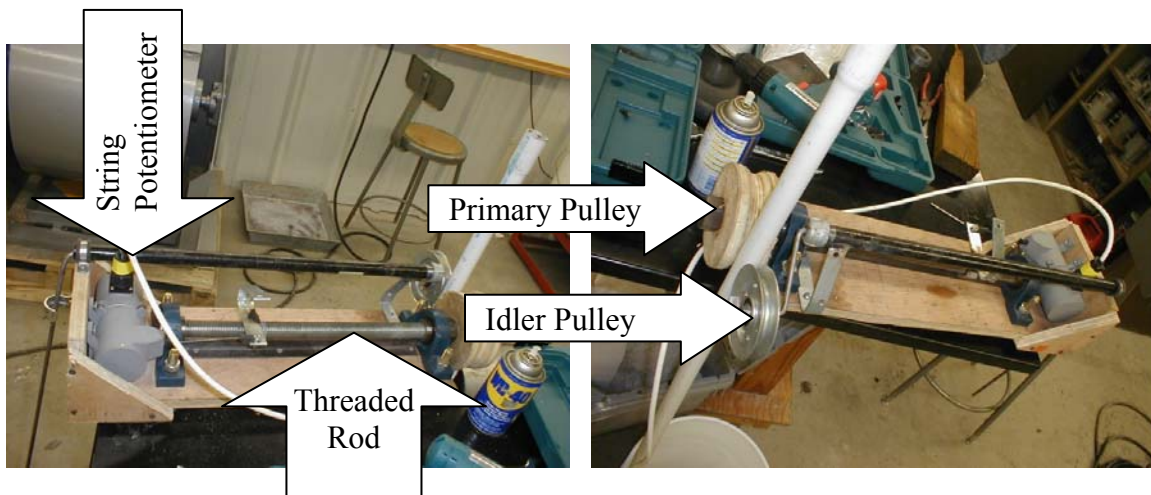


Figure 4.6 - Depth measuring device

4.6 Field Trial #1

Based on the success of the lab scale tests, it was decided to create a field scale test. The field scale test would be a 24 inch diameter, 12 feet long drilled shaft replica. Half of the drilled shaft replica would be buried into the ground and half would be free standing, exposed to the air.

Instrumentation for the test was set up with the OS36-RA infrared thermocouple extending out of a PVC coupling and reducer system that also contained the TX901 transmitter. The sensor, transmitter, coupling and reducer system was mounted to the end of a length of 1" schedule 40 PVC pipe allowing the lead wire to be fed from the Megadac to the temperature transmitter. It should be noted that machining of the PVC couplings and/or reducers was necessary for proper fit of the components and to allow the instrument configuration to be inserted into the 2" diameter schedule 80 access tubes. Additionally, this configuration allowed for vertical and radial control of where the sensor was measuring. See Figure 4.7 through 4.9 for additional information.

In order to maximize heat production, it was decided in lieu of constructing the shaft replica out of concrete, to construct it utilizing cement paste consisting only of Type I portland cement and water. The 24 inch diameter shaft would have three two inch diameter schedule 80 PVC access tubes, similar to those utilized for CSL testing, evenly spaced and extended 12 inches above the top of the simulated shaft. These access tubes, labeled 1 – 3, would allow temperature readings to be taken of the inside wall of the PVC. Further, it was decided to place several anomalies or inclusions in the shaft to mimic possible real life problems. The anomalies were as follows:

- ✧ 6"x12" concrete cylinder mold filled with sand placed 14 inches from the bottom between access tubes 1 and 3.
- ✧ 2"x8"x12" box filled with sand placed 13 inches from the top of the shaft between access tubes 2 and 3.

- ◇ 3"x6" air cylinder placed 28" from the top of the shaft adjacent to access tube 2 towards access tube 1.

In addition to measuring the temperature of the simulated shaft with the IR thermocouple, it was decided to embed standard two wire thermocouples at various locations to record the temperature of the cement paste mix as it hydrated. The thermocouples were inserted into the shaft after placement of the paste, as detailed in the chronology of construction below.

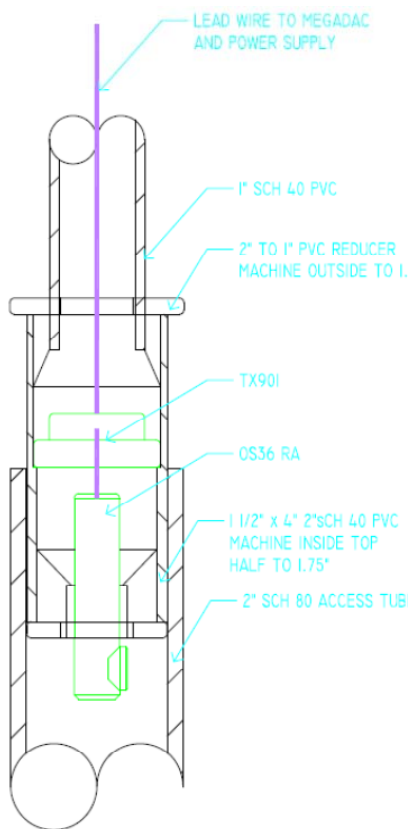


Figure 4.7 - IR sensor mount for field test #1

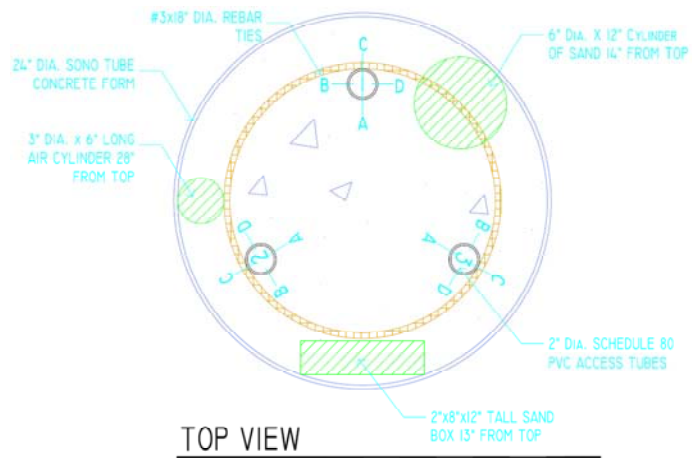


Figure 4.8 - Top view field trial #1

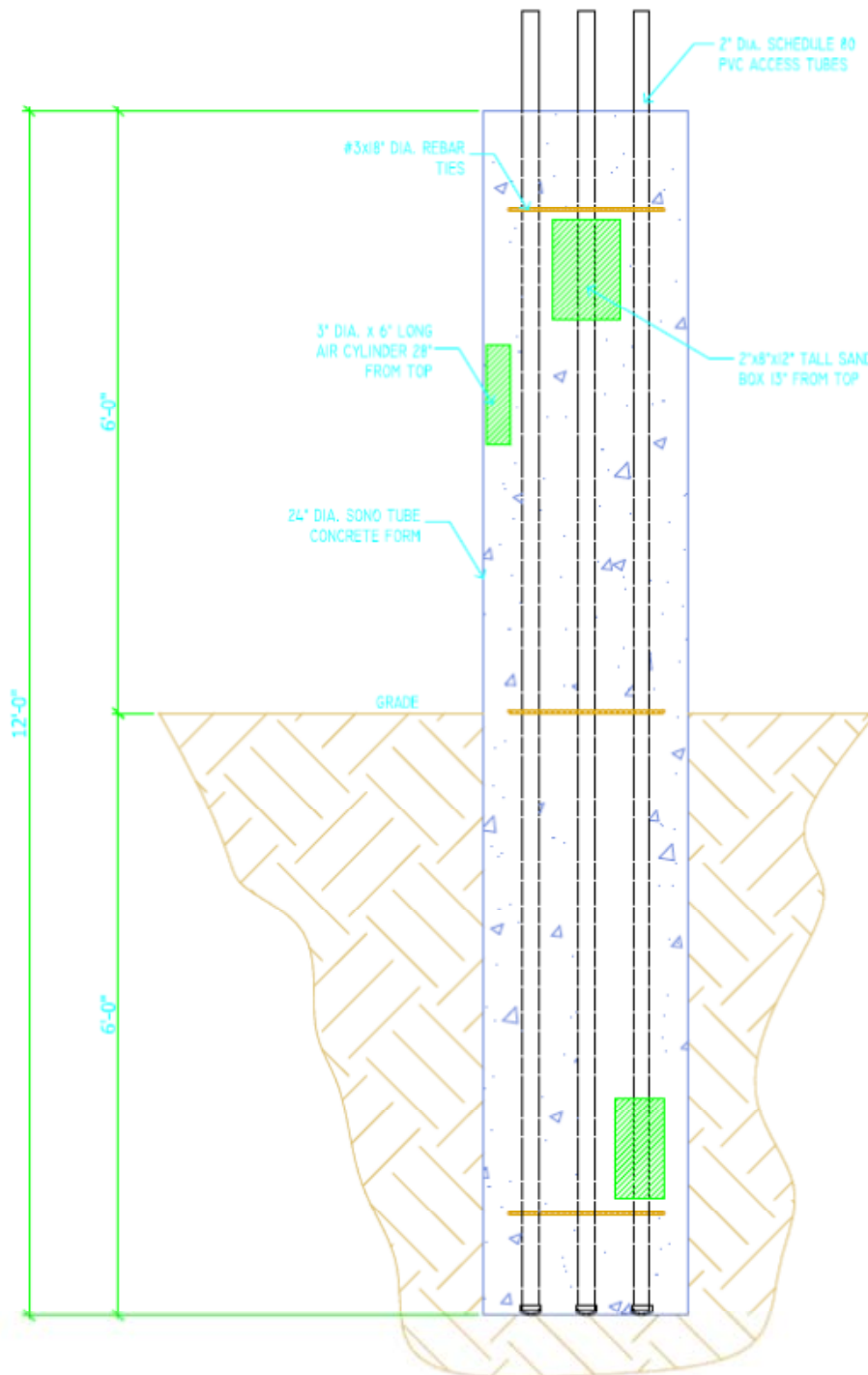


Figure 4.9 - Field trial #1 side view

The shaft was constructed at the Soils Lab on the University of South Florida, Tampa Campus, as shown in Figure 4.10A. Construction began by procuring the necessary materials and then proceeding as follows:



Figure 4.10 - Field trial #1 test set-up, A - location of test shaft, B -securing access tubes to #3 circular ties

1. Three (3) 18 inch diameter #3 grade 40 circular ties placed at the middle and 12 inches from the top and bottom were utilized to secure the access tubes. – Figure 4.10(B)
2. The access tubes and ties were then placed inside of a 24 inch diameter x 12’-0” long Sonotube concrete form. These were secured in place by using standard rebar tie wire.
3. The anomalies as indicated above were then constructed and secured to the inside of the Sonotube.



Figure 4.11 - Placing anomalies for field trial #1, A - inserting and securing access tubes and ties, B - example of anomaly sand box, C - inside of Sonotube showing anomalies, access tubes and ties, D - end or bottom view of replica shaft showing access tubes and anomaly

4. Using a 24inch diameter hydraulic auger attachment mounted to a Bobcat skid steer, a six foot deep hole was augered into the ground.
5. The Sonotube containing the access tubes and the anomalies were then erected in the hole. A work platform was then erected around the replica shaft to allow access to the top of the shaft.



Figure 4.12 - Excavation and erection of test shafts for field trial #1, A - auger attached to skid steer, B - completed hole, C - setting Sonotube into hole, D - final erection of Sonotube



Figure 4.13 - Field trial #1 erected test shaft, A - top view of erected Sonotube, B - work platform and bags of type I cement

6. Since the cement paste mixture consisted only of Type I portland cement and water, it was important to attempt to place the cement paste into the shaft and begin testing as soon as possible. Therefore, two cement mixers along with an overhead crane and a grout chute were utilized to mix and place the paste. While one mixer was being loaded and the paste being mixed, the other was being emptied into the chute and placed into the shaft.

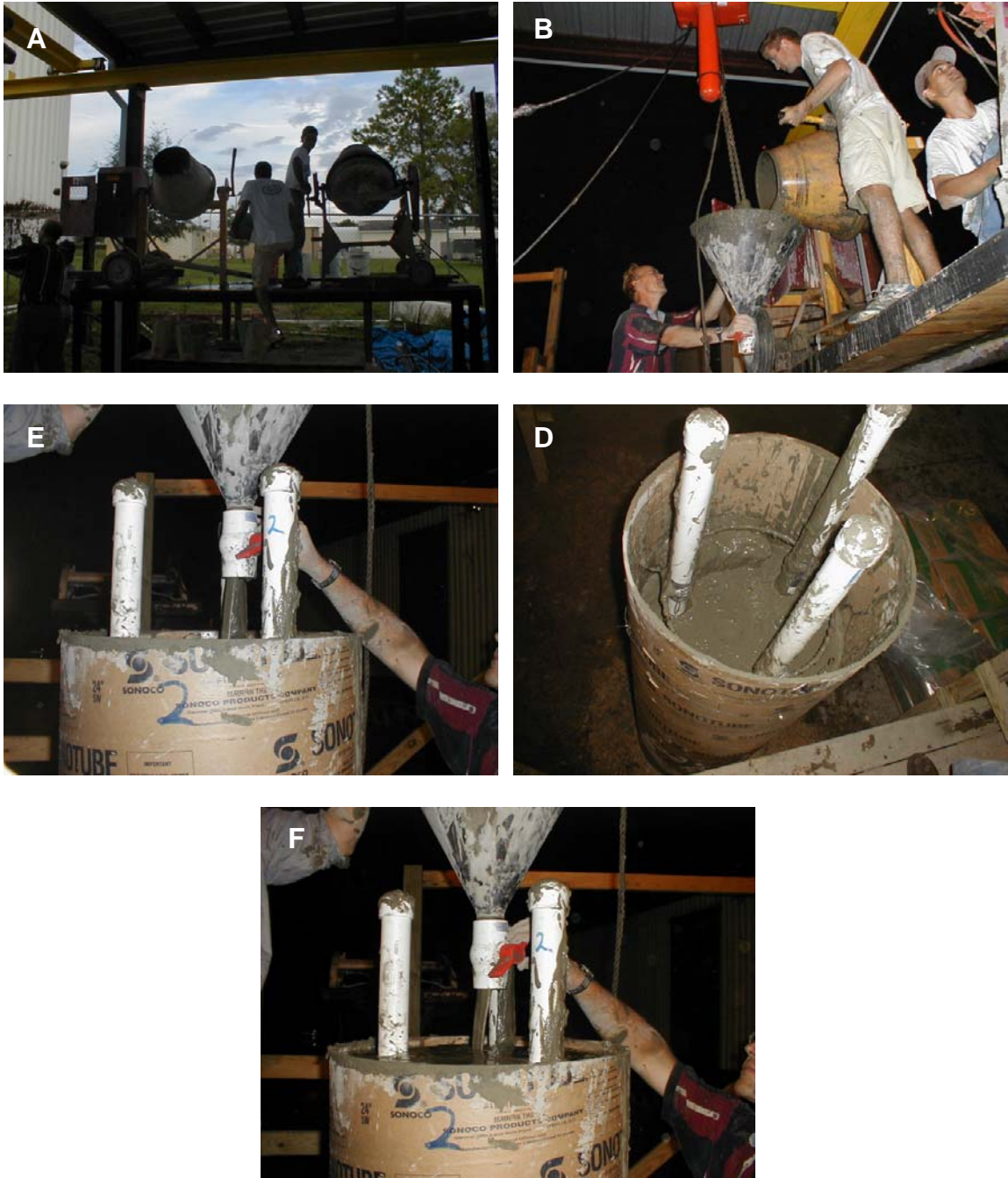


Figure 4.14 - Mixing and Placing Cement for field trial #1, A - double cement mixers, B - transferring paste from mixer into grout chute, C - Placing paste into replica shaft, D - nearing completion of paste placement, E - completion of paste placement

7. Following placement of the paste, six thermocouples were inserted into the replica shaft by first drilling a hole through the Sonotube and then using a stiff welding

rod inside of a rubber tube, the tube was inserted into the center of the shaft. Two thermocouples were then inserted into the rubber tube, one with twelve inches of embedment and the other with six inches of embedment. The rubber tube was then extracted, leaving the thermocouples in place. The thermocouples were then connected to a multi-channel digital readout and the temperature of each thermocouple was recorded.



Figure 4.15 - Installing thermocouples in test shaft for field trial #1, A - inserting rubber tube into drilled shaft utilizing a welding rod, B - inserting two-wire thermocouples into capillary tube, C - removing capillary tube, leaving thermocouple in place

8. The IR thermocouple, transmitter and string potentiometer height measuring devices were then attached to the Megadac and tested to make sure they were operating correctly.

9. First the ambient temperature of the wood on the exterior of the shaft was measured with the IR thermocouple and recorded. This allowed reference temperature.

10. Several tests were then conducted on the outside face of the replica shaft. These tests were necessary to check the device and provide a reference temperature.

11. Next a series of tests were run inside of the access tubes. As stated previously, each tube was numbered 1-3 and quarter direction was established for each tube. Quarter direction "A" was towards the center of the drilled shaft, and then progressing clockwise "B", then "C" was towards the outside of the shaft, and then "D" was the final quarter point.



Figure 4.16 - Running tests field trial #1, A - instrumentation check, B - running tests inside of access tubes, C - running tests in access tubes close-up

12. The first test in the access tube was completed at about 11:39 PM, approximately three hours after completion of the placement of the cement paste. Tests were then completed almost continuously until about 1:55 AM, approximately five hours after placement of the paste.

It is important to note that after the first few tests in the access tube, the access tubes started heating up, causing the probe to stick. Silicone was used in an attempt to lubricate the surface between the probe and the access tube. At approximately 1:15 AM, the surface of the concrete and the access tubes became very hot and the bleed water on top of the replica shaft started to boil; shortly thereafter, the PVC access tubes debonded from the shaft, eliminating the possibility of any additional testing in the access tubes with the IR probe.

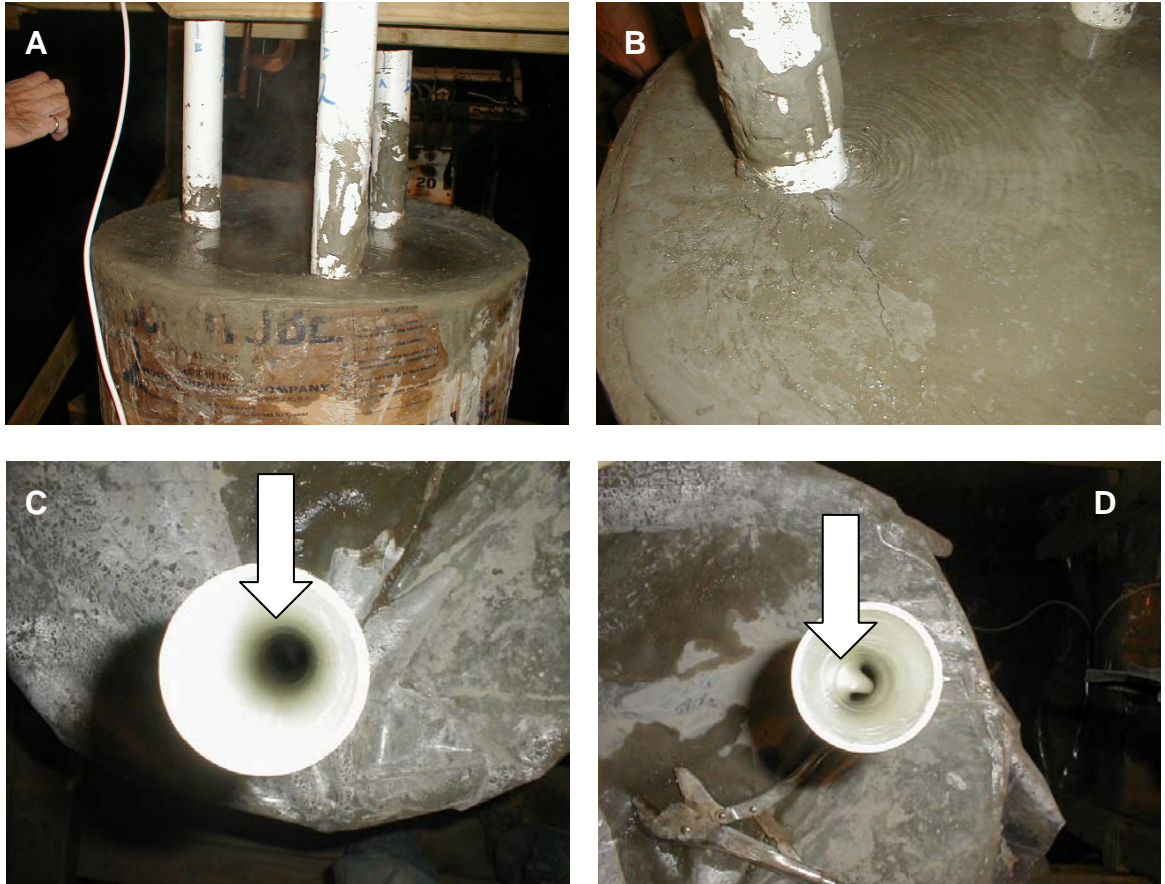


Figure 4.17 - Delamination of PVC access tubes, A - bleed water boiling, B - bleed water boiling and thermal crack, C - delamination of access tube starting, D - full delamination of access tube

The following are samples of the data obtained from the test shaft test along with a brief discussion of the results.

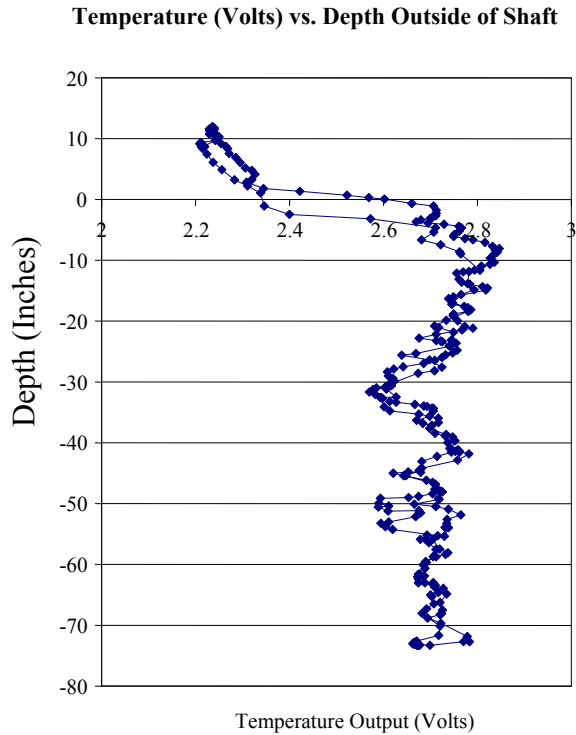


Figure 4.18 - Temperature vs. depth, outside of replica shaft field trial #1

Figure 4.18 indicates the temperature vs. depth taken on the outside of the replica shaft between access tubes 1 and 2. There is an apparent error in the depth recording device, given that the two temperature traces do not align, likely due to the sensor rod slippage on the depth pulley.

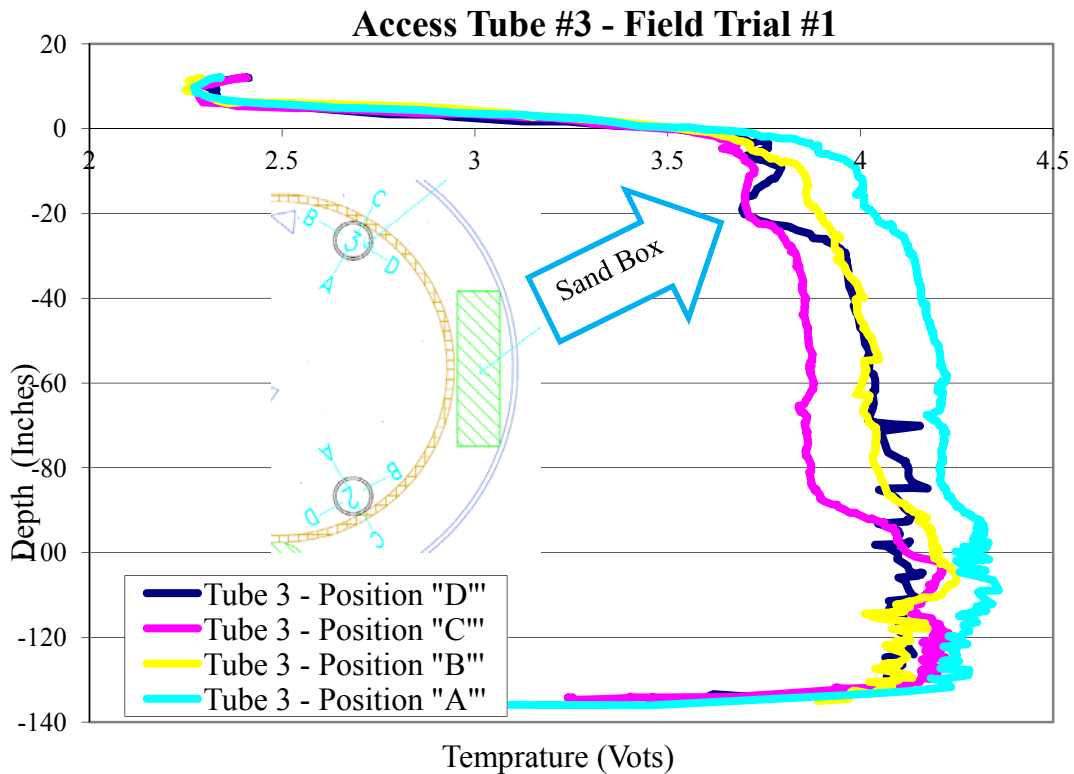


Figure 4.19 - Temperature traces from access tube #3 field trial #1

Figure 4.19 shows the temperature traces from Tube #3 from all four radial directions. The sand box anomaly is apparent in temperature trace "D" which was pointed directly at the anomaly and trace "C" which is 90° away from the anomaly and pointed towards the exterior of the shaft. It is also apparent where the soil level is and the fact that the base of the access tubes is in the soil below the shaft. It is supposed that the temperature traces are cooler when the probe is extracted due to plunging air cooling the access tubes.

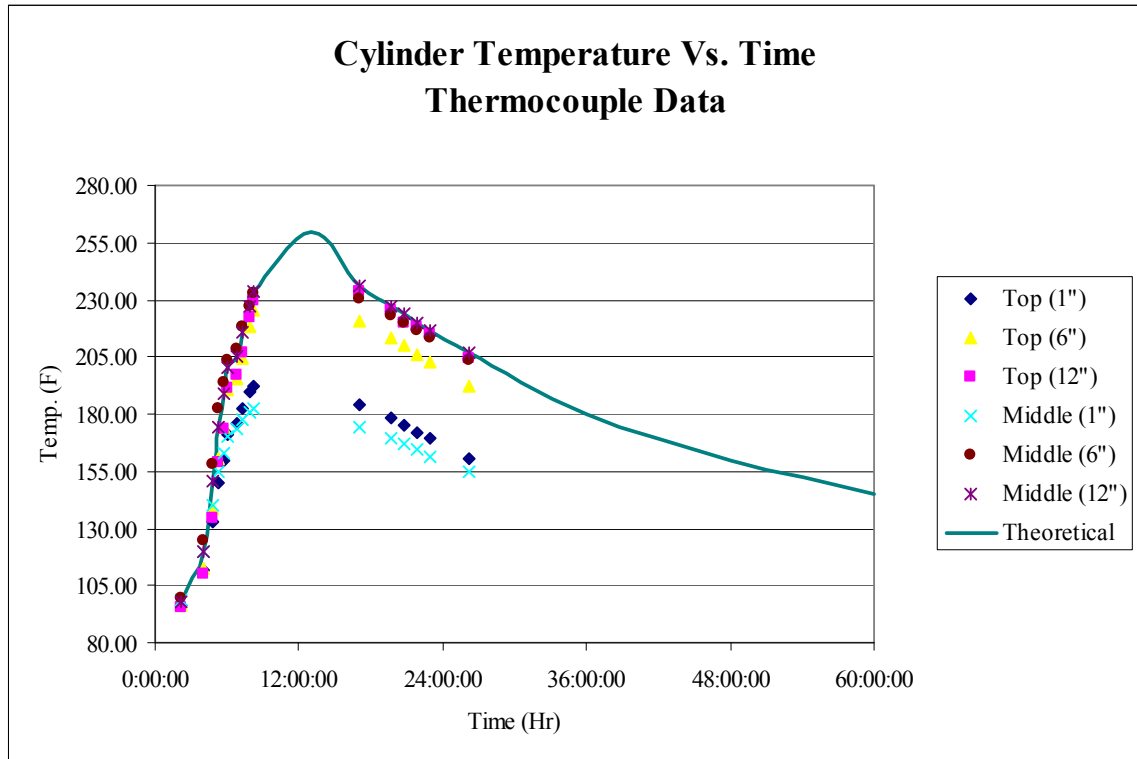


Figure 4.20 - Thermocouple data from replica shaft field trial #1

Figure 4.20 indicates the thermocouple data from the replica shaft. It is apparent that the recording times captured the rise and fall of the shaft temperature, but not the peak temperature. Therefore, a theoretical trace was added to the graph to mimic the temperature curve. Based on this theoretical curve, it is estimated that the peak temperature of the cement paste was approximately 260°F at the core of the test shaft.

Additional information in regards to field trial #1 can be found in Appendix A. Based on the experience gained and the results of Field Test #1, several shortcomings were realized:

- ✧ Utilizing a rigid pipe for the probe was cumbersome and would be impractical when testing real drilled shaft foundations. The length measuring device, which was improvised, needed improvement. The PVC pipe slipped on the wooden wheel.

- ✧ A method would need to be developed so that standard wire could be utilized, similar to CSL testing.

- ✧ Running the test four different times in each access tube is impractical. A method would need to be developed in which the four directions could be tested at once (i.e. four sensors).

- ✧ The temperatures of the cement paste mix were too hot. It is not likely that the temperature of a standard drilled shaft would reach 260°F. Actual concrete would likely produce enough energy to be useable.

- ✧ Continuous monitoring and recording of the embedded thermocouples is necessary to provide a complete understanding of the temperature of the cement as it hydrates.

4.7 Basic Instrumentation – Version 2.0

Drawing from the lessons learned in Field Test #1, a redevelopment of both the infrared thermocouple and the length measuring instrumentation was undertaken.

In order to achieve the desired results of testing all four directions simultaneously, quad-directional infrared thermocouple housing was designed constructed out of Teflon. The housing held each of the OS36RA in one of the four different primary radial directions, i.e. 0°, 90°, 180°, 270°.

One of the shortcomings of the original probe was the size of the TX901 thermal transmitters. Therefore, it was decided that the circuitry for the transmitter should be manufactured, making it as small as possible. Therefore, the housing also contained a signal conditioning area.

Given the apparent need to maintain radial positioning, it was elected to utilize standard 2 ¼ inch outside diameter inclinometer casing. Inclinometer casing contains grooves in which wheels on a standard inclinometer instrument ride in order to keep alignment. Accordingly, the Teflon housing would be attached to an inclinometer alignment mechanism that would also maintain an equidistant from the infrared thermocouple view window to the borehole surface.

Figures 4.21 show drawings of the new device design. The drawings of the assembled device were then divided into four individual pieces. These pieces were then

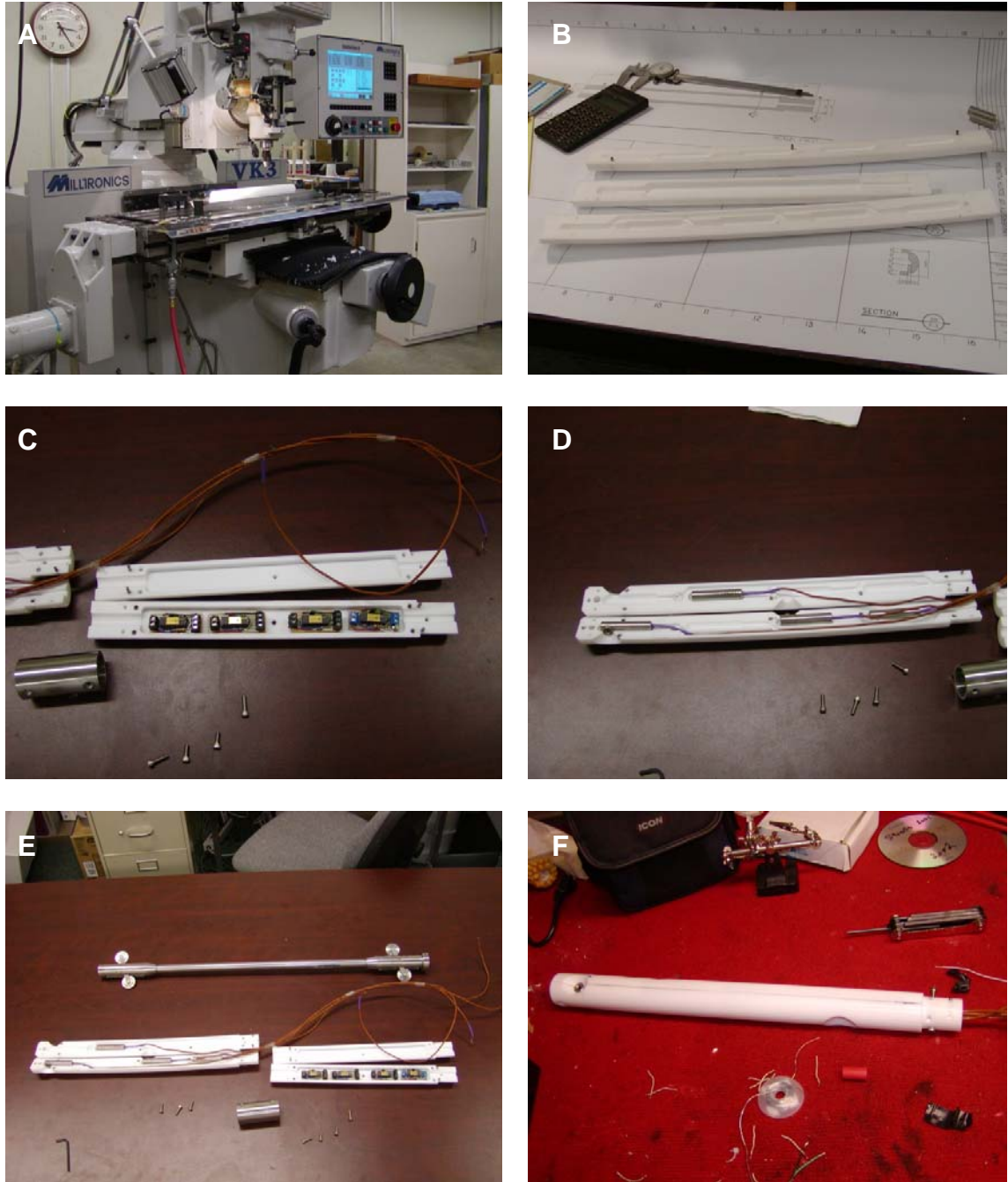
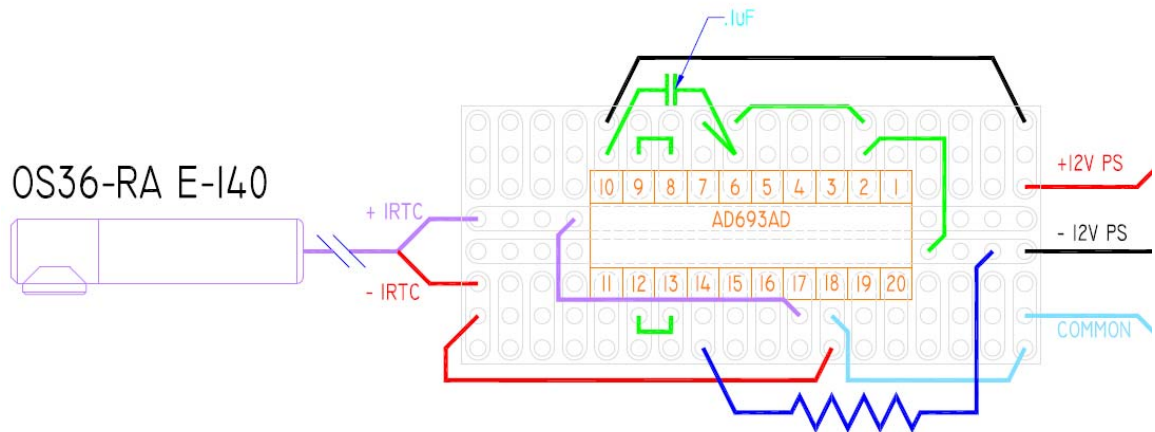


Figure 4.22 - Manufacturing and assembly of version 2.0 instrumentation, A - housing manufacturing, B - completed pieces, C - housing pieces for down hole signal conditioning, D - IR thermocouple housing pieces, E - complete device disassembled, F - IR thermocouple section assembled

The electronic circuitry for the device includes transducer end signal conditioning that transposes the output voltage from the thermocouples into a 4 to 20 mA current loop.

This current loop is required to allow the signal from the thermocouples to be read at the acquisition board without loss or alteration of signal due to the length of the lead wires.

The circuit for the current loop was not commercially available in a scale that allows it to be placed in the instrument body. Therefore, a circuit was developed that met the scaling needs to be placed within the device. Specifically, an Analog Devices Loop-Powered 4-20 mA Sensor transmitter AD693 chip was selected and placed into a circuit as shown in Figure 4.23. The AD693 is a monolithic signal conditioning circuit which accepts low-level inputs from a transducer to control a standard 4-20 mA two wire current loop (ANALOG).



4-20 mA VOLTAGE TO CURRENT LOOP CONVERTER

Figure 4.23 - 4-20 milliamp voltage to current loop converter

In addition, a circuit was also developed to transpose the current loop signal into a differential voltage that can be measured by a data acquisition system. This circuit allows for the differential signal to have a moveable reference for greater accuracy when

recording the readouts. See Figure 4.24 for a wiring diagram of the current to voltage conversion.

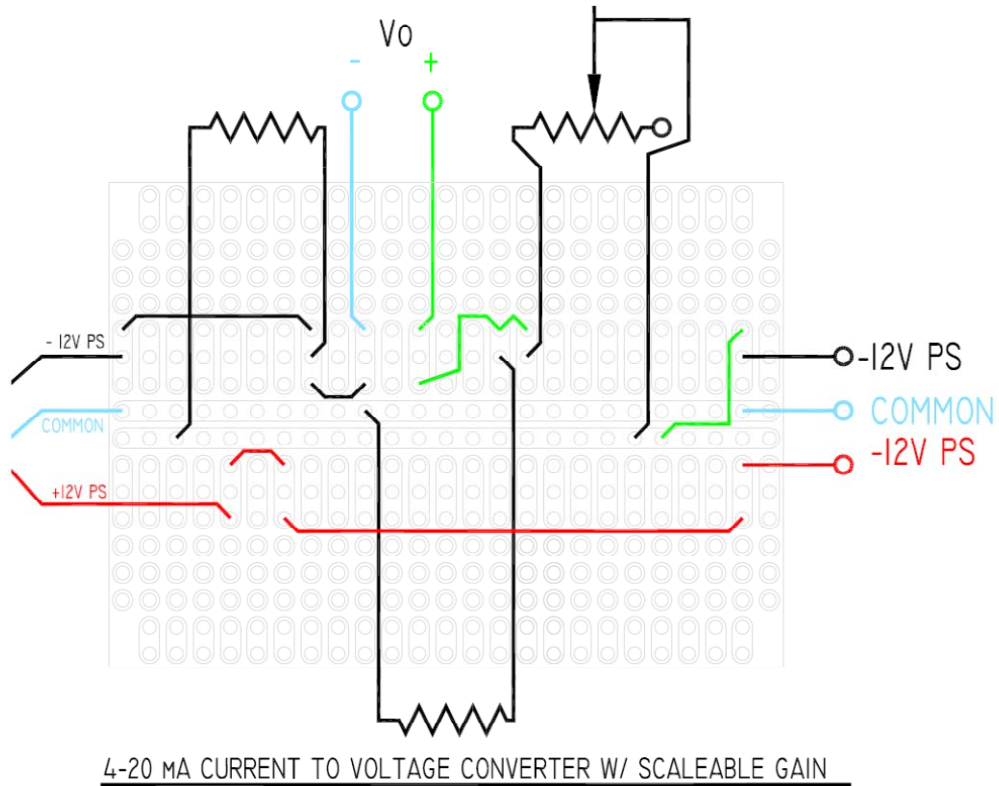


Figure 4.24 - Current to voltage conversion

The overall wiring diagram for one of the thermocouples and the associated signal conditioning is represented in Figure 4.25. Selected pictures from the assembly of the electronic components are shown in Figure 4.26.

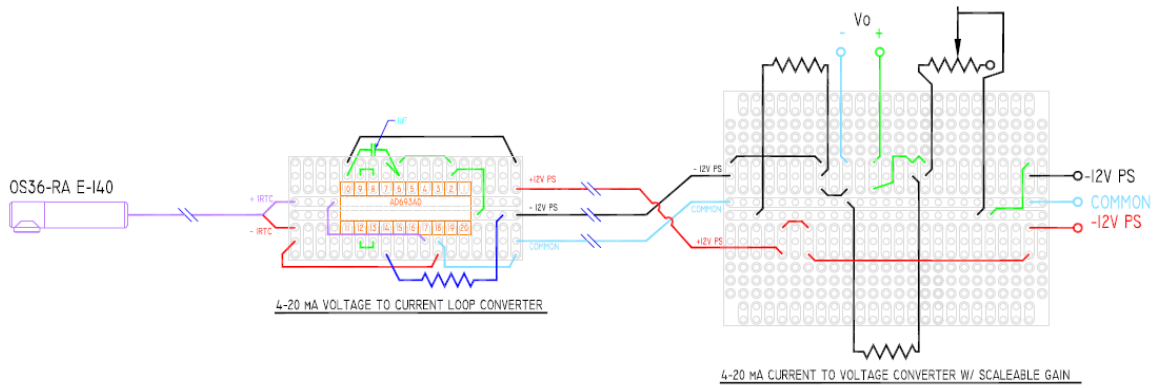


Figure 4.25 - Complete wiring diagram

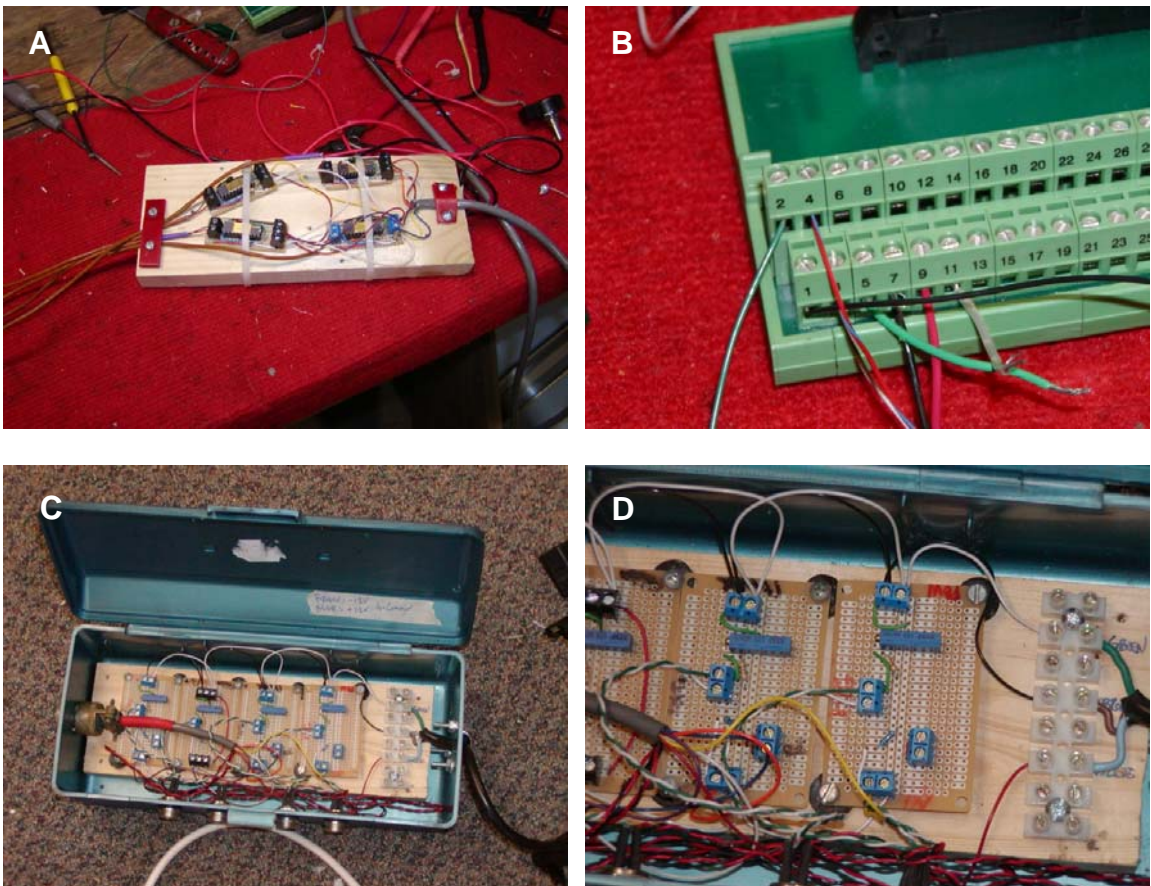


Figure 4.26 - Version 2.0 wiring, A - Voltage to current loop circuits, B - Terminal block to DAQCard, C - current loop to voltage conversion overall, D - current loop to voltage circuitry close up

The second instrument was the replacement for the string potentiometer based position indicator. A position wheel was manufactured with an aluminum body and contained a polyethylene molly wheel that was attached to a central shaft with a set screw. The shaft then extended through a set of high precision bearings on each side held into the aluminum housing. The molly wheel was grooved to ensure intimate contact between the borehole cable and the pulley. This combination provided a high coefficient of friction and a large amount of surface area between the umbilical cable and the wheel, effectively eliminating the likelihood of slippage (Figure 4.27A). One end of the shaft extended to coupling and an optical encoder that was mounted inside of a protective housing (Figure 4.27B). Finally, the position indicator was fitted with a 5/8" x 11 threads per inch threaded opening to allow it to be attached to a standard surveying tripod (Figure 4.27C). The two high precision bearings were pressed into wheel assembly housing. A Clarostat 600EN digital encoder was used to measure the angular motion of the wheel assembly.

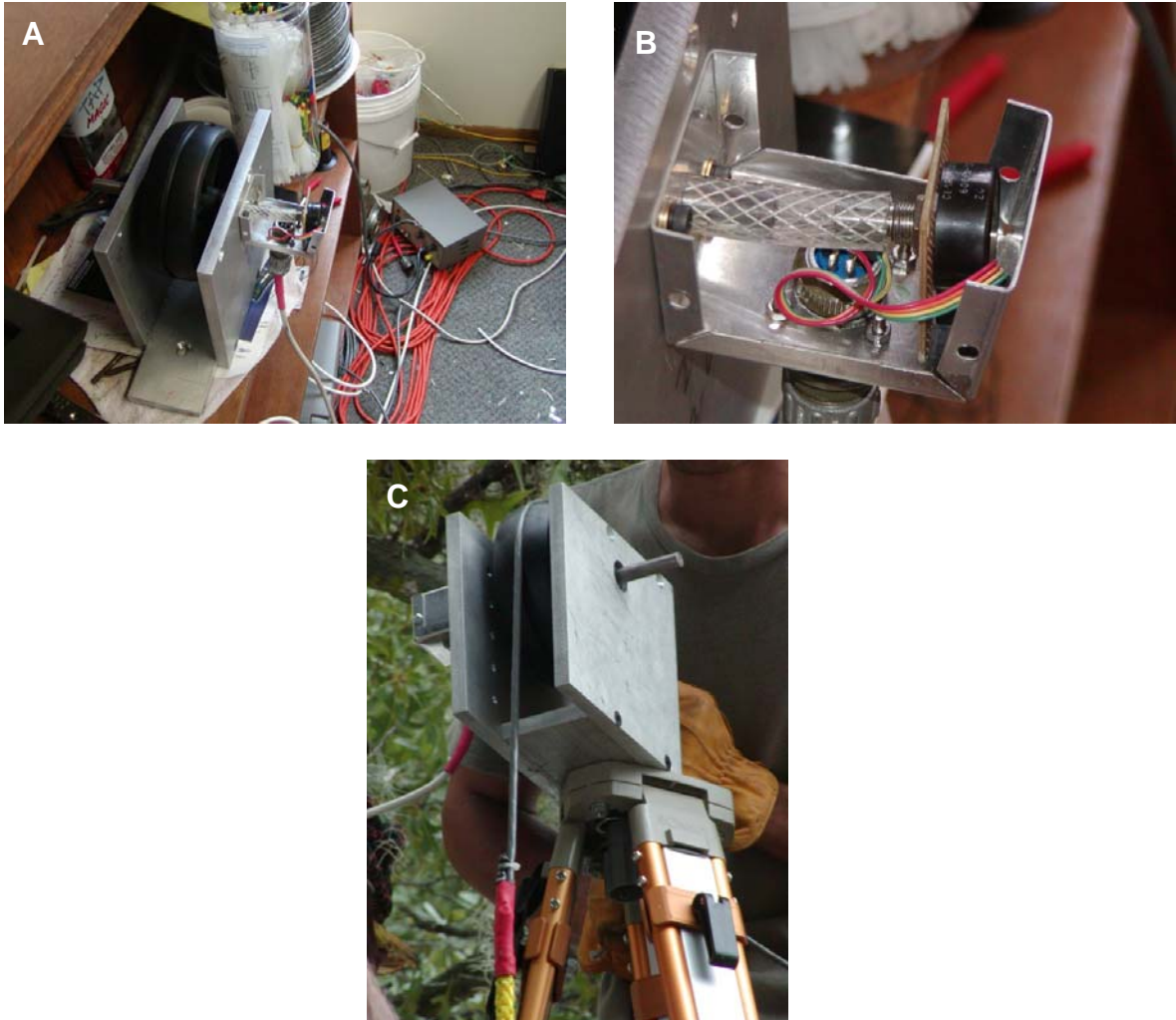


Figure 4.27- Version 2.0 depth measuring device, A –overall view of depth wheel, B - digital encoder and coupling to wheel shaft, C - Umbilical cord, depth wheel and tripod

The circuitry for the infrared thermocouples was completed by transforming the current in the current loop back in to voltage so it could be easily measured and recorded by the data acquisition system. The current to voltage circuit was housed in the electronics “black box” that also housed the connections for the power supply, the depth encoder along with the data acquisition terminal block, the ribbon cable that connected the terminal block to the data acquisition card, and a manual thermocouple output device.

The backbone of the data acquisition system was the National Instruments DAQCard – 700 which provided the hardware interface between the data acquisition terminal board in the Black Box and the portable computer. Software to monitor the input signals from the infrared thermocouples and the depth encoder consisted of a LabView based program that provided real time numerical and graphical representations as well as the ability to adjust calibration factors.

A standard 120 VAC to +/- 15 VDC @ 0.24 amp power supply / transformer was used to provide excitation to the downhole device. Excitation for the depth encoder was provided from the data acquisition card in the portable computer.

A standard surveying tripod was used to position the depth encoder over the access tubes and provide support during testing.

Following the development and testing of the new instrumentation, a second field study was planned.

4.8 Field Trial #2

A second field trial was devised to test the new instrumentation. The goals for this were:

- ✧ Two (2) 24" diameter x 6'-0" long test shafts using 24" Sonotube concrete forms were constructed.
- ✧ The shafts would use standard 4000psi ready mix concrete.
- ✧ One shaft would be constructed with a full rebar cage and one with only three (3) #3 ties to hold the access tubes in place.
- ✧ The shafts would be constructed above ground except approximately one foot below the grade for stability.
- ✧ Anomalies were placed in the shafts similar to Field Trial #1.
- ✧ 2.5" nominal inclinometer casing was used for access tubes in lieu of PVC

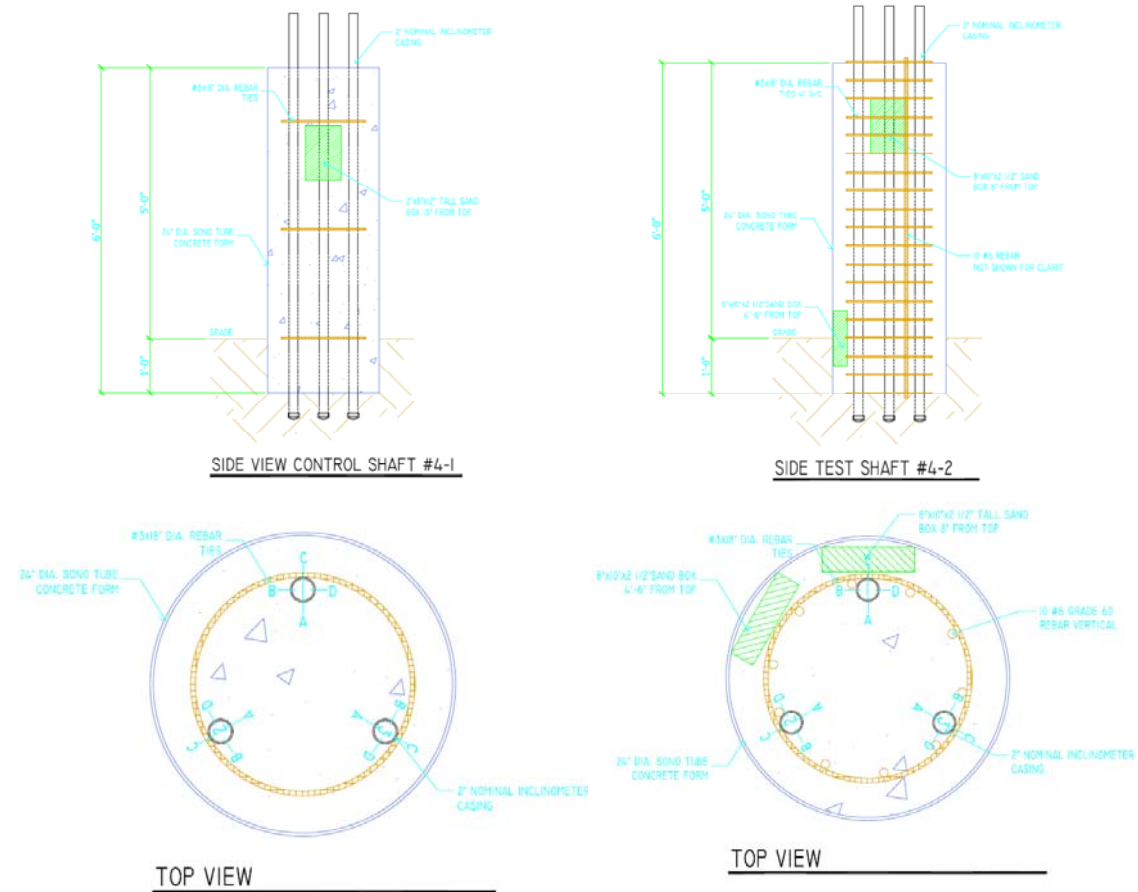


Figure 4.28 - Test set-up for field trial #2, A - side view control shaft, B - side view test shaft, C - top view control shaft, D - top view test shaft

Following procurement of the materials, except the ready mix concrete, construction of the replica shafts progressed as follows at the Soils Lab on the University of South Florida, Tampa Campus.

1. A 12'-0" long Sonotube concrete form was cut into two 6'-0" long sections.
2. The inclinometer casing access tubes for the first shaft was secured with 18 inch diameter #3 grade 40 rebar ties placed at the middle and 12 inches from the top and bottom. As with Trial #1, the access tubes were placed at 0°, 120° and 240°.

3. For the second shaft, the inclinometer casing, ten (10) #6 grade 60 rebar and 18 inch diameter #3 grade 40 ties spaced at approximately 4 inches on center were tied into a “cage”.



Figure 4.29 - Tying rebar cages for field trial #2, A - inclinometer casing and #3 ties, B - inclinometer casing and rebar cage for second shaft

4. The cages were placed along with the anomalies inside of the Sonotubes and secured with standard rebar tie-wire.
5. The Sonotubes and cages were then erected with approximately one foot of embedment into the soil for stability.



Figure 4.30 - Field trial #2 test set-up, A - sand box anomaly, B - anomaly and cage inside of Sonotube, C - erected control shaft top view, D - erected control shaft elevation view

6. Ready mix concrete supplied from RMC Ewell, Inc was then placed inside of the two test shafts. The ready mix design was a f'c 4000 psi drilled shaft mix with #57 rock, 35% fly ash and a water to cement ratio of 0.41 (Ewell's mix number 64405).
7. Following placement of the concrete, 2-wire thermocouples were installed into the drilled shaft in a similar fashion as Field Trial #1. The thermocouples were then attached to a Starlog Pro data logger for continuous data sampling.



Figure 4.31 - Installing thermocouples for field trial #2, A - insertion of 2-wire thermocouples, B - data logger for thermocouples

8. Access scaffolding was then erected along with a shade canopy to limit the amount of direct exposure from the sun to the test shafts.
9. Thermal testing of the shafts was then started and continued on a periodic basis.

The following are samples of data taken during the tests along with a brief discussion.



Figure 4.32 - Field Trial #2 Testing, A - field trial #2 data collection overall, B - field test #2 data collection close-up

Thermocouple Data for Field Trial #2

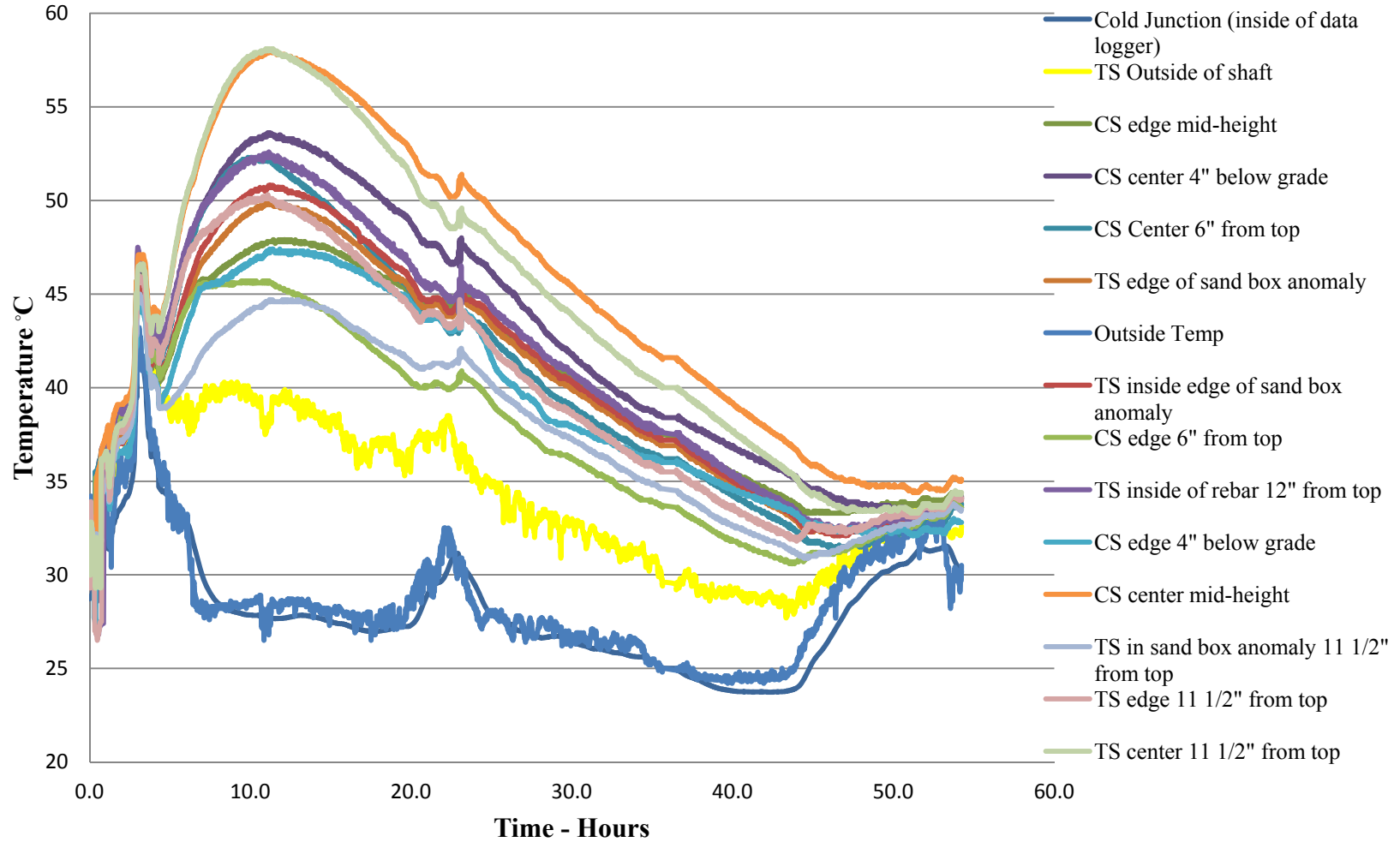


Figure 4.33 - Field trial #2 thermocouple data

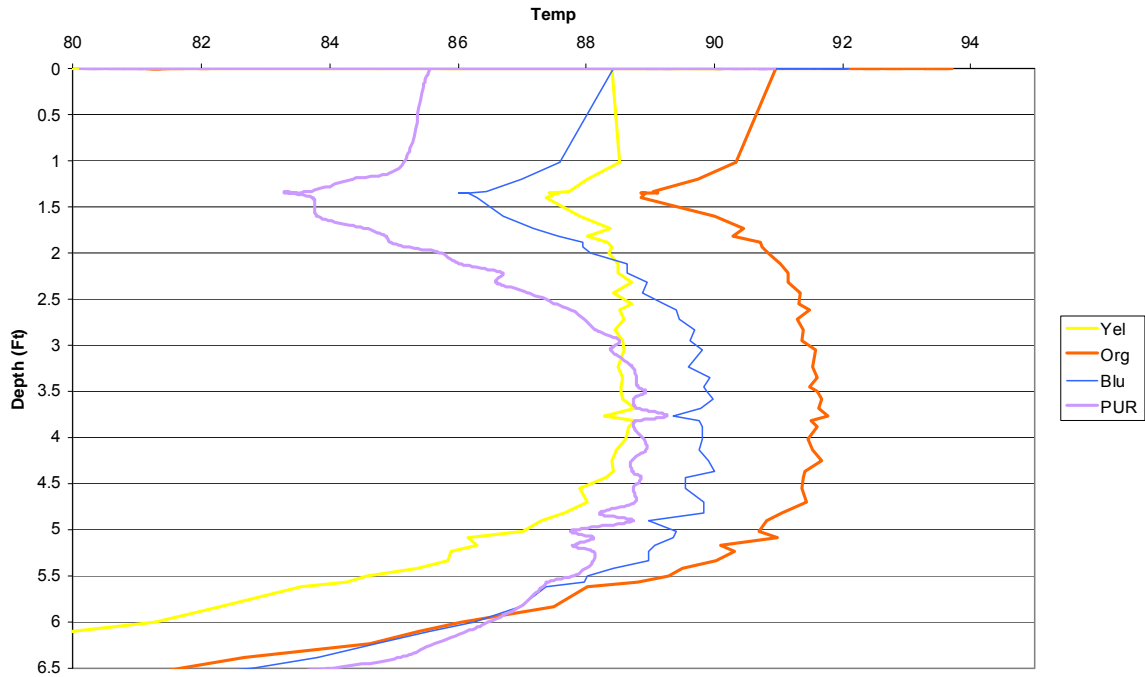


Figure 4.34 - Sample data from field trial #2 - tube E-2



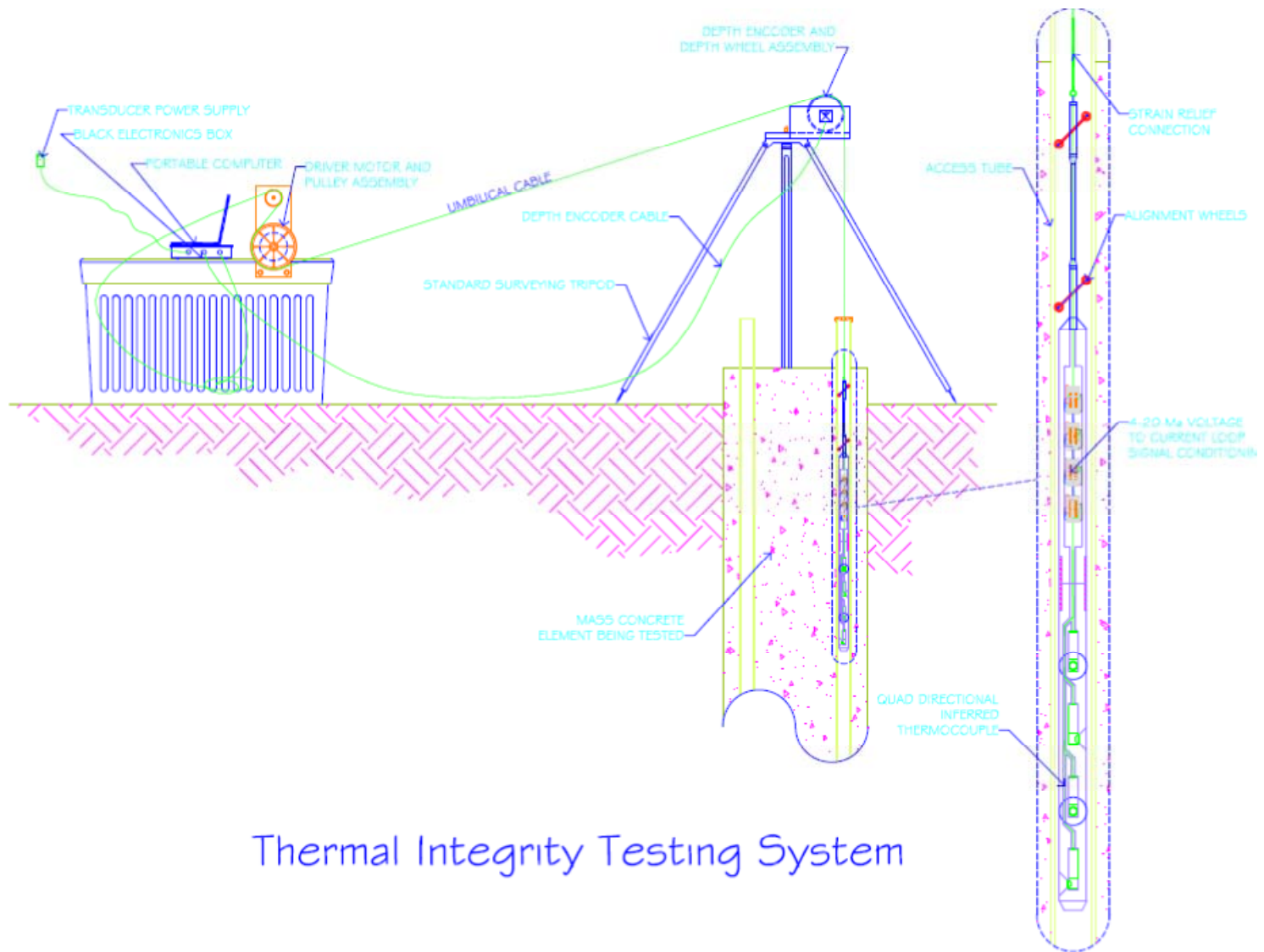
Figure 4.35 - Sand box anomaly found adjacent to tube E-2

Additional information in regards to field trial #2 can be found in Appendix B.

The results of the Field Test #2 showed great promise. It was decided that full scale testing should be performed next. However, several key improvements were desired before continuing with another set of tests.

4.9 Basic Instrumentation – Version 2.1 and Software Development

Drawing from the lessons learned in Field Test #2, several improvements were made. First, the data acquisition end signal conditioning was reconfigured to be housed in a custom made steel “black box”. Next, a driver motor and pulley assembly was added. Specifically, a 2 RPM 110 VAC motor combined with a drive pulley and an idler pulley was configured to lower, and if desired, raise the downhole sensor in the access tubes. This motor was mounted to a portable tool box, allowing the sensors to be raised and lowered at a constant rate and with little effort from the operator. Finally, a Belden 6-conductor 22 AWG shielded cable with a PVC jacket was used to provide excitation to the downhole sensor along with signal return from each of the infrared thermocouples. The cable also acted to lower and raise the sensor in the access tube. This shielded cable provided better resistance to electronic noise and greater strength and durability than the previously used umbilical wire. Figure 4.36 shows the updated testing scheme.



Thermal Integrity Testing System

Figure 4.36 - Thermal integrity profiling system setup

Chapter 5 - Full Scale Testing – Auburn, AL

5.1 Introduction

Based on the lessons learned from the previous tests, a full scale testing program was envisioned. The full scale tests could be completed in conjunction with Auburn University and several different research projects could benefit from the full scale production. Specifically, in addition to Thermal Integrity Profiling methods, the following concepts would be addressed:

1. The drilled shafts would be constructed with a chamber at the base and access tubes to the top of the shaft, allowing the toes of the shafts to be pressure grouted after the concrete for the shafts had cured, thereby mobilizing the toe of the shaft. Load testing on the shafts would then be conducted following the grouting to determine the effect of the post-grouting.
2. Several different concrete mixes with different slumps and coarse aggregate sizes would be utilized. In addition, two shafts would be constructed utilizing self consolidating concrete. The placement of the concrete would be monitored to determine the effect of these different mixes on concrete flow through the reinforcing cages.

3. Adiabatic boxes would be instrumented with standard two wire thermocouples and those thermocouples monitored throughout the curing of the concrete to allow the generation of heat of hydration curves for the different mix designs.
4. In addition to Thermal Integrity Profiling, Cross-hole Sonic Logging (CSL) testing and Sonic Echo Testing would be performed to allow a comparison of the data obtained by Thermal Integrity Profiling.
5. The drilled shaft bore hole and placement of the concrete would also be monitored using a Drilled Shaft Inspection Device (SID) which is a video camera and light system especially developed and equipped for inspecting drilled shafts both submerged and dry.

5.2 Test Site Set-Up

This full scale testing program would be located at the Auburn University's National Geotechnical Experimental Site (NGES) which is adjacent to the National Center for Asphalt Technology (NCAT) test track at Auburn University, in Opelika, Alabama and was made available by Dan Brown, Ph.D., of Auburn University. The site was chosen due to several factors. First, the unique silt soil that exists at the site and the depth to the water table allows for 25 feet deep drilled shafts to be constructed without casing the openings. Secondly, many tests had been conducted at the site in the past, and there was a wealth of information available regarding the geotechnical and geological

conditions of the site. The remnants of said research could be found readily on the property. Figure 5.1 shows an aerial image of the site.

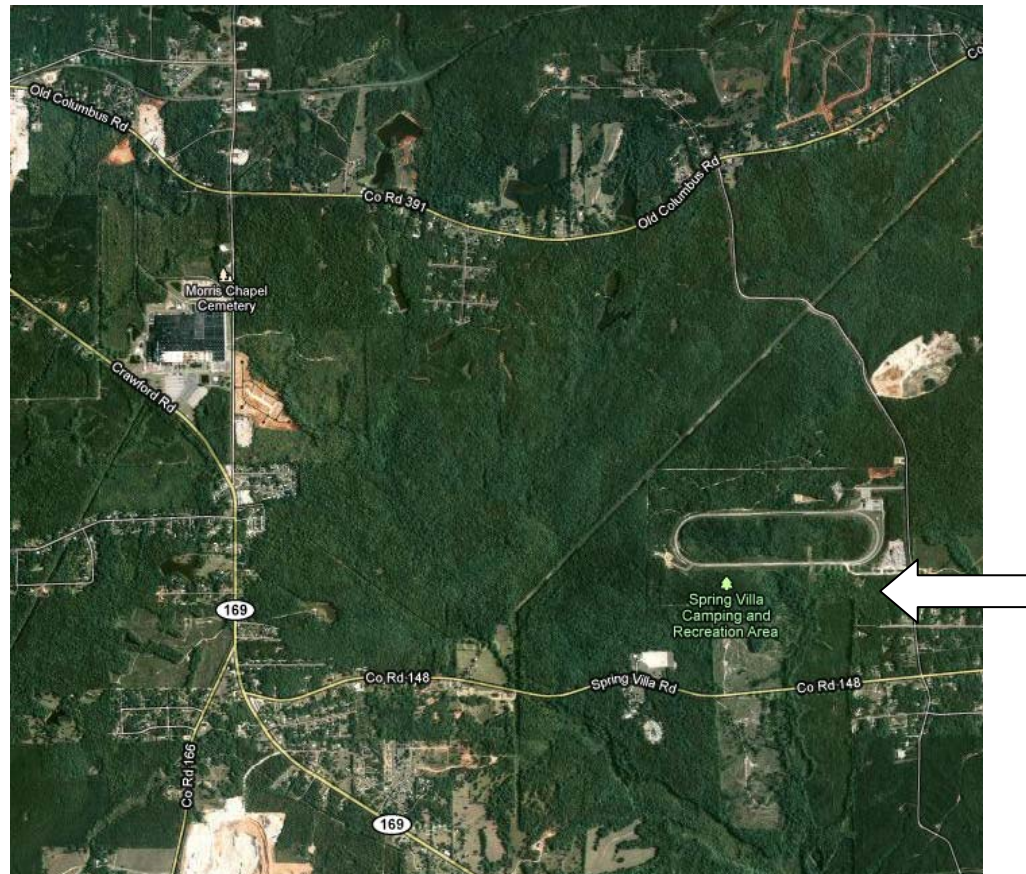


Figure 5.1 - Auburn University's NGES Test Site, Opelika, Alabama (Google Maps)

It was decided that five different drilled shafts would be constructed; each would be 3'-6" in diameter and 24 feet deep. Using the USF miniature cone penetrometer, a subsurface investigation was carried out prior to any site layout (Figure 5.2). Virgin material was located in the northwest corner of the property, and the area was large enough to contain the proposed shafts. Cone penetration tests (CPT) were performed at the centerline locations of each test shaft. Figure 5.3 thru Figure 5.7 shows the CPT soundings for TS-1 through TS-5, respectively. The soil in this area was mainly a reddish-brown clayey silt with some gravel, mostly near the surface. Full documentation

of the various geotechnical investigations can be found in Brown and Drew (2000), Mayne, et al. (2000), and Brown and Vinson (1998).



Figure 5.2 - Alabama site soil testing, A - CPT soundings in test area, B - subsurface exploration using the USF mini-CPT rig

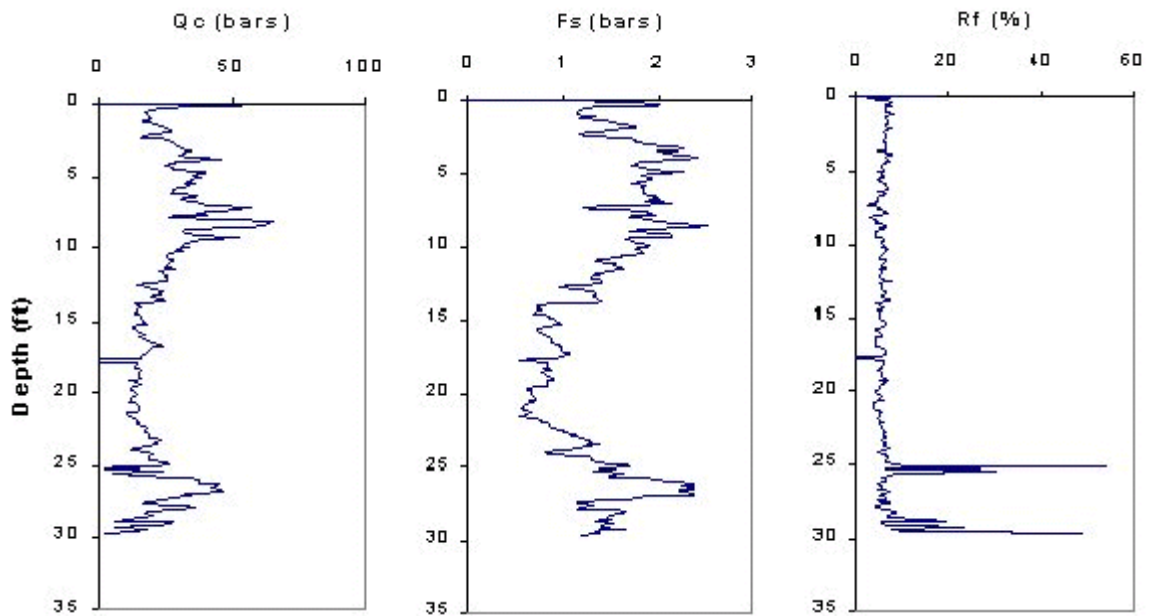


Figure 5.3 - TS-1 mini CPT sounding

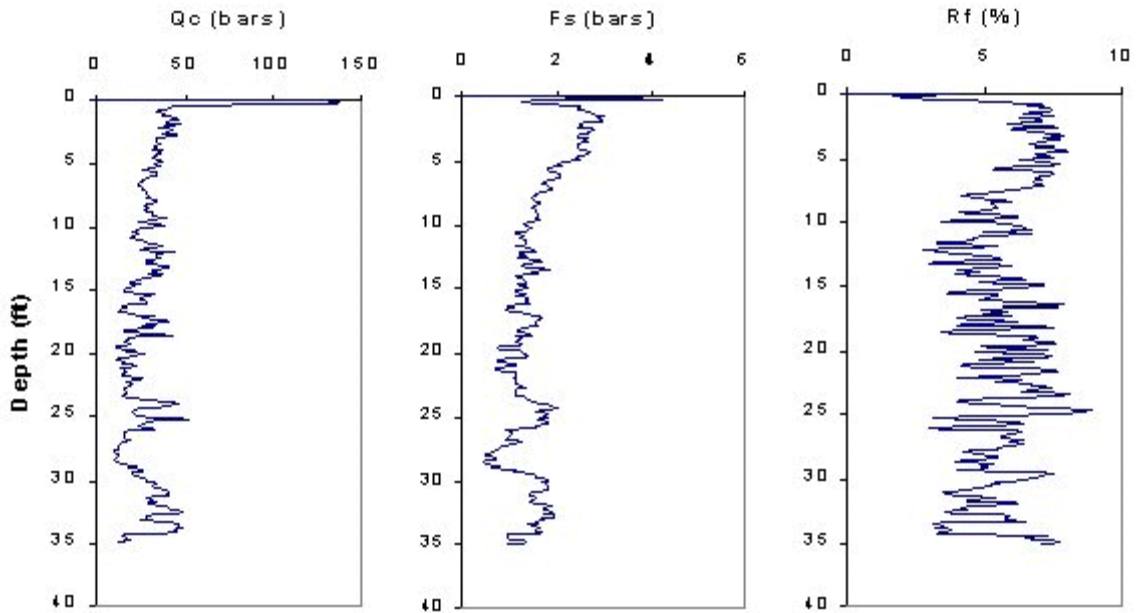


Figure 5.4 - TS-2 mini CPT sounding

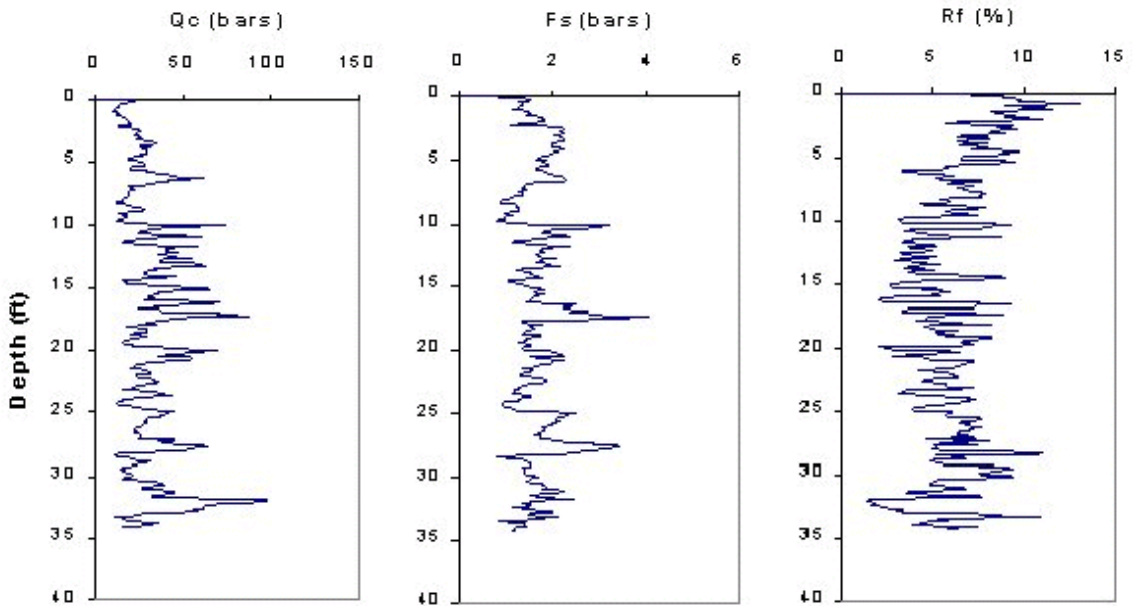


Figure 5.5 - TS-3 mini CPT sounding

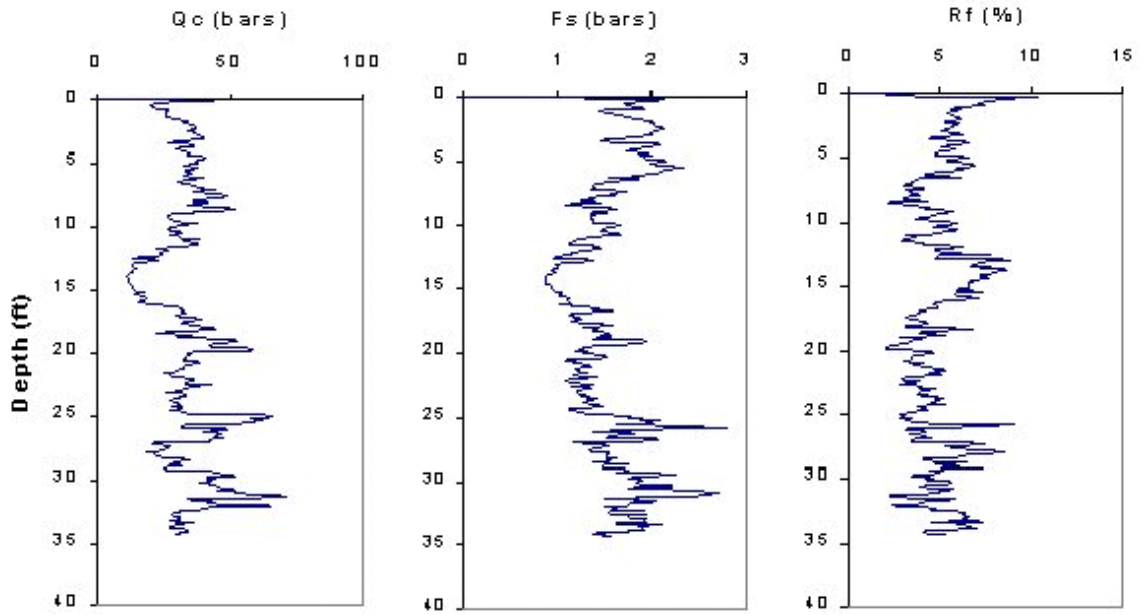


Figure 5.6 - TS-4 mini CPT sounding

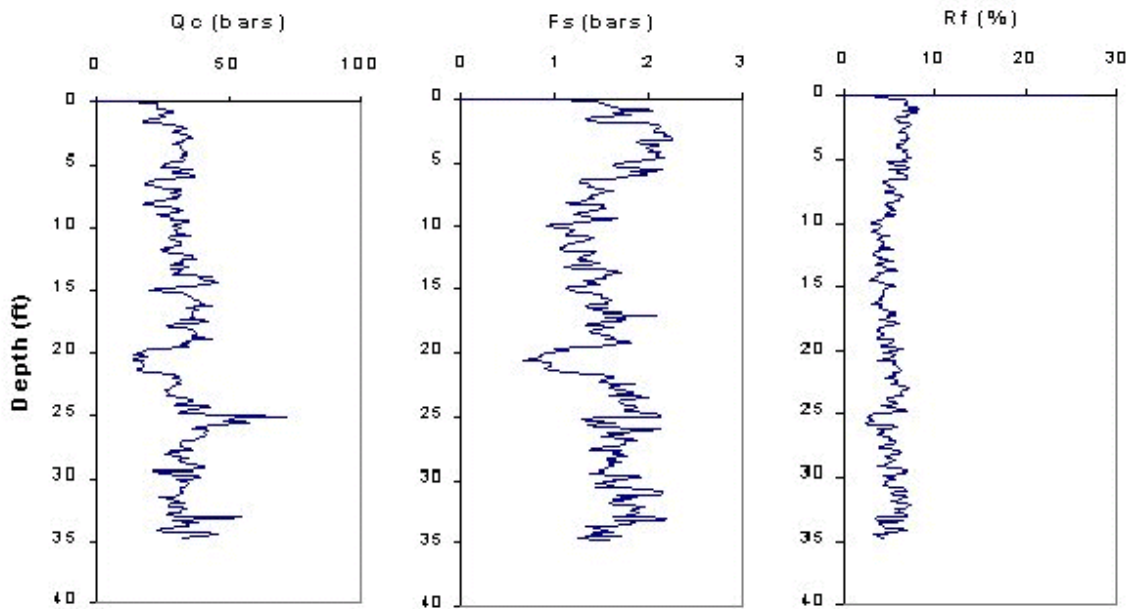


Figure 5.7 - TS-5 mini CPT sounding

The shafts were laid out as shown in Figure 5.8. Two rows of shafts were excavated, with the inside-to-inside spacing equal to 17.5 feet, which is approximately 5 shaft diameters. This same spacing was also used between the two rows of shafts. This was done to ensure that the radial zone of influence from each shaft did not interfere with that of adjacent shafts. Five shaft diameters is greater than the value recommended in recent literature to minimize group effects in drilled shafts (O'Neill, 1981; Poulos, 1980).

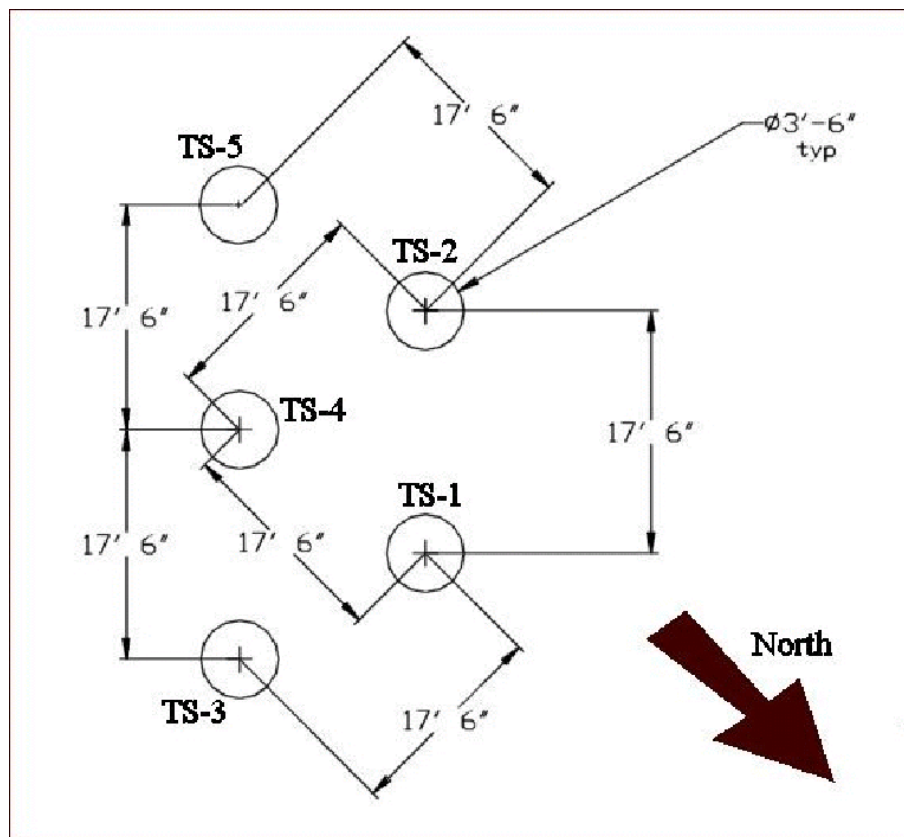


Figure 5.8 - Test shaft layout

5.3 Rebar Cage Preparation Auburn Test Site

The contractor delivered the five rebar cages to the site already assembled according to specifications by Dr. Brown. These cages had an outer diameter of 31 inches and a length of 25 feet. This allowed for 12 inches of rebar stick-up in each of the finished shafts, which would make future extraction of the shafts easier. Longitudinal steel consisted of two DYWIDAG bars, 16 #9 bars, and 75 #4 shear hoops spaced at 4 inches on edge (clear spacing). One of the cages (TS-5) was observed to have tighter shear steel spacing, measured to be 3.2 inches on edge. This cage had 93 hoops. The DYWIDAG bars would be used to extract the drilled shafts.

Sister bars were installed at the toe on each cage (four per cage). These were configured with full bridge strain gauge devices, and were placed at quarter points around the circumference of each cage. The wiring for the gauges was collected in a single harness that was secured to the shear stirrups along the length of each cage, and a service loop was left at the top for future access. The purpose of the gauges was to provide a method to measure the strain of the reinforcement on the interior of the drilled shaft.

Every cage was fitted with steel CSL access tubes installed at third points along the circumference. These tubes were sealed at the bottom to prevent concrete from entering them, which would render them unusable; however later it would be shown that they were not sealed well enough to prevent grout from entering them during the post grouting procedure.

Four of the five cages had post grout cells installed at the toe. The type of cell used on these shafts is known as a “flat jack” system (Dapp, 2002). PVC grout tubes were installed along the length of the cage and mate with ports installed on the steel plate of the cell. Also for four of the five cages, prefabricated anomalies were incorporated. This was done by attaching sand bags full of local material to predetermined locations on each cage. Location TS-1 contained a cluster of bags at the toe, resting atop the post grout cell within the rebar cage. Location TS-2 had an annular neck centered on a CSL tube and located approximately 3/4 the shaft length down from the top. This neck encompassed an area on the cage measuring 18 inches in depth by 34 inches along the circumference. Location TS-3 had an annular neck installed at mid-height on the cage. This anomaly measured 23 inches in depth by 56 inches along the circumference. Location TS-5 contained an anomaly similar to that of TS-2, however this one was placed between CSL access tubes and approximately 1/4 the shaft length down from the top of shaft. The area it encompassed measured 18 inches in depth by 31 inches along the circumference. Only the cage placed in location TS-4 was left without a post grout cell. This cage also contained no prefabricated anomaly. Figure 5.9 shows the different stages of rebar cage, anomaly and instrumentation placement.

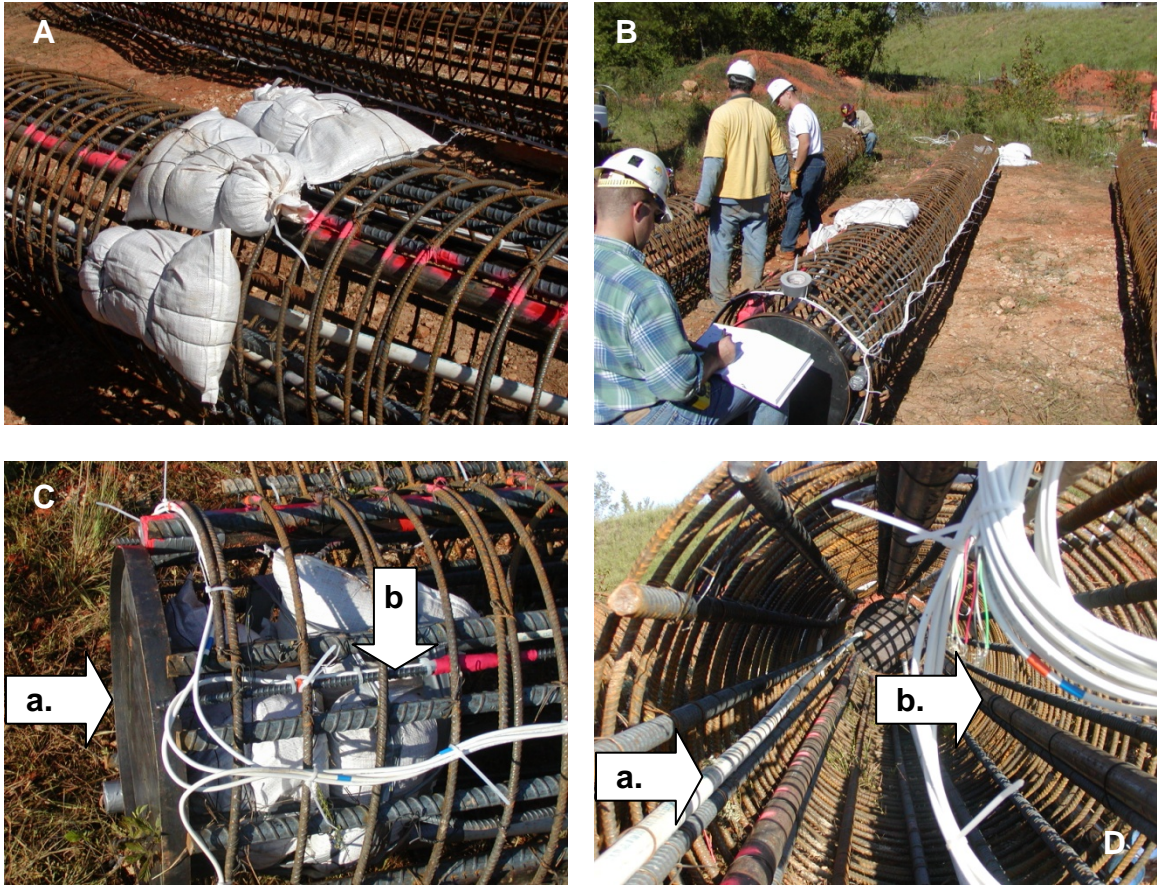


Figure 5.9 - Auburn test shafts set-up, A - example of sand bag anomaly attached to rebar cage, B - overall picture of rebar cage, C - close up view of toe of TS-1 (a. post grout cell, b. sister bar), D - inside of rebar cage (a. grout tube, b. CSL / thermal access tube)

5.4 Drilled Shaft Excavation and Cage Placement

The excavation of the five shafts was completed in one afternoon and each shaft was poured on that day. A truck-mounted, diesel drill rig equipped with a double-flight rotary auger with stinger was supplied by the contractor, as shown in Figure 5.10.

Each of the five shafts was excavated in dry conditions with no casing. This was appropriate because the soil was non-caving and the water table was below the proposed bottom elevation of the borehole, as shown in Figure 5.10. Because of this, drilling proceeded quickly and each excavation was finished in approximately 30 minutes. Also, the clean-out bucket was not used because there was little loose material left at the bottom of the excavation once auger drilling was complete. This was verified using the borescope.

As noted, the water table was below the bottom elevation of each excavation, so the holes remained relatively dry. Tremie placed concrete under water was chosen for constructing the control shaft. Therefore, the excavation denoted TS-4 was filled with water prior to placing the rebar cage. This was performed using water stored in a tank onsite. After the hole was filled with water, the borescope was again used to verify the final quality of the excavation before placement of the rebar cage.

Following the excavations, the rebar cages were lowered into the excavated holes using a crane. Nylon centralizers were utilized to maintain clearance between the rebar cage and the sides of the shaft.

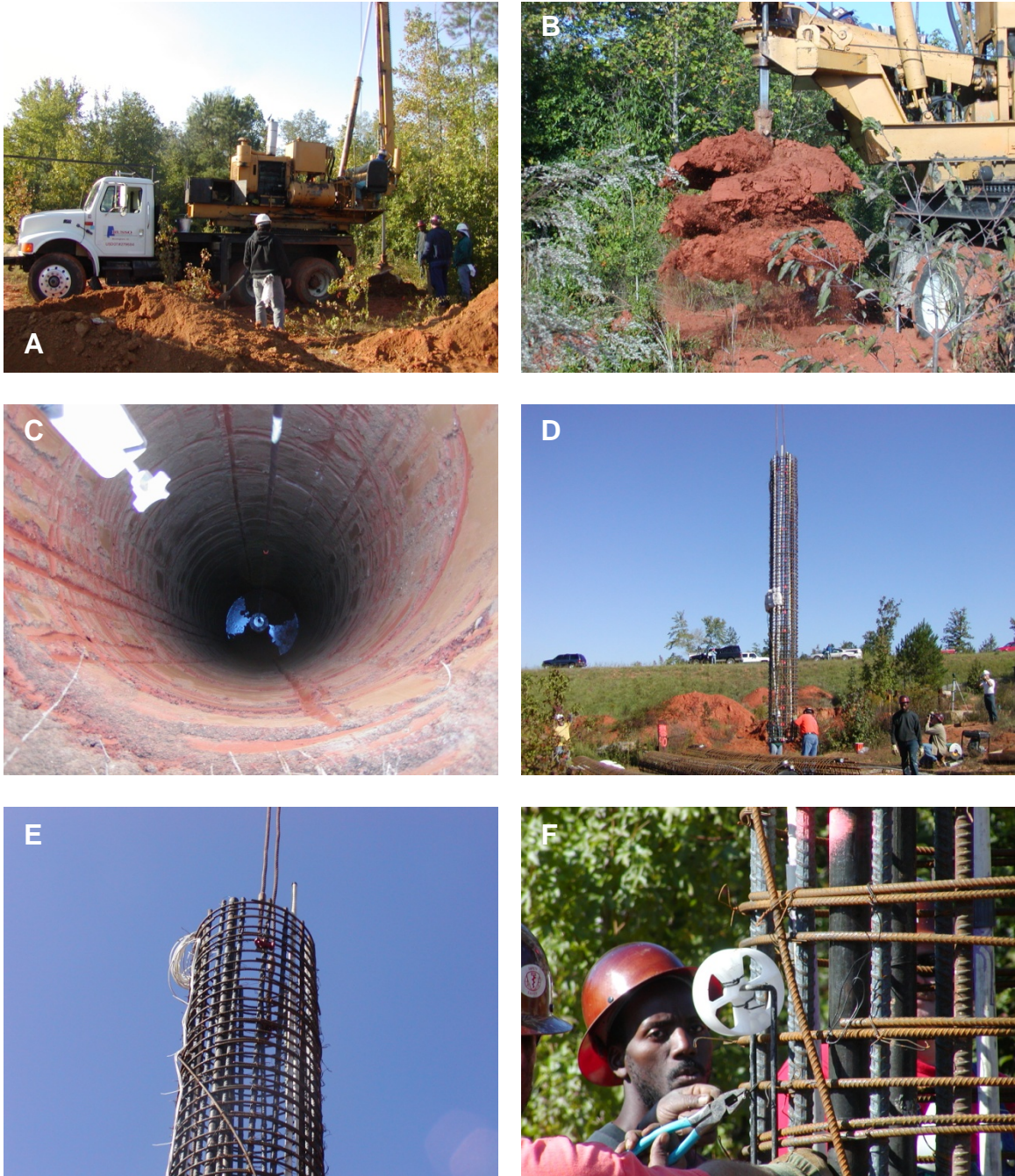


Figure 5.10 – Excavation and erection for Auburn test shafts, A - truck mounted drill rig, B - close up of double flight rotary auger, C - completed excavation being inspected with bore scope, D - centralizer

5.5 Mix Specifications

Several different concrete mix designs were used in this study. The first two shafts poured used a standard portland cement concrete with #57 angular stone (maximum aggregate size of 1 inch). These two mixes were identical except for the slump. One of the mixes was required to have a slump of 8 to 9 inches, while the other needed a slump of 5 to 7 inches. FDOT recommends a slump of 7 to 9 inches for all drilled shafts constructed using the tremie placed method, so this governed the selection of slumps for the test mixes.

One shaft was constructed using a standard portland cement concrete and #7 river rock. This particular aggregate is rounded and has a maximum aggregate size of ½ inch. Number 7 stone is not typically used on FDOT drilled shaft projects. However, it was anticipated that this mix design should perform much better than the #57 stone mix in terms of tremie placement and flow-ability.

The remaining two shafts, one of which was the control shaft constructed under water, used a mix known as a “Self Compacting Concrete” (SCC). Part of the research being conducted during this multiple phase study was the performance characteristics of SCC; therefore, additional comments are warranted. SCC mix design is a very fluid, high slump (>10 inches) material that is designed to exhibit very favorable flow characteristics even in the presence of tight rebar spacing. Because of this, a different assessment of workability is normally used with a SCC mix. The apparatus, pictured in Figure 5.11, measures the flow of the material through a series of rebar sections. Detailed information

regarding this method of testing can be found in literature by Hodgson (2003) at Auburn University.

SCC mixes generally have higher cement contents and higher fines, with lower water to cement ratios and high dosages of high range water reducers (W.R. Grace, 2003). The first SCC mix was modified at the site by the addition of Glenium 3000NS to reach the required slump. This delayed addition of the high range water reducer could be responsible for different characteristics between the mixes for TS-4 and TS-5. Of other significance is the high water to cementitious ratio. Generally SCC mixes have lower water to cement ratios, 0.32 to 0.38, to avoid excess bleed water and segregation which can result from the high dosages of high range water reducers. Figure 5.11 indicates flow tests performed on the SCC mix and Table 5.1 details the 5 mixes used for the Auburn test shaft series.

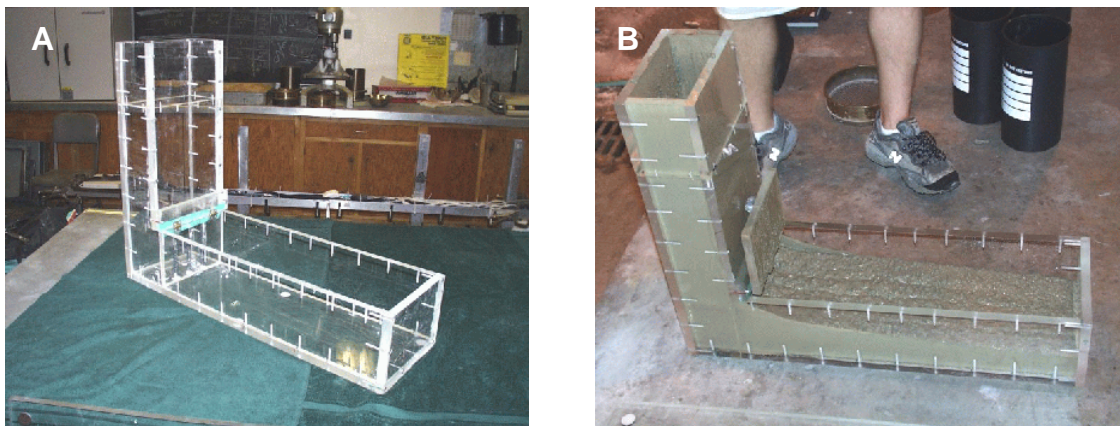


Figure 5.11 - Flow tests for SCC mixes, A - “L”-box flow test device used for measuring the flow of SCC mixes, B - material flows through lower gate and drop height is recorded

Table 5.1 - Detailed summary of concrete mixes

Material	TS-1 & 3	TS-2	TS-4 & 5
Cement Type I	560 lbs/cy	560 lbs/cy	420 lbs/cy
Fly Ash Class F	140 lbs/cy	140 lbs/cy	-
Fly Ash Class C	-	-	227 lbs/cy
GGBF Slag	-	-	97 lbs/cy
Sand	1075 lbs/cy	1075 lbs/cy	1595 lbs/cy
#57 Limestone	1900 lbs/cy	-	-
#7 Pea Gravel	-	1900 lbs/cy	1231 lbs/cy
Water	34 gals/cy	34 gals/cy	40 gals/cy
Micro Air (Air Ent.)	4.5 oz/cwt	4.5 oz/cwt	-
Delvo (HRWR)	40 oz	40 oz	-
Glenium 3000NS	-	-	4.0 oz/cwt
Water / Cementitious Ratio	0.4	0.4	0.45

5.6 Quality Assurance

The deliberate placement of anomalous regions within the shafts offered an opportunity to compare different non-destructive quality assurance methods. Cross-hole Sonic Logging and Thermal Integrity Profiling were performed on each shaft shortly following construction. Sonic Integrity Testing was also performed on each shaft during the curing of the shaft. Once fully cured, the four shafts containing grout cells were tip-grouted while monitoring both the grout pressure and upward displacement.

5.7 Cross-Hole Sonic Logging Auburn Test Shafts

Cross-Hole Sonic Logging readings for each shaft were taken at approximate 12 hour intervals for two days following shaft construction. A review of several of the completed tests and a discussion of each are included below. Refer to CSL Test Data from Auburn in the Appendix for additional information. Test shaft TS-3 included an anomaly at the mid-depth of the shaft centered on access tube B or tube 2. The signal does not show significant change from these readings. The Velocity and Arrival Time, Energy plots for this series of tests are shown in Figure 5.12 and the Anomaly placed in TS-3 is shown in Figure 5.13.

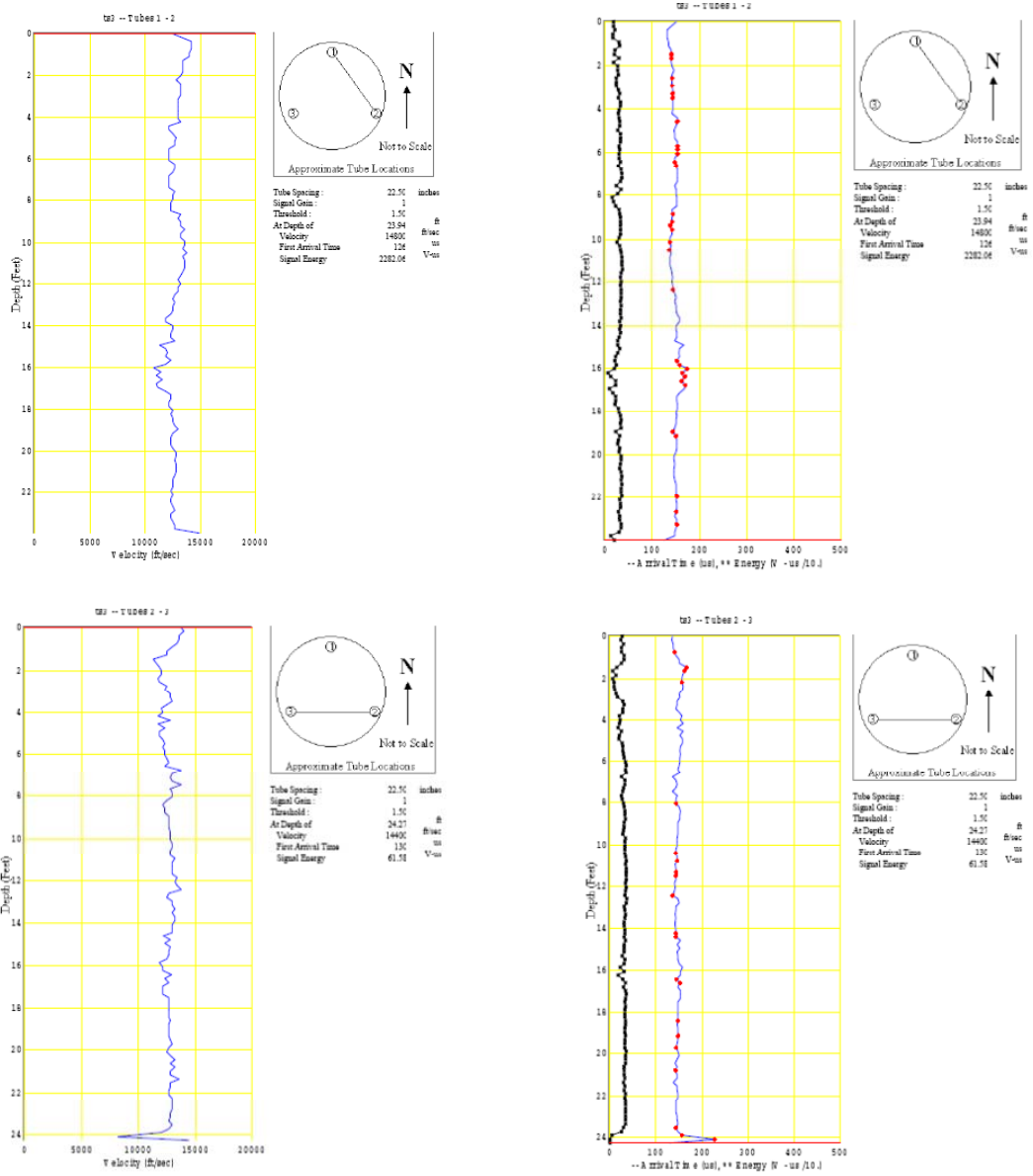


Figure 5.12 - CSL velocity and energy plots for test shaft TS-3 - all tube pairs

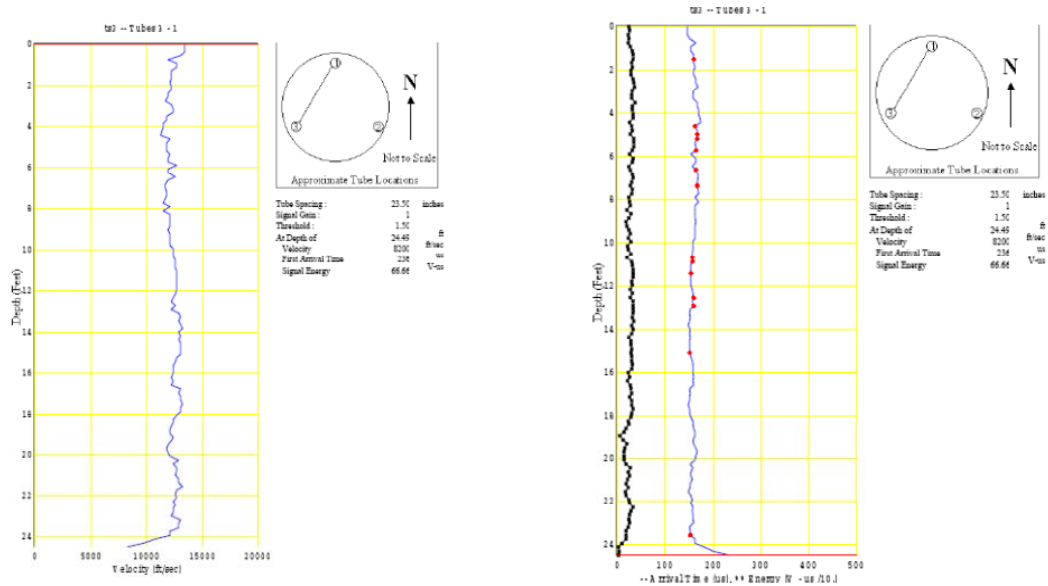


Figure 5.12 (Continued)



Figure 5.13 - Sand bag anomaly centered on tube B (2) for TS-3 Auburn test site

As can be seen from the above information, the results from these CSL tests failed to identify this substantial inclusion on the side of the drilled shaft. Similarly, results from TS-2 and TS-5 do not indicate the presence of anomalous regions in the test shafts. This is due to the fact that the included anomalies for these shafts are not arranged inside of the triangulated path between the 3 CSL tubes, but rather attached to the outside of the rebar cage.

The control shaft, TS-4 as shown in Figure 5.14 shows no significant change in velocity for all readings, although when excavated, TS-4 had a bullet shaped toe with CSL tubes exposed.

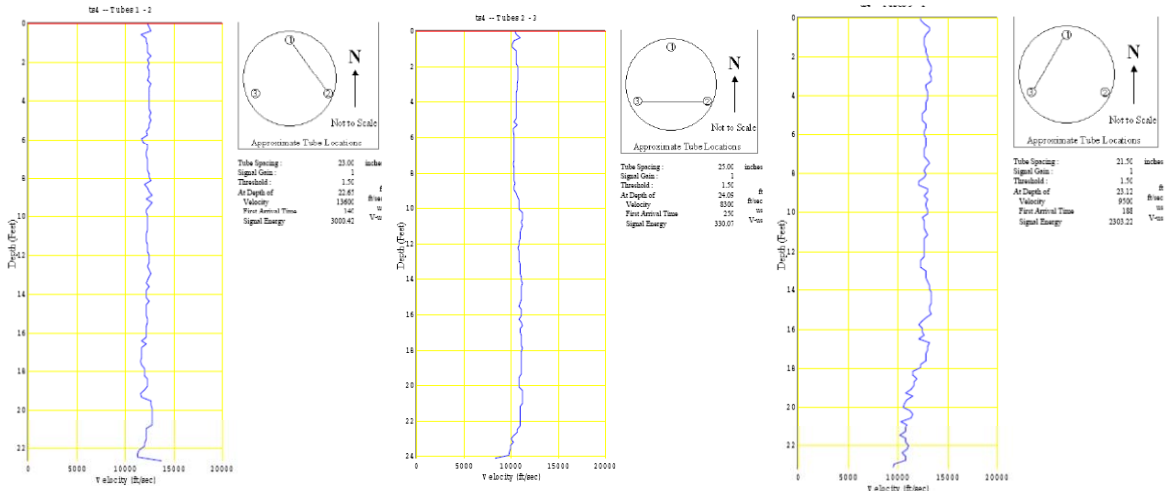


Figure 5.14 - Control shaft TS-4 and the CSL test results for TS-4 Auburn test site

The results of the CSL test from TS-1 shows a decreasing velocity in tube pair 1-2 from 23 to 24 feet. This indicates a less dense material within this region which is indicative of the included sand bags at the toe. The decrease in density was not evident in the other two tube pairs in the shaft. The results of these tests along with pictures of the anomaly are included in Figure 5.15.

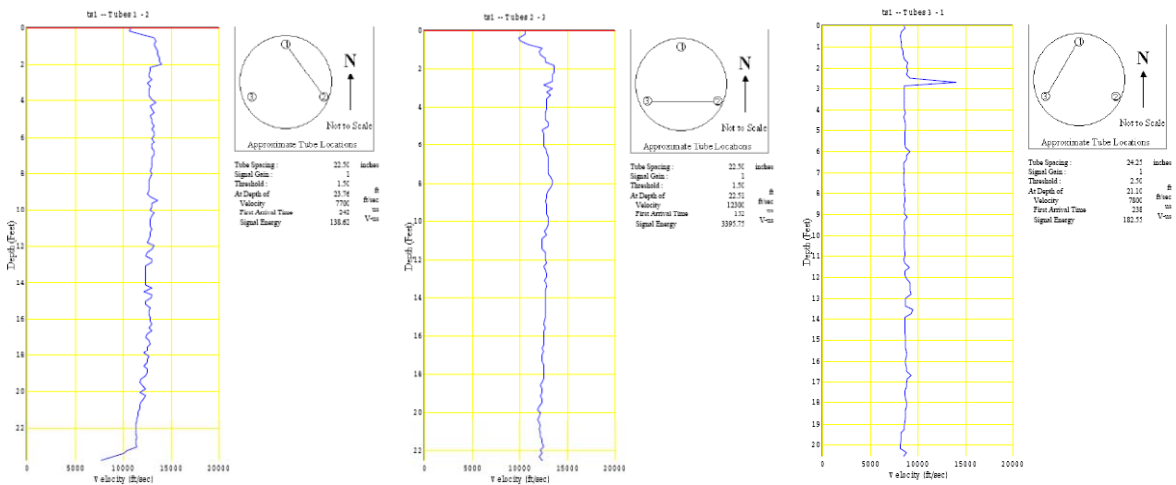


Figure 5.15 - TS-1 CSL data and toe anomaly Auburn test site

5.8 Shaft Integrity Testing Auburn Test Shafts

The goal of this non-destructive testing was to detect the anomalous regions placed within the test shafts and compare this testing method with both CSL and Thermal Integrity Profiling. The first SET test was completed approximately 48 hours following the placement of the concrete in the test shafts and the second test was completed at approximately 72 hours following concrete placement. The results of the first two SET tests found a large attenuation of the signal due to the concrete still being fresh. See Figure 5.16 for SET test set-up showing the impact hammer, accelerometer and data acquisition system.



Figure 5.16 - SET test set-up for Auburn test site

Additional SET soundings were taken prior to post grouting, after load testing, and after extraction. These readings were taken to show the additional effects of post grouting, load testing, and the influence of the surrounding soil.

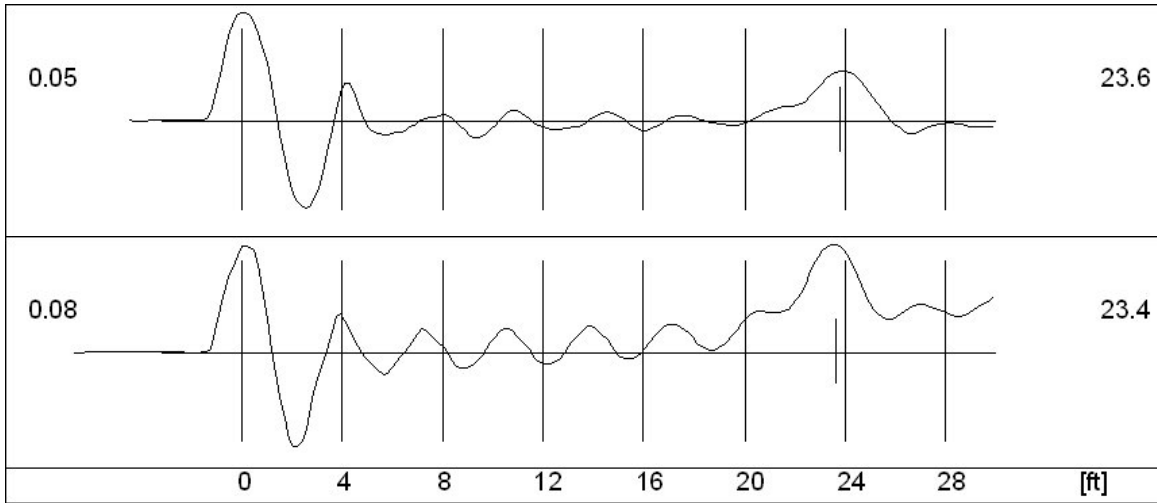


Figure 5.17 - SET data for TS-1 before grouting (top) and after load testing (bottom)

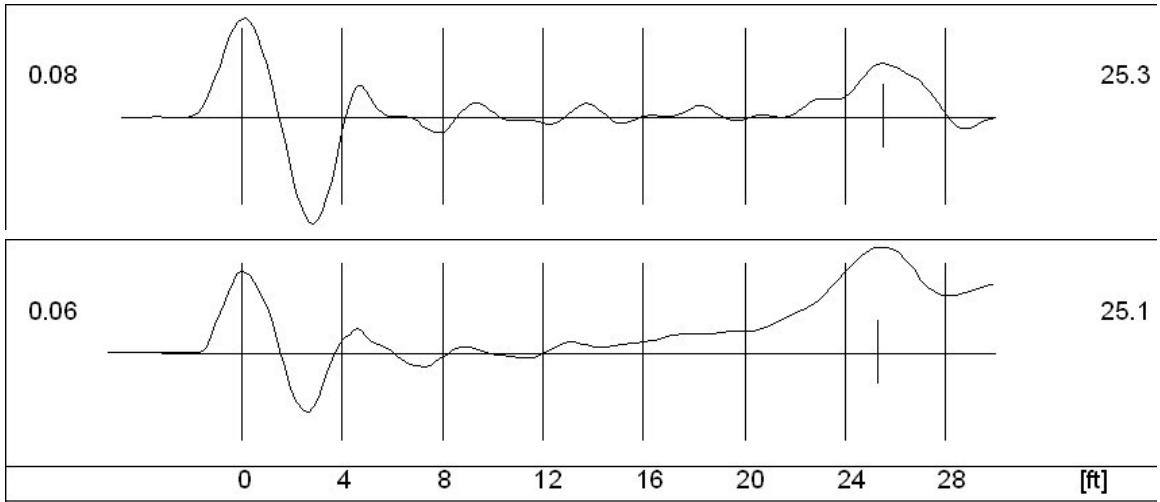


Figure 5.18 - SET data for TS-2 before grouting (top) and after load testing (bottom)

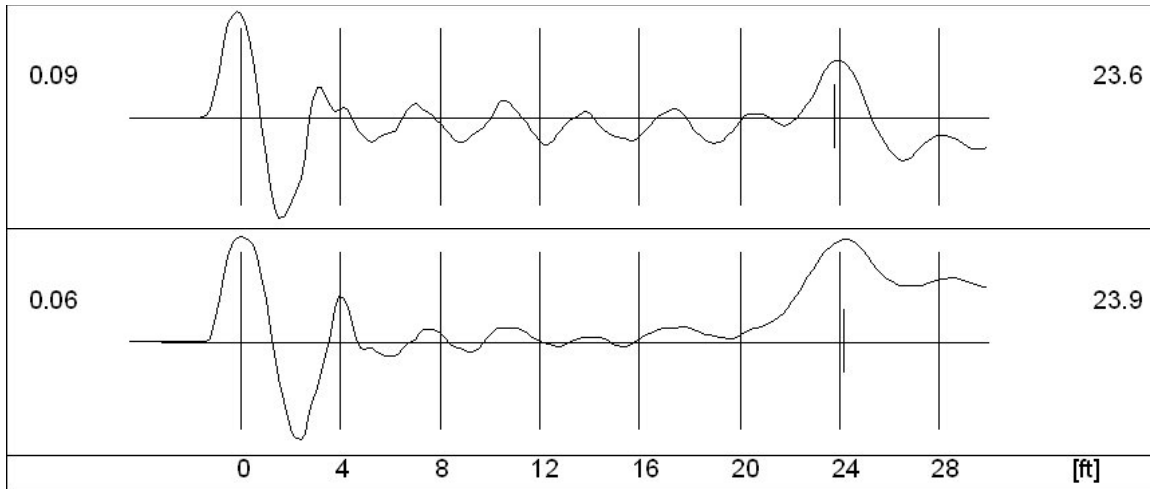


Figure 5.19 - SET data for TS-3 before grouting (top) and after load testing (bottom)

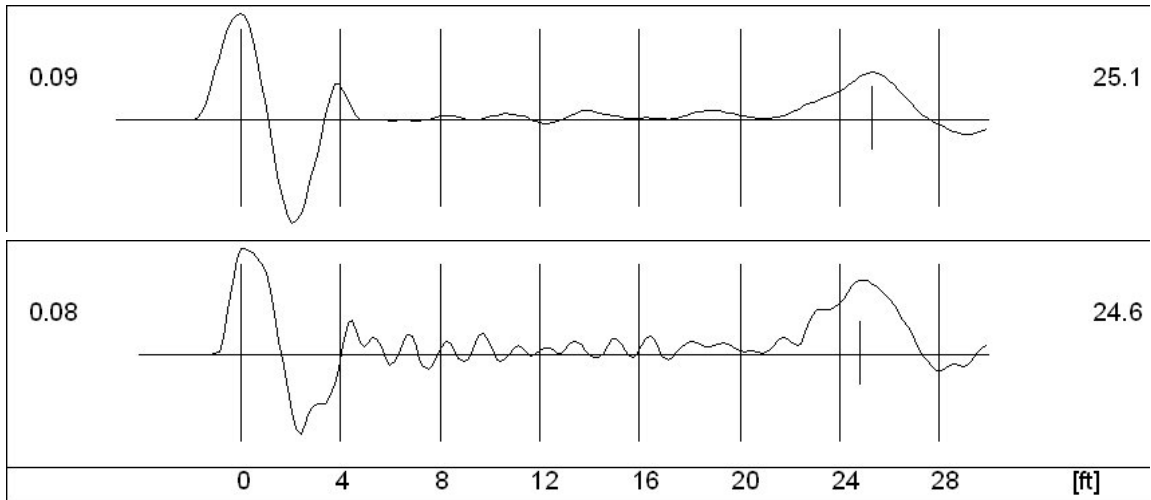


Figure 5.20 - SET data for TS-4 before grouting (top) and after load testing (bottom)

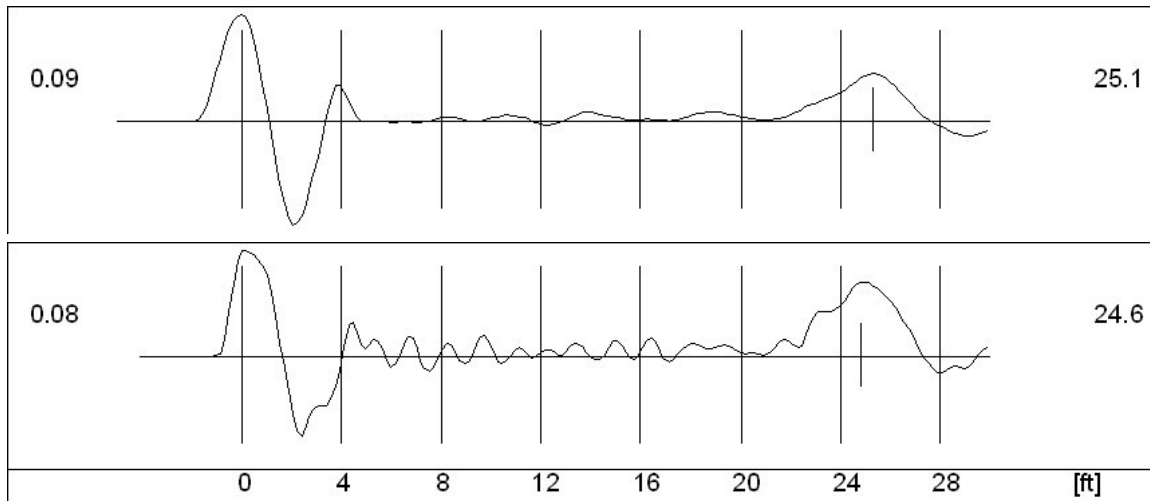


Figure 5.21 - SET data for TS-5 before grouting (top) and after load testing (bottom)

Figures 5.17 through 5.21 show the results from the SIT soundings prior to post grouting and after load testing for TS-1 through TS-5, respectively. Comparing all of the SIT test data sets to the control shaft, it is only slightly apparent in TS-3 that a problem may exist in the test shaft in that there are several different intermediate reflector sets. As may be expected, TS-1, TS-2, and TS-3 show a stronger toe reflection after grouting and load testing. Additional information on the effects of post grouting can be found in Mullins and Winters (2004).

5.9 Thermal Integrity Profiling – Auburn Test Shafts

Thermal temperature readings were taken in the same fashion as CSL and in similar manners as taken in the earlier tests; however, the results proved more promising. Temperature soundings were taken in each of the three access tubes for all 5 shafts roughly every 4-6 hours over a 2 day period. Despite the very high thermal conductivity

of the steel access tubes, the thermal signal was repeatable and sensitive on the order of 0.1° F. See Figure 5.22 for thermal test setup and testing in progress.



Figure 5.22 - TIP testing at Auburn test site, A - tripod, depth wheel, tripod and down hole sensor, B - driver motor and pulleys, signal conditioning and portable computer, C - overall test setup, D - screen shot showing real time thermal sensors

As stated earlier, the CSL data failed to show any significant anomalies in test shaft TS-2. However, the thermal data taken from shaft TS-2B show the effects that boundary conditions and diffusivity changes of various materials have on the heat flow regime of a drilled shaft. The data show sharply increasing temperature curves at the top of the shaft, with peak temperatures occurring at a depth of 7 to 8 feet. Below this depth temperatures are decreasing somewhat steeply, with a flattening of the curves occurring around the shaft midpoint. At 13 feet deep, a 6 inch pipe coupling induces a temperature increase on all the traces, below which is the sandbag anomaly. Pipe coupling anomalies are identifiable in all shaft traces where a coupling exists. Below this point, the thermal signal decreases steeply as some of the heat flow is diminished due to changing boundary conditions: increasing free water in pore spaces in the capillary fringe (previously noted GWT below tip of shafts >24 feet) and the end condition, requiring outward heat flow with both radial and vertical components. The anomaly at the third quarter point can be seen in all four traces at approximately 17 to 22 feet, with the coolest temperature trace (outward-facing) showing the greatest anomaly. The base of the anomalous signal is clearly defined by the sharply increasing temperature curve beginning at 20 feet, progressing toward the non-anomalous temperature. This upward temperature change occurs over approximately a 1 foot vertical span in which the purely outward radial heat flow of a cylinder is disrupted, adding a vertical component of heat flow. The placement of the sandbag adjacent to the coupling enhances the heat flow (vertically and radially) through the coupling and around the sandbag. This “heat channeling” effect may raise the temperature above that of the neighboring material, which appears to contradict

Fourier's Law $Q = -k \frac{dT}{dx}$ (where k is the thermal conductivity), but which is only valid in a constant- k domain.

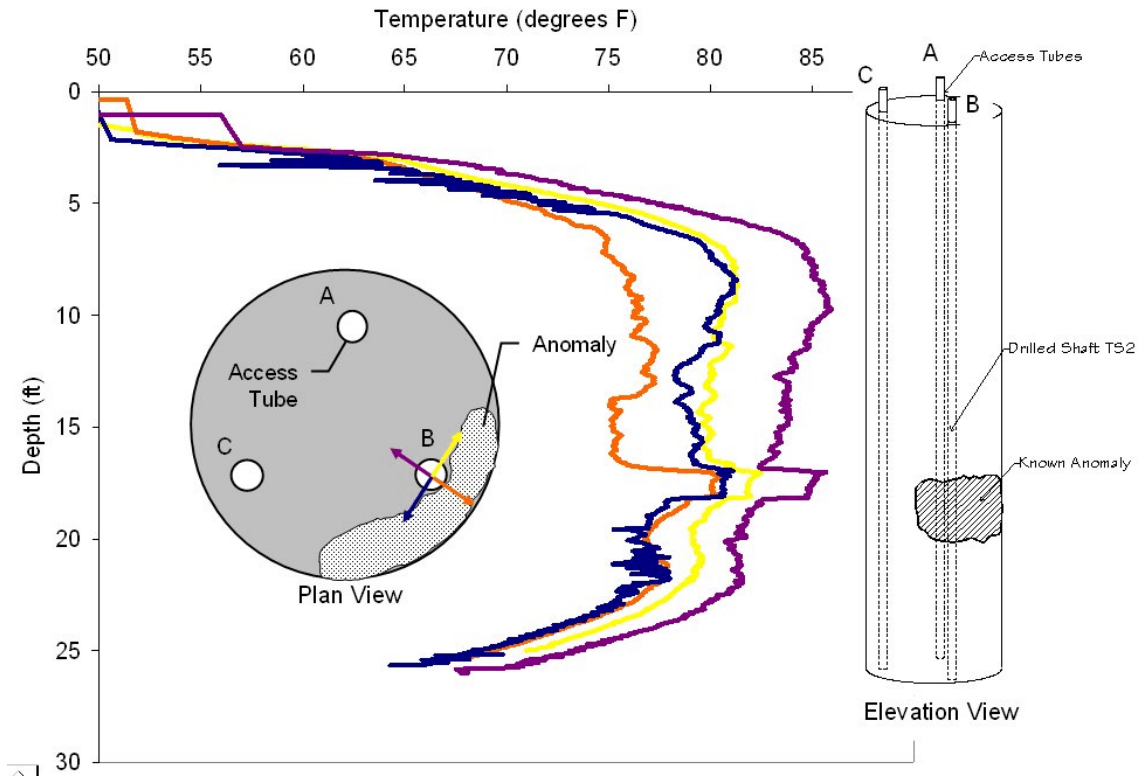


Figure 5.23 - Temperature traces vs. depth for test shaft TS-2 Auburn test site

During the process of doing the production Thermal Integrity Profiling Tests, the author noticed apparent problems associated with both sensitivity and noise. Specifically, the manufacturer's specification of the infrared thermocouple gives a repeatability error for any device without temperature control, such as in this design of 1 to 2% of reading value, and for complete ambient temperature control an error of 0.01% of value. This is a large range of values, and an analysis of sampled signal and noise may more accurately place the expected values of error and signal/noise for this design.

Figure 5.24 shows the magnitude spectrum of the outward-facing sensor data from access tube A of shaft TS-3. Note that this spectral peak at 0 Hz resides in the decade 100-1000 degrees, so that magnitude percentages can be read approximately from the log plot. The plot was generated using 441 data from the trace TS-3A (outward), and was zero-padded to 512 points, and Fourier transformed using the “boxcar” window only. Without any filter windows the boxcar will yield spectra that are factorable into sinc functions, where $\text{sinc}(x) = \sin(x)/x$, which produce the lobes seen throughout the data. This effect itself introduces noise to the transformed data.

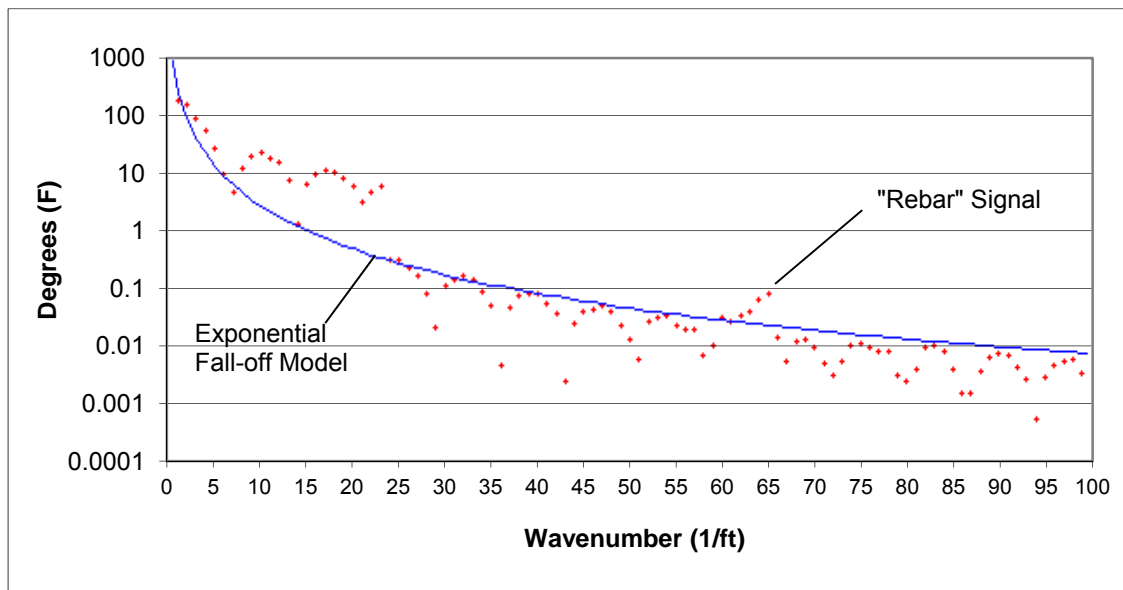


Figure 5.24 - Fourier analysis of inward-facing sensor temperature data for shaft TS-3 (tube A) Auburn test site

The data exhibit a 0.5dB amplitude falloff per wavenumber and a total drop of ~15dB for wavenumbers < 30. This spatial frequency (wavenumber = 30) represents a wavelength of 8.8 inches, and it suggests that important information in the data can be restricted statistically to length scales larger than 8.8 inches. Also at this wavenumber, spectral magnitude falls below approximately 1% of the maximum value, the nominal

signal error. The data “noise” appears to follow an exponential falloff which is shown by the curve in Figure 5.24. The exception to this trend occurs at wavenumber equal to 62 to 65, which were in part masked by the lobular character of the data, but which clearly stands above the curve. These wavenumbers have equivalent wavelengths of 4.06 to 4.26 inches, indicating rebar signal in the data, which is concordant with the placement of circular hoop rebar at nominal 4 inch separations, although some cages had smaller clear spacing.

Figure 5.25 shows four “rebar-filtered” traces of shaft TS-3A and the unfiltered trace. The unfiltered trace shows a strong heat transfer coupling between the circular rebar hoops and the access tube nearby which the data was taken. Although the rebar “signals” are readily apparent in the trace, their magnitude is $<0.1\%$, higher than that of a temperature controlled device, but much less than expected in this device. This signal is sufficiently greater than the combination of all sources of noise, including uncontrolled ambient temperature and those introduced by poor data transformations (i.e., the unwindowed FFT). It should be concluded that the sensitivity and signal/noise ratio have surpassed the predicted values for this design.

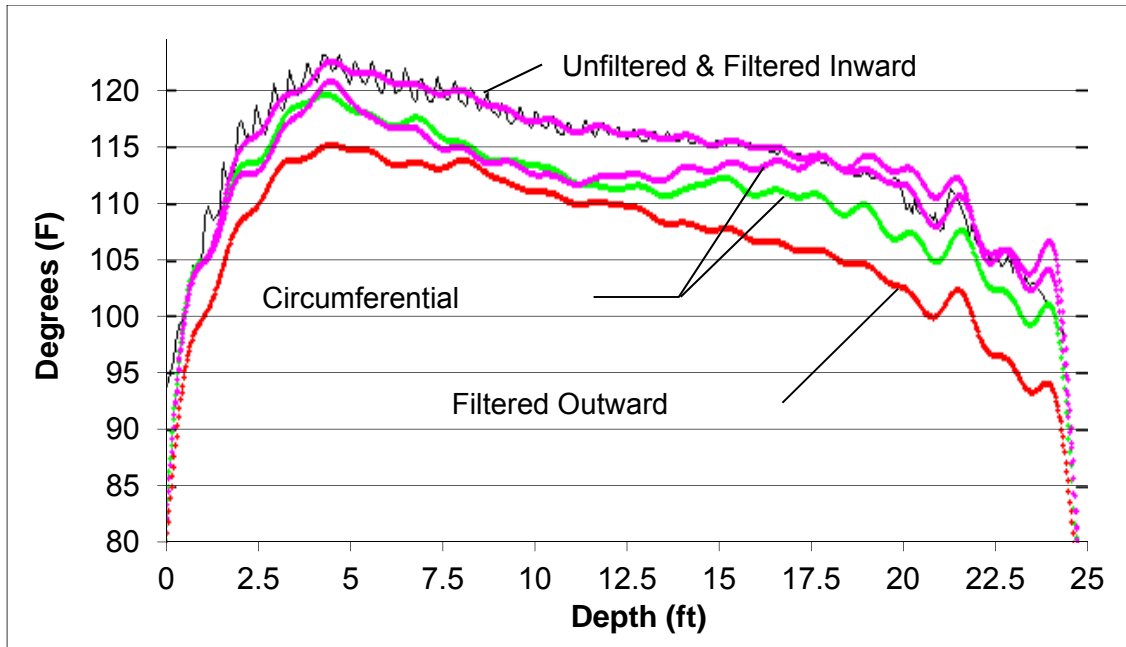


Figure 5.25 - Low-passed (“rebar-filtered”) temperature traces and one unfiltered trace of the inward-facing channel from shaft TS-3 (tube A) Auburn test site

As stated earlier, several problems became apparent during the various tests, these will be discussed further at the close of this chapter. Additional information in regards to the Auburn tests can be found in Appendix C.

5.10 Post Grout– Auburn Test Site

Post grouting was performed on four of the five test shafts (TS-1, TS-2, TS-3, and TS-5) approximately 13 days after initial concrete placement. portland type I cement with a w/c ratio of 0.55 was pumped to the tip of each shaft. Figure 5.26 shows the grouting process and test setup.

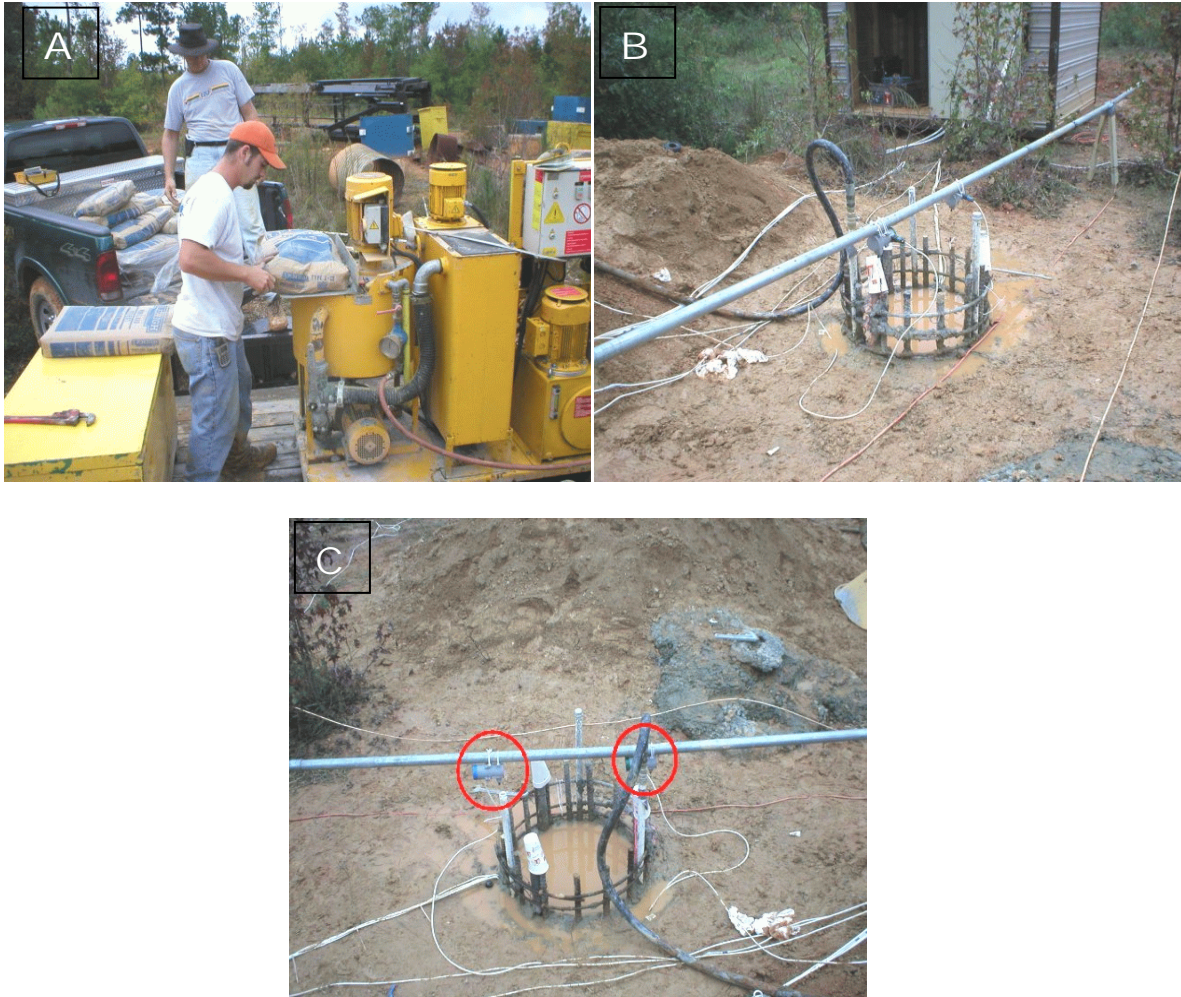


Figure 5.26 - Post Grouting at Auburn test site, A - grout pump and mixing of grout, B - injection of grout into top of shaft, C - string potentiometers used to measure vertical displacement of shaft

The specified upward displacement was set at 2.5% the diameter (approximately 1 inch for the 42 inch diameter shafts). The displacement and grout pressure were monitored during the grouting process with string potentiometers and a pressure transducer. The strains at the toe of the test shafts were also measured by four resistive strain gauges. The post grouting results are summarized as follows:

- ✧ TS-1 maximum grout pressure of 82 psi and uplift of 0.105 inches

- ✧ TS-2 maximum grout pressure of 88 psi and uplift of 0.074 inches

- ✧ TS-3 maximum grout pressure of 100 psi and uplift of 0.132 inches

- ✧ TS-5 maximum grout pressure of 109 psi and uplift of 0.075 inches

Additional information on the post grouting and the results of the post grouting program may be found in (Mullins and Ashmawy, 2005).

5.11 Additional Testing – Auburn Test Site

In addition to the aforementioned tests, researchers from the University of South Florida and Auburn University performed the following tests on the shafts:

1. As shown in figure 5.27, the test shafts were load tested utilizing an axial compressive force pulse (rapid) testing method. This testing method which is commonly referred to as statnamic load testing was performed on all shafts using a 4 MN statnamic device, equipped with the hydraulic catching mechanism. Two load cycles were performed on each shaft; the target displacement was set at 2.5% the shaft diameter. The strain gauges located at the toe of each shaft made it possible to separate the applied load into side friction and end bearing

components. A sample of the side shear results from the first load cycles can be seen in Figure 5.28. The figure also shows the respective slumps for each test shaft. The results show that within this test program the slump does not affect the side shear component.



Figure 5.27 - 4MN static load test setup Auburn test site

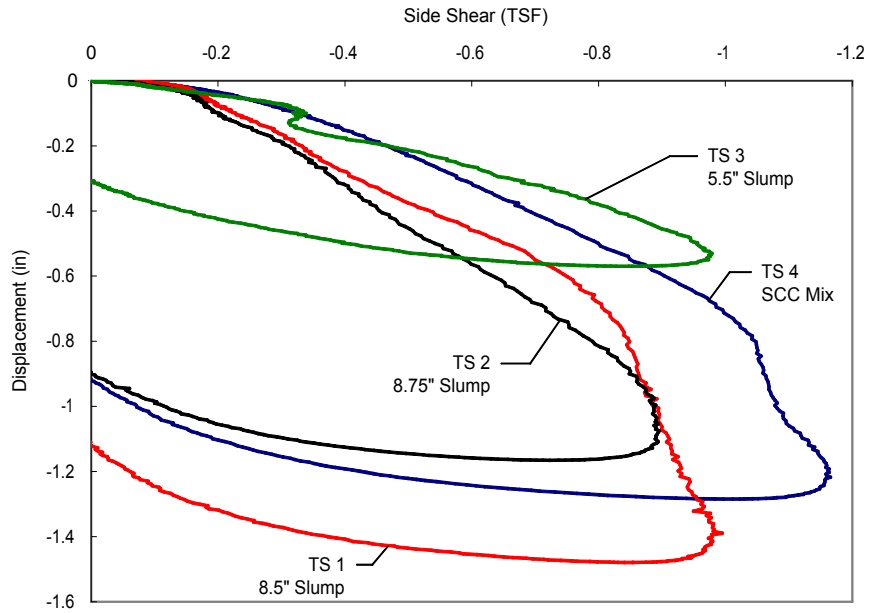


Figure 5.28 - Sample of rapid load test results on Auburn test shafts

2. Following the load testing, the shafts were exhumed and dissected to fully document the condition of the final shafts. Examples of this process can be seen in Figure 5.29.



Figure 5.29 - Exhuming, coring and dissecting the test shafts at the Auburn test site

3. Following the excavation, coring and dissecting of the test shafts, the shafts were examined for confirmation of placed anomalies and aggregate distribution. Permeability tests were completed on the test shafts.

5.12 Lessons Learned from Thermal Integrity Profiling - Auburn Test Site

Although several sets of very good data was retrieved at the Auburn test site that showed great promise, the testing was not as successful as originally envisioned. Several distinct lessons were learned from the Auburn Test Program.

First, during one of the initial tests, the alignment wheels on the down hole portion of the thermal device became lodged in between two segments of the steel pipe access tube at the location of a couple. This caused the down hole assembly to become stuck inside of the shaft and took several hours to dislodge. This led to the conclusion that either a completely smooth access tube is required or the development of an alignment that had more tolerance was required. The use of a completely smooth access tube is not reasonable in a production scenario. In future tests, it would be shown that it is not necessary to have an alignment device. The temperature traces from each of the four sensors could be radially adjusted based on the fact that the exterior of the shaft is cooler than the interior.

Second, although the access tubes were excavated of water prior to the testing and the tests were completed in rain free conditions, there was moisture present in both the access tubes and in the atmosphere. Given that the down hole sensor and the depth encoder were enclosed, but not hermetically sealed, the electronic components were susceptible to moisture which caused signal problems. Future versions of the down hole sensor would need to be completely sealed to prevent moisture intrusion.

Third, the use of an alternating current (A/C) driver motor and pulley assembly, which was intended to allow a uniform rate of descent and retrieval of the down hole sensor introduced 60 Hz noise into the signal. This occurred, even though a properly grounded and shielded wire was used. The signal strength from the down hole sensors was not strong enough to not be adversely affected from the alternating current of the motor. Future versions of the system would need to eliminate the driver motor and pulley assembly. If a constant rate of descent / retrieval was necessary, a mechanical solution would need to be developed.

One of the most basic concepts of thermocouple operation, which is discussed in detail in chapter three, is the cold junction. To re-cap, a millivolt signal is produced due to the difference in temperature between two different junctions of differing metal. The first junction is the reference, where the temperature is being measured. The second, where the thermocouple signal is measured, is commonly referred to as the cold junction. During the course of developing the device, the cold junction and the effect that the change of temperature of the connection from the infrared thermocouple to the current loop had on the recorded signal had not been considered. Given that the connection of the infrared thermocouple to the current loop occurred down hole, it meant that this connection was susceptible to the same temperature variants as the infrared thermocouple itself. This cold junction problem led to temperature signals that were not a true reflection of the inside of the access tube. To complicate the problem, there was not an embedded thermocouple in the device that would provide an actual temperature of the device. Having an actual temperature of the device would have allowed for the

correction of the data to account for the cold junction error. This problem was further complicated by the dissimilar metal used on the circuit board at the infrared thermocouple to current loop connection. Future versions of the device would need to either incorporate measures such as a different circuit to eliminate the cold junction problem or the current loop would need to be eliminated, thereby allowing the cold junction to occur at the surface where it would not be susceptible to extreme changes in temperature.

Chapter 6 - Summary and Conclusions

6.1 Overview

This thesis has shown that the development of the instrumentation necessary to provide in-situ thermal imaging for the determination of homogeneity of concrete is theoretically sound.

Drilled shafts are large diameter underground cast-in-place columns that necessarily rely on sound integrity to properly withstand imposed loadings. As a by-product of the most common construction techniques, the entire process is often completely blind whereby the excavation and concreting processes are conducted beneath the surface of the water table (or slurry level). This results in an inability to inspect the final product and in many cases allows anomalous inclusions (soil cave-ins, slurry pockets, etc) to go undetected especially when they are formed outside the steel reinforcing cage.

In an effort to gain verification of the as-built, below ground structure, numerous non-destructive test methods have been devised, all of which have strengths and weaknesses with regards to the full extent of the tested concrete volume. To further this cause, a new methodology was developed that uses the energy from hydrating concrete to assess the presence or absence of an intact concrete. Therein, the temperature generated

by the curing concrete can be measured and correlated to the probable dimensions of the drilled shaft.

This thesis outlines the development of the instrumentation capable of making in-situ temperature measurement of drilled shafts to assure the homogeneity of concrete is acceptable. To that end, several configurations of instrumentation approach were tested on varying scales from small lab specimens to full-size field constructed drilled shafts. The bulk of this work was conducted several years before the completion of the thesis and has the benefit of noting later developments. For instance, this study was used to seed future research and led to subsequent FDOT and WSDOT (Washington State DOT) funded research for the express purpose of identifying capabilities of thermal testing in those states. Likewise, present day practice and use of the approach has also been documented.

6.2 Present Practice

Integrity testing using the thermal method is now being used as an accepted method of drilled shaft integrity testing in multiple states. The frequency of testing is commensurate with other test methods wherein a minimum of 10% of shafts are tested when redundant load paths exist and 100% testing is performed on single shaft non-redundant foundations.

Access tubes (previously only used for CSL or GGL) have been standardized to be 1.5” inner diameter black steel pipe and are installed with the general rule of no less than 1 tube per ft of shaft diameter with a minimum of 4 tubes. This changed from 2 inch I.D. steel (galvanized or black) and a minimum of 3 tubes since this exploratory study was conducted.

Present day equipment is far improved from that used in this study. The field equipment used today has undergone further refinements whereby the infrared sensors are now digital and the data collectors are miniaturized. The depth measurement technique remains essentially unchanged.

Data analysis at the time of the study was basic in nature reporting only temperature as a function of depth for each tube. Present day analysis techniques have evolved to a point where the eccentricity of the cage alignment, the radius of the shaft, and the concrete cover can all be determined. This provides an overall view of the shaft shape and concrete quality throughout that is not possible from other test methods.

List of References

1. AASHTO (2010). "AASHTO LRFD Bridge Design Specifications Customary U.S. Units, Fourth Edition," ISBN: 1-56051-250-4 Publication Code: LRFDUS-4.
2. Alabama Department of Transportation (ADOT), Special Provision No. 01-0712, Section 506, Drilled Shaft Construction, November 28, 2001.
3. Baker, C.N., Parikh, G., Briaud, J.L., Drumright, E.E. and Mensah, F. (1993), *Drilled Shafts for Bridge Foundations*, FHWA Publication No. FHWA-RD-92-004, Federal Highway Administration, McLean, Virginia, August.
4. Blitz, J. (1971). *Ultrasonics: Methods and Applications*, Van Nostrand Reinhold Company, New York, pp. 151.
5. Branagan & Associates, Inc., *Using Crosshole Sonic Logging (CSL) To Test Drilled-Shaft Foundations*, (2002), Branagan & Associates, Inc., Las Vegas, NV.
6. Briaud et al. Briaud J.L., Ballouz M., and Nasr, N., "Defect And Length Predictions by NDT Methods For Nine Bored Piles," 2002, Texas A&M University, Austin, TX.
7. Caltrans (2005). Method of ascertaining the homogeneity of concrete in cast-in-drilled-hole (CIDH) piles using the gamma-gamma test method. California Department of Transportation Specifications, California Test 233.
8. Caltrans (2010). Gamma-gamma logging (GGL).
9. Caltrans, <http://www.dot.ca.gov/hq/esc/geotech/ft/gamma.htm>
10. Davis, A.G. & Hertlein, B.H. (1993), *Evaluation of the Integrity of Some Large Concrete Structures Using NDT*, American Concrete Institute Spring Convention, Vancouver, March.
11. Davis, A.G., & Robertson, S.A. (1976), *Vibration Testing of Piles*, Structural Engineering, June, pp. A7-A10.
12. Doebelin, Ernest O. Measurement systems: Application and Design – 5th ed.; The McGraw-Hill Companies, Inc., New York, NY; 2004.

13. Duarte, A., Campos, T., Araruna, J., and Filho, P. (2006). Thermal properties of unsaturated soils. *Unsaturated Soils*, GSP, ASCE, pp. 1707-1718.
14. Farouki, O. (1966). Physical properties of granular materials with reference to thermal resistivity. Highway Research Record 128, National Research Council, Washington, DC, pp 25-44.
15. FDOT (2010). Standard specifications for road and bridge construction. Florida Department of Transportation, <ftp://ftp.dot.state.fl.us/LTS/CO/Specifications>.
16. FHWA, 2009 - <http://www.cflhd.gov/resources/agm/bibliography/index.cfm>
17. Finno, R.J. & Prommer, P.J. (1994). *Evaluation on Inaccessible Drilled Shafts Using the Impulse Response Method*: Northwestern University, Infrastructure Technology Institute: ITI Publications Directory.
18. Galperin, E.I. (1985), Vertical Seismic Profiling and its Exploration Potential, D. Reidel Publishing Company, Boston, 316 p.
19. Garbin, E.J. (2001), *Drilled Shaft Integrity Study*, University of South Florida Department of Civil and Environmental Engineering, <http://www.eng.usf.edu/~garbin/dshafts/background.htm>
20. Harris, M. (1999). *Sams Teach Yourself Microsoft Excel 2000 Programming in 21 Days*. Sams Publishing, Indianapolis, Indiana.
21. Herne, T.M., Stokoe, K.H. & Reese, L.C. (1981). *Drilled-Shaft Integrity by Wave Propagation Method,*” Journal of Geotechnical Engineering, American Society of Civil Engineers, Volume 107, No. 10, October, pp. 1327-1344.
22. Hertlein, B. (2001). Are our client’s expectations realistic? Geo-Strata, Geo-Institute of the American Society of Civil Engineers, January, p.11.
23. Higgs, J.S. and Robertson, S.A. (1979), *Integrity Testing of Concrete Piles by Shock Method,*” Concrete, October, pp. 31-33.
24. <http://www.dot.ca.gov/hq/esc/geotech/ft/gamma.htm>
25. http://www.dot.ca.gov/hq/esc/geotech/gg/geophysics2002/049rucker_fhwa2002finalgammadensitypaper.pdf
26. Johansen, O. (1975). Thermal conductivity of soils and rocks. Proceedings of the Sixth International Congress of the Foundation Francaise d’Etudes Nordiques, Vol. 2, pp.407-420.
27. Johnson, K. and Mullins, G. (2007). Concrete temperature control via voiding drilled shafts. *Contemporary Issues in Deep Foundations*, ASCE Geo Institute, GSP No.158, Vol. I, pp. 1-12.

28. Kranc, S.C. and Mullins, G. (2007). Inverse method for the detection of voids in drilled shaft concrete piles from longitudinal temperature scans. Inverse Problems Design and Optimization Symposium, Miami, FL, April 16-18, 2007.
29. Lew, M.; Zadoorian, C.J.; Carpenter, L.D., *Integrity Testing of Drilled Piles for Tall Buildings*, Structure, A joint publication of: National Council of Structural Engineers Associations; Council of American Structural Engineers, Structural Engineering Institute, (October 2002), pp. 14-17.
30. MacGregor, J.G., Reinforced Concrete: Mechanics and Design (3rd Edition), (1996), Prentice Hall.
31. Mullins and Kranc, 2004 - U.S. Patent Application
32. Mullins, A.G. and Kranc, S.C. (2004), "Method for Testing Integrity of Concrete Shafts," US Patent No.: US6,783,273 B1, filed April 22, 2002.
33. Mullins, G. (2010). Thermal integrity profiling of drilled shafts. *DFI Journal*, Deep Foundations Institute, Vol. 4, No. 2, pp. 54-64.
34. Mullins, G. and Ashmawy, A. (2005). Factors affecting anomaly formation in drilled shafts. Final Report, FDOT Project BC353-19, March.
35. Mullins, G. and Kranc, S. (2007). "Thermal Integrity Testing of Drilled Shafts - Final Report." FDOT Grant #BD544-20, May.
36. Mullins, G., Winters, D., and Johnson, K. (2009). "Attenuating Mass Concrete Effects in Drilled Shafts." FDOT Grant #BD-544-39, September.
37. O'Neill, M.W. & Reese, L.C. (1999), *Drilled Shafts: Construction Procedures and Design Methods*, U.S. Department of Transportation, Federal Highway Administration (FHWA), Washington D.C.
38. O'Neill, M.W. and Reese, L. C. (1999). *Drilled shafts: construction procedures and design methods*. U.S. Department of Transportation, Publication No. FHWA-IF-99-025, ADSC-TL 4, Volume II.
39. Olson Engineering, *Crosshole Sonic Logging (CSL)*, (2003), www.olsonengineering.com/CSL.html.
40. Omega(2). "Infrared Thermocouples – The Infrared Thermocouple", Accessed August 31, 2011 <http://www.omega.com/literature/transactions/volume1/infrared2.html>
41. OMEGA(4). "Omega Operator's Manual – TX901 Field Rangeable Thermocouple Two-Wire Temperature Transmitters"

42. OMEGA-5. “International Thermocouple Color Codes”, Accessed August 31, 2011, <http://www.omega.com/techref/thermcolorcodes.html>
43. Paikowsky, Samuel G. et al., *Examination of a New Cross-Hole Sonic Logging System for Integrity Testing of Drilled Shafts*, (2000), Geotechnical Engineering Research Laboratory, University of Massachusetts, Lowell, Mass., USA
44. Paquet, J. (1968). “Etude Vibratoire des Pieux en Beton: Response Harmonique,” *Annales Inst. Tech. Batim*, 21st year, No. 245, May, pp. 789-803.
45. Pauly, N. (2010). Thermal conductivity of soils from the analysis of boring logs. Master’s Thesis, University of South Florida Department of Civil and Environmental Engineering, December.
46. Rucker, M.L. & Verquer, M.D., *Gamma Density Logging of Drilled Shafts – Some Observations and Interpretations*, AMEC Earth & Environmental, Inc., Phoenix, AR.,
47. Schindler, A. and Folliard, K. (2005). Heat of hydrations models for cementitious materials. *ACI Materials Journal*, Vol. 102, No.1, pp. 24-33.
48. Schneider, D.I. (1999). *An Introduction to Programming Using Visual Basic 6.0* Fourth Edition. Prentice Hall, Upper Saddle River, New Jersey.
49. Speer, D, *The Use of NDE for Deep Shaft Foundation Construction Compliance*, (1997), 5th ITI Bridge NDE Users Group Conference (Proceedings), California Department of Transportation (Caltrans) – Department of Transportation – Office of Structural Foundations – Foundations Testing and Instrumentation Section.
50. Stain, R.T. (1982), *Integrity Testing*, *Civil Engineering*, April and May, pp. 55-59 and 71-73.
51. Stain, R.T. and Williams, H.T. (1987), *Integrity Testing of Piles – Horses for Courses,*” *International Conference on Piling and Deep Foundations*, London, March.
52. Stokes, Michael J., *Advancements in Rapid Load Test Data Regression*. Dissertation, University of South Florida, Tampa, 2007.
53. U.S. Department of the Interior (2004). Story of Hoover dam; concrete. Bureau of Reclamation, <http://www.usbr.gov/lc/hooverdam/History/essays/concrete.html>.
54. U.S. FHWA, Geotechnical Engineering Circular (GEC) No. 8 Design And Construction Of Continuous Flight Auger Piles Final, April 2007, Chapter 7: Quality Control (QC) / Quality Assurance (QA) Procedures. <http://www.fhwa.dot.gov/engineering/geotech/pubs/gec8/07.cfm#s05c>

55. Whitfield, T. (2006). "Effect of C₃S content on expansion due to ettringite formation. Master's Thesis, University of South Florida Department of Civil and Environmental Engineering, June.
56. WSDOT (2009). "Report of CSL Testing, Pier 6 Shaft A & Shaft C," Nalley Valley I-16 Bridge Project, Tacoma, WA, Washington State Department of Transportation, Olympia, WA.
57. WSDOT, (2009). "Report of CSL Testing, Pier 6 Shaft A & Shaft C," Nalley Valley I-16 Bridge Project, Tacoma, WA, Washington State Department of Transportation, Olympia, WA.
58. Omega(3). "Infrared Thermocouples", Accessed August 31, 201, <http://www.omega.com/literature/transactions/volume1/infrared1.html>
59. Analog Devices Loop-Powered 4-20mA Sensor Transmitter Technical Manual, Norwood, MA
60. AEO Technology, "Infrared Light", Accessed August 31, 2011, <http://www.aeotechnology.com/about.html>
61. Google Maps. "Opelika, AL", Accessed August 31, 2011, http://maps.google.com/maps?q=Handbook+of+Temperature+Measurement+%26+Control,+Omega+Press,+1997&rlz=1I7GZEZ_en&oe=UTF-8&um=1&ie=UTF-8&sa=N&hl=en&tab=wl
62. Omega(1). "Thermocouple Basics", Accessed August 31, 2011, http://www.omega.com/literature/transactions/volume1/infrared1.html#thermocouple_basics
63. OMEGA-H1. "A Historical Perspective-1", Accessed August 31, 2011, <http://www.omega.com/literature/transactions/volume1/historical1.html>
64. OMEGA-H2. "A Historical Perspective-2", Accessed August 31, <http://www.omega.com/literature/transactions/volume1/historical2.html>
65. Suite 101. "Visible Light Spectrum", Accessed August 31, 2011 http://www.suite101.com/view_image_articles.cfm/1028854

Appendices

Appendix A - Additional Information from Field Trial #1

The information contained in this appendix is additional information and test results from field trial #1

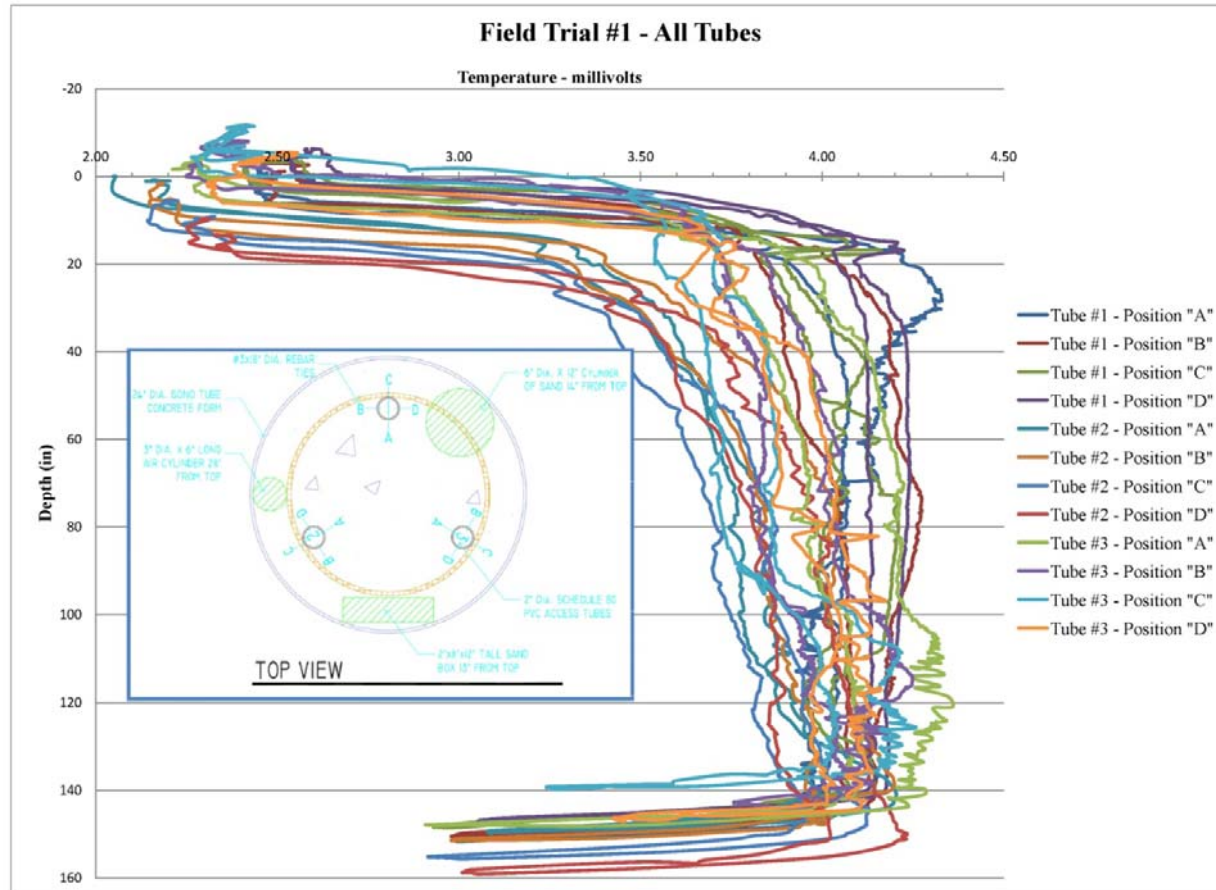


Figure A1 - TIP data from field trial #1 all tubes

Appendix A (Continued)

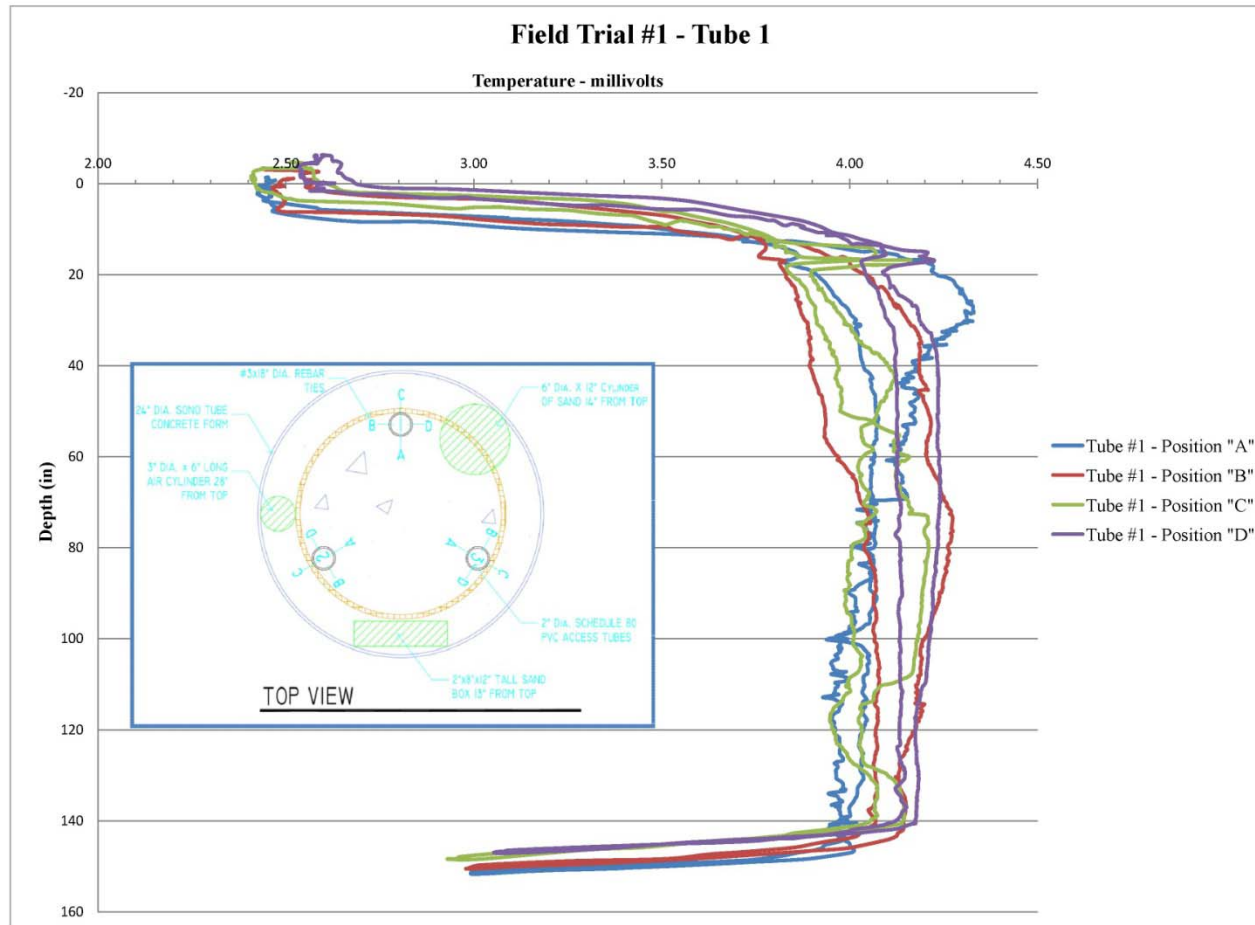


Figure A2 - TIP data from field trial #1 tube 1

Appendix A (Continued)

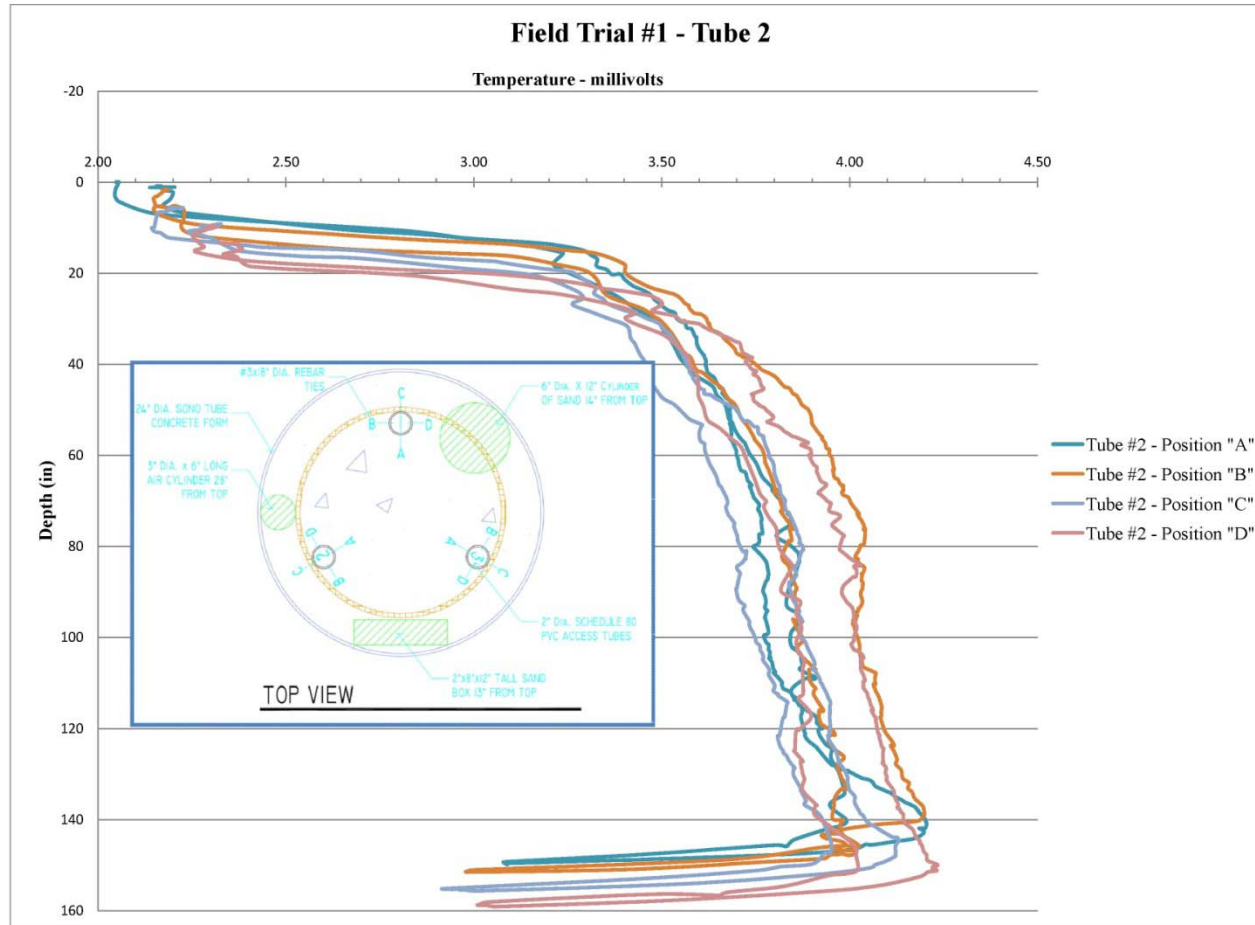


Figure A3 - TIP data from field trial #1 tube 2

Appendix A (Continued)

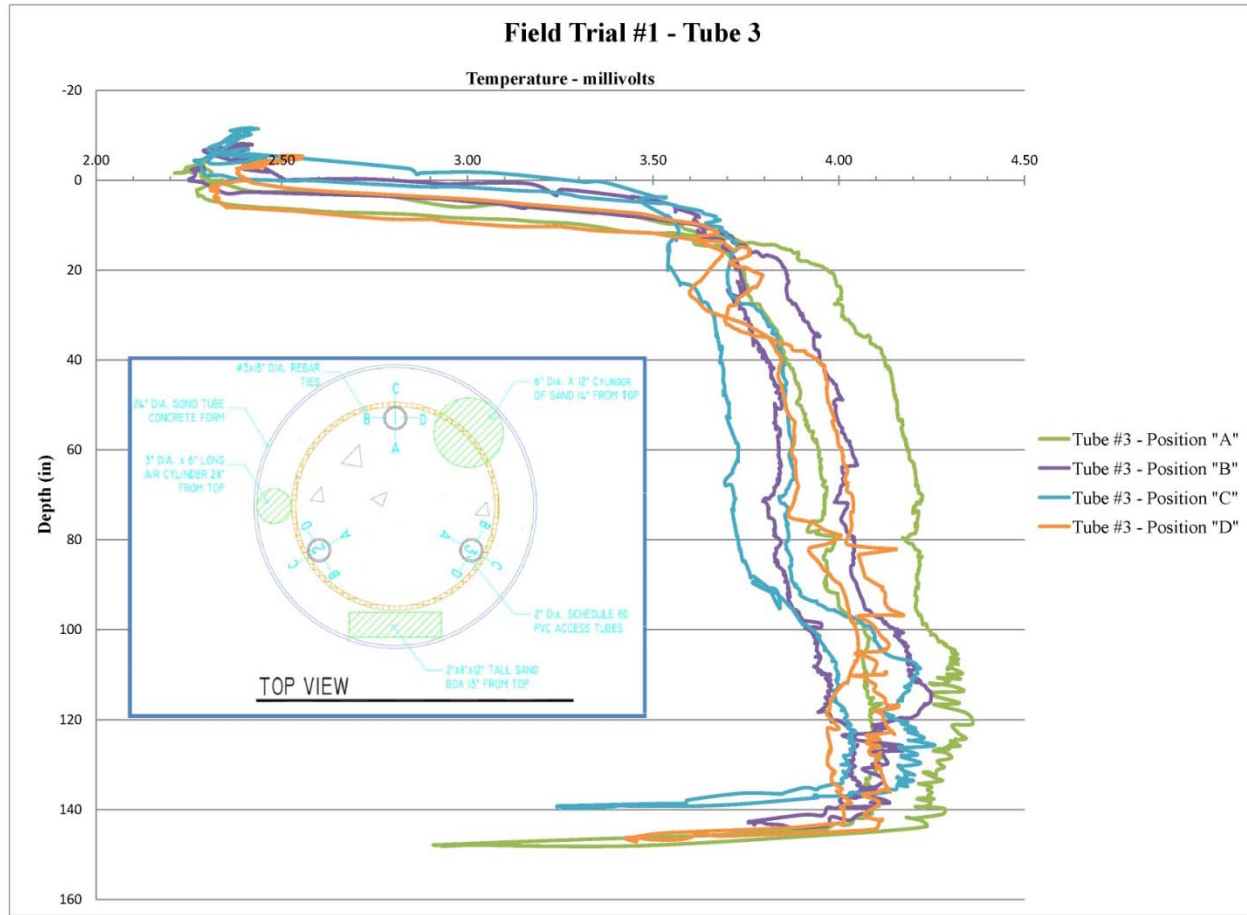


Figure A4 - TIP data from field trial #1 tube 3

Appendix A (Continued)

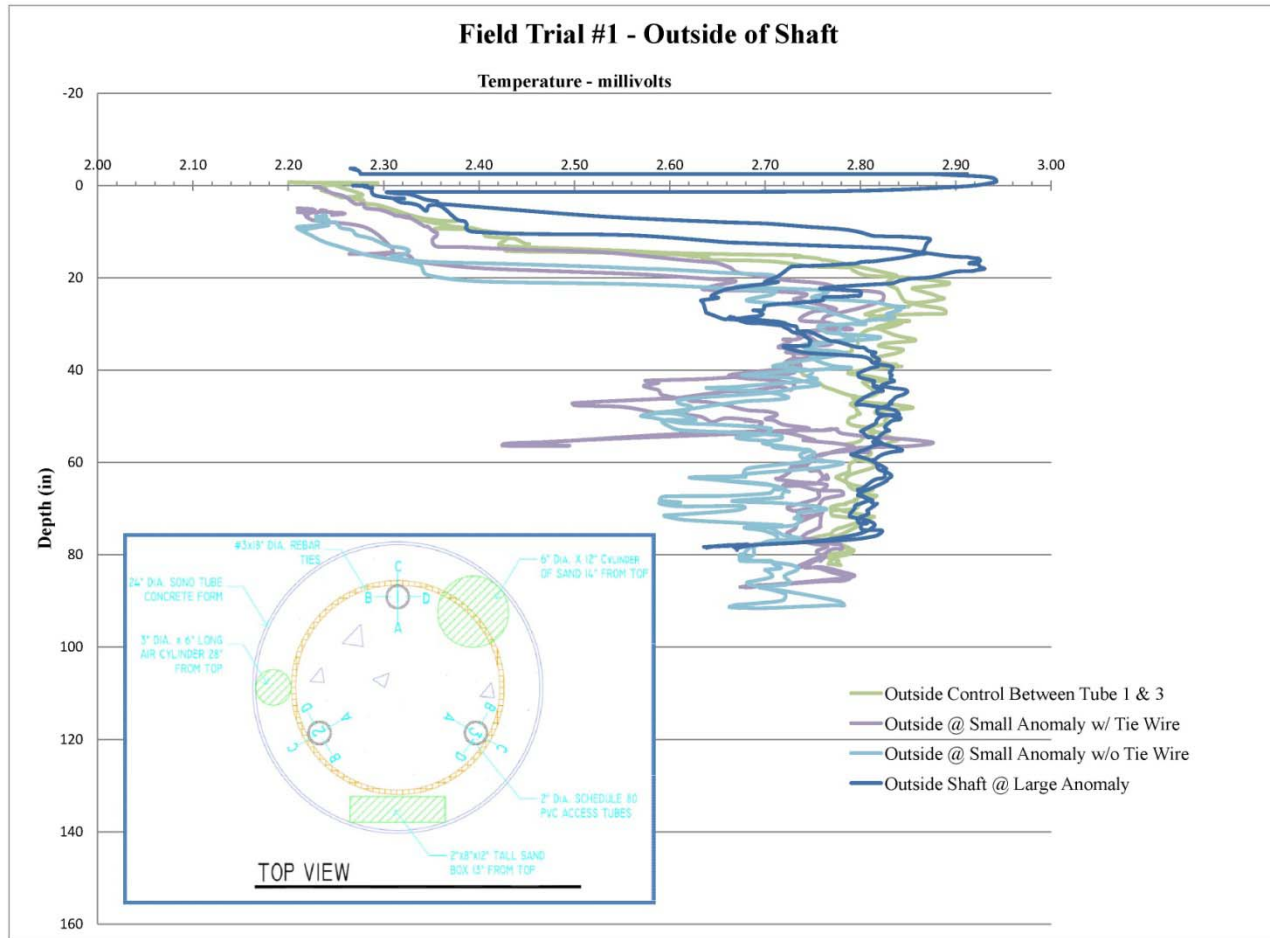


Figure A5 - TIP data from field trial #1 outside of shaft

Appendix B - Additional Information from Field Trial #2

The information contained in this appendix is additional information and test results from field trial #1.




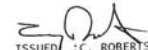
<p>05/30/2002 11:22 FAX 8136842892 RMC EWELL, INC-BRANDON 001</p>	<p>05/30/2002 11:22 FAX 8136842892 RMC EWELL, INC-BRANDON 002</p>																																								
<p>RMC Ewell, Inc. </p>	<p> ISSUED: C. ROBERTS REVIEWED: K. WEST DATE: 05/29/01 MIX NO.: 07-0615 Ewell ** G4405</p>																																								
<p>facsimile transmittal</p>	<p>CONCRETE MIX DESIGN</p>																																								
<p>To: Byron Anderson Fax: 984-9177 Company: USF From: Michelle Taylor Date: 8/30/02 Re: drill shaft mix Pages: 2 CC: n/a <input type="checkbox"/> Urgent <input type="checkbox"/> For Review <input type="checkbox"/> Please Comment <input type="checkbox"/> Please Reply <input type="checkbox"/> Please Recycle</p>	<p>CONCRETE SUPPLIER: RMC EWELL, INC ADDRESS: 311 FALKENBURG ROAD SOUTH TAMPA, FLORIDA 33619 PLANT LOCATION: TAMPA TELEPHONE NO: 813/643-4650 FDOT ASSIGNED PLANT NO.: 10-012 PROJECT NO: 25845915201 DATE: 04/25/01</p>																																								
<p>Notes: Attached is a copy of the 4000 psi Class IV drill shaft mix design you and I discussed. This mix has had the FDOT laboratory testing, and is approved under FDOT Road & Bridge Specifications, Section #346 (FDOT mix #07-0615). All that is required for use on an FDOT drill shaft project is a slump loss test.</p>	<p>CLASS CONCRETE: IV DRILL SHAFT(4000)</p>																																								
<p>Technical Services Dept. 311 Falkenburg Road South Tampa, FL 33619 Phone 813-643-4650 Fax 813-684-2892</p>	<p>SOURCE OF MATERIALS</p>																																								
	<table border="0"> <tr> <td>COARSE AGGREGATE: VULCAN</td> <td>GRADE: 57 S.G.(SSD): 2.40</td> </tr> <tr> <td>FINE AGGREGATE: E.R. JAHNA</td> <td>F.M.: 2.20 S.G.(SSD): 2.30</td> </tr> <tr> <td>PIT NO.(COARSE): TM-416</td> <td>TYPE: CRUSHED LIMESTONE</td> </tr> <tr> <td>PIT NO.(FINE): 11-490</td> <td>TYPE: SILICA SAND</td> </tr> <tr> <td>CEMENT: LAFARGE</td> <td>SPEC: AASHTO M-85 TYPE I</td> </tr> <tr> <td>AIR ENTR. ADMIX: MBAE 90</td> <td>SPEC: AASHTO M-154</td> </tr> <tr> <td>1ST ADMIX: POZZ 80</td> <td>MASTER BUILDERS</td> </tr> <tr> <td>2ND ADMIX: ----</td> <td>MASTER BUILDERS</td> </tr> <tr> <td>3RD ADMIX: ----</td> <td>SPEC: AASHTO M-194 TYPE D</td> </tr> <tr> <td>FLY ASH: BORAL</td> <td>SPEC: ----</td> </tr> <tr> <td></td> <td>SPEC: ASTM C-618 CLASS F</td> </tr> </table>	COARSE AGGREGATE: VULCAN	GRADE: 57 S.G.(SSD): 2.40	FINE AGGREGATE: E.R. JAHNA	F.M.: 2.20 S.G.(SSD): 2.30	PIT NO.(COARSE): TM-416	TYPE: CRUSHED LIMESTONE	PIT NO.(FINE): 11-490	TYPE: SILICA SAND	CEMENT: LAFARGE	SPEC: AASHTO M-85 TYPE I	AIR ENTR. ADMIX: MBAE 90	SPEC: AASHTO M-154	1ST ADMIX: POZZ 80	MASTER BUILDERS	2ND ADMIX: ----	MASTER BUILDERS	3RD ADMIX: ----	SPEC: AASHTO M-194 TYPE D	FLY ASH: BORAL	SPEC: ----		SPEC: ASTM C-618 CLASS F																		
COARSE AGGREGATE: VULCAN	GRADE: 57 S.G.(SSD): 2.40																																								
FINE AGGREGATE: E.R. JAHNA	F.M.: 2.20 S.G.(SSD): 2.30																																								
PIT NO.(COARSE): TM-416	TYPE: CRUSHED LIMESTONE																																								
PIT NO.(FINE): 11-490	TYPE: SILICA SAND																																								
CEMENT: LAFARGE	SPEC: AASHTO M-85 TYPE I																																								
AIR ENTR. ADMIX: MBAE 90	SPEC: AASHTO M-154																																								
1ST ADMIX: POZZ 80	MASTER BUILDERS																																								
2ND ADMIX: ----	MASTER BUILDERS																																								
3RD ADMIX: ----	SPEC: AASHTO M-194 TYPE D																																								
FLY ASH: BORAL	SPEC: ----																																								
	SPEC: ASTM C-618 CLASS F																																								
	<p>HOT WEATHER CONCRETE DESIGN MIX</p>																																								
	<table border="0"> <tr> <td>CEMENT (Kg) LBS</td> <td>: 528</td> <td>SLUMP RANGE</td> <td>: 7.00 TO 9.00 (mm) IN</td> </tr> <tr> <td>COARSE AGG (Kg) LBS</td> <td>: 1493.538</td> <td>AIR CONTENT</td> <td>: 0.0 % TO 6.0 %</td> </tr> <tr> <td>FINE AGG (Kg) LBS</td> <td>: 952</td> <td>UNIT WEIGHT (WET)</td> <td>: 133.0 (kg/M3) PCF</td> </tr> <tr> <td>AIR ENT ADMX (mL) OZ</td> <td>: 8.0</td> <td>W/C RATIO (PLANT)</td> <td>: 0.41 (kg/Kg) LBS/LB</td> </tr> <tr> <td>1ST ADMIXTURE (mL) OZ</td> <td>: 114.0</td> <td>W/C RATIO (FIELD)</td> <td>: 0.41 (kg/Kg) LBS/LB</td> </tr> <tr> <td>2ND ADMIX (mL) OZ</td> <td>: 0.0</td> <td>THEO YIELD</td> <td>: 27.00 (M3) CU FT</td> </tr> <tr> <td>3RD ADMIX (mL) OZ</td> <td>: 0.0</td> <td></td> <td></td> </tr> <tr> <td>WATER (mL) GAL</td> <td>: 40.00</td> <td></td> <td></td> </tr> <tr> <td>WATER (Kg) LBS</td> <td>: 333.0</td> <td></td> <td></td> </tr> <tr> <td>FLY ASH (Kg) LBS</td> <td>: 284</td> <td></td> <td></td> </tr> </table>	CEMENT (Kg) LBS	: 528	SLUMP RANGE	: 7.00 TO 9.00 (mm) IN	COARSE AGG (Kg) LBS	: 1493.538	AIR CONTENT	: 0.0 % TO 6.0 %	FINE AGG (Kg) LBS	: 952	UNIT WEIGHT (WET)	: 133.0 (kg/M3) PCF	AIR ENT ADMX (mL) OZ	: 8.0	W/C RATIO (PLANT)	: 0.41 (kg/Kg) LBS/LB	1ST ADMIXTURE (mL) OZ	: 114.0	W/C RATIO (FIELD)	: 0.41 (kg/Kg) LBS/LB	2ND ADMIX (mL) OZ	: 0.0	THEO YIELD	: 27.00 (M3) CU FT	3RD ADMIX (mL) OZ	: 0.0			WATER (mL) GAL	: 40.00			WATER (Kg) LBS	: 333.0			FLY ASH (Kg) LBS	: 284		
CEMENT (Kg) LBS	: 528	SLUMP RANGE	: 7.00 TO 9.00 (mm) IN																																						
COARSE AGG (Kg) LBS	: 1493.538	AIR CONTENT	: 0.0 % TO 6.0 %																																						
FINE AGG (Kg) LBS	: 952	UNIT WEIGHT (WET)	: 133.0 (kg/M3) PCF																																						
AIR ENT ADMX (mL) OZ	: 8.0	W/C RATIO (PLANT)	: 0.41 (kg/Kg) LBS/LB																																						
1ST ADMIXTURE (mL) OZ	: 114.0	W/C RATIO (FIELD)	: 0.41 (kg/Kg) LBS/LB																																						
2ND ADMIX (mL) OZ	: 0.0	THEO YIELD	: 27.00 (M3) CU FT																																						
3RD ADMIX (mL) OZ	: 0.0																																								
WATER (mL) GAL	: 40.00																																								
WATER (Kg) LBS	: 333.0																																								
FLY ASH (Kg) LBS	: 284																																								
	<p>CC: D. W. E. 1 & 7 TEST FILE</p>																																								
	<p>PRODUCER TEST DATA CHLORIDE CONT: 0.153 (kg/M3) LB/CY SLUMP: 8.00 (MM) IN AIR CONTENT: 3.50 % TEMPERATURE: 95 DEG (C) F COMPRESSIVE STRENGTH (MPA) PSI 28 -DAY- 5500 -DAY- -DAY- -DAY-</p>																																								

Figure B1 - Concrete mix design for field trial #2

Appendix B (Continued)

<p>05/30/2002 11:22 FAX 8136842892 RMC EWELL, INC-BRANDON 0002</p> <p style="text-align: center;"> ISSUED: C. ROBERTS REVIEWED: K. WEST DATE: 05/29/01 MIX NO.: 07-0615 Ewell **64405</p> <p style="text-align: center;">CONCRETE MIX DESIGN</p> <p>CONCRETE SUPPLIER: RMC EWELL, INC ADDRESS: 311 FALKENBURG ROAD SOUTH TAMPA, FLORIDA 33619 PLANT LOCATION: TAMPA TELEPHONE NO: 813/643-4650 FDOT ASSIGNED PLANT NO.: 10-012 PROJECT NO: 25845915201 DATE: 04/25/01</p> <p style="text-align: center;">CLASS CONCRETE: IV DRILL SHAFT(4000)</p> <p style="text-align: center;">SOURCE OF MATERIALS</p> <table border="0" style="width: 100%;"> <tr> <td style="width: 50%;">COARSE AGGREGATE: VULCAN</td> <td style="width: 50%;">GRADE: 57 S.G.(SSD): 2.40</td> </tr> <tr> <td>FINE AGGREGATE: E.R. JAHNA</td> <td>F.M.: 2.20 S.G.(SSD): 2.330</td> </tr> <tr> <td>PIT NO.(COARSE): TM-416</td> <td>TYPE: CRUSHED LIMESTONE</td> </tr> <tr> <td>PIT NO.(FINE): 11-490</td> <td>TYPE: SILICA SAND</td> </tr> <tr> <td>CEMENT: LAFARGE</td> <td>SPEC: AASHTO M-85 TYPE I</td> </tr> <tr> <td>AIR ENTR.ADMIX: MBAE 90 MASTER BUILDERS</td> <td>SPEC: AASHTO M-154</td> </tr> <tr> <td>1ST ADMIX: POZZ 80 MASTER BUILDERS</td> <td>SPEC: AASHTO M-194 TYPE D</td> </tr> <tr> <td>2ND ADMIX: ----</td> <td>SPEC: ----</td> </tr> <tr> <td>3RD ADMIX: ----</td> <td>SPEC: ----</td> </tr> <tr> <td>FLY ASH: BORAL</td> <td>SPEC: ASTM C-618 CLASS F</td> </tr> </table> <p>HOT WEATHER CONCRETE DESIGN MIX</p> <table border="0" style="width: 100%;"> <tr> <td style="width: 30%;">CEMENT (Kg) LBS : 528</td> <td style="width: 30%;">SLUMP RANGE : 7.00 TO 9.00 (mm)IN</td> </tr> <tr> <td>COARSE AGG (Kg) LBS : 1493</td> <td>AIR CONTENT : 0.0 % TO 6.0 %</td> </tr> <tr> <td>FINE AGG (Kg) LBS : 952</td> <td>UNIT WEIGHT (WET): 133.0 (kg/M3)PCF</td> </tr> <tr> <td>AIR ENT ADMX (mL) OZ : 8.0</td> <td>W/C RATIO(PLANT): 0.41 (kg/kg)LBS/LB</td> </tr> <tr> <td>1ST ADMIXTURE (mL) OZ : 114.0</td> <td>W/C RATIO (FIELD): 0.41 (kg/kg)LBS/LB</td> </tr> <tr> <td>2ND ADMIX (mL) OZ : 0.0</td> <td>THEO YIELD : 27.00 (M3)CU FT</td> </tr> <tr> <td>3RD ADMIX (mL) OZ : 0.0</td> <td></td> </tr> <tr> <td>WATER (ML) GAL : 40.00</td> <td></td> </tr> <tr> <td>WATER (Kg) LBS : 333.0</td> <td></td> </tr> <tr> <td>FLY ASH (Kg) LBS : 284</td> <td></td> </tr> </table> <p style="text-align: center;">PRODUCER TEST DATA</p> <table border="0" style="width: 100%;"> <tr> <td style="width: 50%;">CHLORIDE CONT : 0.153 (kg/M3)LB/CY</td> <td style="width: 50%;">SLUMP : 8.00 (MM)IN</td> </tr> <tr> <td>AIR CONTENT : 3.50 %</td> <td>TEMPERATURE : 95 DEG (C)F</td> </tr> <tr> <td>COMPRESSIVE STRENGTH (MPA)PSI</td> <td></td> </tr> <tr> <td>28 -DAY- 5500</td> <td>-DAY-</td> </tr> <tr> <td>-DAY-</td> <td>-DAY-</td> </tr> </table> <p>CC: D. M. E. 1 & 7 TEST FILE</p>	COARSE AGGREGATE: VULCAN	GRADE: 57 S.G.(SSD): 2.40	FINE AGGREGATE: E.R. JAHNA	F.M.: 2.20 S.G.(SSD): 2.330	PIT NO.(COARSE): TM-416	TYPE: CRUSHED LIMESTONE	PIT NO.(FINE): 11-490	TYPE: SILICA SAND	CEMENT: LAFARGE	SPEC: AASHTO M-85 TYPE I	AIR ENTR.ADMIX: MBAE 90 MASTER BUILDERS	SPEC: AASHTO M-154	1ST ADMIX: POZZ 80 MASTER BUILDERS	SPEC: AASHTO M-194 TYPE D	2ND ADMIX: ----	SPEC: ----	3RD ADMIX: ----	SPEC: ----	FLY ASH: BORAL	SPEC: ASTM C-618 CLASS F	CEMENT (Kg) LBS : 528	SLUMP RANGE : 7.00 TO 9.00 (mm)IN	COARSE AGG (Kg) LBS : 1493	AIR CONTENT : 0.0 % TO 6.0 %	FINE AGG (Kg) LBS : 952	UNIT WEIGHT (WET): 133.0 (kg/M3)PCF	AIR ENT ADMX (mL) OZ : 8.0	W/C RATIO(PLANT): 0.41 (kg/kg)LBS/LB	1ST ADMIXTURE (mL) OZ : 114.0	W/C RATIO (FIELD): 0.41 (kg/kg)LBS/LB	2ND ADMIX (mL) OZ : 0.0	THEO YIELD : 27.00 (M3)CU FT	3RD ADMIX (mL) OZ : 0.0		WATER (ML) GAL : 40.00		WATER (Kg) LBS : 333.0		FLY ASH (Kg) LBS : 284		CHLORIDE CONT : 0.153 (kg/M3)LB/CY	SLUMP : 8.00 (MM)IN	AIR CONTENT : 3.50 %	TEMPERATURE : 95 DEG (C)F	COMPRESSIVE STRENGTH (MPA)PSI		28 -DAY- 5500	-DAY-	-DAY-	-DAY-	<p>05/30/2002 11:22 FAX 8136842892 RMC EWELL, INC-BRANDON 0002</p> <p style="text-align: center;"> ISSUED: C. ROBERTS REVIEWED: K. WEST DATE: 05/29/01 MIX NO.: 07-0615 Ewell **64405</p> <p style="text-align: center;">CONCRETE MIX DESIGN</p> <p>CONCRETE SUPPLIER: RMC EWELL, INC ADDRESS: 311 FALKENBURG ROAD SOUTH TAMPA, FLORIDA 33619 PLANT LOCATION: TAMPA TELEPHONE NO: 813/643-4650 FDOT ASSIGNED PLANT NO.: 10-012 PROJECT NO: 25845915201 DATE: 04/25/01</p> <p style="text-align: center;">CLASS CONCRETE: IV DRILL SHAFT(4000)</p> <p style="text-align: center;">SOURCE OF MATERIALS</p> <table border="0" style="width: 100%;"> <tr> <td style="width: 50%;">COARSE AGGREGATE: VULCAN</td> <td style="width: 50%;">GRADE: 57 S.G.(SSD): 2.40</td> </tr> <tr> <td>FINE AGGREGATE: E.R. JAHNA</td> <td>F.M.: 2.20 S.G.(SSD): 2.330</td> </tr> <tr> <td>PIT NO.(COARSE): TM-416</td> <td>TYPE: CRUSHED LIMESTONE</td> </tr> <tr> <td>PIT NO.(FINE): 11-490</td> <td>TYPE: SILICA SAND</td> </tr> <tr> <td>CEMENT: LAFARGE</td> <td>SPEC: AASHTO M-85 TYPE I</td> </tr> <tr> <td>AIR ENTR.ADMIX: MBAE 90 MASTER BUILDERS</td> <td>SPEC: AASHTO M-154</td> </tr> <tr> <td>1ST ADMIX: POZZ 80 MASTER BUILDERS</td> <td>SPEC: AASHTO M-194 TYPE D</td> </tr> <tr> <td>2ND ADMIX: ----</td> <td>SPEC: ----</td> </tr> <tr> <td>3RD ADMIX: ----</td> <td>SPEC: ----</td> </tr> <tr> <td>FLY ASH: BORAL</td> <td>SPEC: ASTM C-618 CLASS F</td> </tr> </table> <p>HOT WEATHER CONCRETE DESIGN MIX</p> <table border="0" style="width: 100%;"> <tr> <td style="width: 30%;">CEMENT (Kg) LBS : 528</td> <td style="width: 30%;">SLUMP RANGE : 7.00 TO 9.00 (mm)IN</td> </tr> <tr> <td>COARSE AGG (Kg) LBS : 1493</td> <td>AIR CONTENT : 0.0 % TO 6.0 %</td> </tr> <tr> <td>FINE AGG (Kg) LBS : 952</td> <td>UNIT WEIGHT (WET): 133.0 (kg/M3)PCF</td> </tr> <tr> <td>AIR ENT ADMX (mL) OZ : 8.0</td> <td>W/C RATIO(PLANT): 0.41 (kg/kg)LBS/LB</td> </tr> <tr> <td>1ST ADMIXTURE (mL) OZ : 114.0</td> <td>W/C RATIO (FIELD): 0.41 (kg/kg)LBS/LB</td> </tr> <tr> <td>2ND ADMIX (mL) OZ : 0.0</td> <td>THEO YIELD : 27.00 (M3)CU FT</td> </tr> <tr> <td>3RD ADMIX (mL) OZ : 0.0</td> <td></td> </tr> <tr> <td>WATER (ML) GAL : 40.00</td> <td></td> </tr> <tr> <td>WATER (Kg) LBS : 333.0</td> <td></td> </tr> <tr> <td>FLY ASH (Kg) LBS : 284</td> <td></td> </tr> </table> <p style="text-align: center;">PRODUCER TEST DATA</p> <table border="0" style="width: 100%;"> <tr> <td style="width: 50%;">CHLORIDE CONT : 0.153 (kg/M3)LB/CY</td> <td style="width: 50%;">SLUMP : 8.00 (MM)IN</td> </tr> <tr> <td>AIR CONTENT : 3.50 %</td> <td>TEMPERATURE : 95 DEG (C)F</td> </tr> <tr> <td>COMPRESSIVE STRENGTH (MPA)PSI</td> <td></td> </tr> <tr> <td>28 -DAY- 5500</td> <td>-DAY-</td> </tr> <tr> <td>-DAY-</td> <td>-DAY-</td> </tr> </table> <p>CC: D. M. E. 1 & 7 TEST FILE</p>	COARSE AGGREGATE: VULCAN	GRADE: 57 S.G.(SSD): 2.40	FINE AGGREGATE: E.R. JAHNA	F.M.: 2.20 S.G.(SSD): 2.330	PIT NO.(COARSE): TM-416	TYPE: CRUSHED LIMESTONE	PIT NO.(FINE): 11-490	TYPE: SILICA SAND	CEMENT: LAFARGE	SPEC: AASHTO M-85 TYPE I	AIR ENTR.ADMIX: MBAE 90 MASTER BUILDERS	SPEC: AASHTO M-154	1ST ADMIX: POZZ 80 MASTER BUILDERS	SPEC: AASHTO M-194 TYPE D	2ND ADMIX: ----	SPEC: ----	3RD ADMIX: ----	SPEC: ----	FLY ASH: BORAL	SPEC: ASTM C-618 CLASS F	CEMENT (Kg) LBS : 528	SLUMP RANGE : 7.00 TO 9.00 (mm)IN	COARSE AGG (Kg) LBS : 1493	AIR CONTENT : 0.0 % TO 6.0 %	FINE AGG (Kg) LBS : 952	UNIT WEIGHT (WET): 133.0 (kg/M3)PCF	AIR ENT ADMX (mL) OZ : 8.0	W/C RATIO(PLANT): 0.41 (kg/kg)LBS/LB	1ST ADMIXTURE (mL) OZ : 114.0	W/C RATIO (FIELD): 0.41 (kg/kg)LBS/LB	2ND ADMIX (mL) OZ : 0.0	THEO YIELD : 27.00 (M3)CU FT	3RD ADMIX (mL) OZ : 0.0		WATER (ML) GAL : 40.00		WATER (Kg) LBS : 333.0		FLY ASH (Kg) LBS : 284		CHLORIDE CONT : 0.153 (kg/M3)LB/CY	SLUMP : 8.00 (MM)IN	AIR CONTENT : 3.50 %	TEMPERATURE : 95 DEG (C)F	COMPRESSIVE STRENGTH (MPA)PSI		28 -DAY- 5500	-DAY-	-DAY-	-DAY-
COARSE AGGREGATE: VULCAN	GRADE: 57 S.G.(SSD): 2.40																																																																																																				
FINE AGGREGATE: E.R. JAHNA	F.M.: 2.20 S.G.(SSD): 2.330																																																																																																				
PIT NO.(COARSE): TM-416	TYPE: CRUSHED LIMESTONE																																																																																																				
PIT NO.(FINE): 11-490	TYPE: SILICA SAND																																																																																																				
CEMENT: LAFARGE	SPEC: AASHTO M-85 TYPE I																																																																																																				
AIR ENTR.ADMIX: MBAE 90 MASTER BUILDERS	SPEC: AASHTO M-154																																																																																																				
1ST ADMIX: POZZ 80 MASTER BUILDERS	SPEC: AASHTO M-194 TYPE D																																																																																																				
2ND ADMIX: ----	SPEC: ----																																																																																																				
3RD ADMIX: ----	SPEC: ----																																																																																																				
FLY ASH: BORAL	SPEC: ASTM C-618 CLASS F																																																																																																				
CEMENT (Kg) LBS : 528	SLUMP RANGE : 7.00 TO 9.00 (mm)IN																																																																																																				
COARSE AGG (Kg) LBS : 1493	AIR CONTENT : 0.0 % TO 6.0 %																																																																																																				
FINE AGG (Kg) LBS : 952	UNIT WEIGHT (WET): 133.0 (kg/M3)PCF																																																																																																				
AIR ENT ADMX (mL) OZ : 8.0	W/C RATIO(PLANT): 0.41 (kg/kg)LBS/LB																																																																																																				
1ST ADMIXTURE (mL) OZ : 114.0	W/C RATIO (FIELD): 0.41 (kg/kg)LBS/LB																																																																																																				
2ND ADMIX (mL) OZ : 0.0	THEO YIELD : 27.00 (M3)CU FT																																																																																																				
3RD ADMIX (mL) OZ : 0.0																																																																																																					
WATER (ML) GAL : 40.00																																																																																																					
WATER (Kg) LBS : 333.0																																																																																																					
FLY ASH (Kg) LBS : 284																																																																																																					
CHLORIDE CONT : 0.153 (kg/M3)LB/CY	SLUMP : 8.00 (MM)IN																																																																																																				
AIR CONTENT : 3.50 %	TEMPERATURE : 95 DEG (C)F																																																																																																				
COMPRESSIVE STRENGTH (MPA)PSI																																																																																																					
28 -DAY- 5500	-DAY-																																																																																																				
-DAY-	-DAY-																																																																																																				
COARSE AGGREGATE: VULCAN	GRADE: 57 S.G.(SSD): 2.40																																																																																																				
FINE AGGREGATE: E.R. JAHNA	F.M.: 2.20 S.G.(SSD): 2.330																																																																																																				
PIT NO.(COARSE): TM-416	TYPE: CRUSHED LIMESTONE																																																																																																				
PIT NO.(FINE): 11-490	TYPE: SILICA SAND																																																																																																				
CEMENT: LAFARGE	SPEC: AASHTO M-85 TYPE I																																																																																																				
AIR ENTR.ADMIX: MBAE 90 MASTER BUILDERS	SPEC: AASHTO M-154																																																																																																				
1ST ADMIX: POZZ 80 MASTER BUILDERS	SPEC: AASHTO M-194 TYPE D																																																																																																				
2ND ADMIX: ----	SPEC: ----																																																																																																				
3RD ADMIX: ----	SPEC: ----																																																																																																				
FLY ASH: BORAL	SPEC: ASTM C-618 CLASS F																																																																																																				
CEMENT (Kg) LBS : 528	SLUMP RANGE : 7.00 TO 9.00 (mm)IN																																																																																																				
COARSE AGG (Kg) LBS : 1493	AIR CONTENT : 0.0 % TO 6.0 %																																																																																																				
FINE AGG (Kg) LBS : 952	UNIT WEIGHT (WET): 133.0 (kg/M3)PCF																																																																																																				
AIR ENT ADMX (mL) OZ : 8.0	W/C RATIO(PLANT): 0.41 (kg/kg)LBS/LB																																																																																																				
1ST ADMIXTURE (mL) OZ : 114.0	W/C RATIO (FIELD): 0.41 (kg/kg)LBS/LB																																																																																																				
2ND ADMIX (mL) OZ : 0.0	THEO YIELD : 27.00 (M3)CU FT																																																																																																				
3RD ADMIX (mL) OZ : 0.0																																																																																																					
WATER (ML) GAL : 40.00																																																																																																					
WATER (Kg) LBS : 333.0																																																																																																					
FLY ASH (Kg) LBS : 284																																																																																																					
CHLORIDE CONT : 0.153 (kg/M3)LB/CY	SLUMP : 8.00 (MM)IN																																																																																																				
AIR CONTENT : 3.50 %	TEMPERATURE : 95 DEG (C)F																																																																																																				
COMPRESSIVE STRENGTH (MPA)PSI																																																																																																					
28 -DAY- 5500	-DAY-																																																																																																				
-DAY-	-DAY-																																																																																																				

Bl (Continued)

Appendix B (Continued)

RMC Ewell, Inc.
 P.O. BOX 3858
 LAKELAND, FL 33802
 TELEPHONE (863) 688-5787
 1-800-282-4657

RMC
 CORPORATE OFFICE

56TH STREET RM
 813/628-4627

CUSTOMER NAME / ADDRESS		SPECIAL INSTRUCTIONS	DELIVERY TICKET NUMBER
CASH/U. S. F.-BYRON WESTERN CASH SALE TAMPA FL 33802		COME IN OFF FLETCHER UNDER WATER TOWER	20400753
DELIVERY ADDRESS			PLANT
SOILS LAB/UNDER WATER TOWER NO CHARGE ORDERED BY: ZONE: 139* SLUMP: 5.00		CAUTION: Freshly mixed cement, mortar concrete or grout may cause skin injury. Avoid contact with skin where possible and wash exposed skin areas promptly with water. If any cement mixtures get into the eye, rinse immediately and repeatedly with water and get prompt medical attention. When sawing or grinding concrete blocks, wear approved respirator and goggles to prevent eye and nose irritation. KEEP OUT OF REACH OF CHILDREN.	204
			DATE
			09/04/02
			COUNTY
			139*

PURCHASE ORDER #	LOT #	JOB #	TRUCK #	DRIVER	TIME OUT	TIME IN	CASH
NO CHG/PRED		143	6477	MCCALL, MICHAEL	1140		

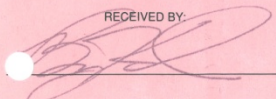
QUANTITY	PRODUCT CODE	DESCRIPTION	UNIT PRICE	EXTENSION
3.00	64405	4000 57 LR 35% FA 0.41 W/C CC-IV D		SEP 4 AM 11:32
	999001 999102	FUEL SUR ENVIRONMENTAL FEE		
PLEASE CONFIRM DELIVERY ADDRESS NOTE ANY CHANGES OF DELIVERY ADDRESS IF DIFFERENT FROM ADDRESS PRINTED ABOVE				
TOTAL TODAY:	3.00	WATER ADDED ON THE JOB:	GALS: 0	SUB TOTAL
ANY WATER ADDED TO THE MIX ON THE JOB SITE WILL BE AT THE CUSTOMER'S RISK				SALES TAX
The Company, when delivering materials beyond curb line, will not assume liability for damage to sidewalk, driveway, septic tank or other property when directed onto property by Purchaser or Purchaser's agent(s). Purchaser or Purchaser's agent(s) shall be responsible to provide safe and adequate access. One (1) hour allowed for unloading. Overtime beyond Allowed Unloading Time, or after normal working hours will be charged per current price list. Diversion of a load from one job to another will carry a Diversion Charge per current price list. A Handling/Restock fee, per current price list, will be charged for all materials picked up by company equipment from the curb line of the Purchaser's property. Only materials in resalable condition, as determined by the Company, will receive full credit. The purchaser of materials delivered agrees to pay for same within credit payment terms, and upon failure to pay for same, and the necessity of placing the account in the hands of an attorney for collection, will pay all cost of said collection including a reasonable attorney's fee. Interest will be charged on delinquent accounts at the maximum rate allowed by law. Proper venue for suit will be Polk County, Florida.				TOTAL
RECEIVED BY: 				CROSS CURB RELEASE
				TIME ON JOB: 1216
				TIME OFF JOB:
				CUSTOMER'S COPY
				FORMS CONTROLS # 760405

Figure B2 - Ready mix delivery ticket for concrete used in Field Trial #2

Appendix B (Continued)

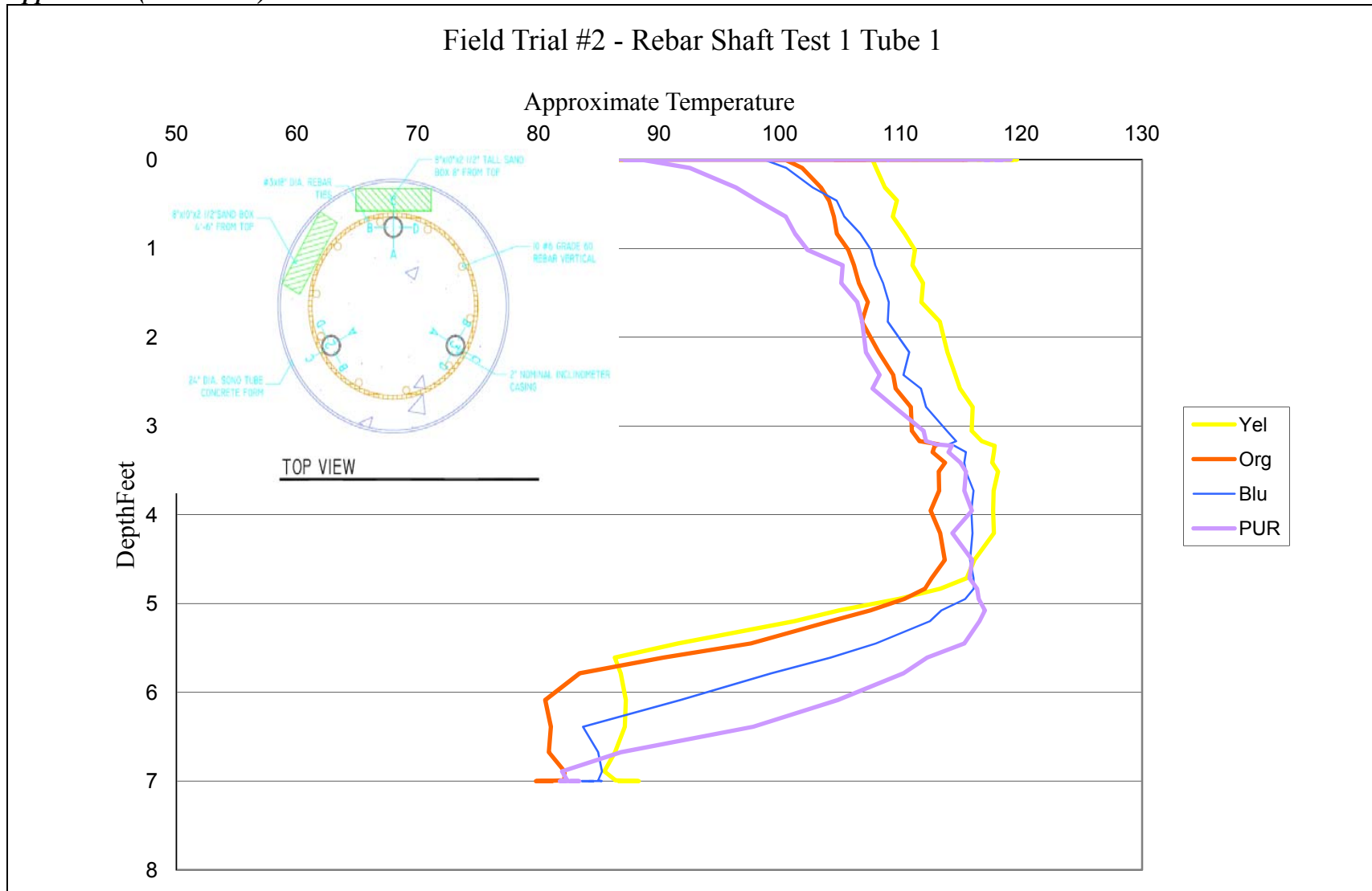


Figure B3 - Field trial #2 TIP test #1 rebar shaft tube 1

Appendix B (Continued)

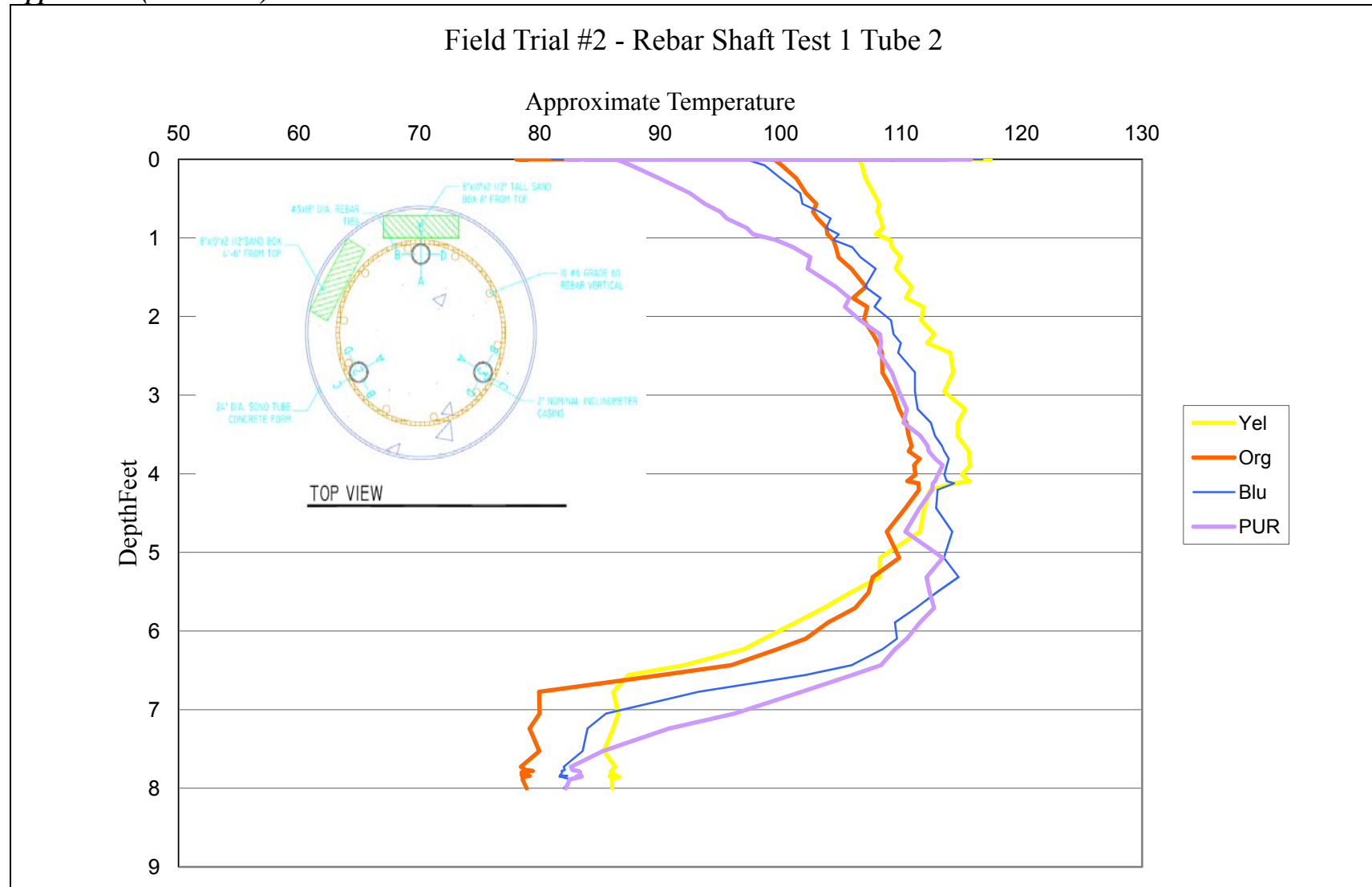


Figure B4 - Field trial #2 TIP test #1 rebar shaft tube 2

Appendix B (Continued)

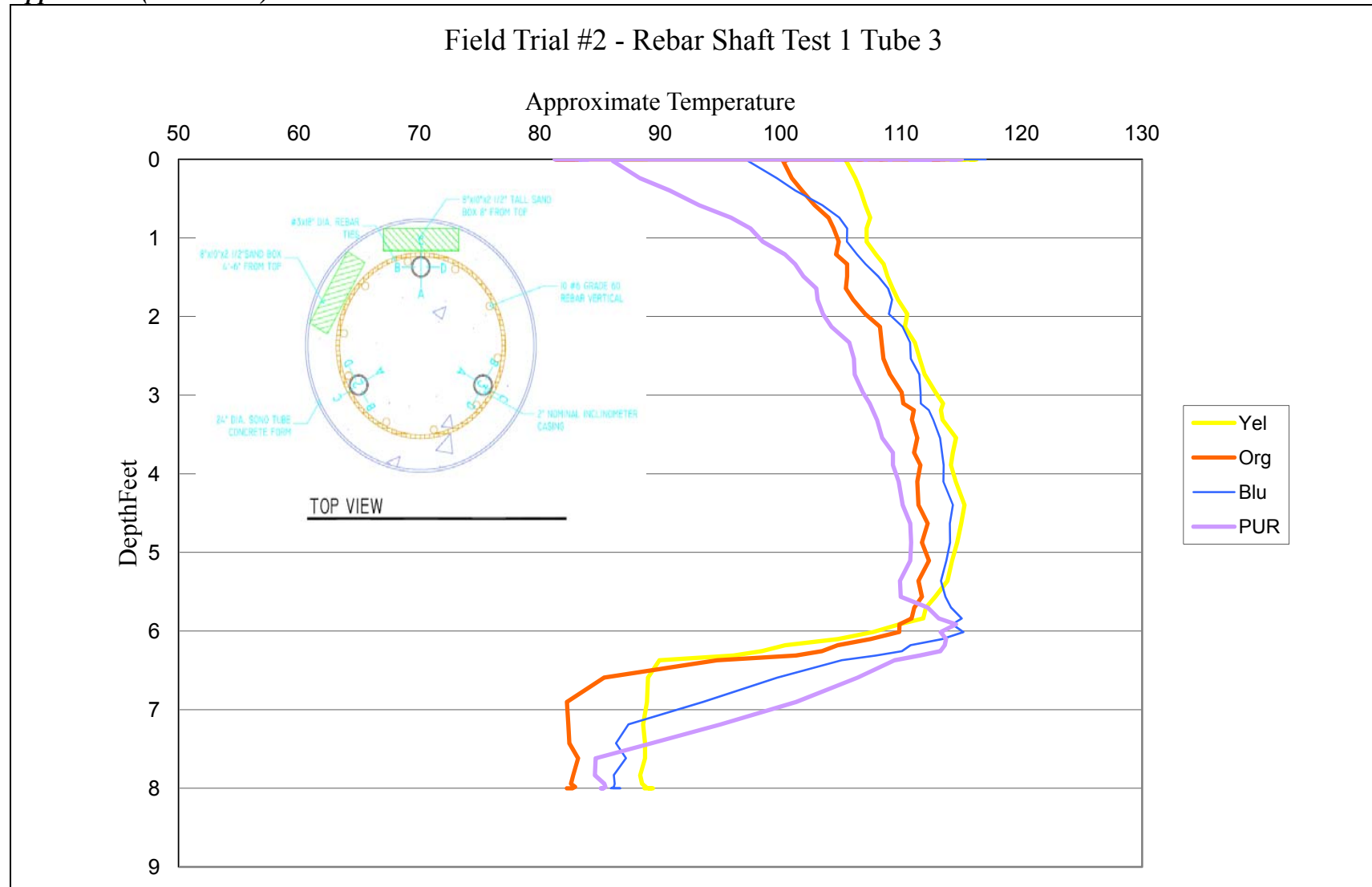


Figure B5 - Field trial #2 TIP test #1 rebar shaft tube 3

Appendix B (Continued)

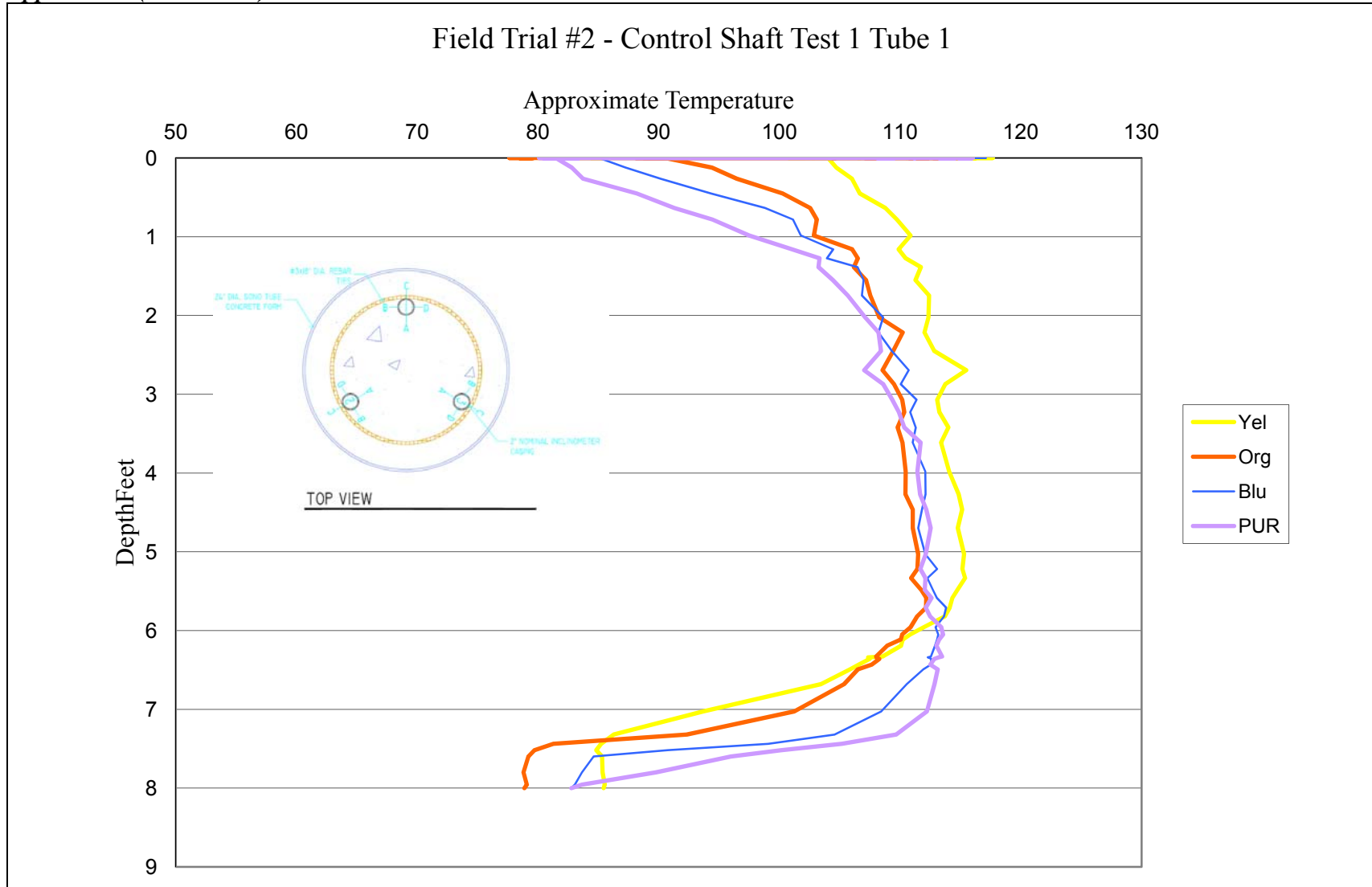


Figure B6 - Field trial #2 TIP test #1 control shaft tube 1

Appendix B (Continued)

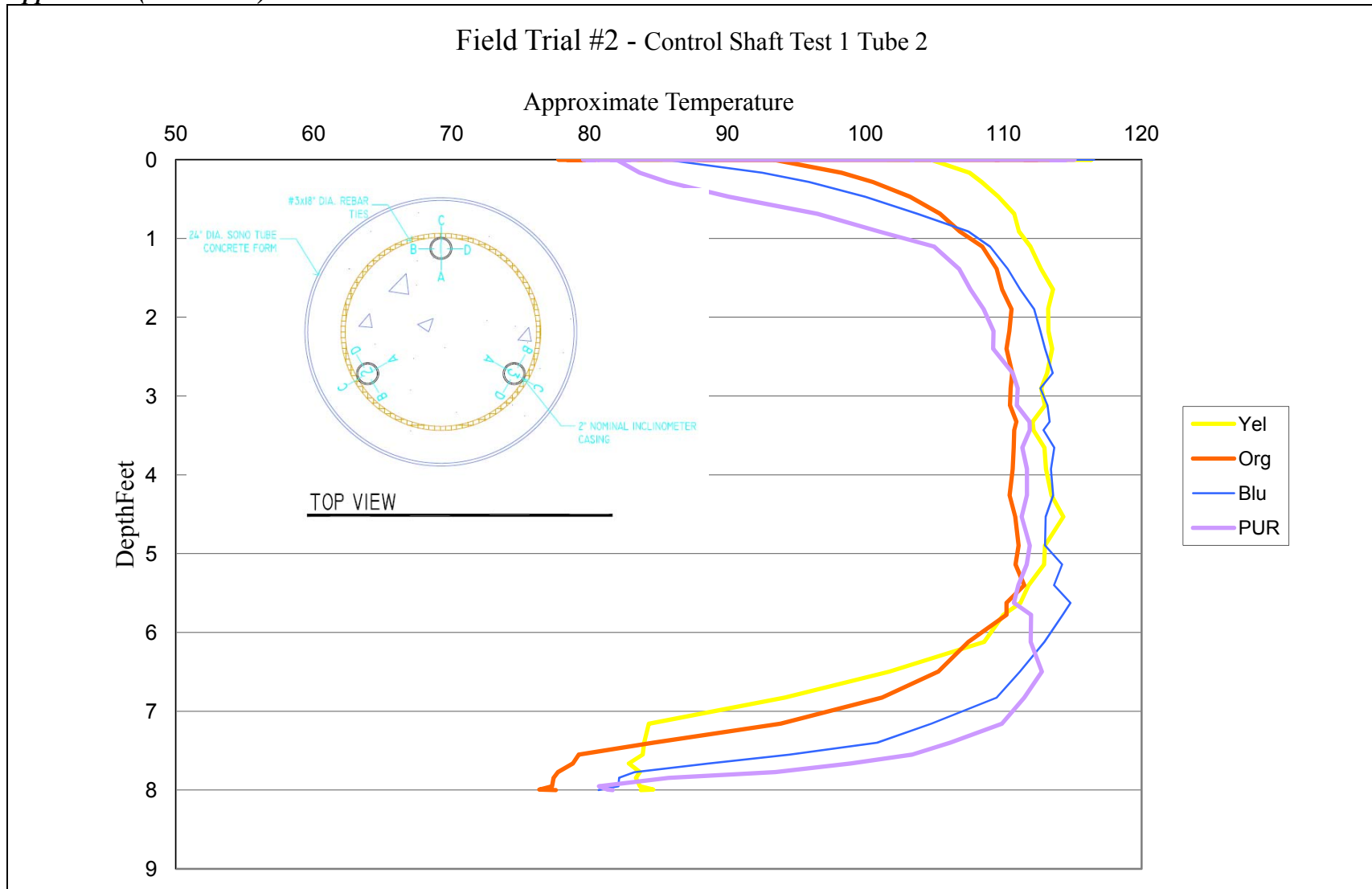


Figure B7 - Field trial #2 TIP test #1 control shaft tube 2

Appendix B (Continued)

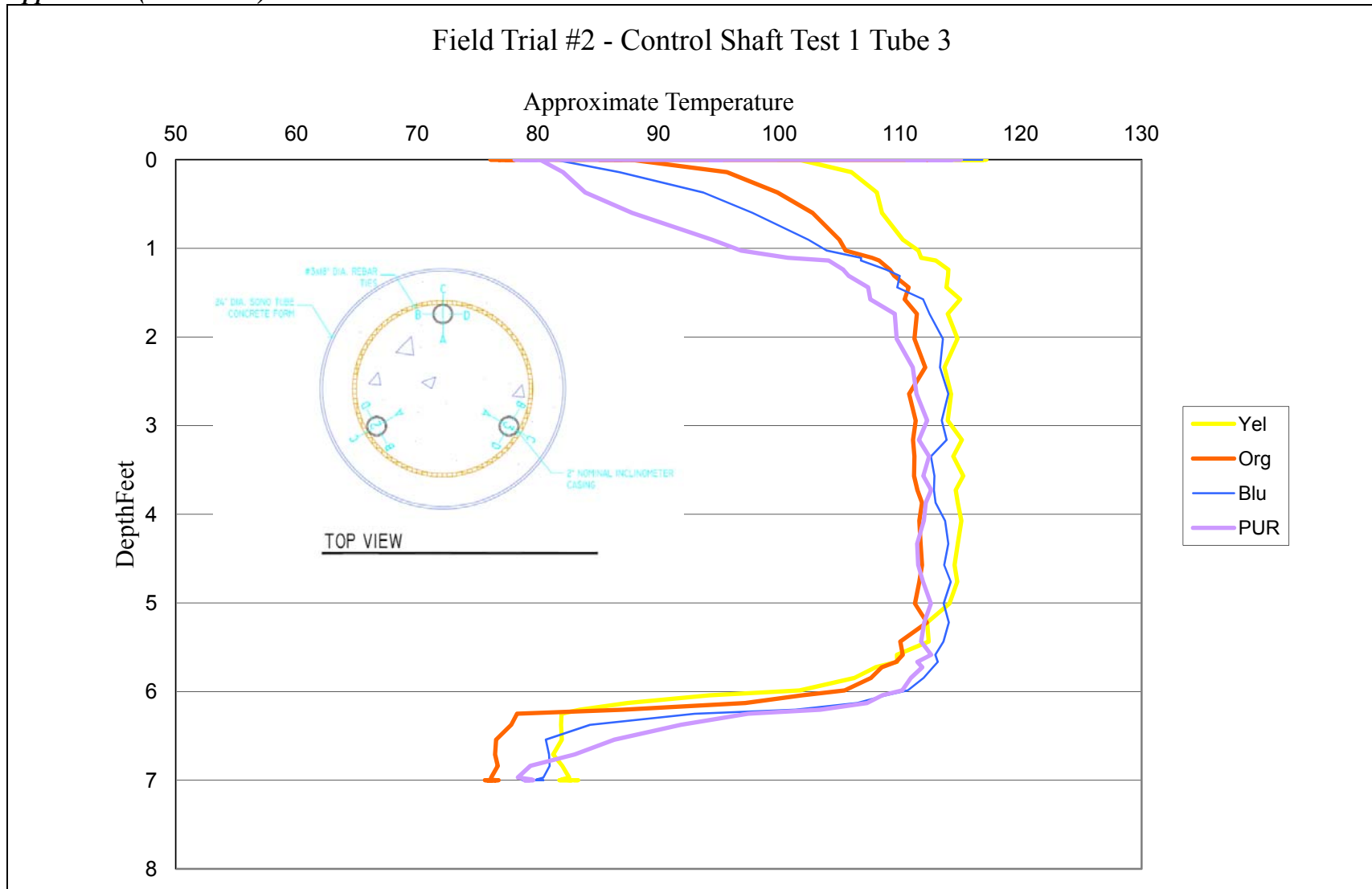


Figure B8 - Field trial #2 TIP test #1 control shaft tube 3

Appendix B (Continued)

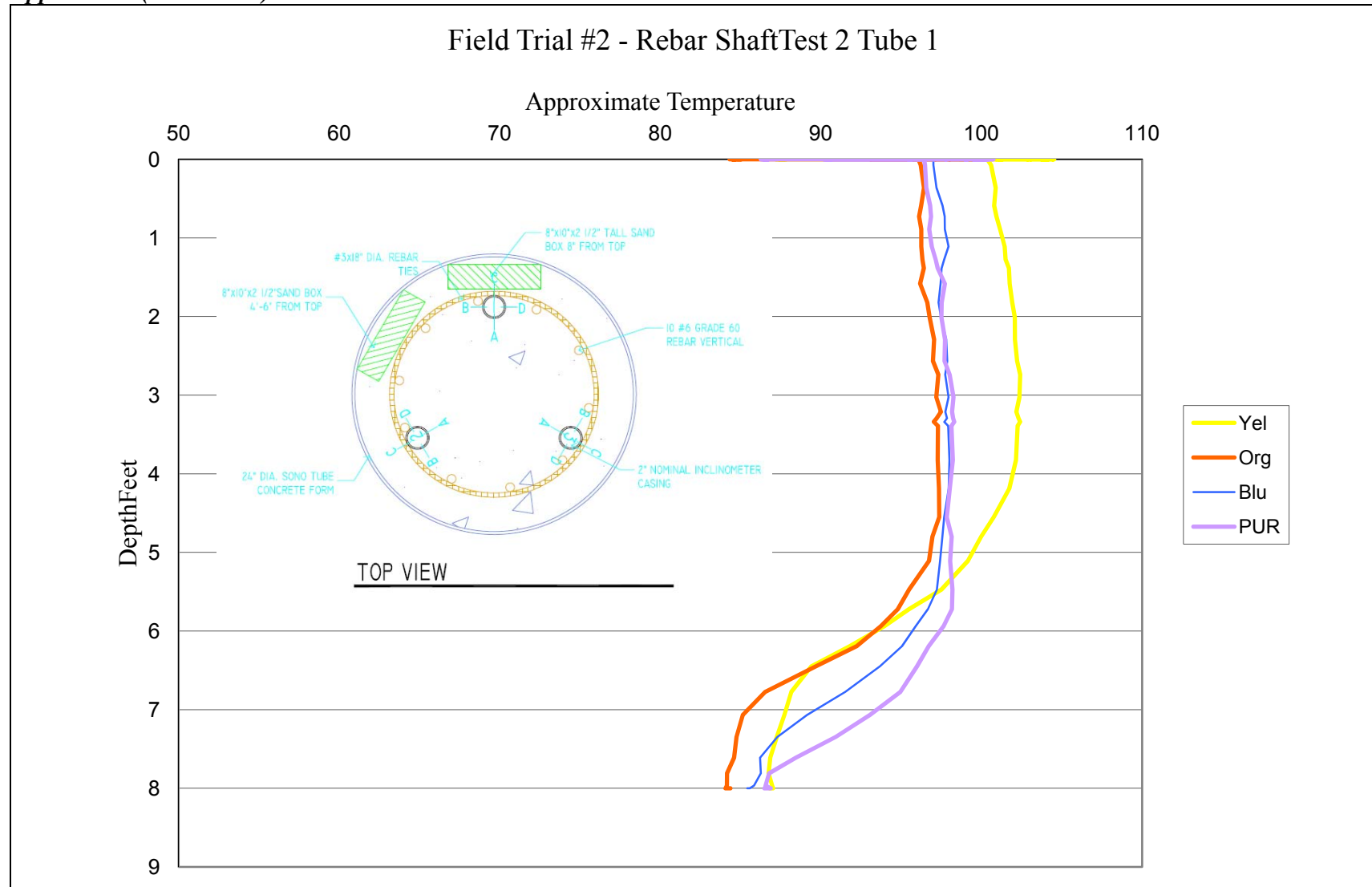


Figure B9 - Field trial #2 TIP test #2 rebar shaft tube 1

Appendix B (Continued)

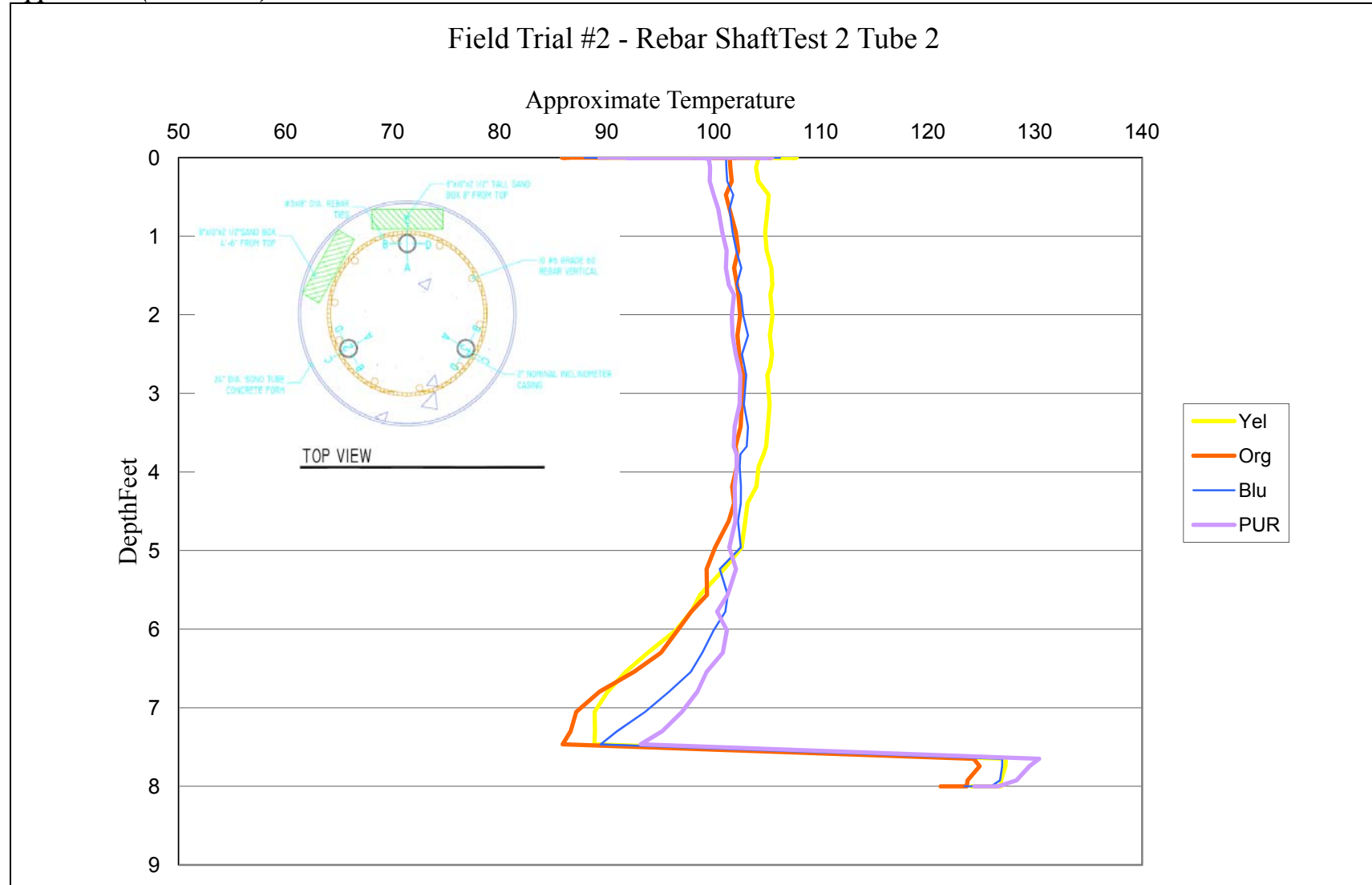


Figure B10 - Field trial #2 TIP test #2 rebar shaft tube 2

Appendix B (Continued)

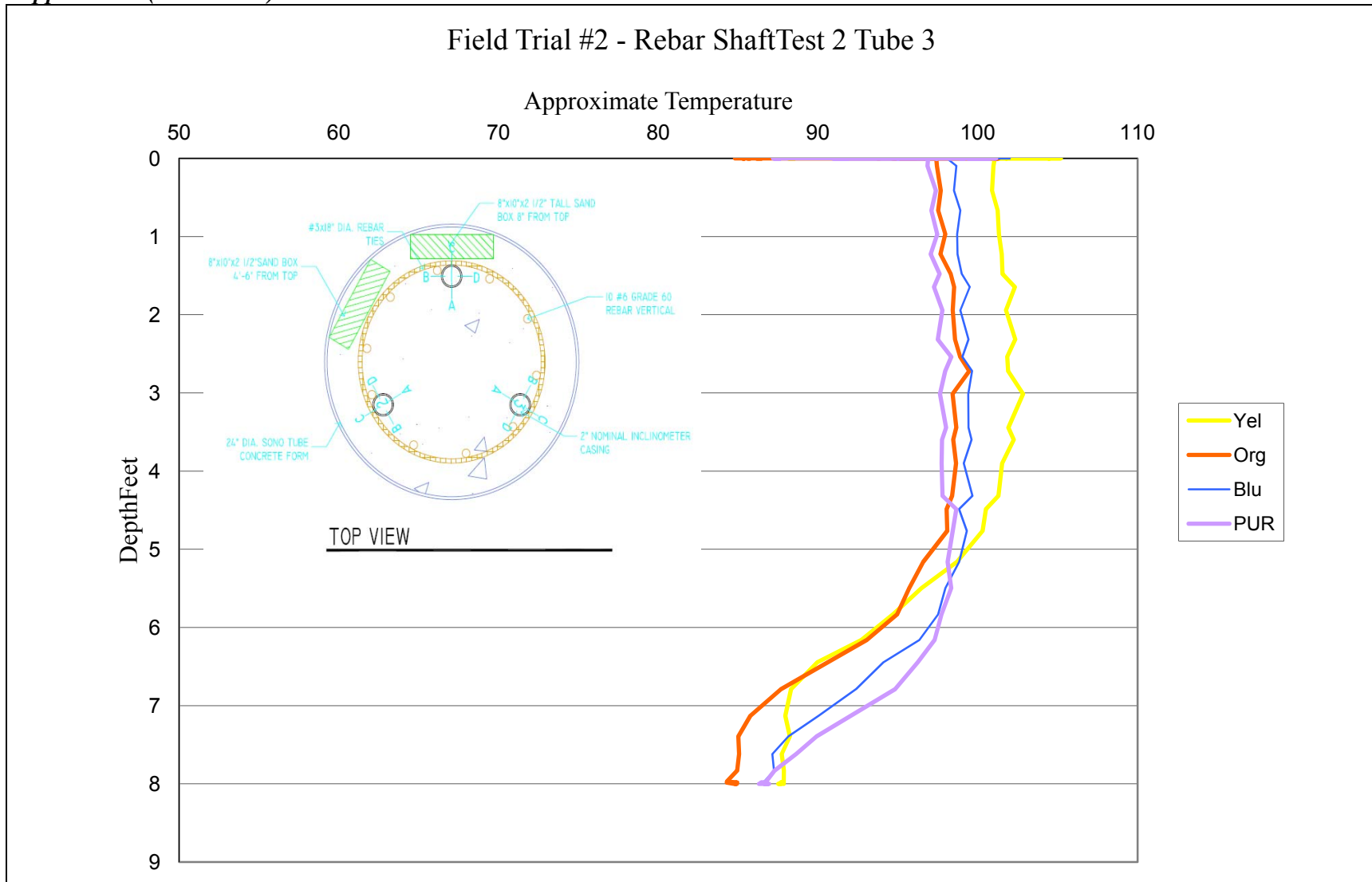


Figure B11 - Field trial #2 TIP test #2 rebar shaft tube 3

Appendix B (Continued)

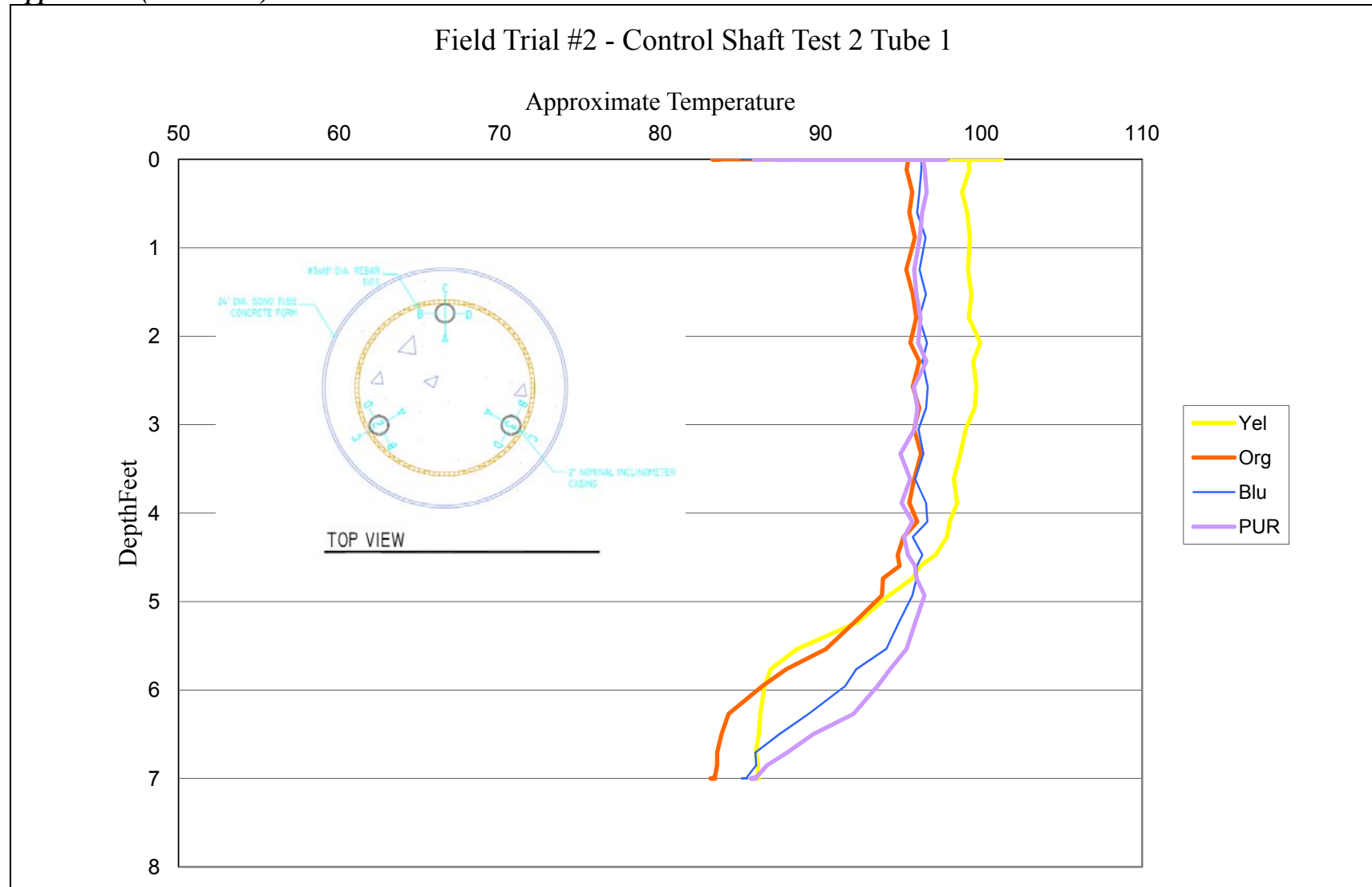


Figure B12 - Field trial #2 TIP test #2 control shaft tube 1

Appendix B (Continued)

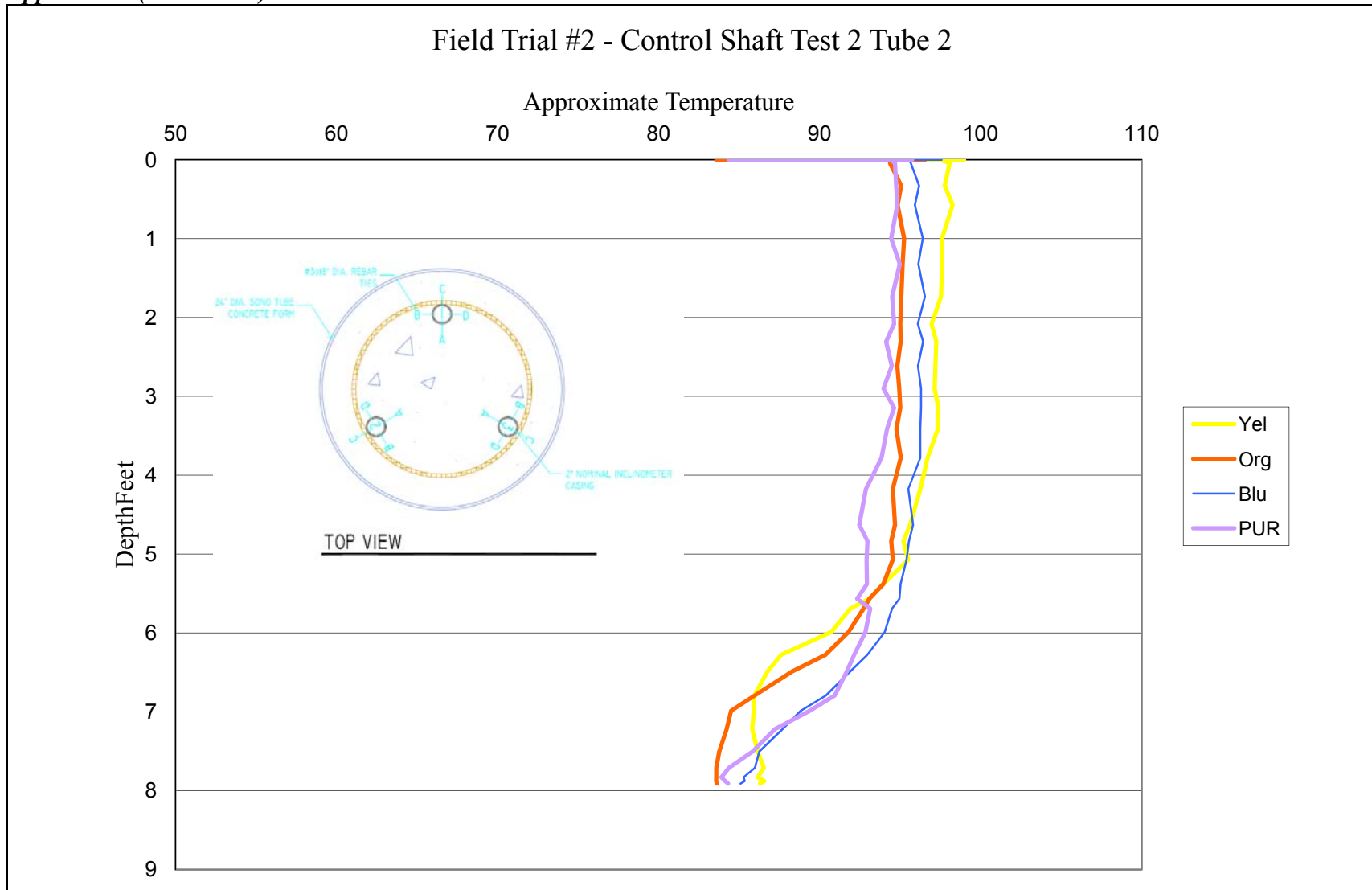


Figure B13 - Field trial #2 TIP test #2 control shaft tube 2

Appendix B (Continued)

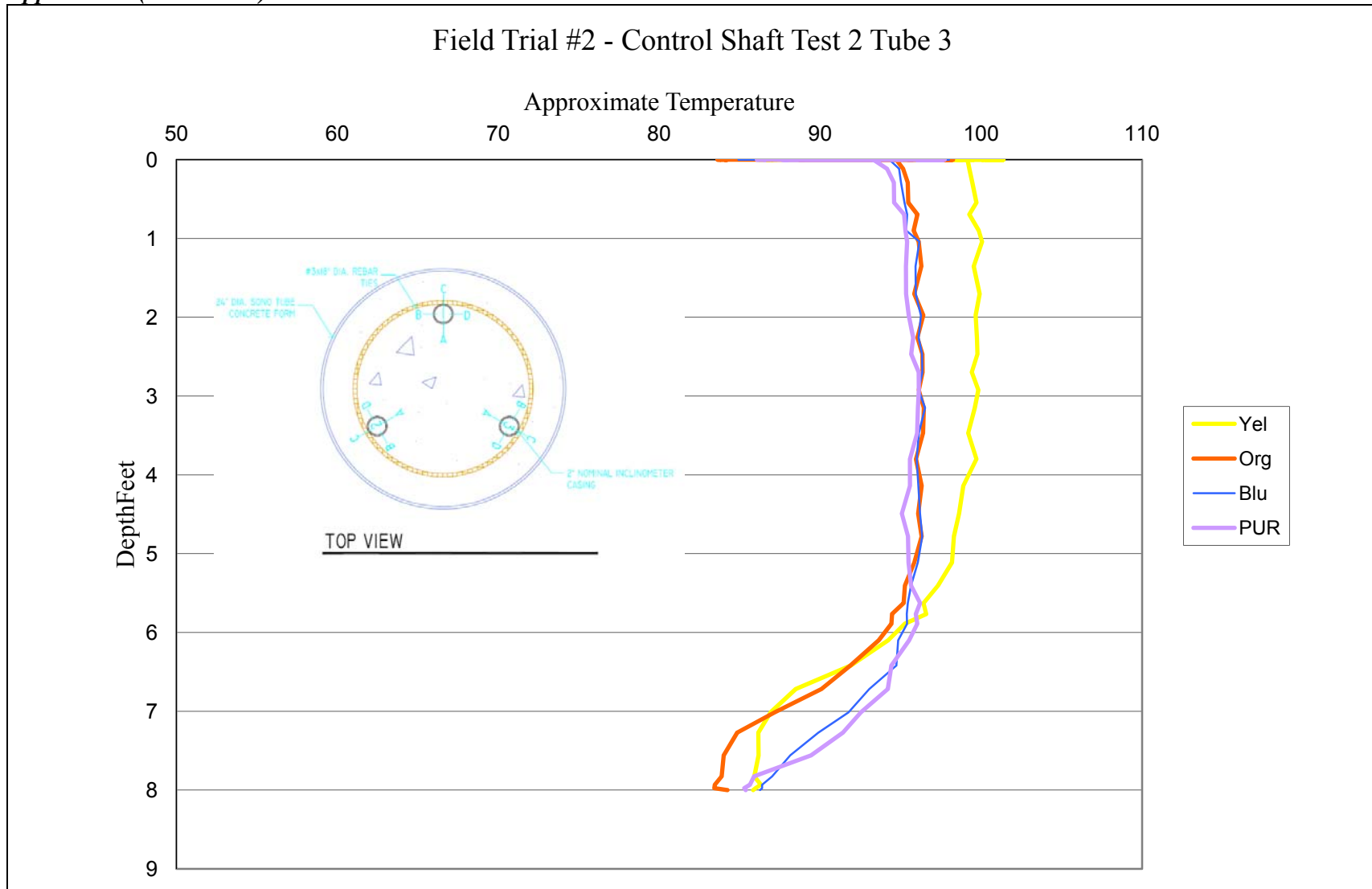


Figure B14 - Field trial #2 TIP test #2 control shaft tube 3

Appendix B (Continued)

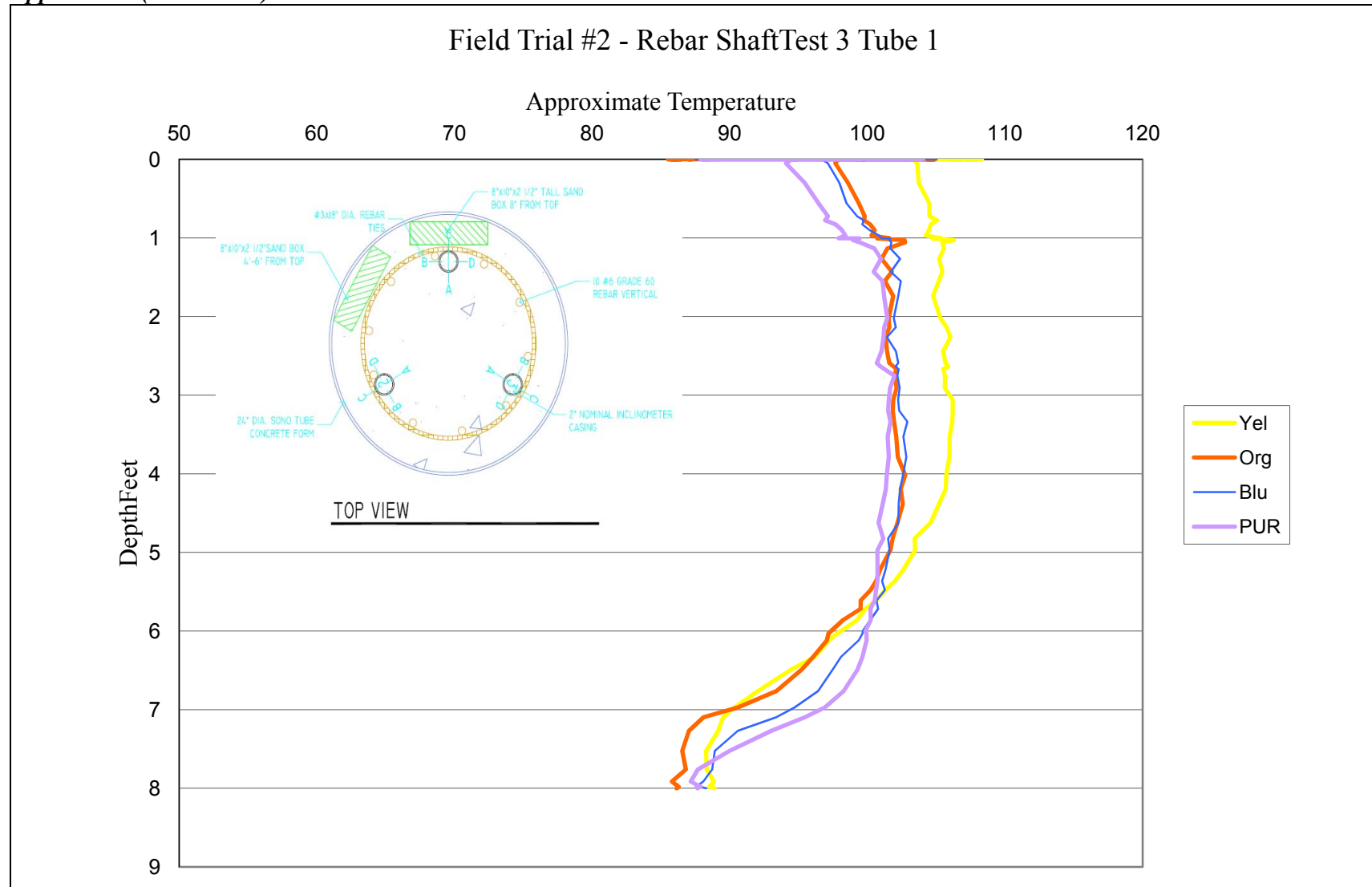


Figure B15 - Field trial #2 TIP test #3 rebar shaft tube 1

Appendix B (Continued)

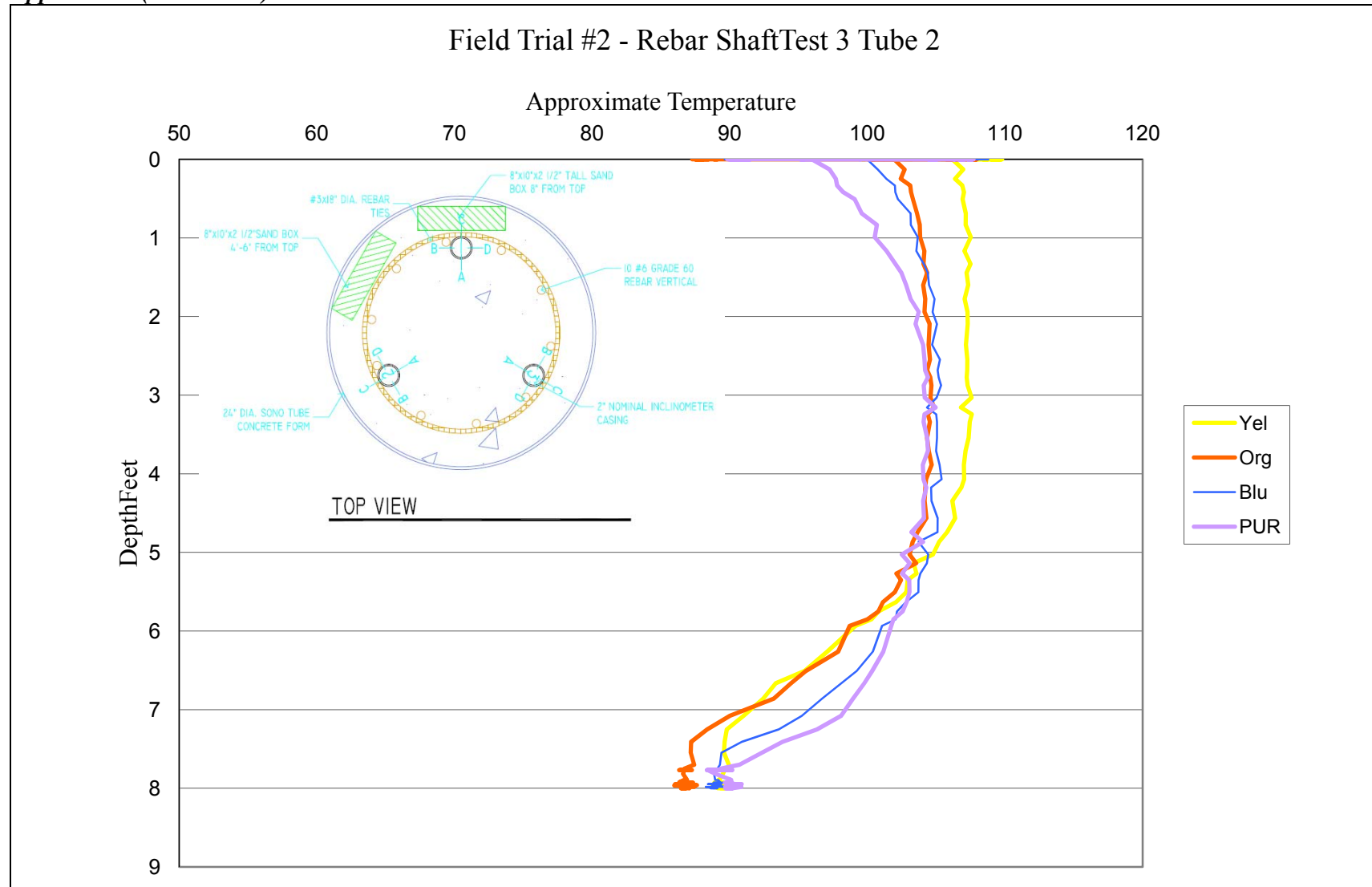


Figure B16 - Field trial #2 TIP test #3 rebar shaft tube 2

Appendix B (Continued)

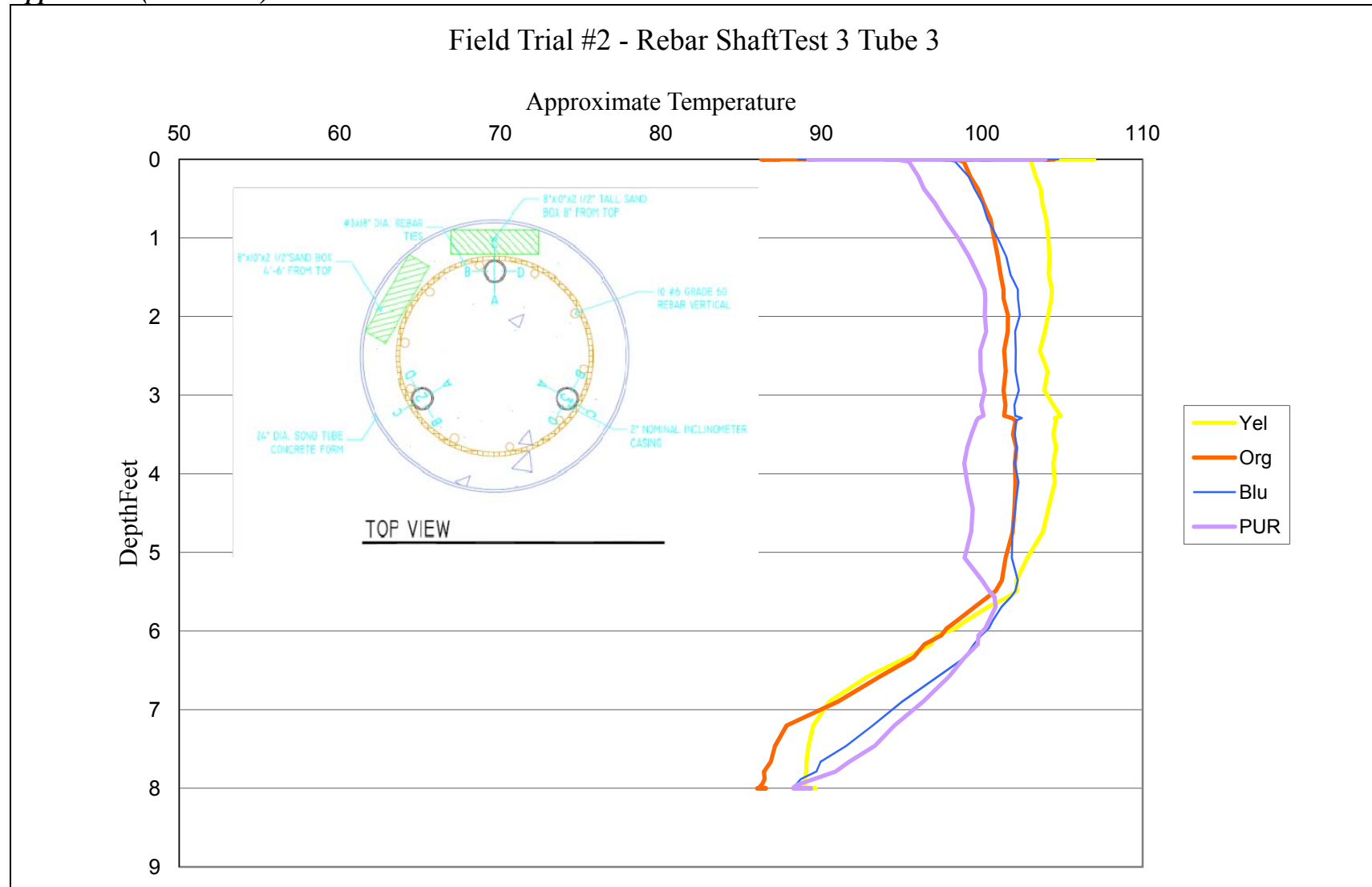


Figure B17 - Field trial #2 TIP test #3 rebar shaft tube 3

Appendix C - Additional Information Auburn Test Site

The information contained in this appendix is additional information and test results from the Auburn test site.

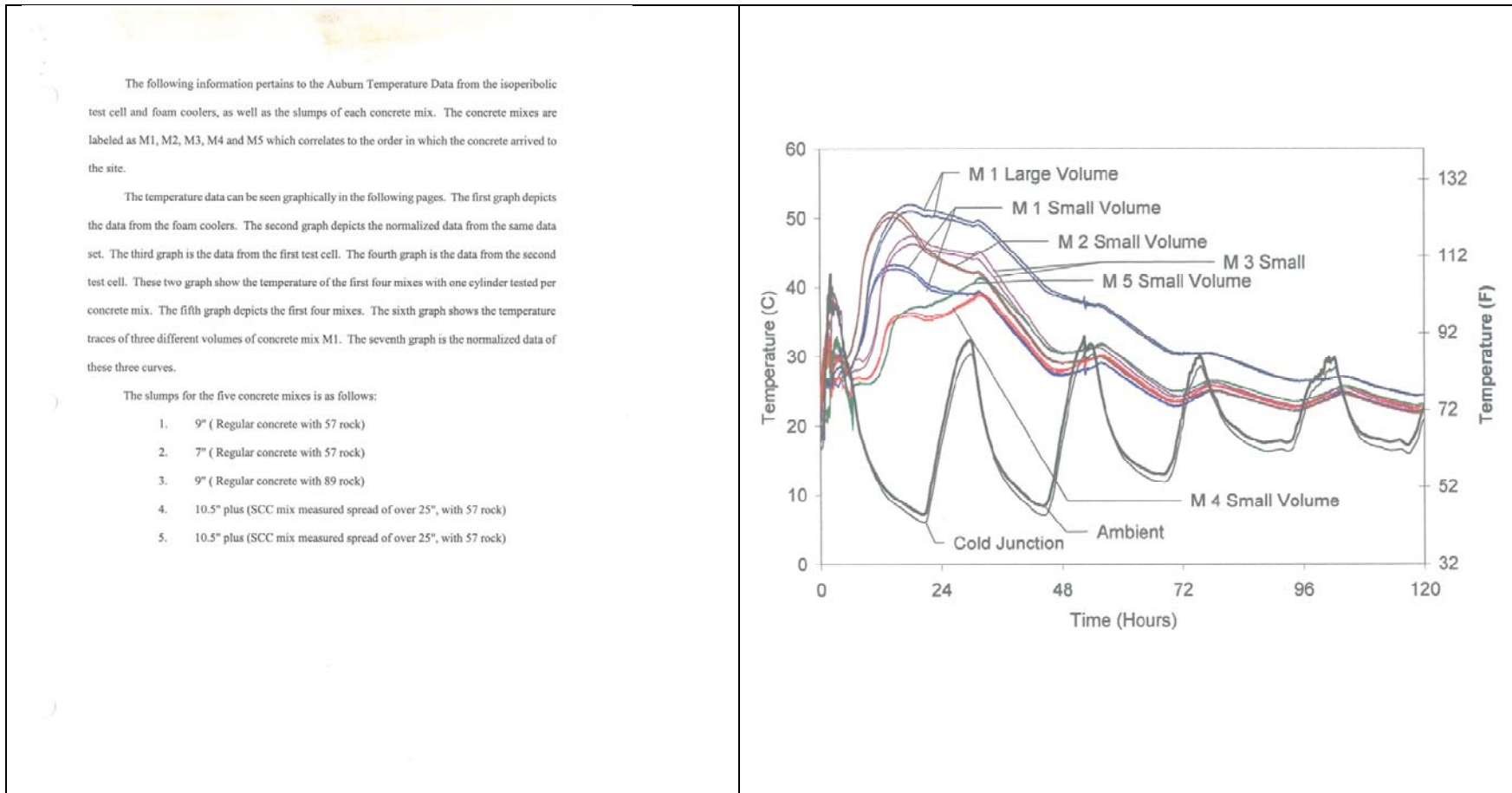


Figure C1 - Explanation of thermocouple data from Auburn test site

Figure C2 - Auburn test site thermocouple data from foam coolers

Appendix C (Continued)

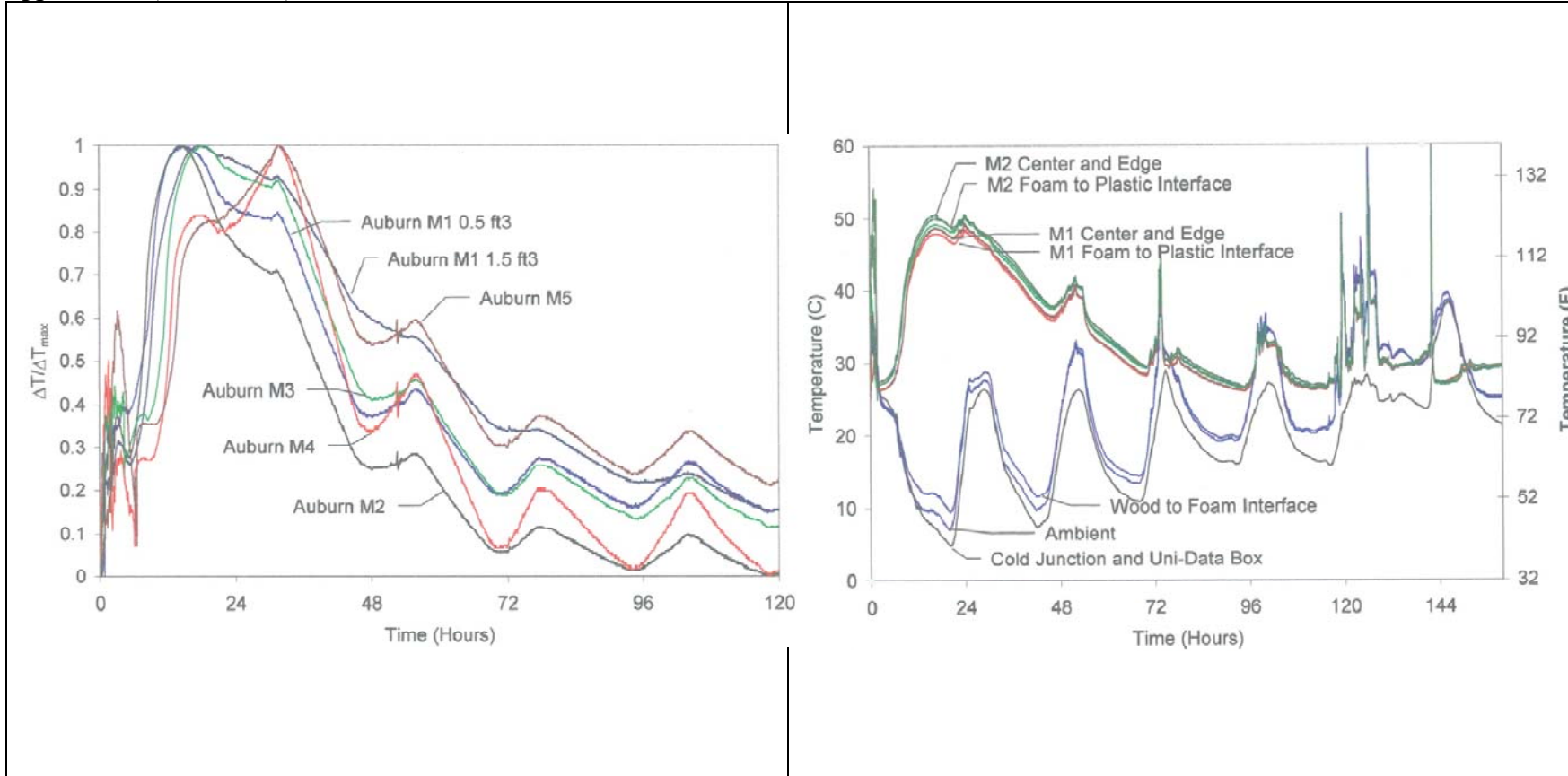


Figure C3 - Auburn test site thermocouple data normalized

Figure C4 - Auburn test site thermocouple data from adiabatic box #1

Appendix C (Continued)

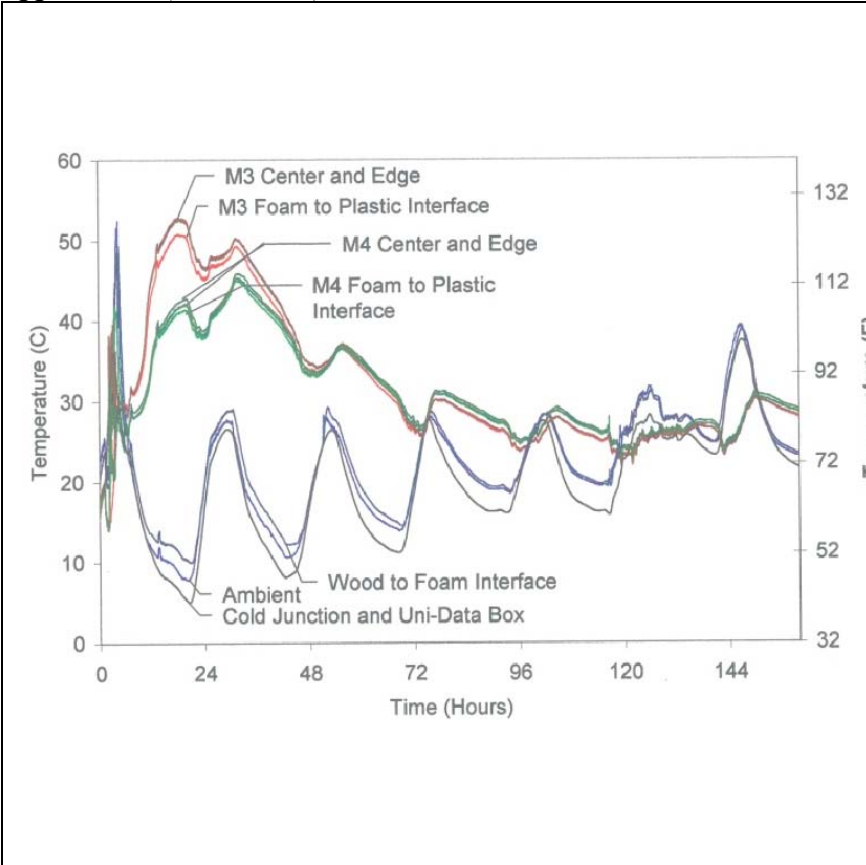


Figure C5 - Auburn test site thermocouple data from adiabatic box #2

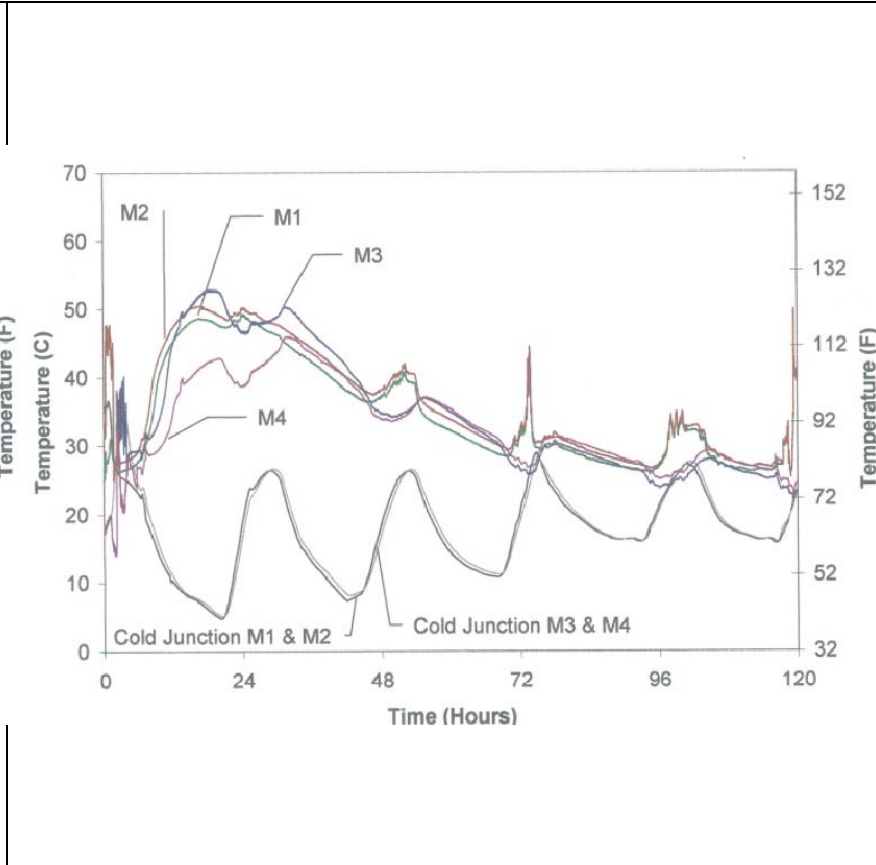


Figure C6 - Auburn test site thermocouple data from first four mixes

Appendix C (Continued)

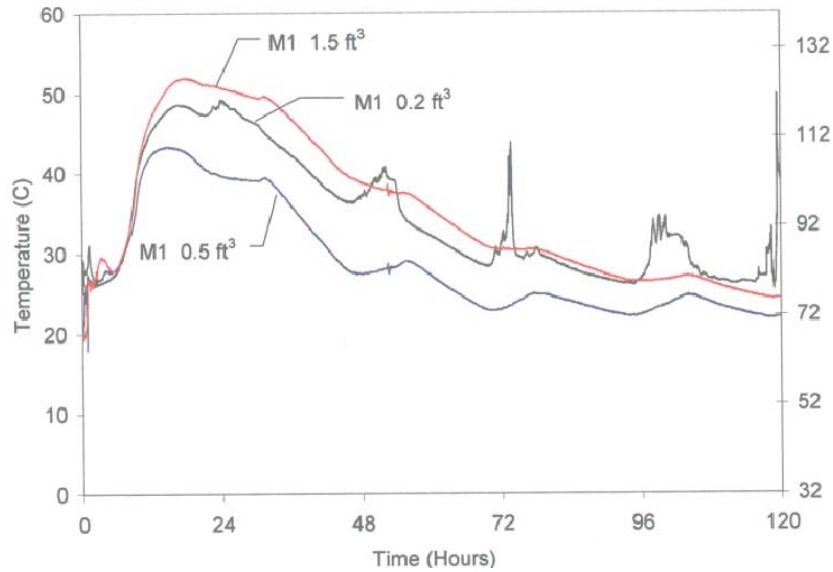


Figure C7 - Auburn test site thermocouple data for three different volumes of the same mix (M1)

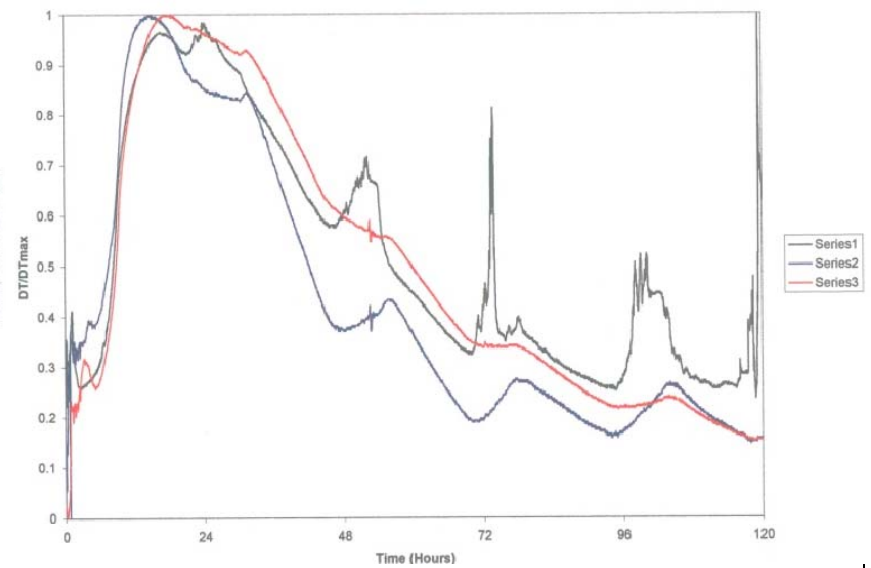


Figure C8 - Auburn test site normalized thermocouple data for three different volumes of mix M1

Appendix C (Continued)

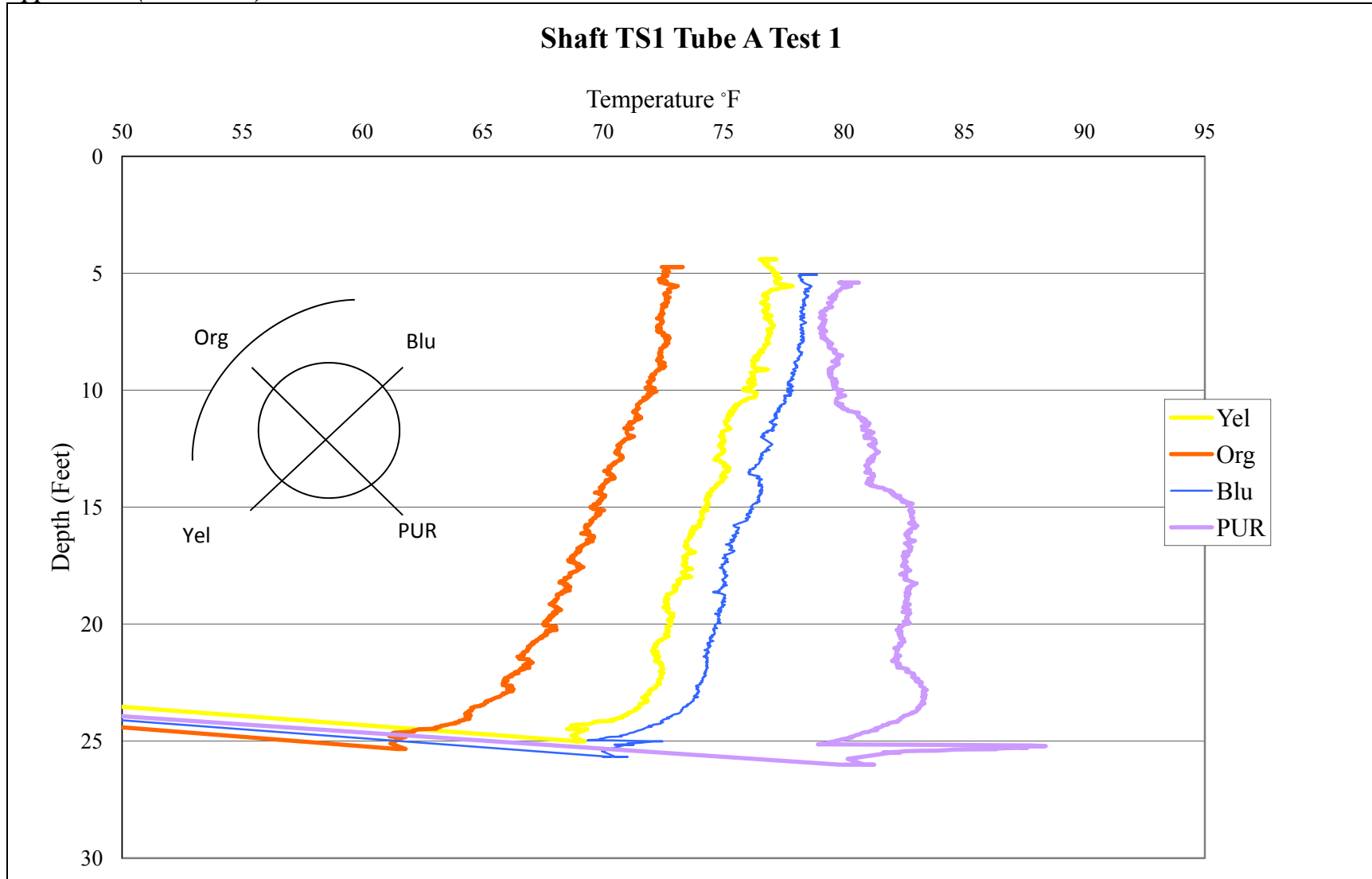


Figure C9 - Auburn test site TIP test results TS1 tube A Test 1

Appendix C (Continued)

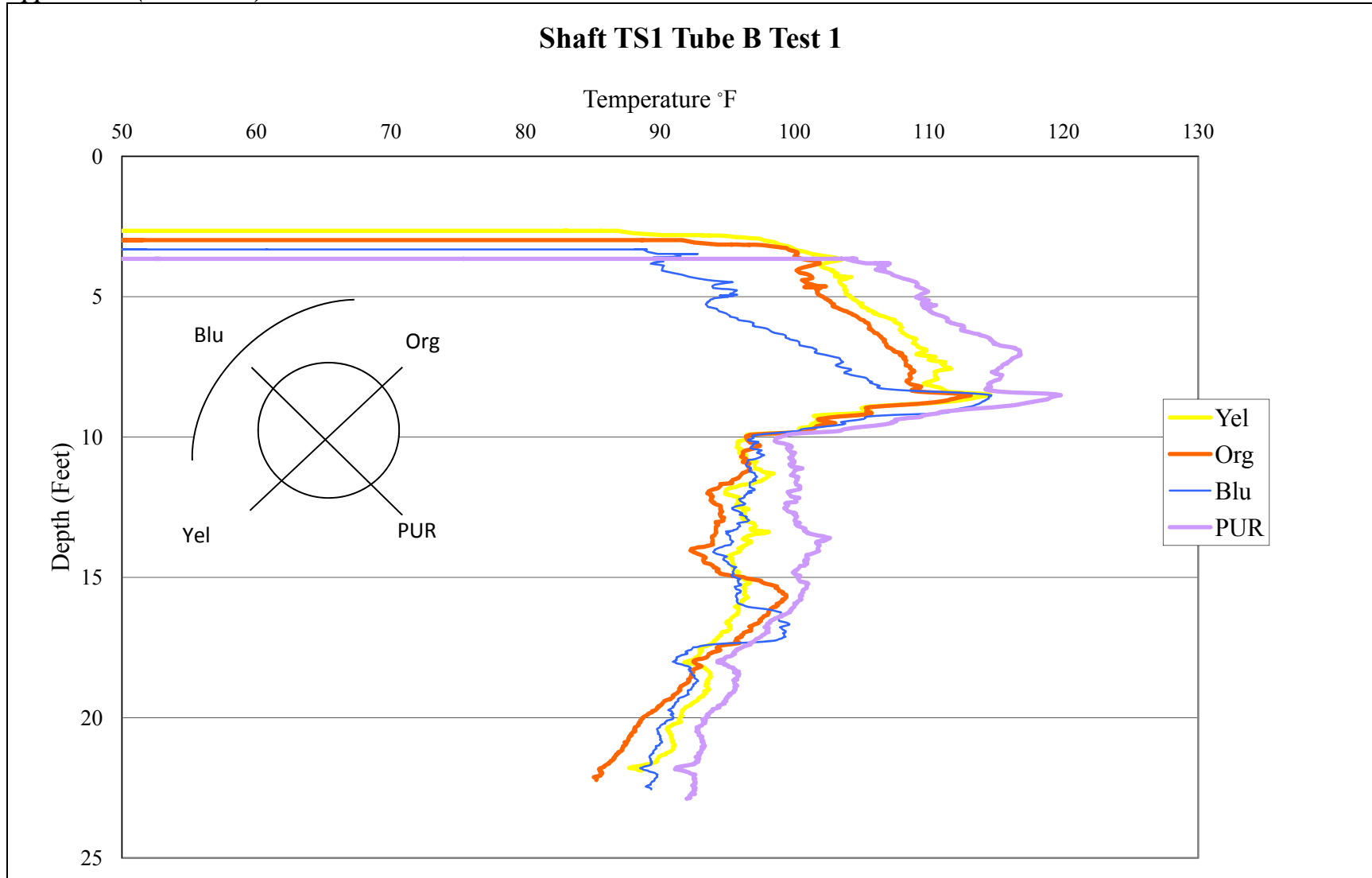


Figure C10 - Auburn test site TIP test results TS1 tube B Test 1

Appendix C (Continued)

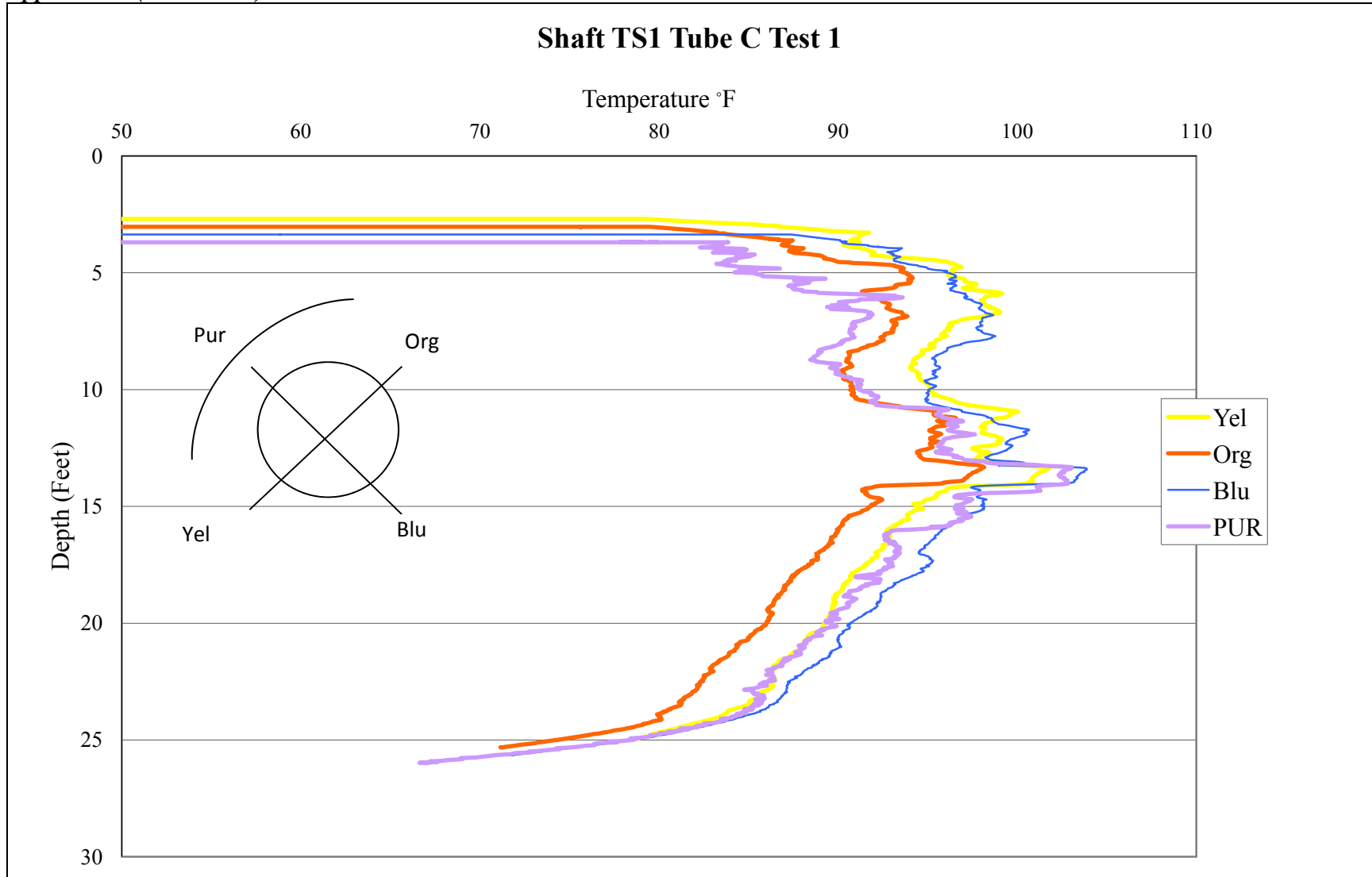


Figure C11 - Auburn test site TIP test results TS1 tube C Test 1

Appendix C (Continued)

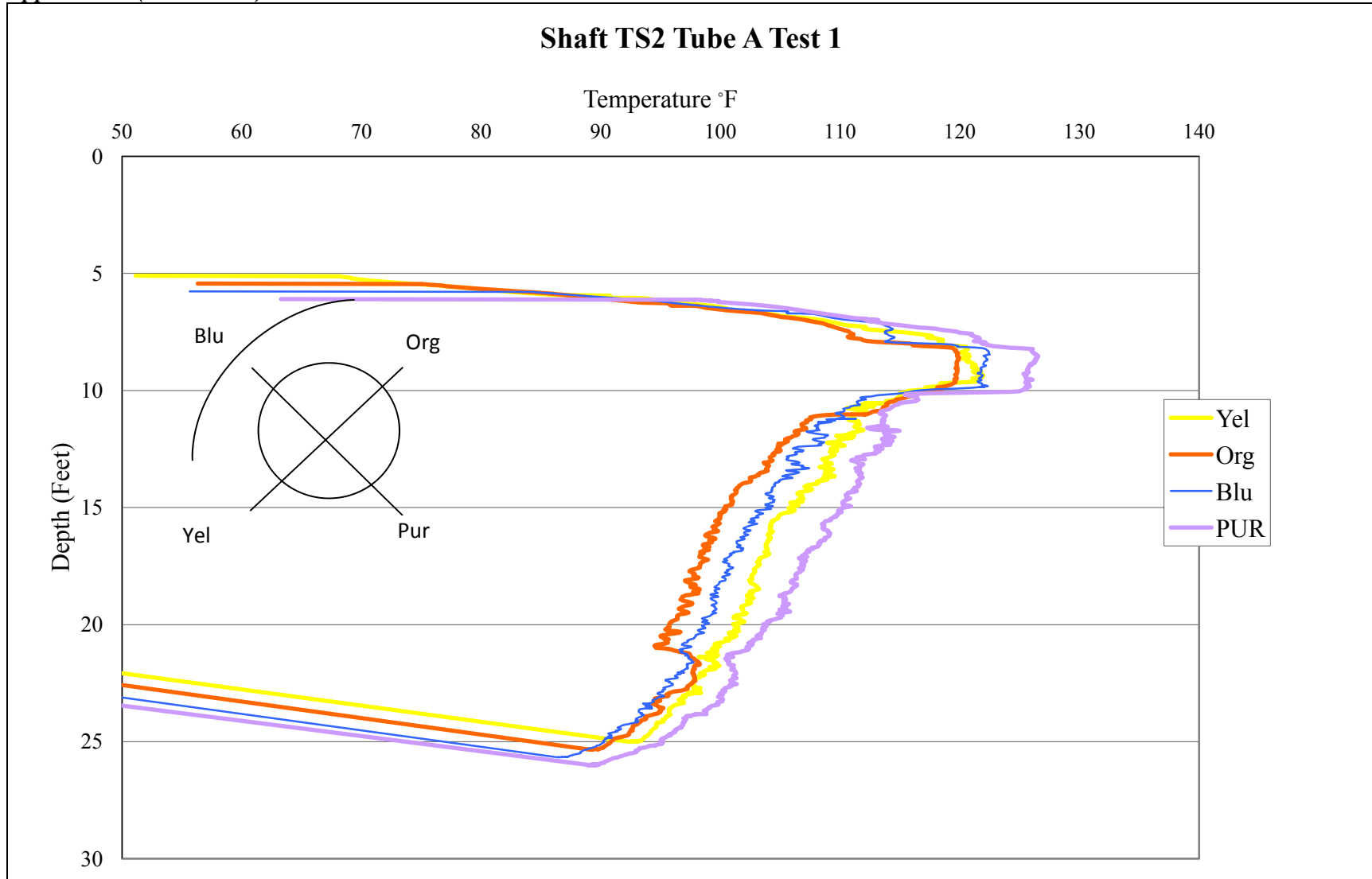


Figure C12 - Auburn test site TIP test results TS2 tube A Test 1

Appendix C (Continued)

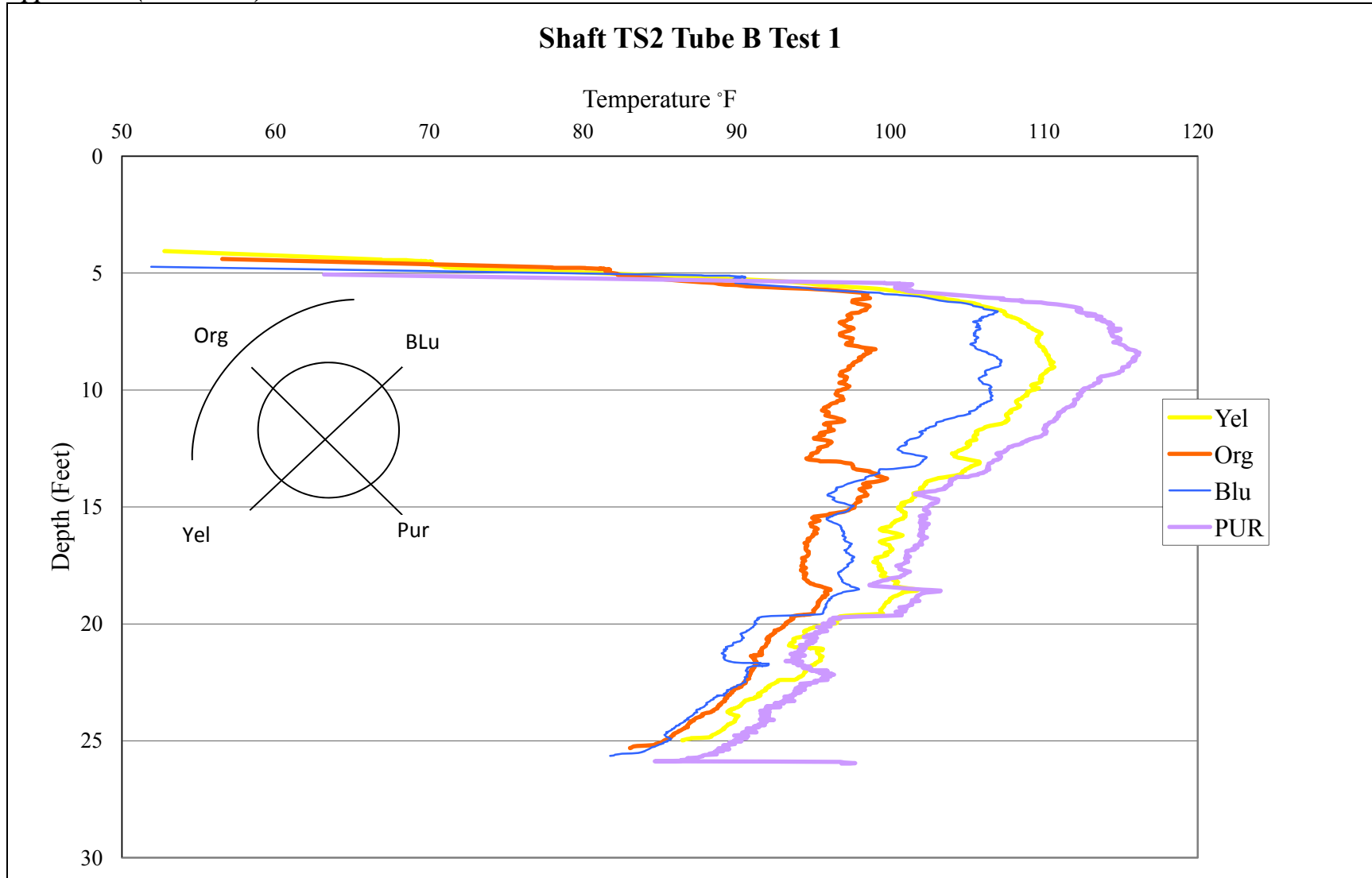


Figure C13 - Auburn test site TIP test results TS2 Tube B Test 1

Appendix C (Continued)

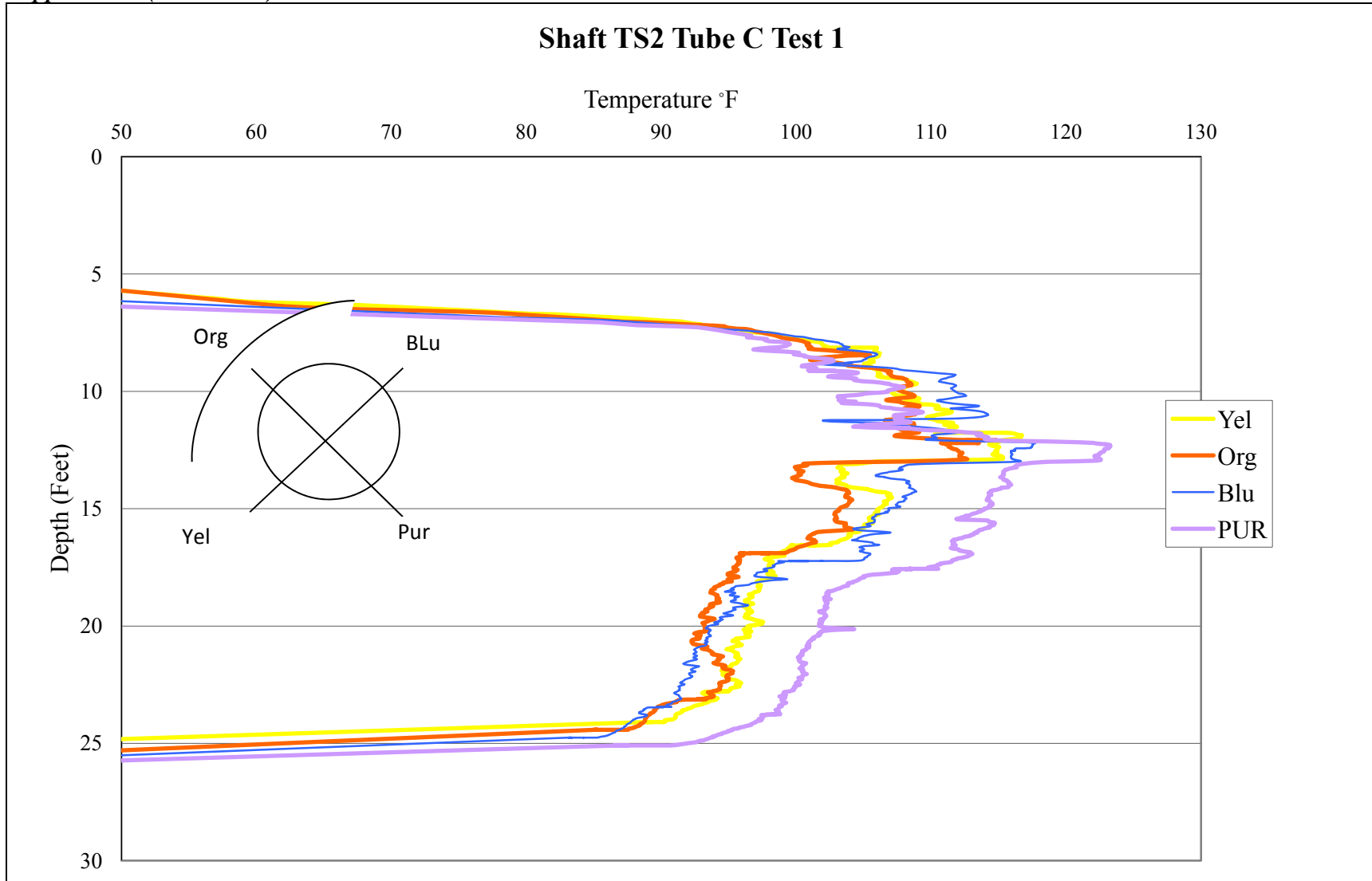


Figure C14 - Auburn test site TIP test results TS2 Tube C Test 1

Appendix C (Continued)

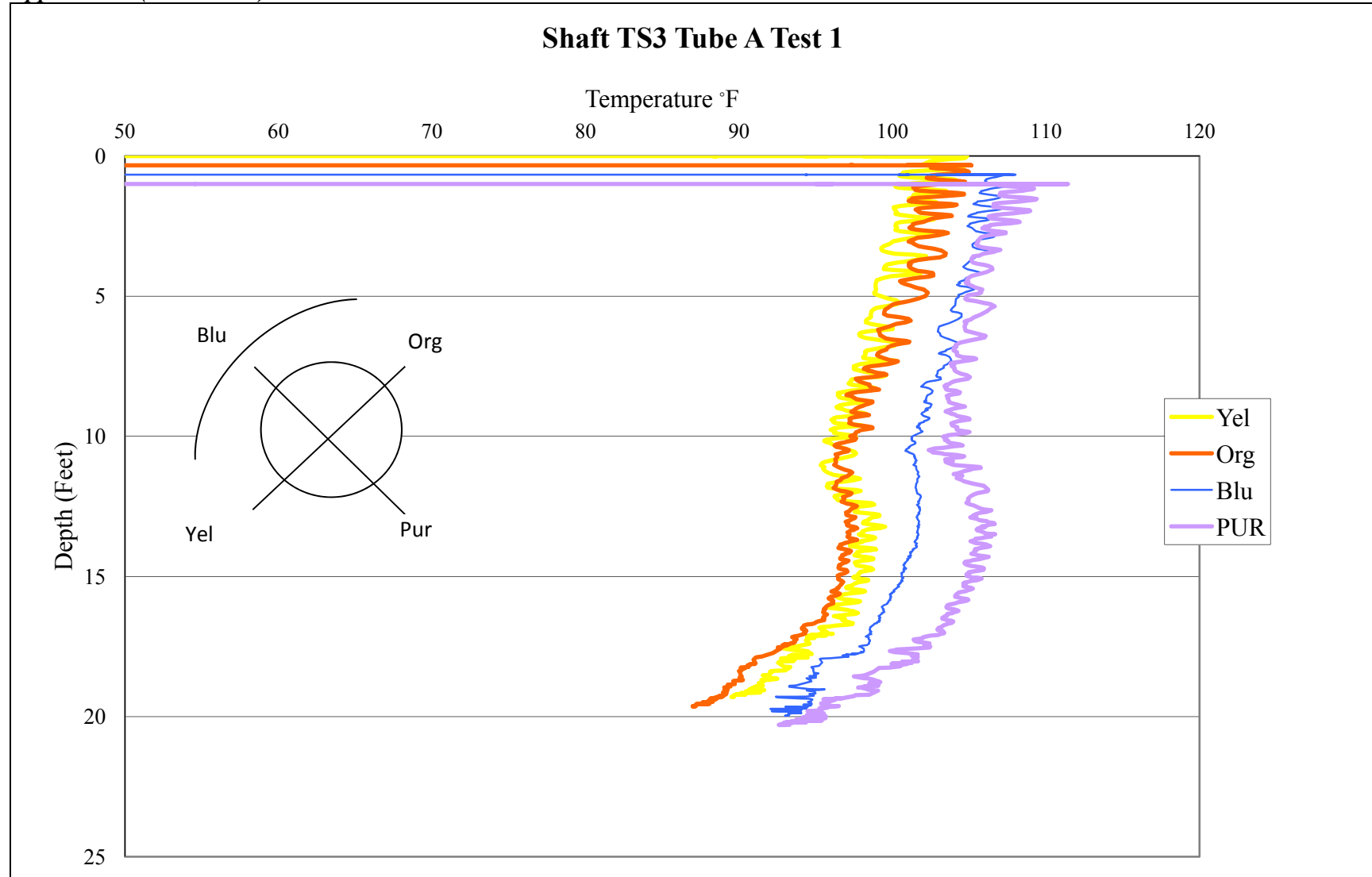


Figure C15 - Auburn test site TIP test results TS3 Tube A Test 1

Appendix C (Continued)

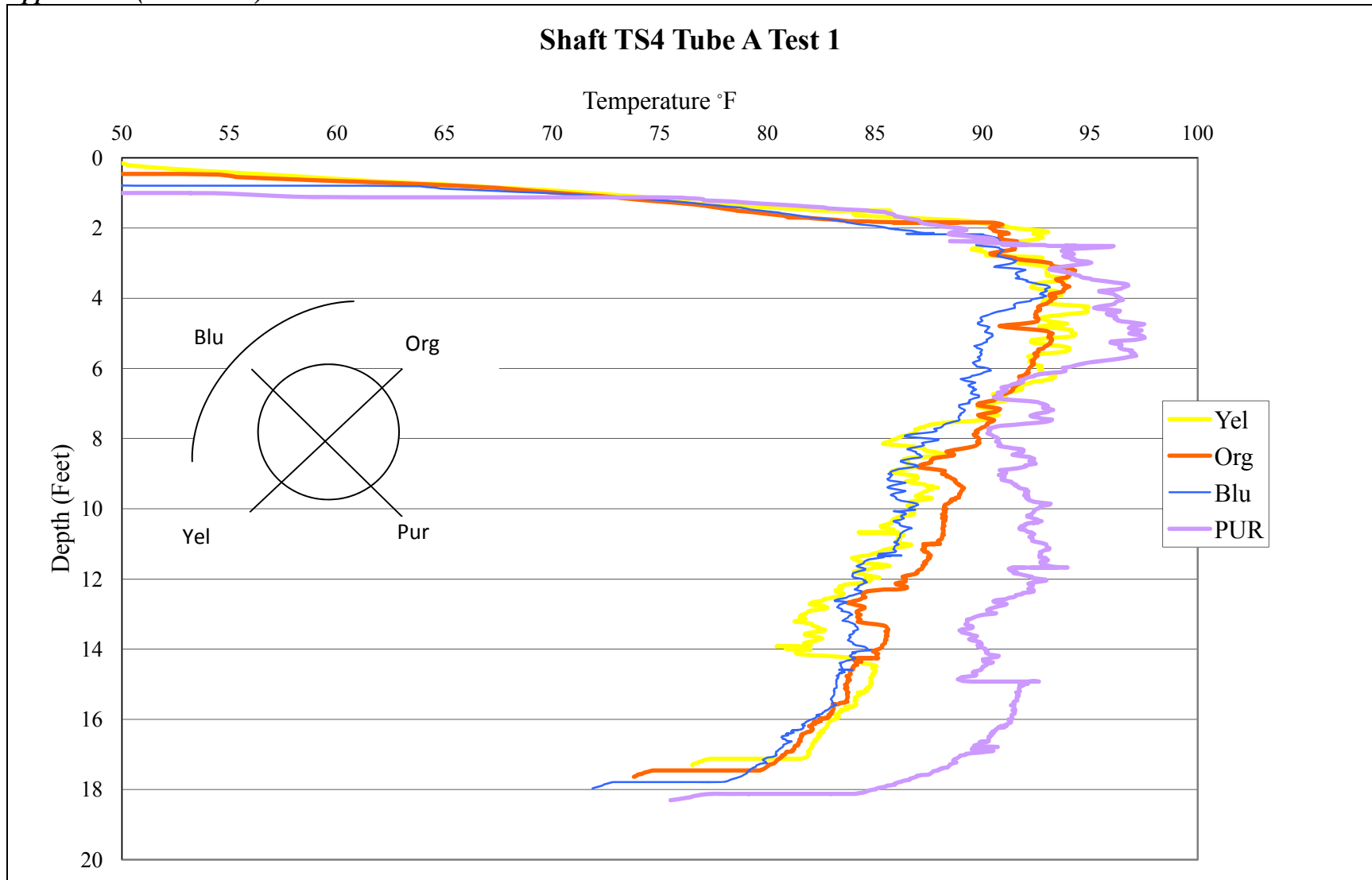


Figure C16 - Auburn test site TIP test results TS4 Tube A Test 1

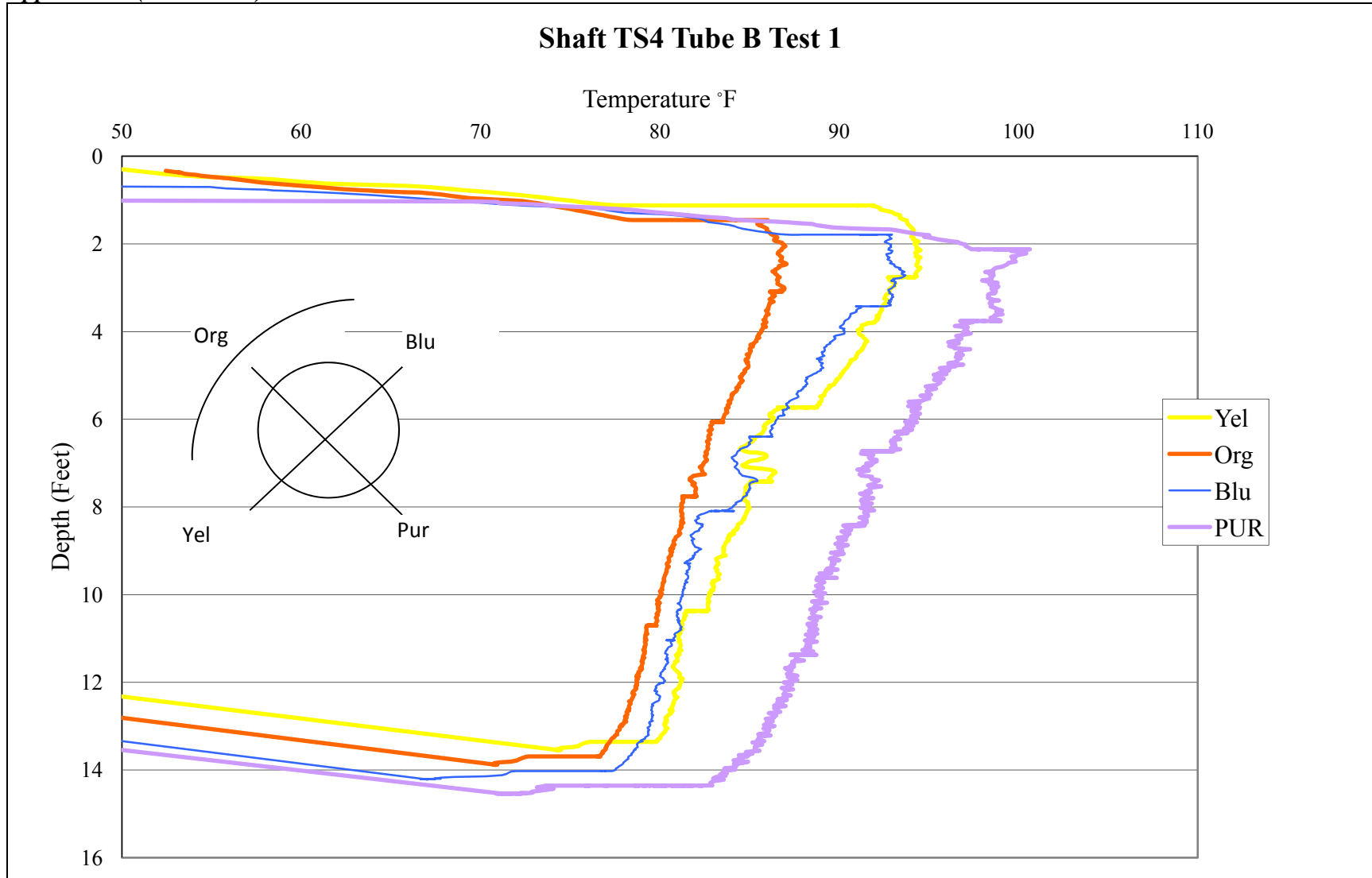


Figure C17 - Auburn test site TIP test results TS4 Tube B Test 1

Appendix C (Continued)

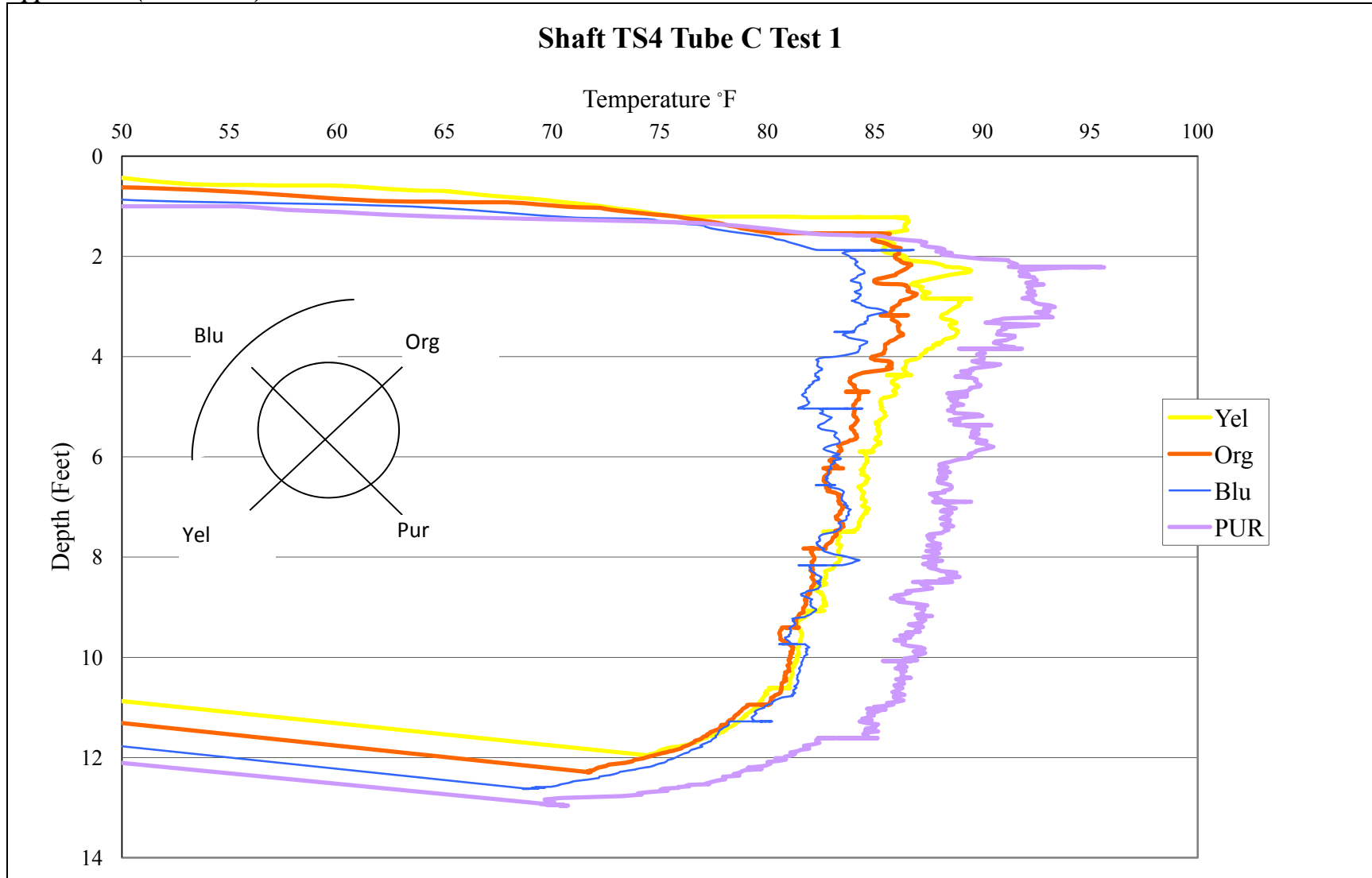


Figure C18 - Auburn test site TIP test results TS4 Tube C Test 1

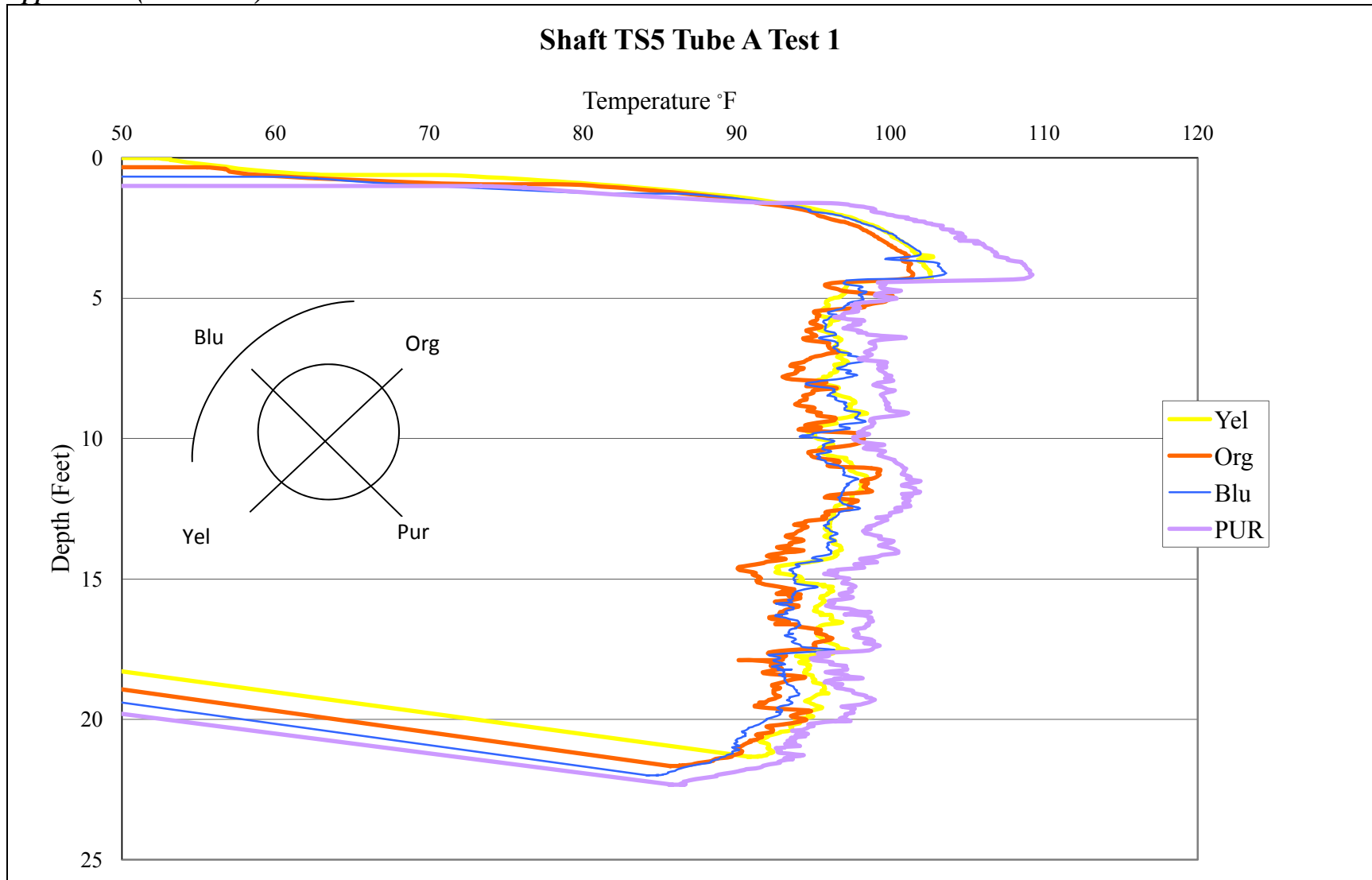


Figure C19 - Auburn test site TIP test results TS5 Tube A Test 1

Appendix C (Continued)

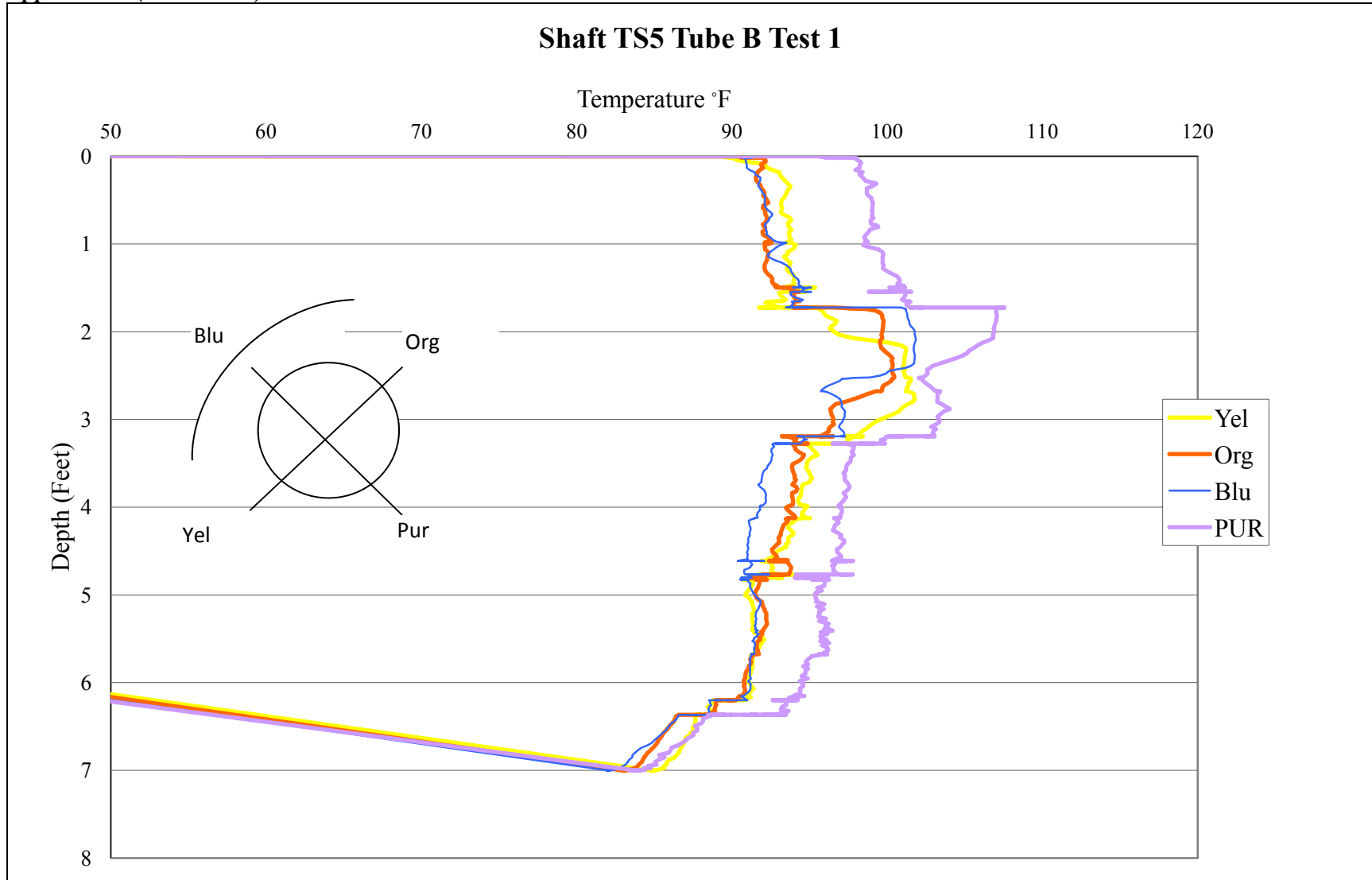


Figure C20 - Auburn test site TIP test results TS5 Tube B Test 1

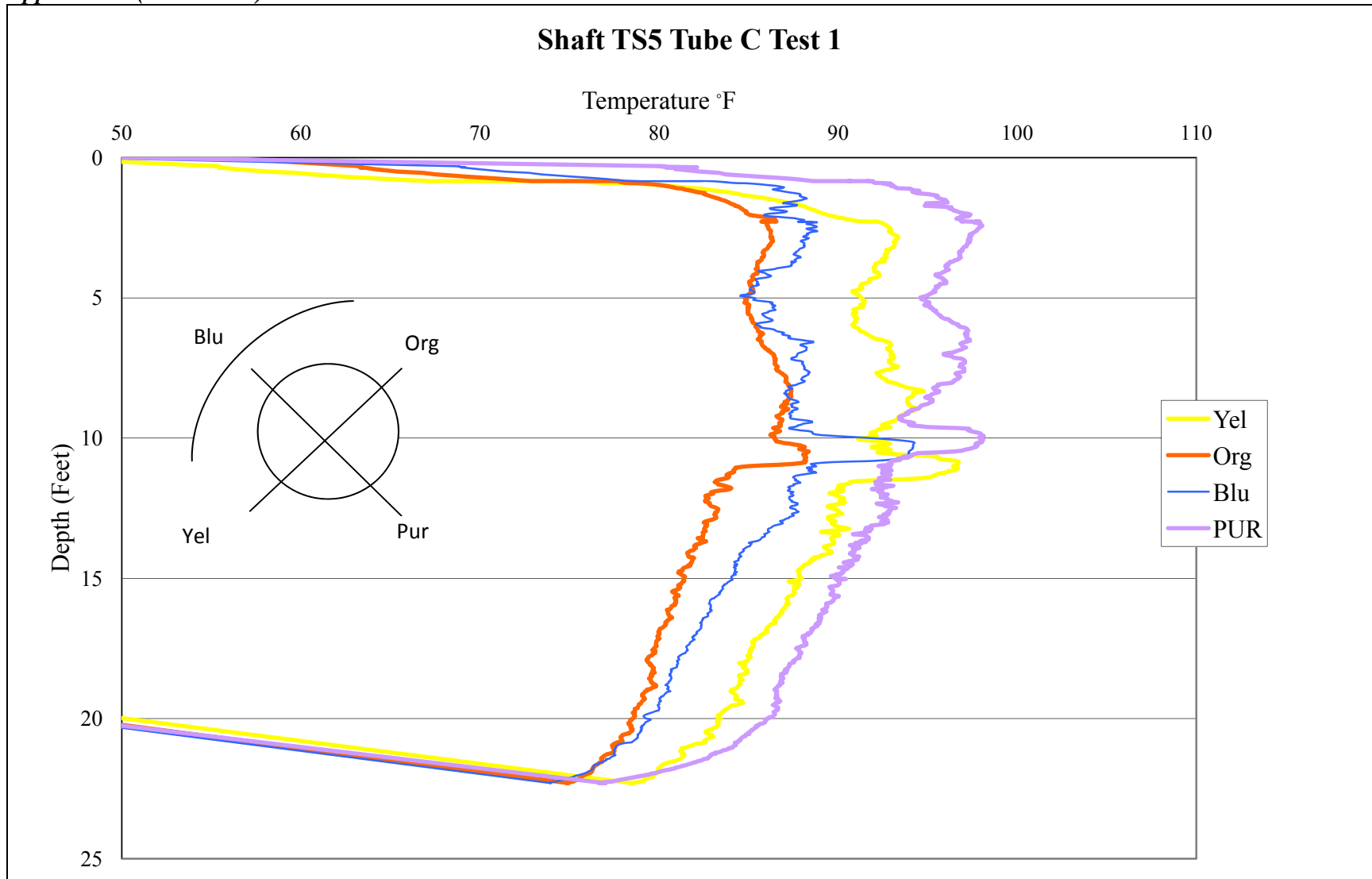


Figure C21 - Auburn test site TIP test results TS5 Tube C Test 1

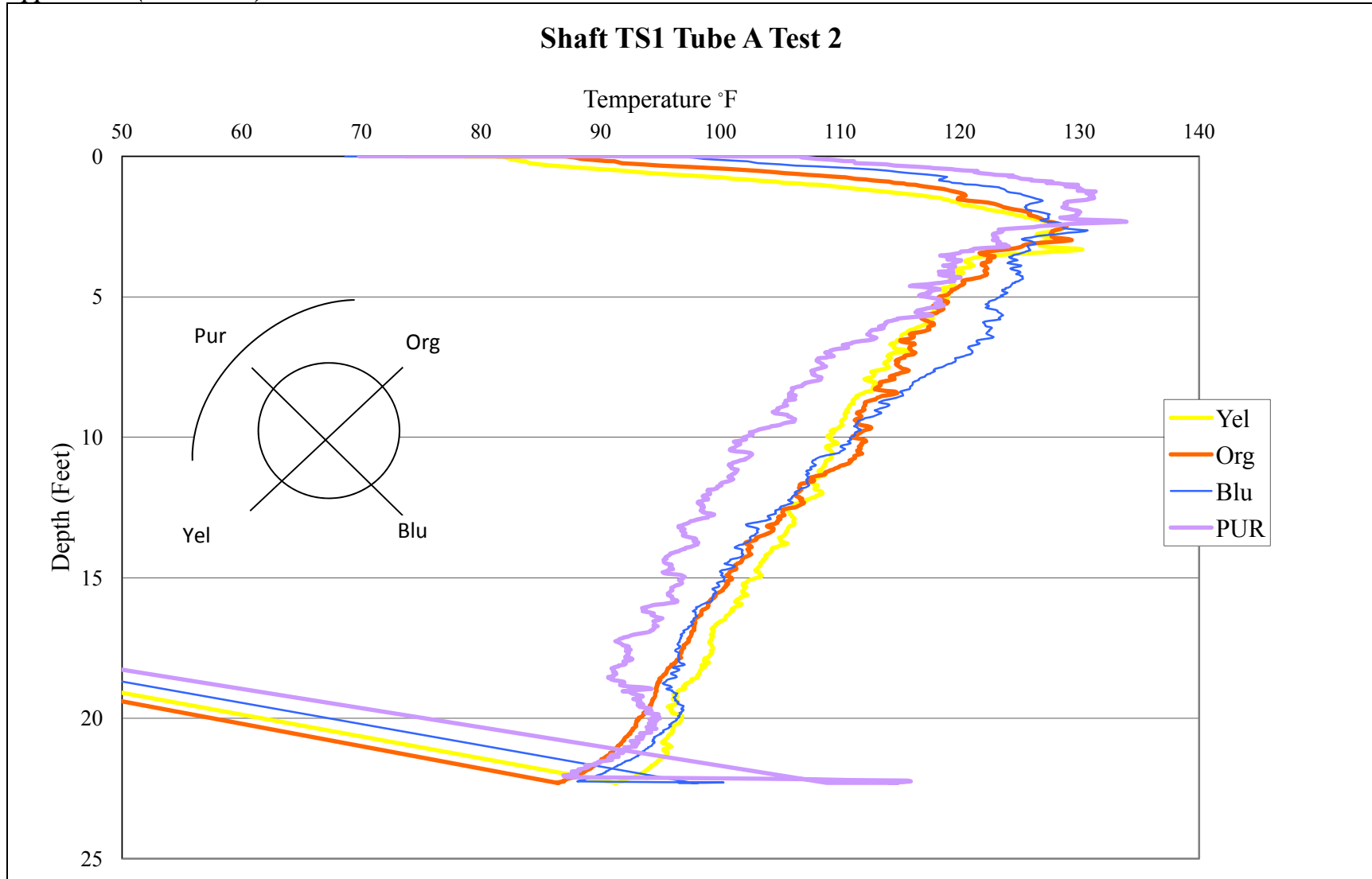


Figure C22 - Auburn test site TIP test results TS1 Tube A Test 2

Appendix C (Continued)

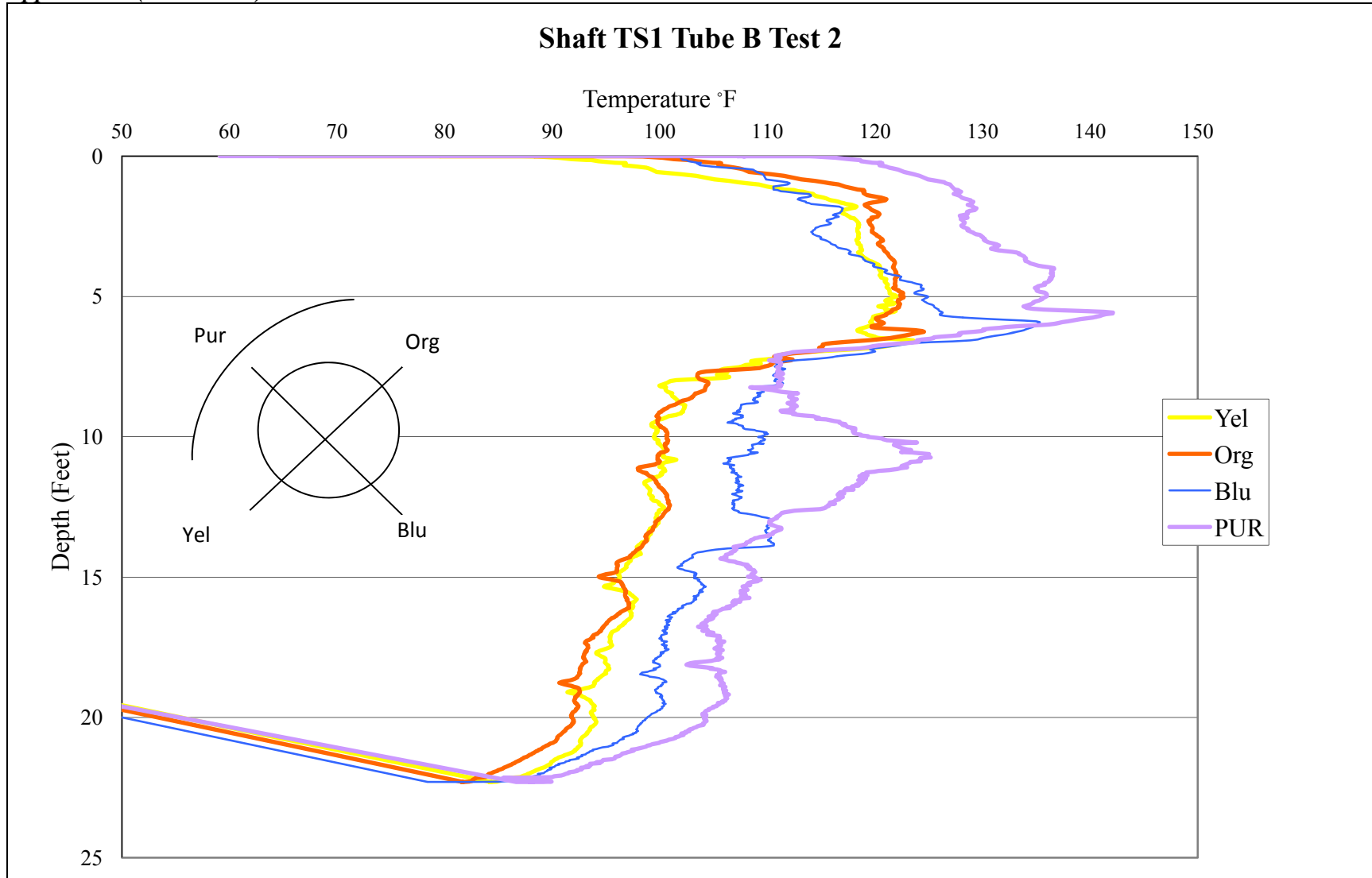


Figure C23 - Auburn test site TIP test results TS1 Tube B Test 2

Appendix C (Continued)

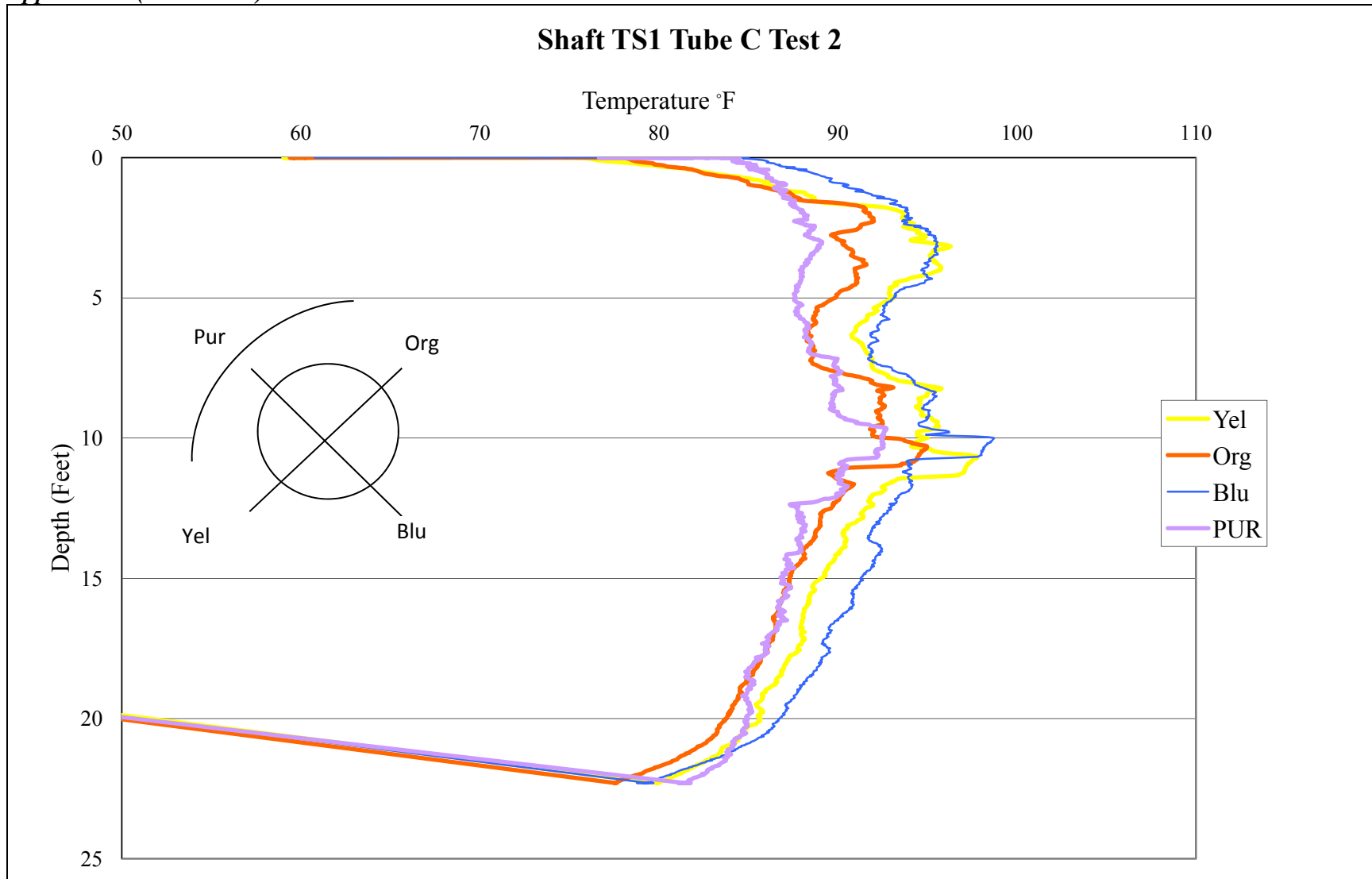


Figure C24 - Auburn test site TIP test results TS1 Tube C Test 2

Appendix C (Continued)

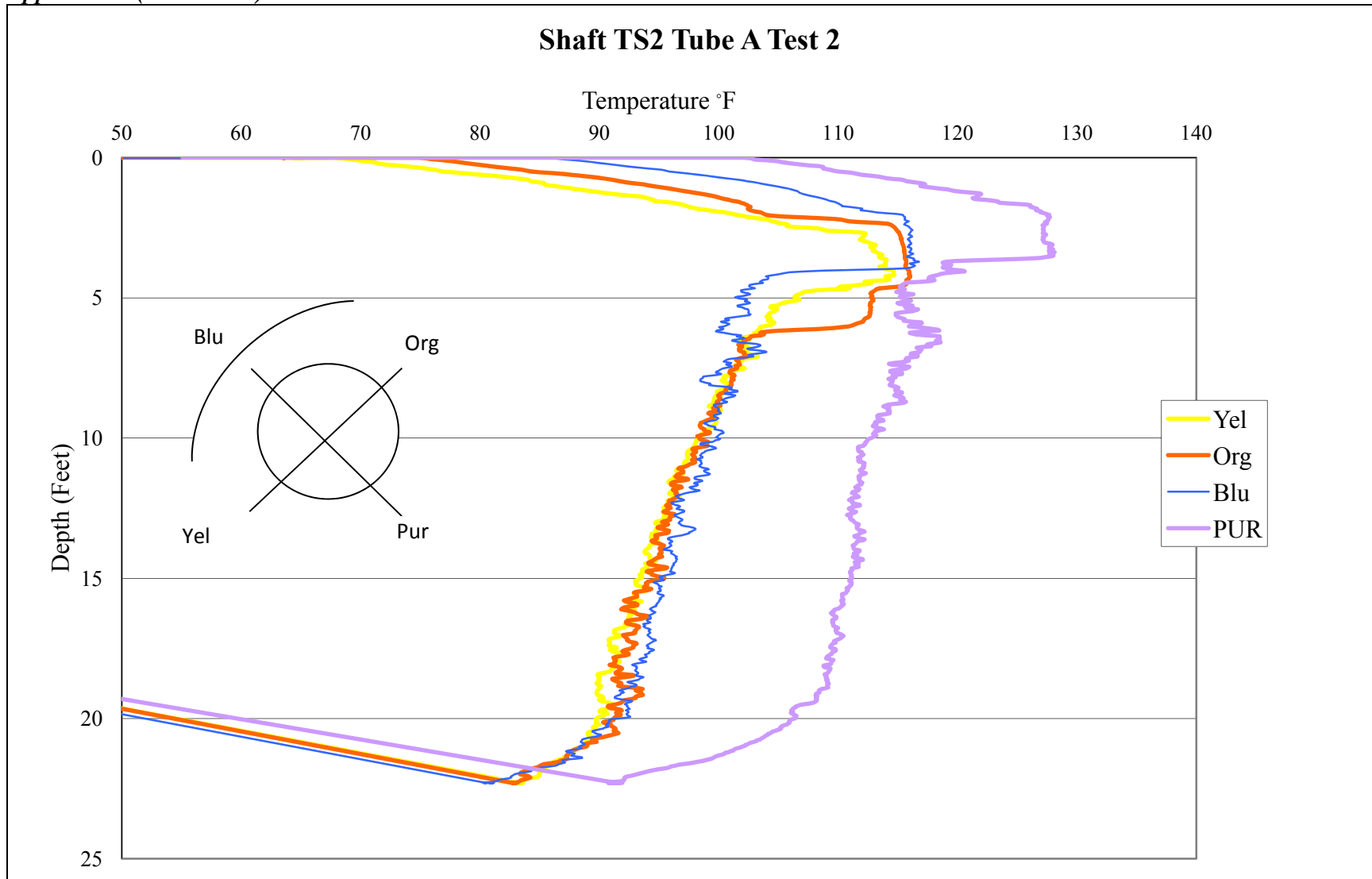


Figure C25 - Auburn test site TIP test results TS2 Tube A Test 2

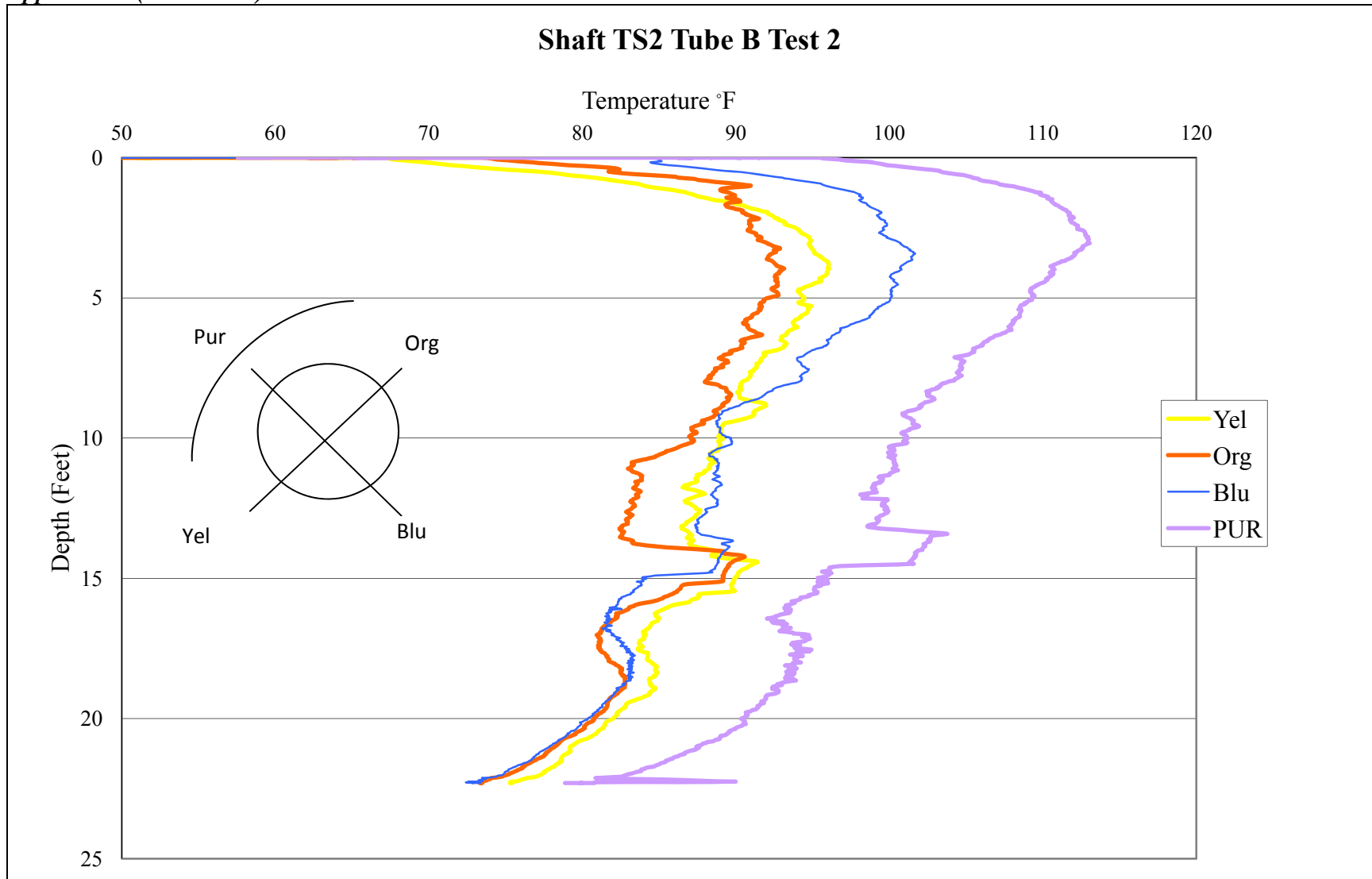


Figure C26 - Auburn test site TIP test results TS2 Tube B Test 2

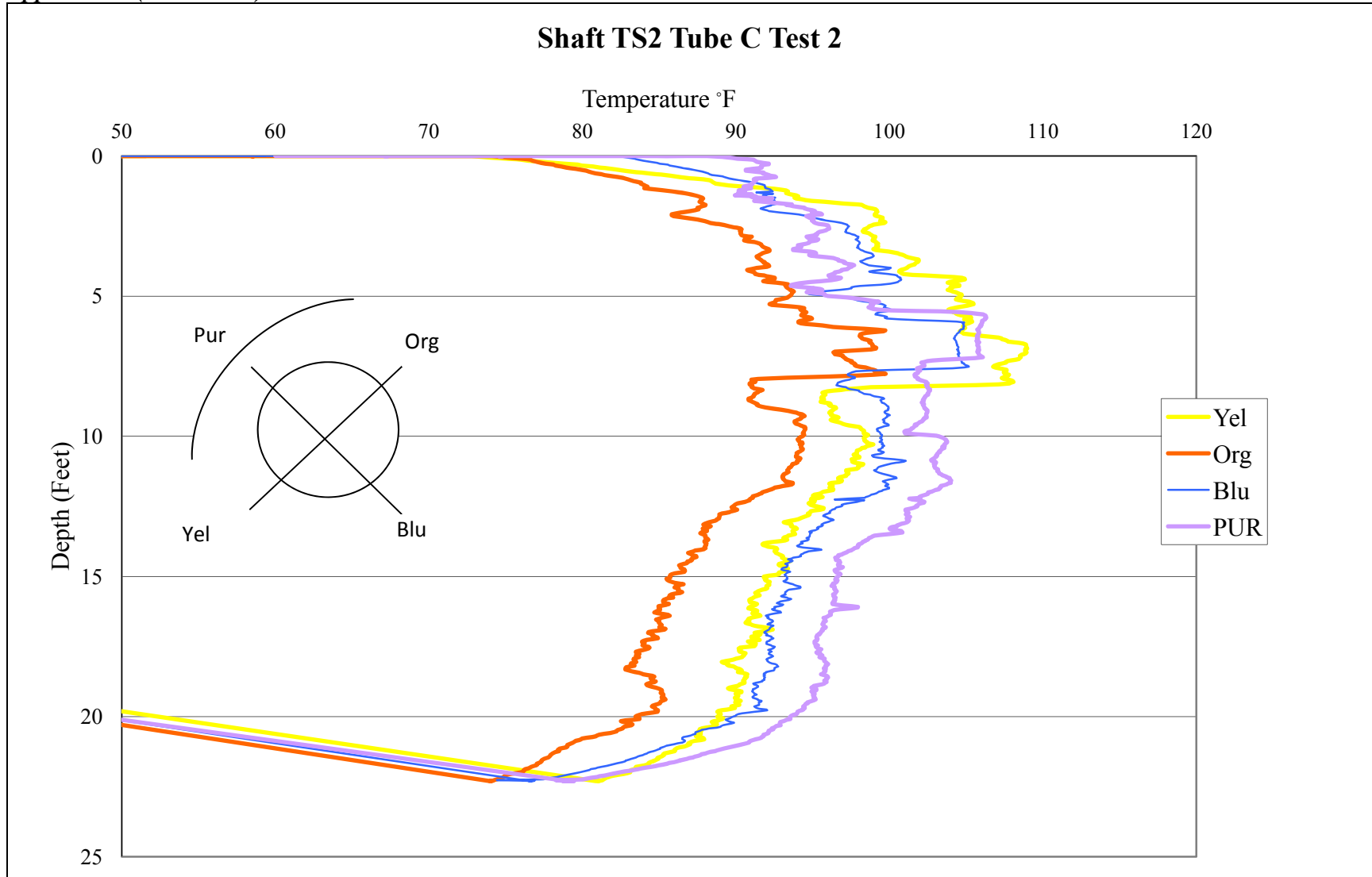


Figure C27 - Auburn test site TIP test results TS2 Tube C Test 2

Appendix C (Continued)

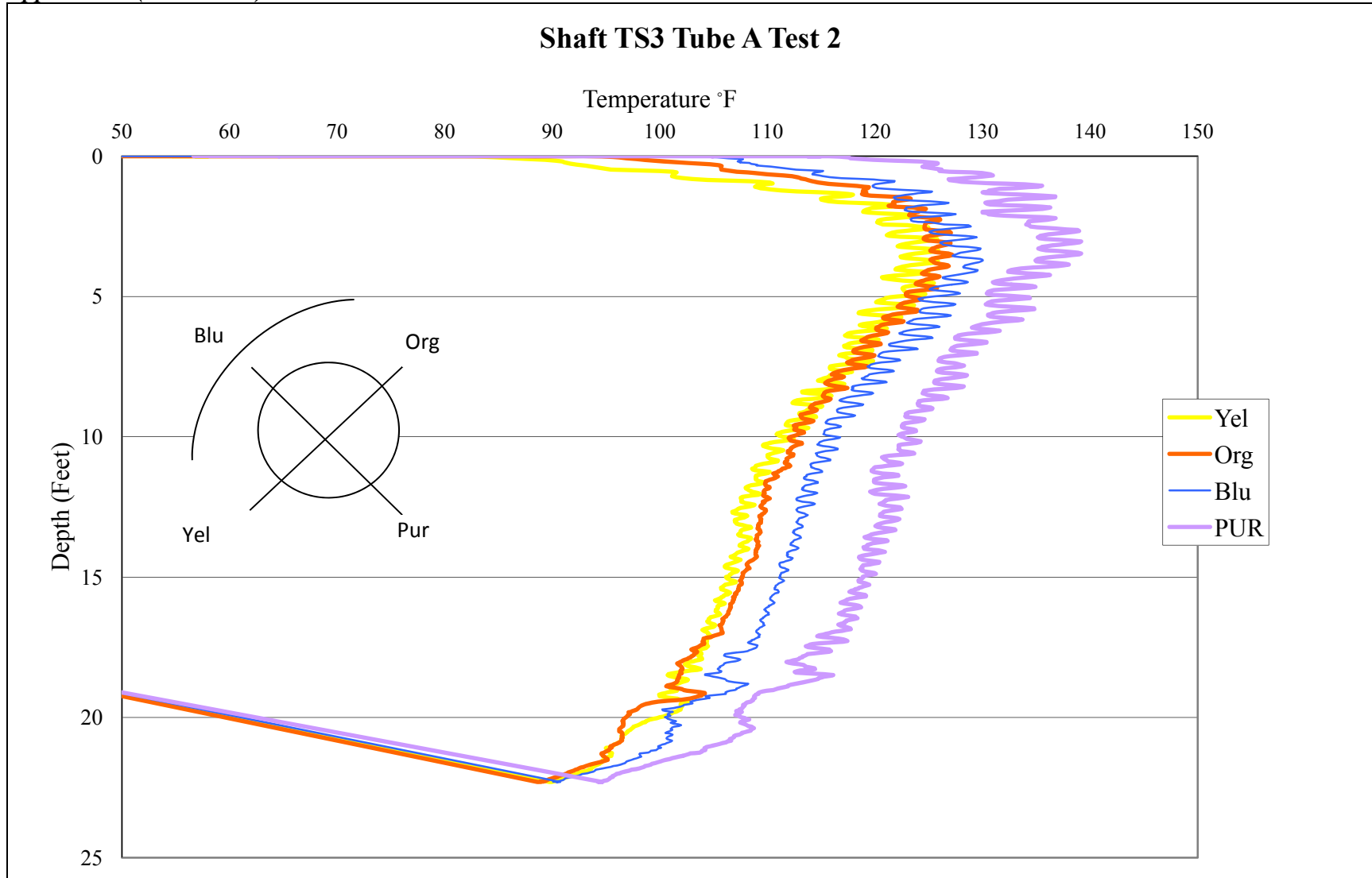


Figure C28 - Auburn test site TIP test results TS3 Tube A Test 2

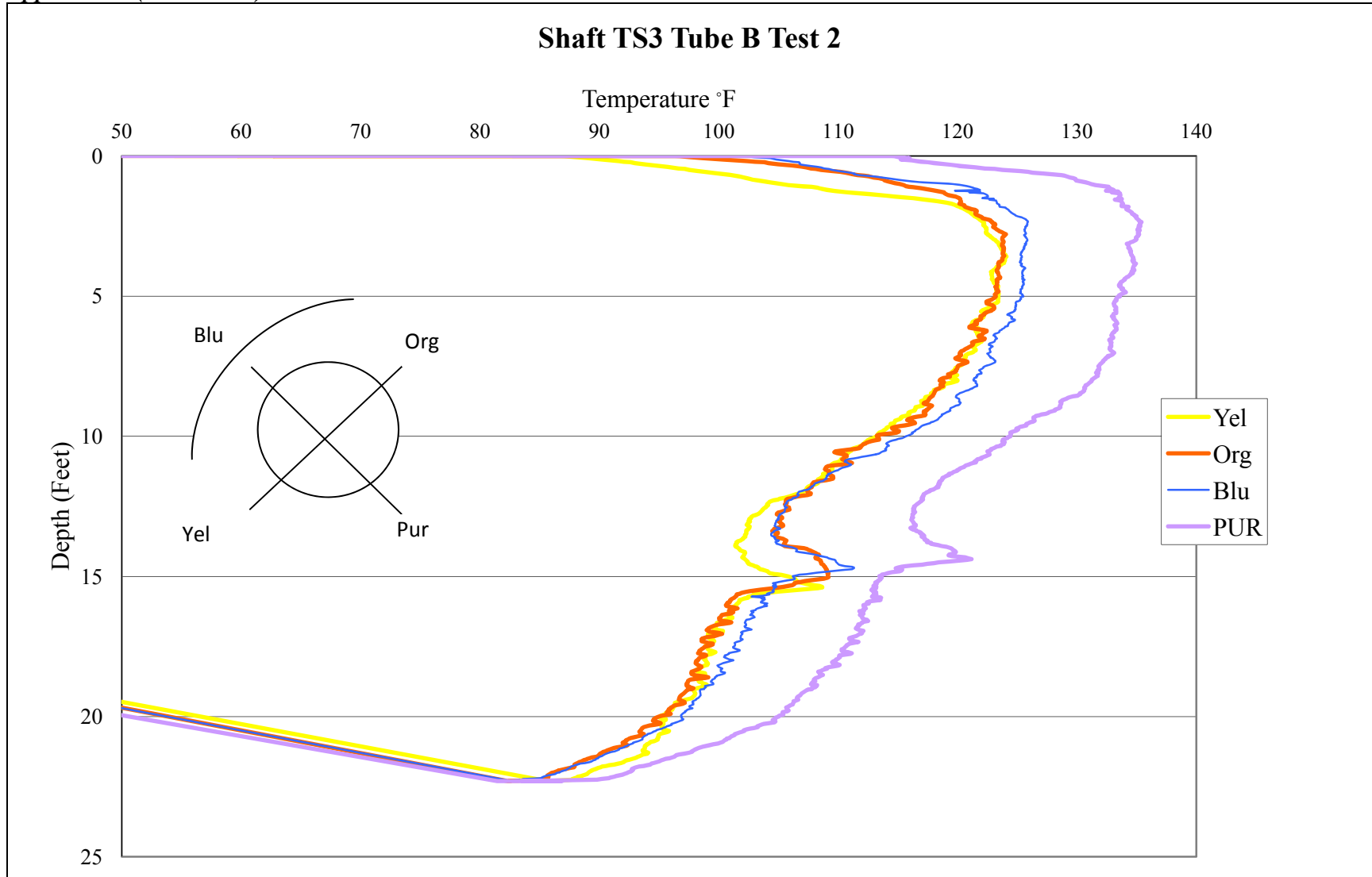


Figure C29 - Auburn test site TIP test results TS3 Tube B Test 2

Appendix C (Continued)

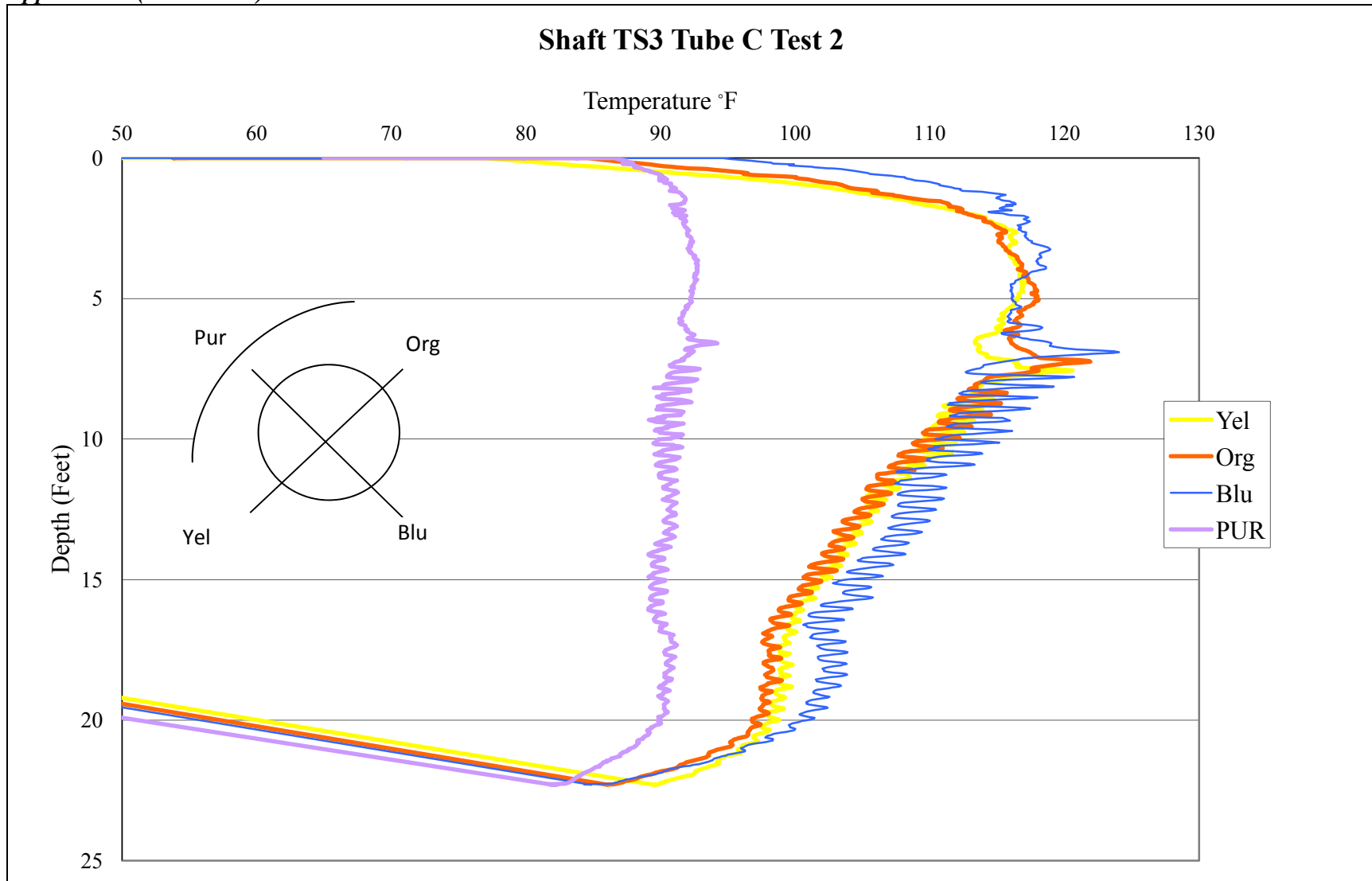


Figure C30 - Auburn test site TIP test results TS3 Tube C Test 2

Appendix C (Continued)

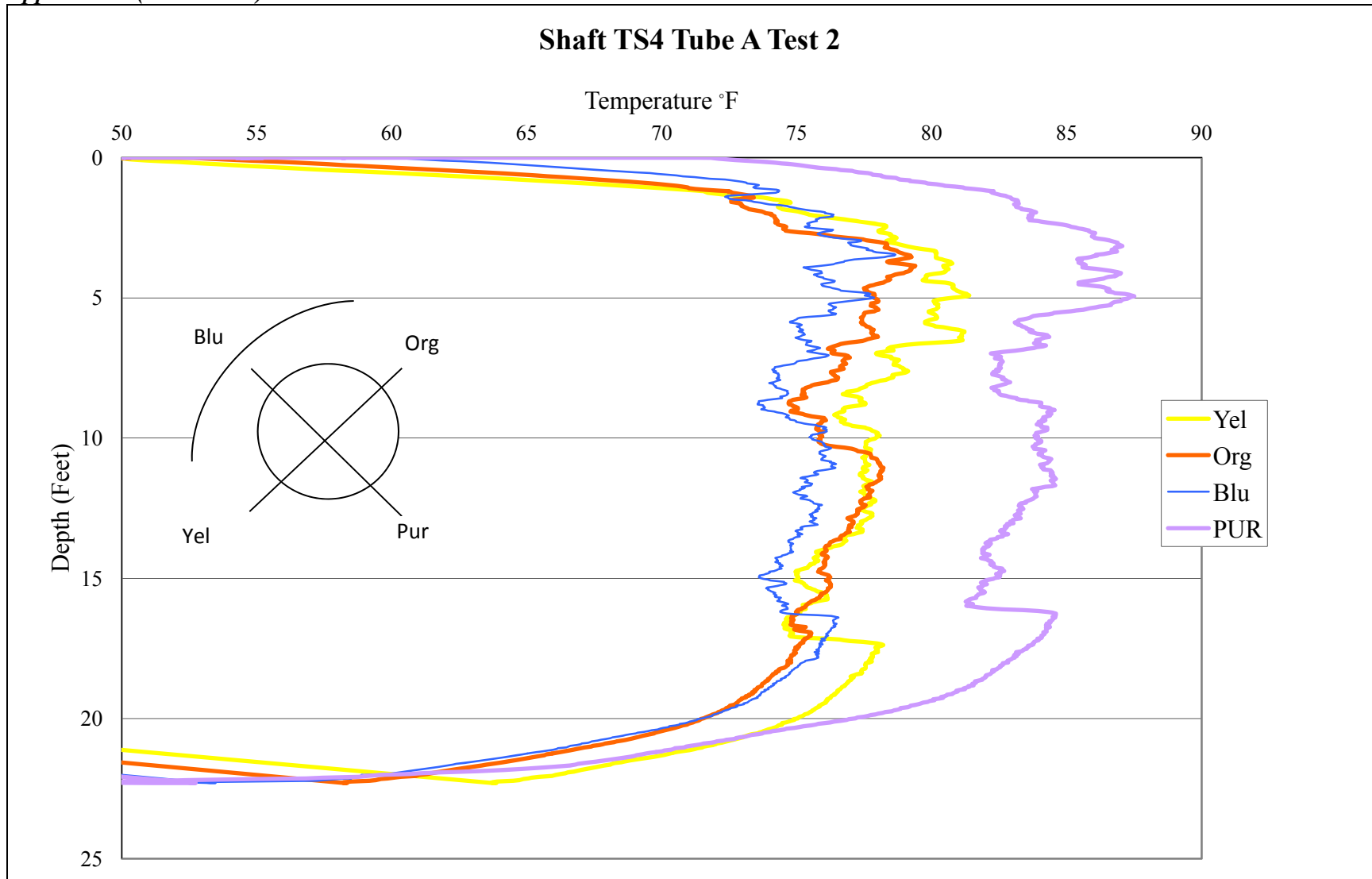


Figure C31 - Auburn test site TIP test results TS4 Tube A Test 2

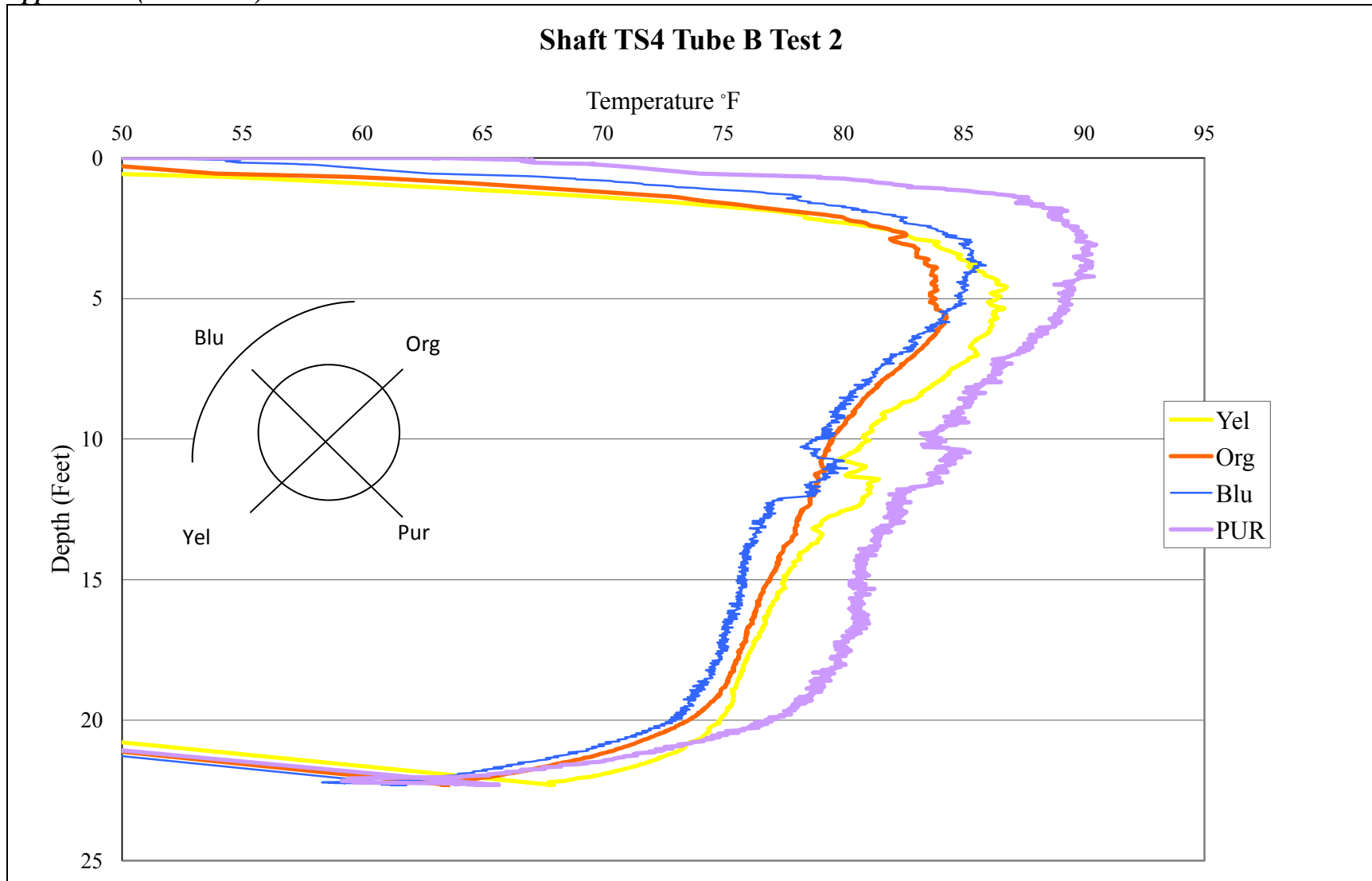


Figure C32 - Auburn test site TIP test results TS4 Tube B Test 2

Appendix C (Continued)

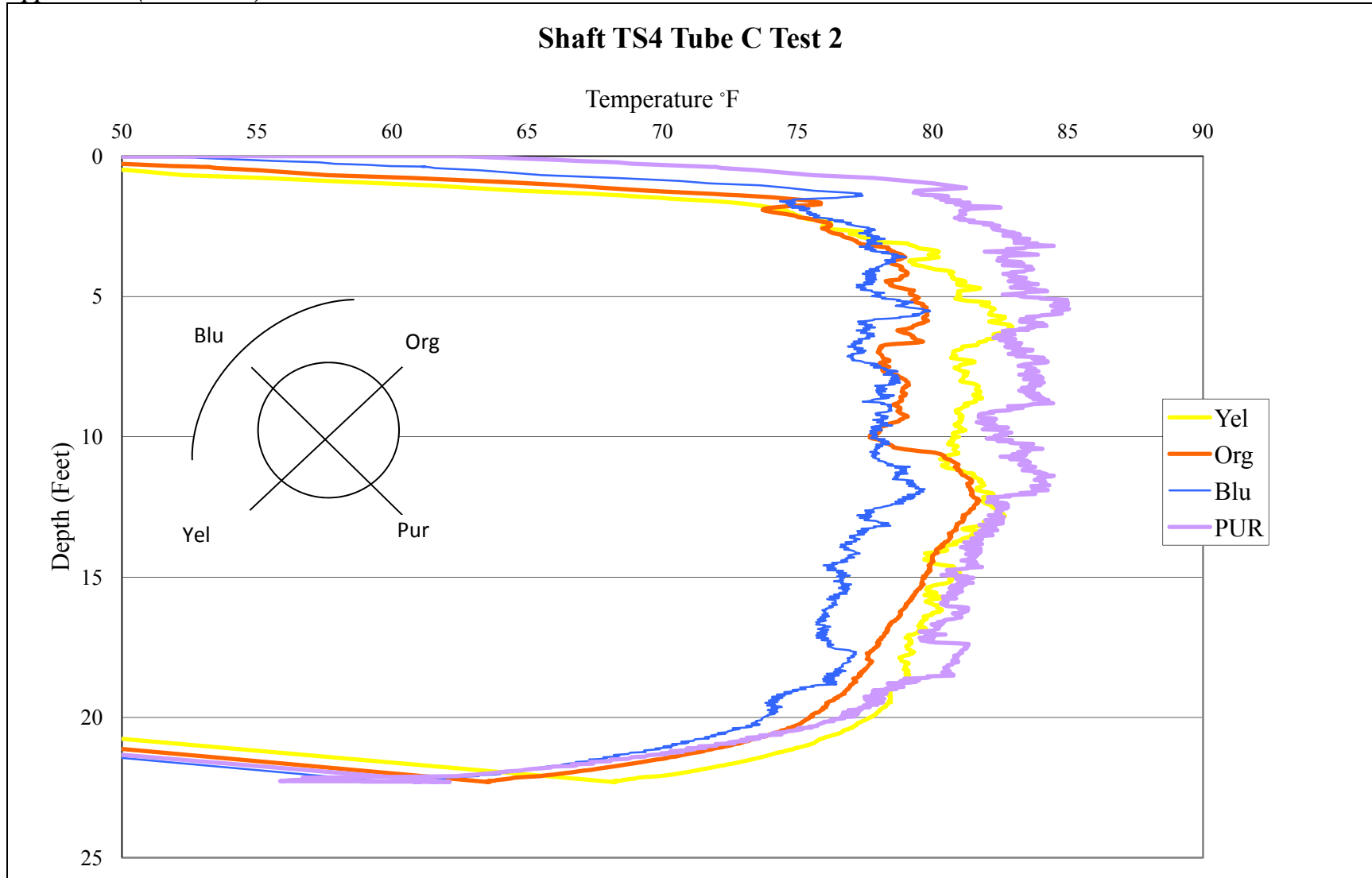


Figure C33 - Auburn test site TIP test results TS4 Tube C Test 2

Appendix C (Continued)

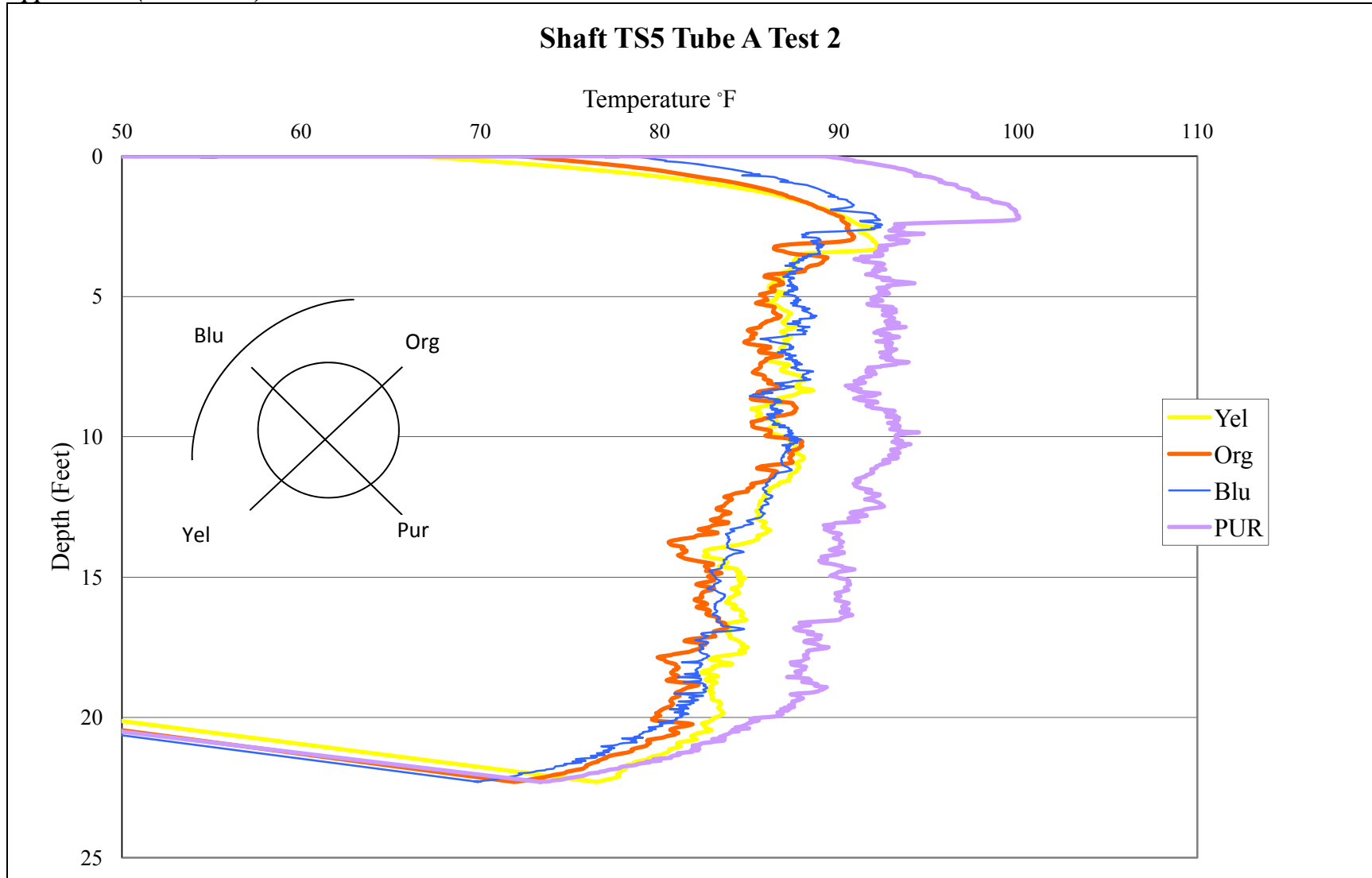


Figure C34 - Auburn test site TIP test results TS5 Tube A Test 2

Appendix C (Continued)

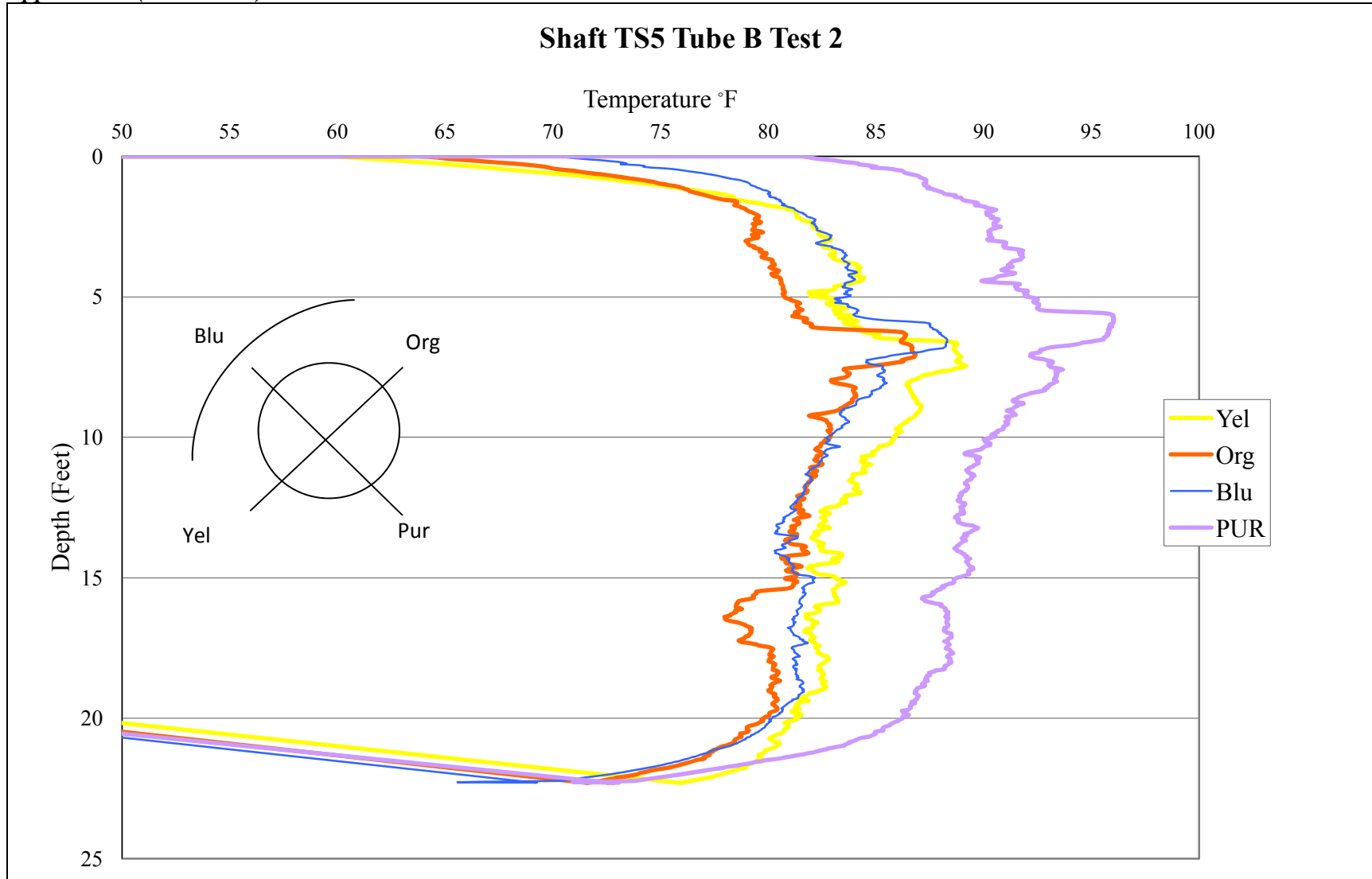


Figure C35 - Auburn test site TIP test results TS5 Tube B Test 2

Appendix C (Continued)

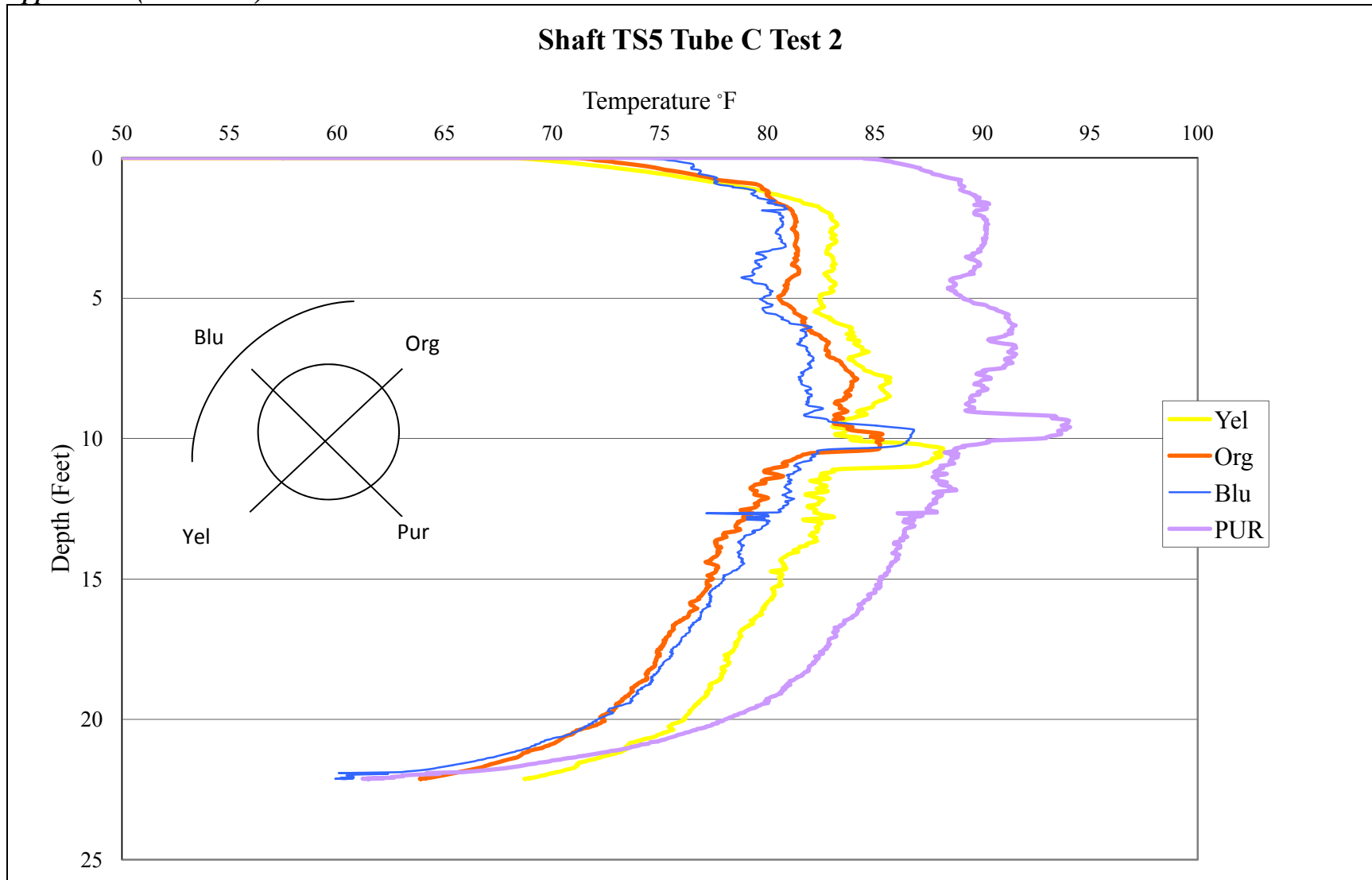


Figure C36 - Auburn test site TIP test results TS5 Tube C Test 2

Appendix C (Continued)

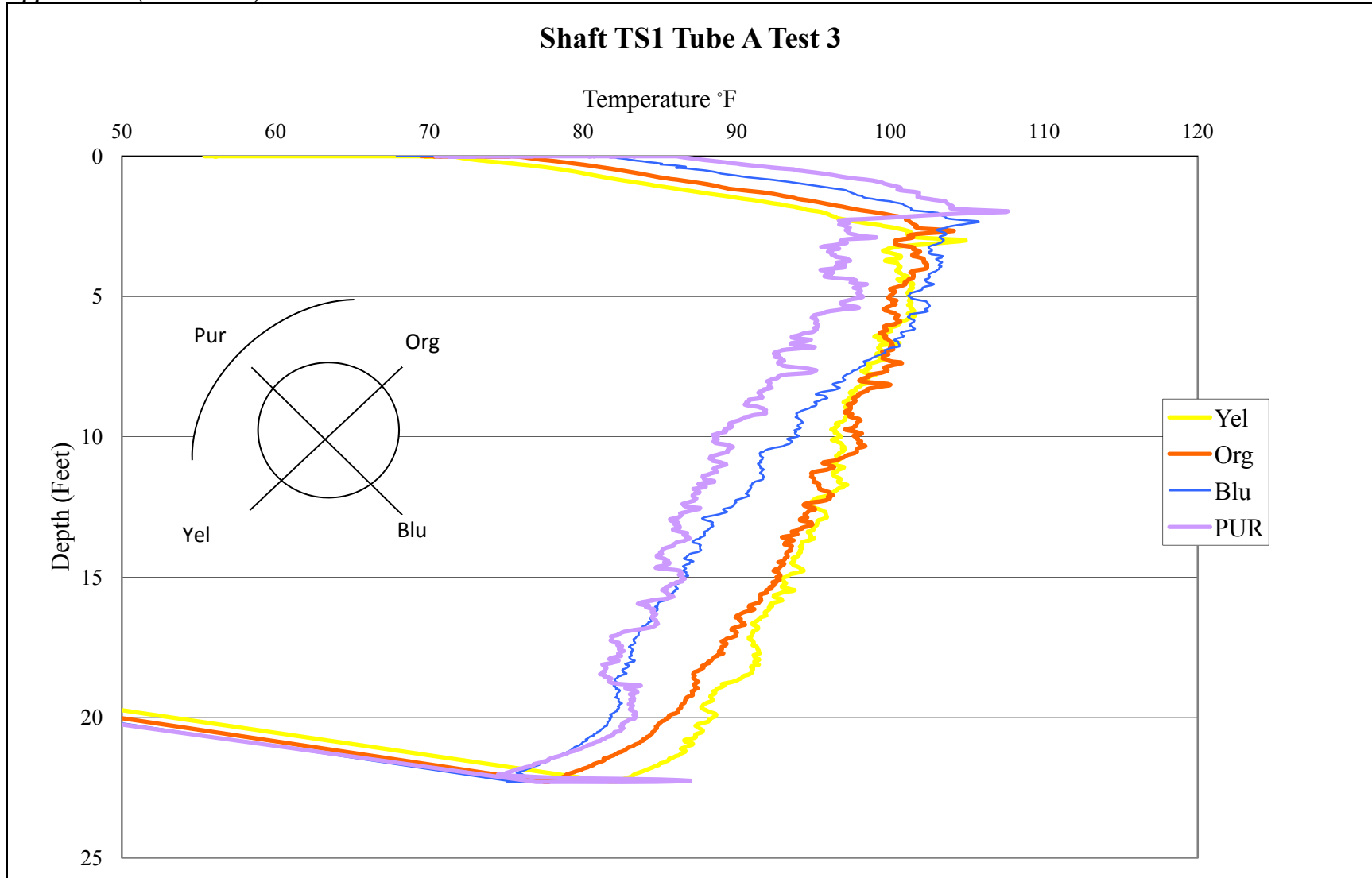


Figure C37 - Auburn test site TIP test results TS1 Tube A Test 3

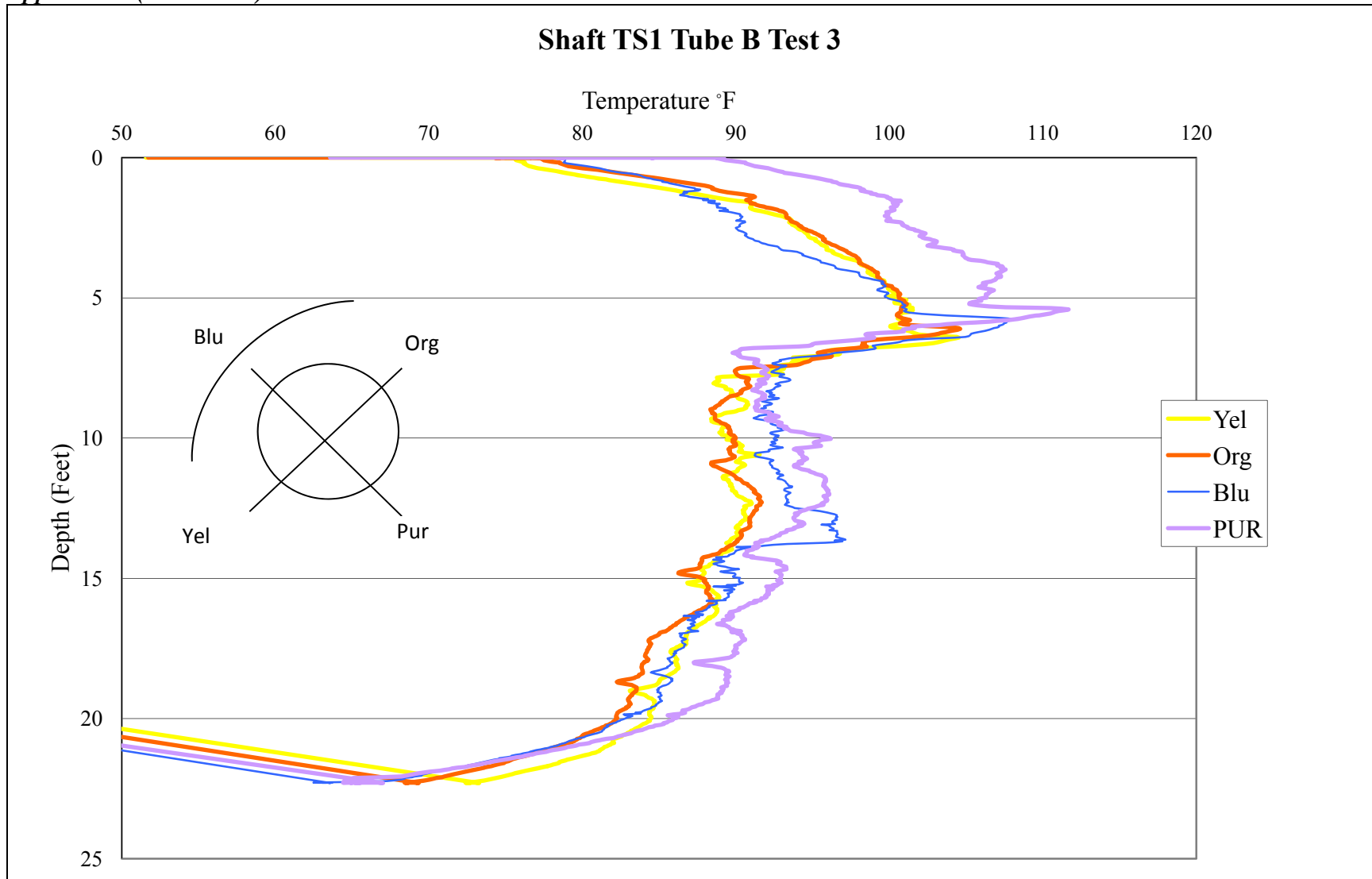


Figure C38 - Auburn test site TIP test results TS1 Tube B Test 3

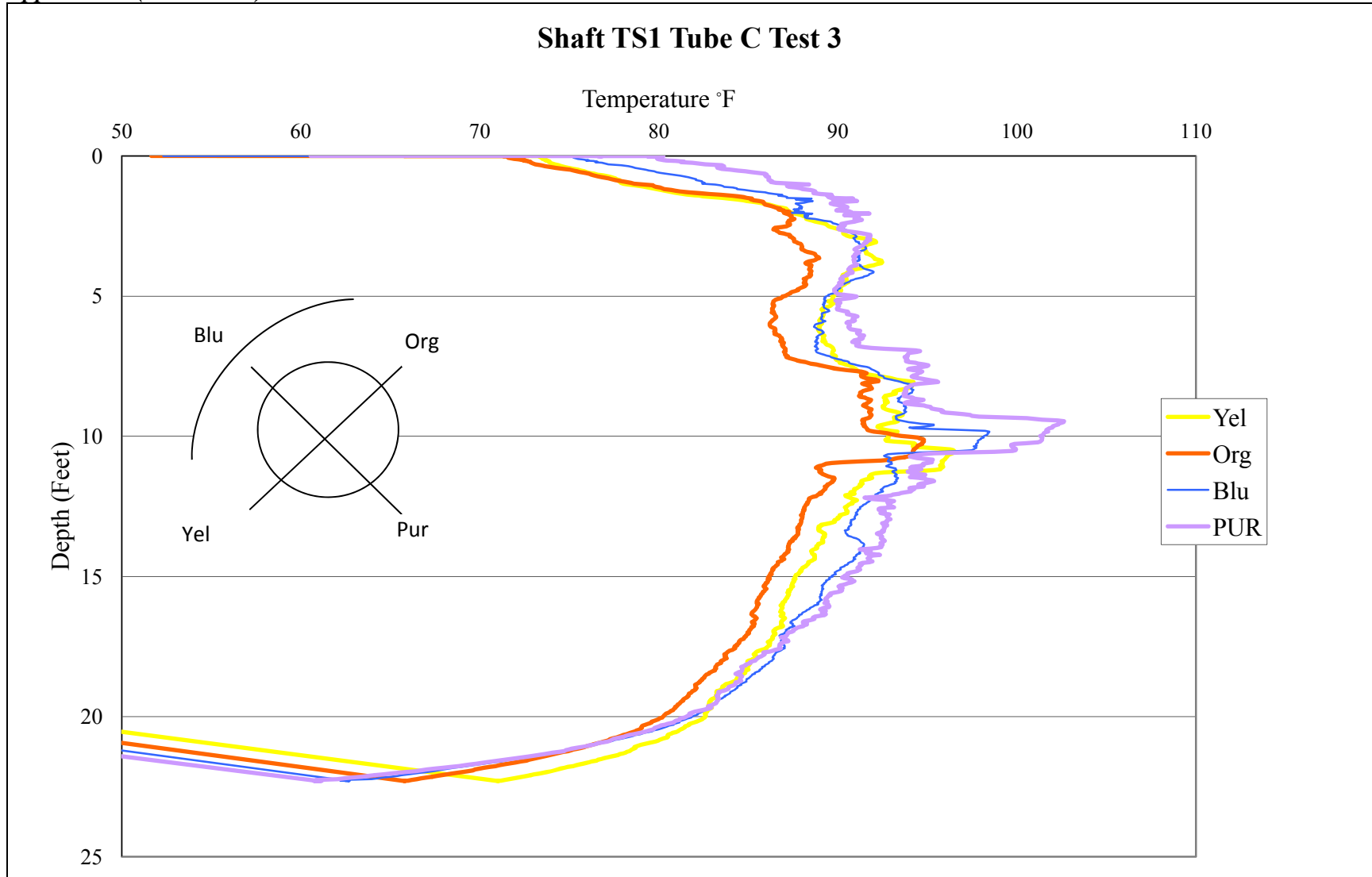


Figure C39 - Auburn test site TIP test results TS1 Tube C Test 3

Appendix C (Continued)

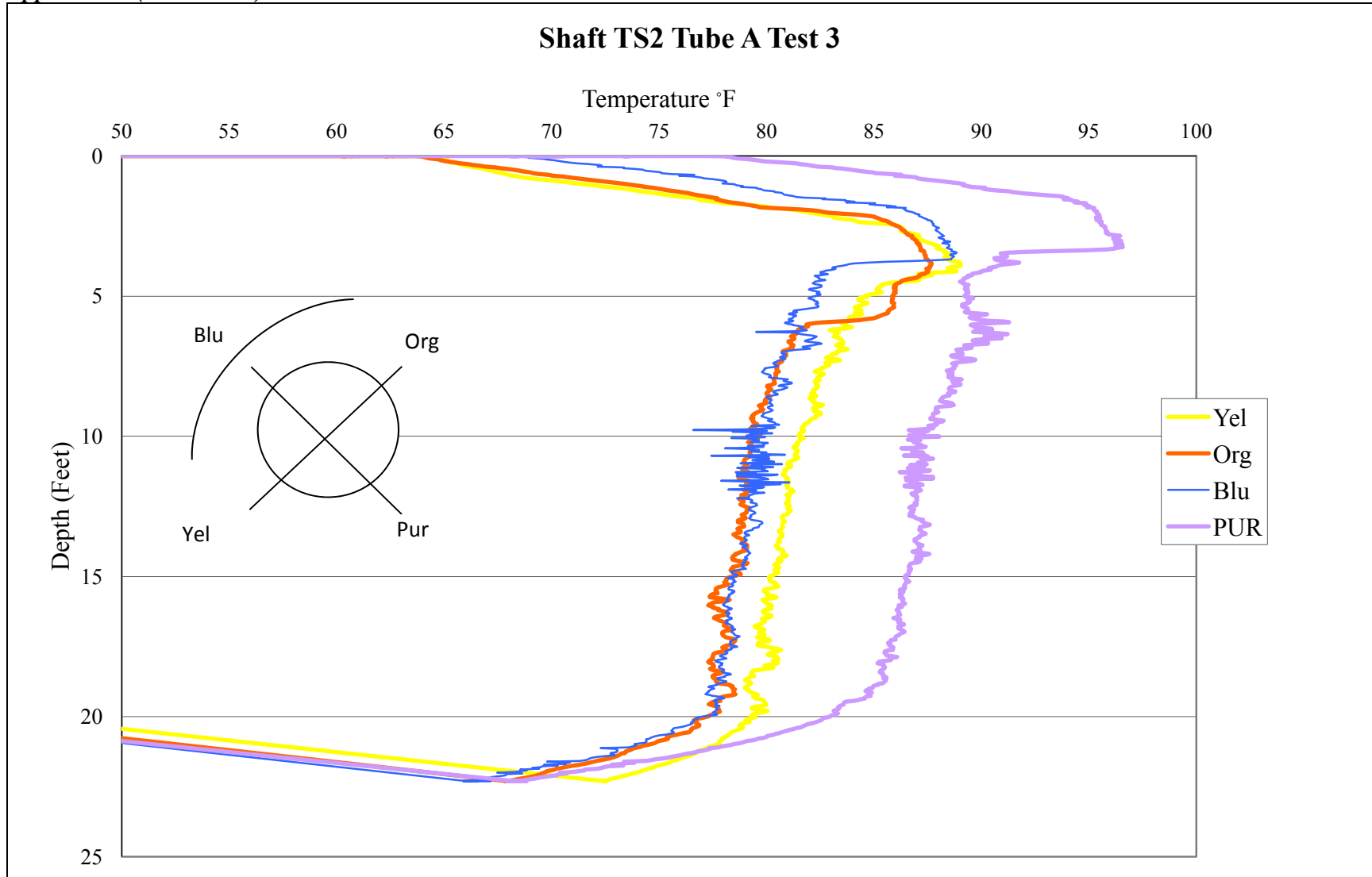


Figure C40 - Auburn test site TIP test results TS2 Tube A Test 3

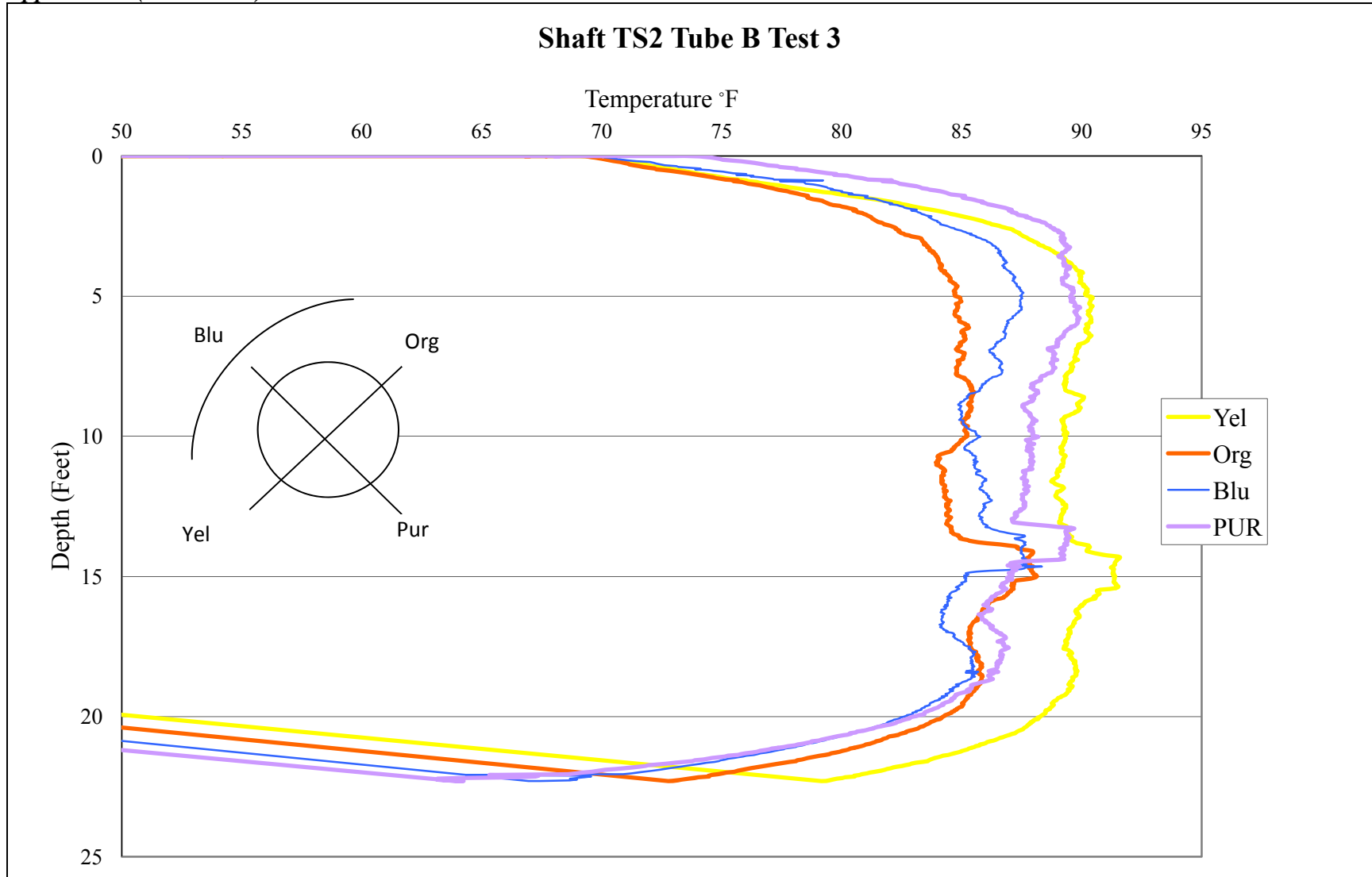


Figure C41 - Auburn test site TIP test results TS2 Tube B Test 3

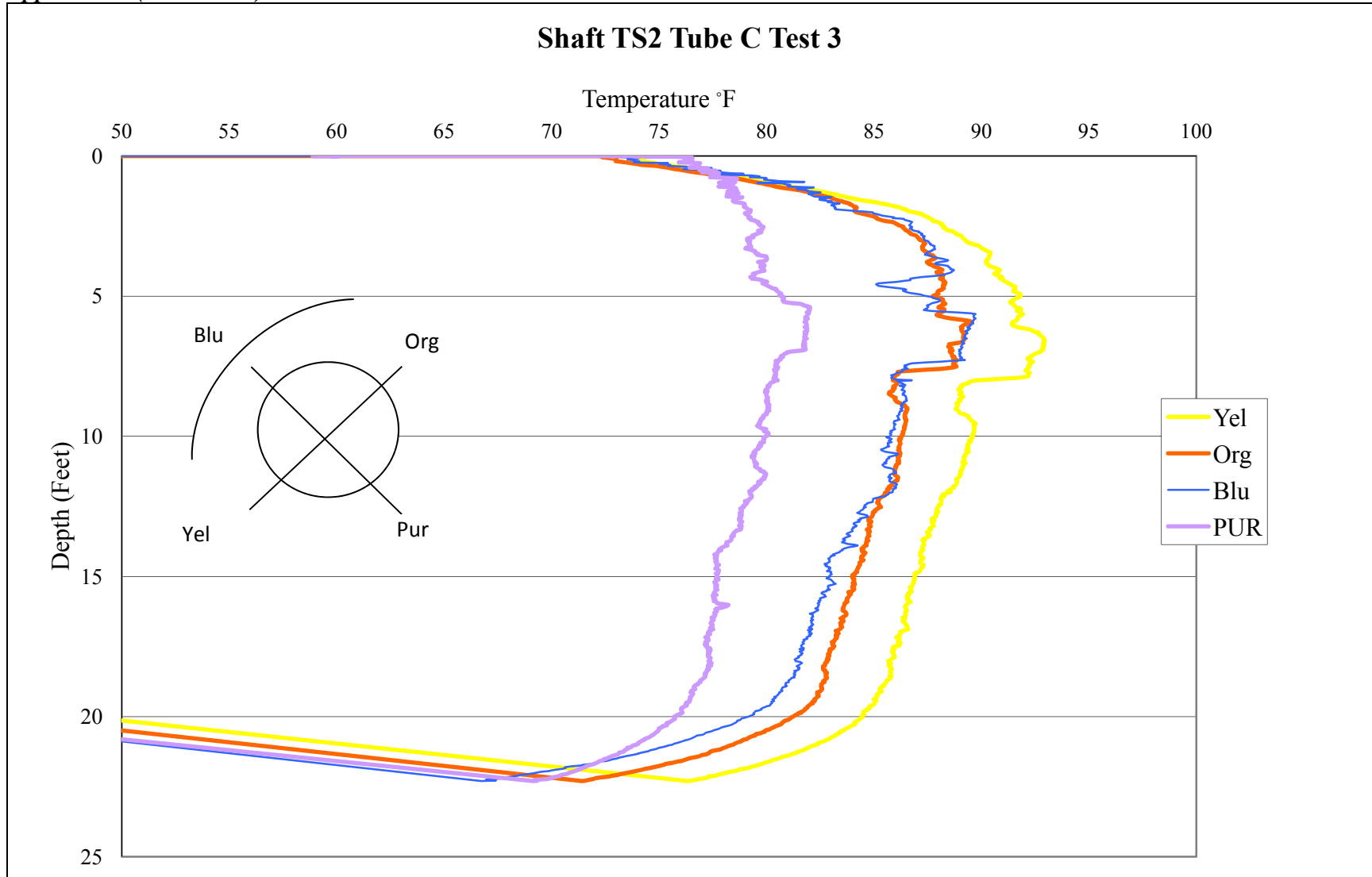


Figure C42 - Auburn test site TIP test results TS2 Tube C Test 3

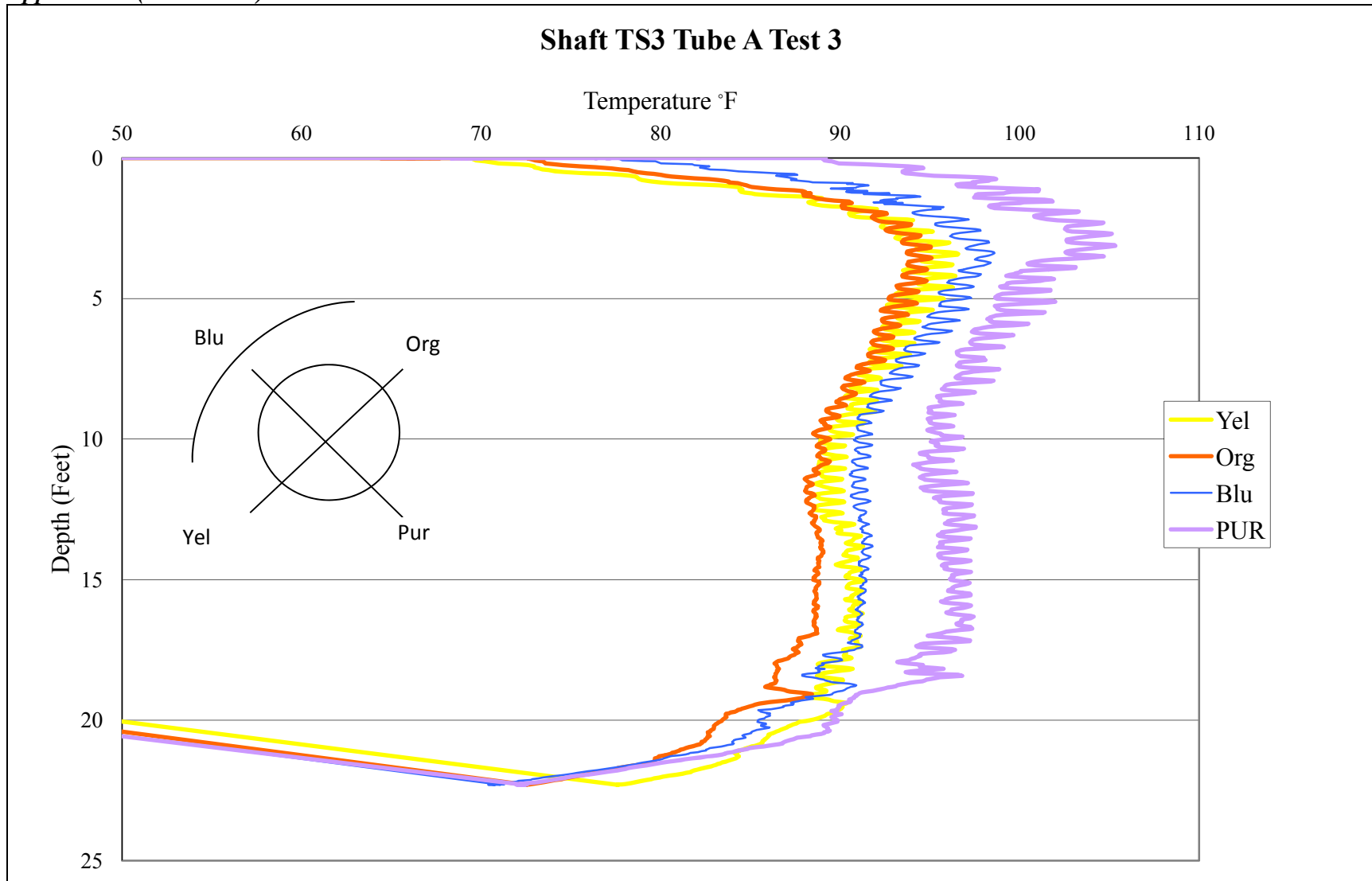


Figure C43 - Auburn test site TIP test results TS3 Tube A Test 3

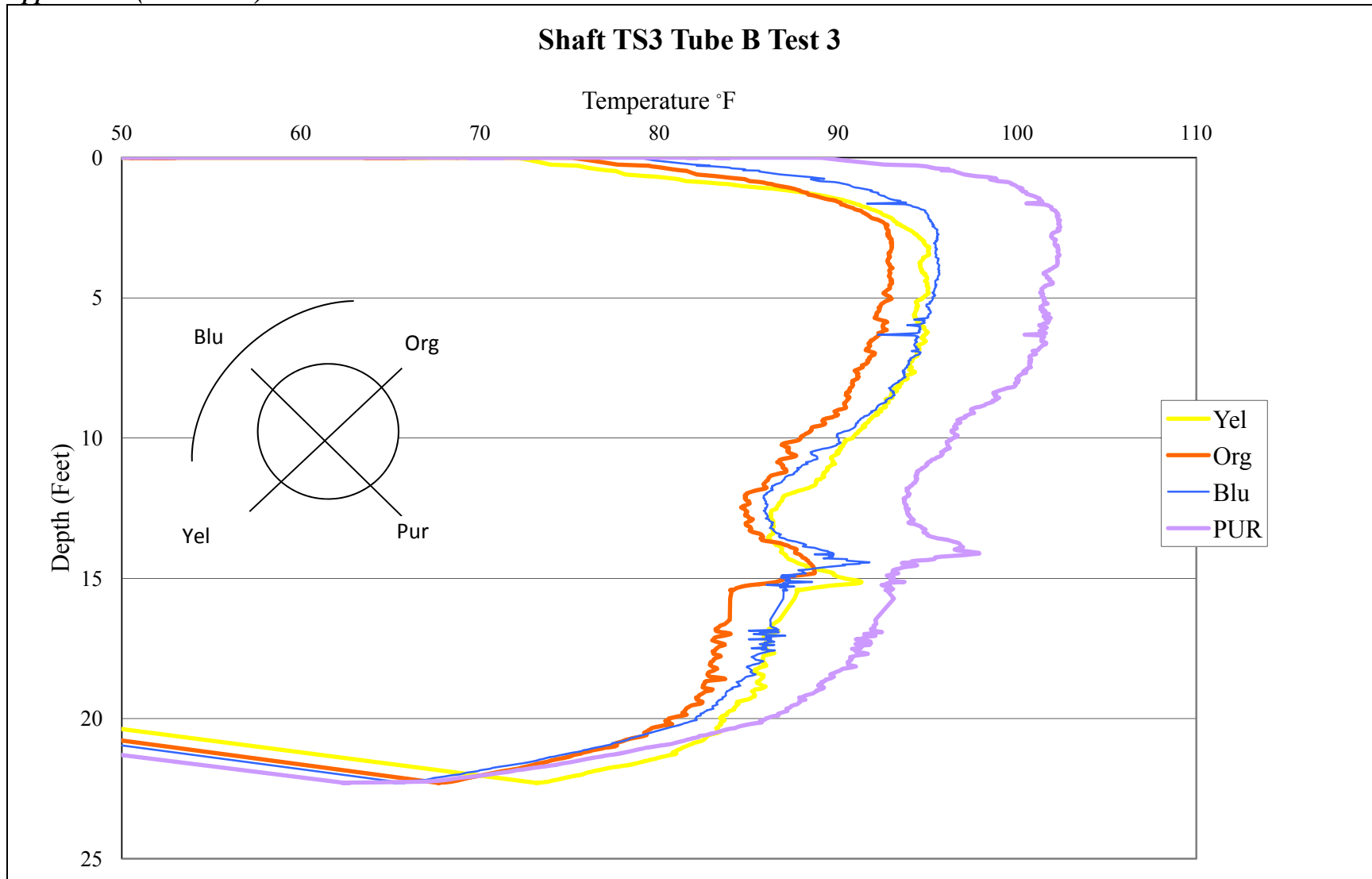


Figure C44 - Auburn test site TIP test results TS3 Tube B Test 3

Appendix C (Continued)

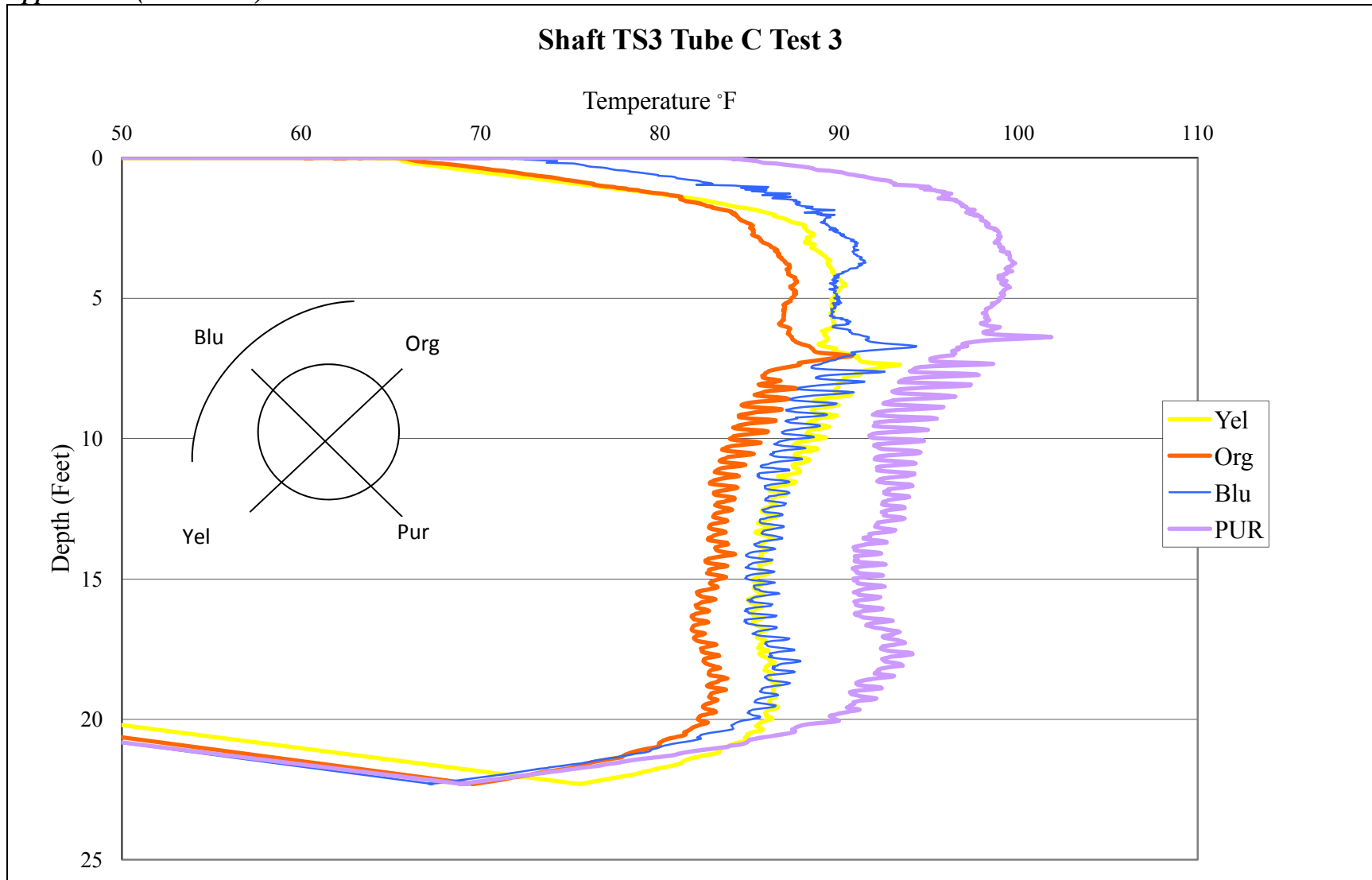


Figure C45 - Auburn test site TIP test results TS3 Tube C Test 3

Appendix C (Continued)

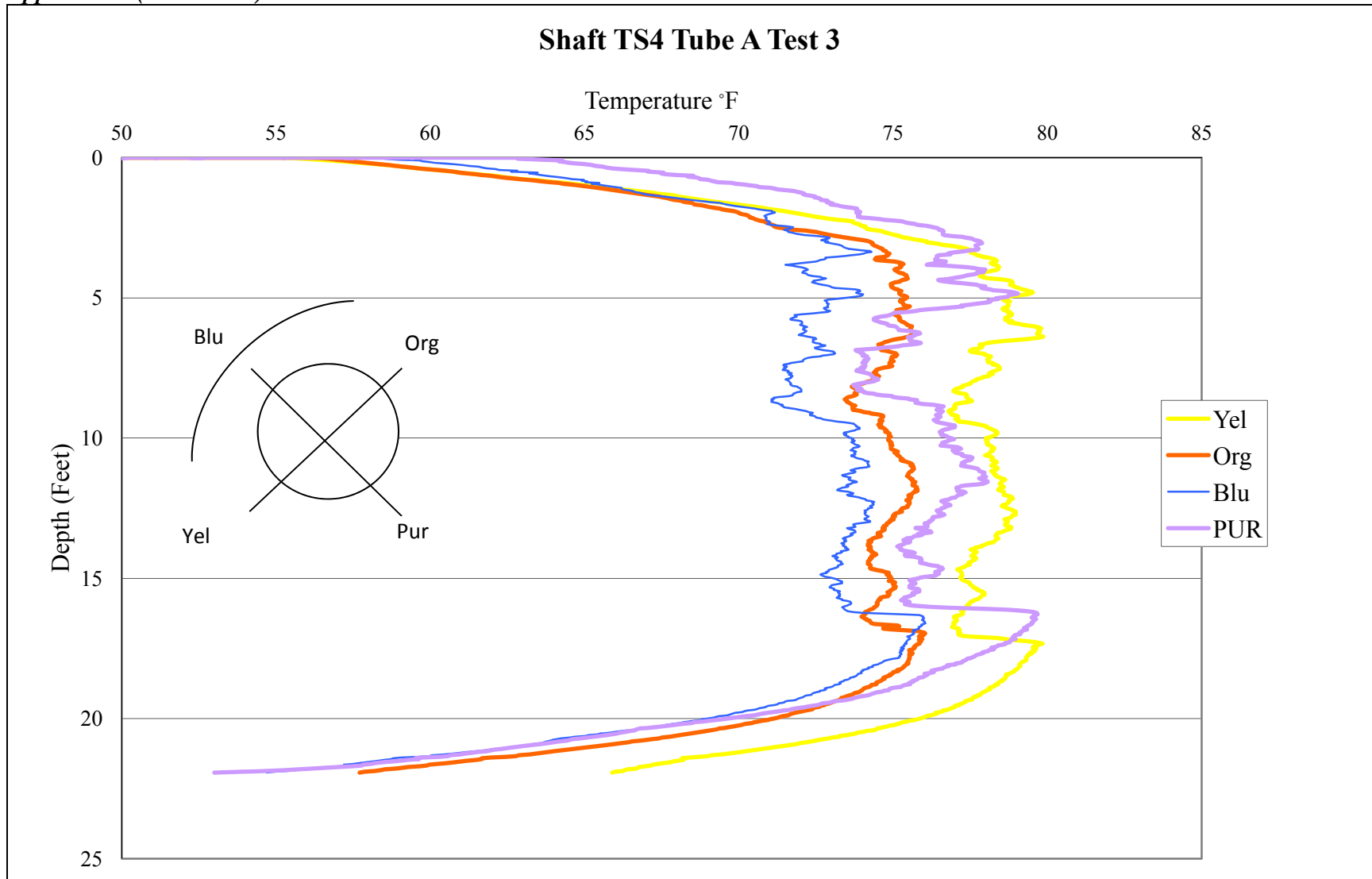


Figure C46 - Auburn test site TIP test results TS4 Tube A Test 3

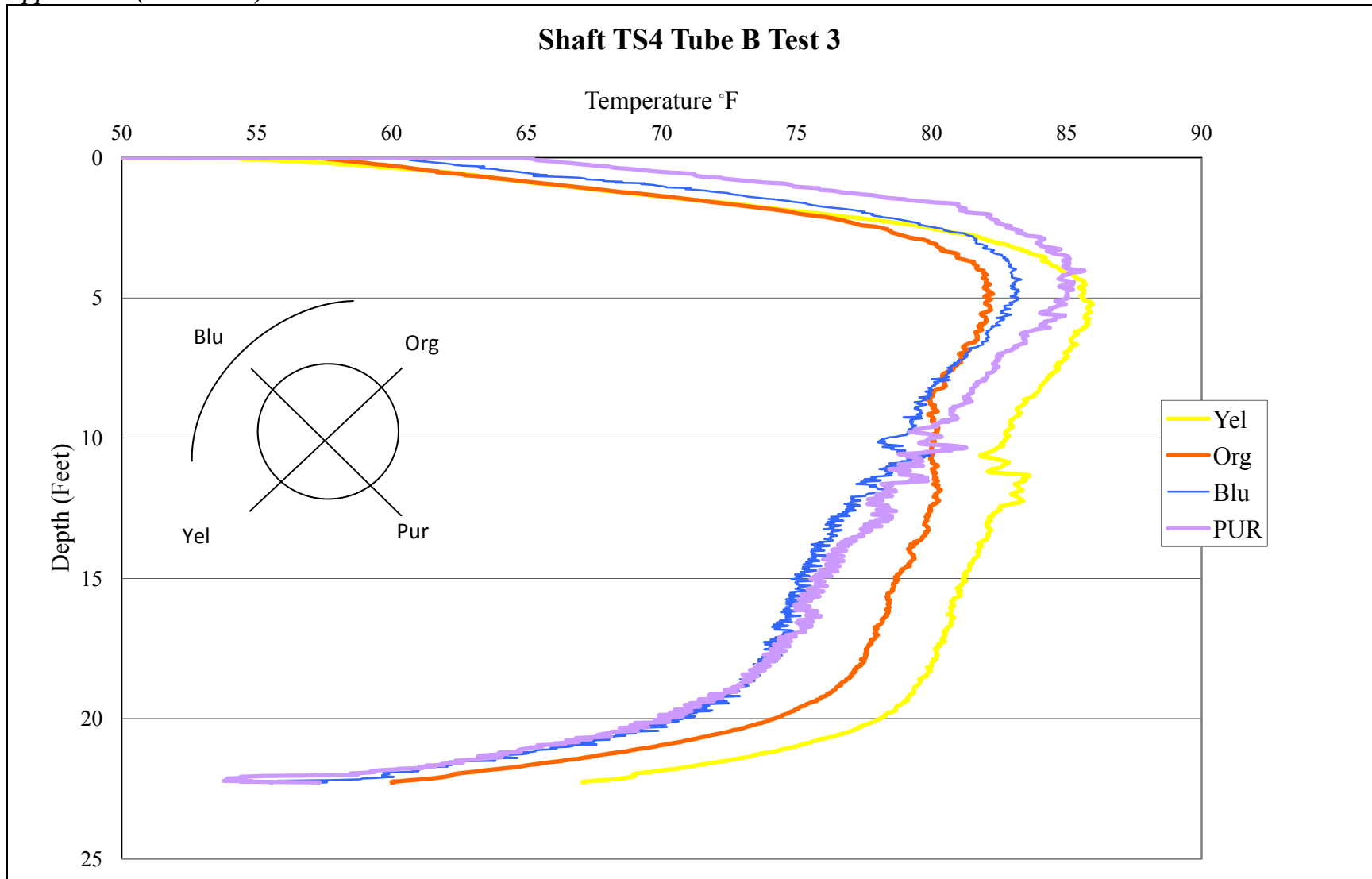


Figure C47 - Auburn test site TIP test results TS4 Tube B Test 3

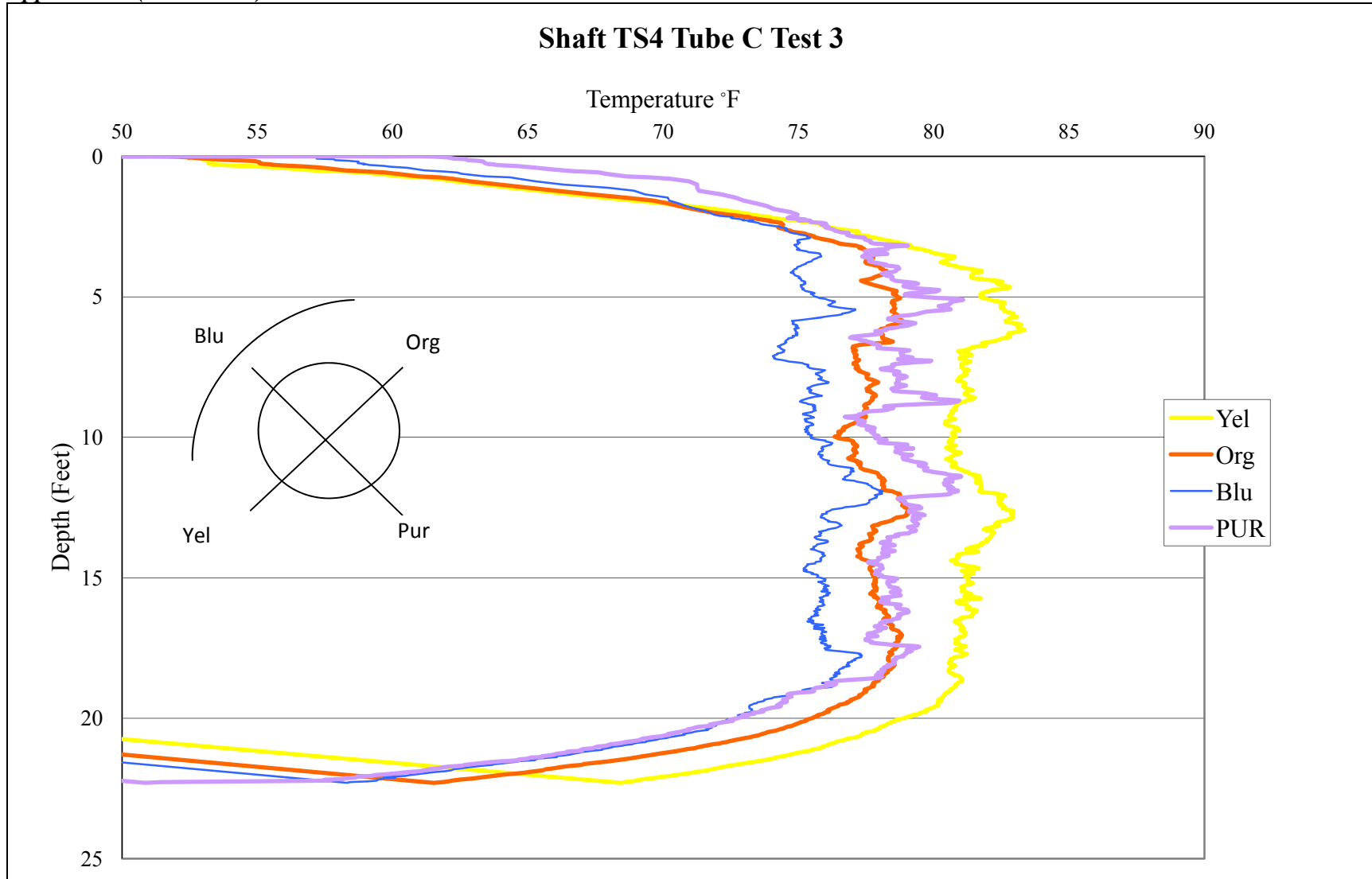


Figure C48 - Auburn test site TIP test results TS4 Tube C Test 3

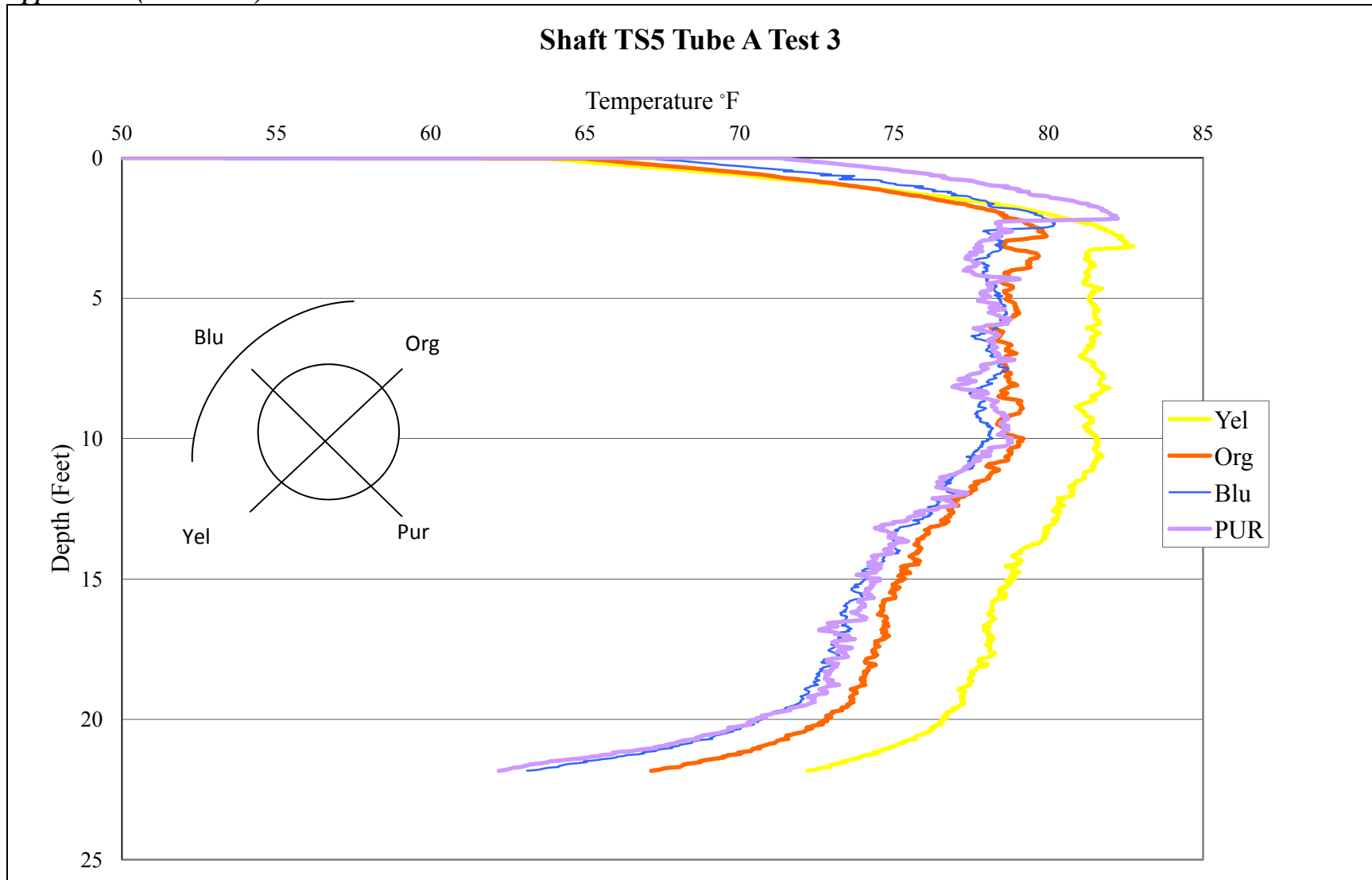


Figure C49 - Auburn test site TIP test results TS5 Tube A Test 3

Appendix C (Continued)

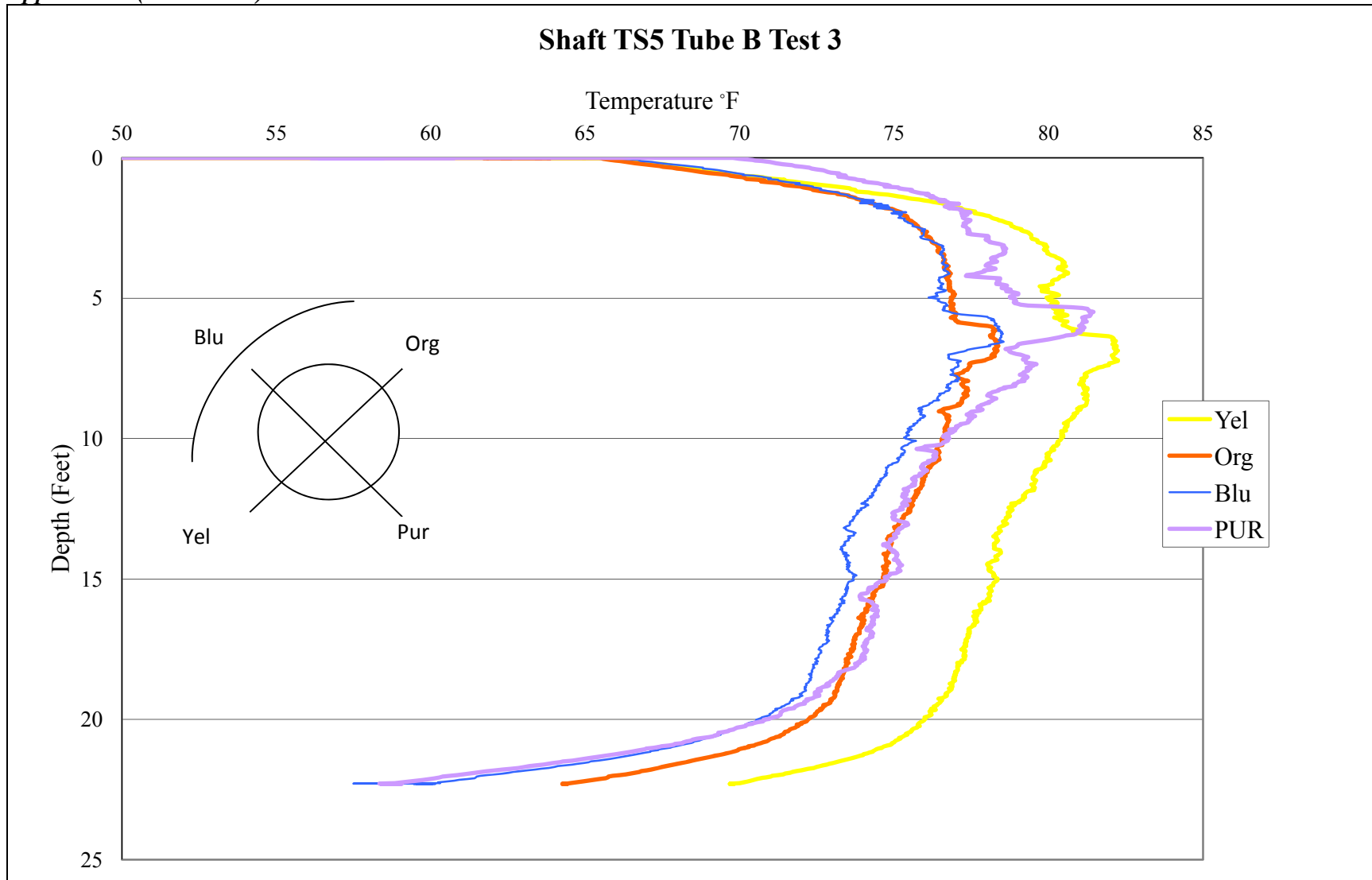


Figure C50 - Auburn test site TIP test results TS5 Tube B Test 3

Appendix C (Continued)

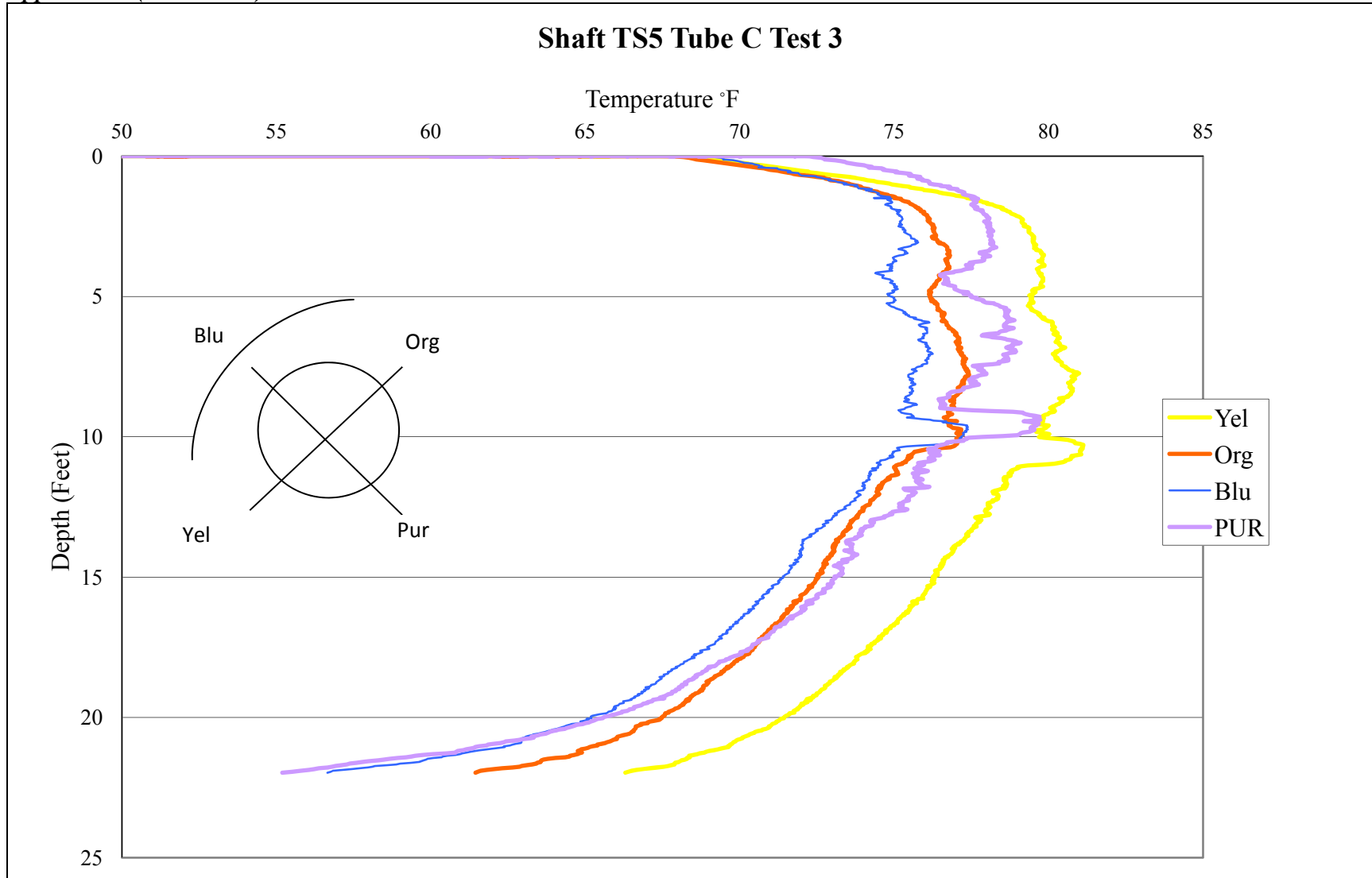


Figure C51 - Auburn test site TIP test results TS5 Tube C Test 3

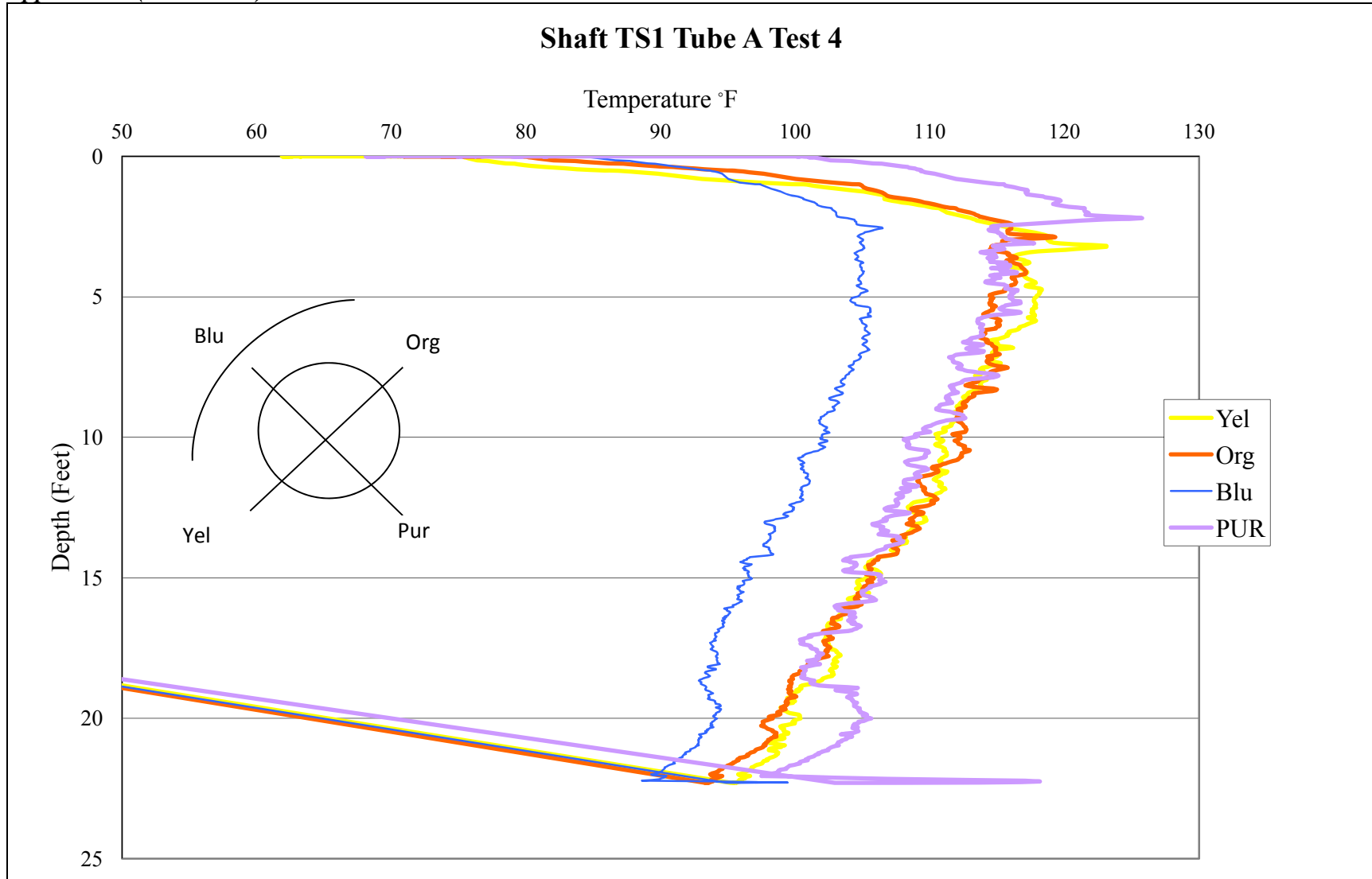


Figure C52 - Auburn test site TIP test results TS1 Tube A Test 4

Appendix C (Continued)

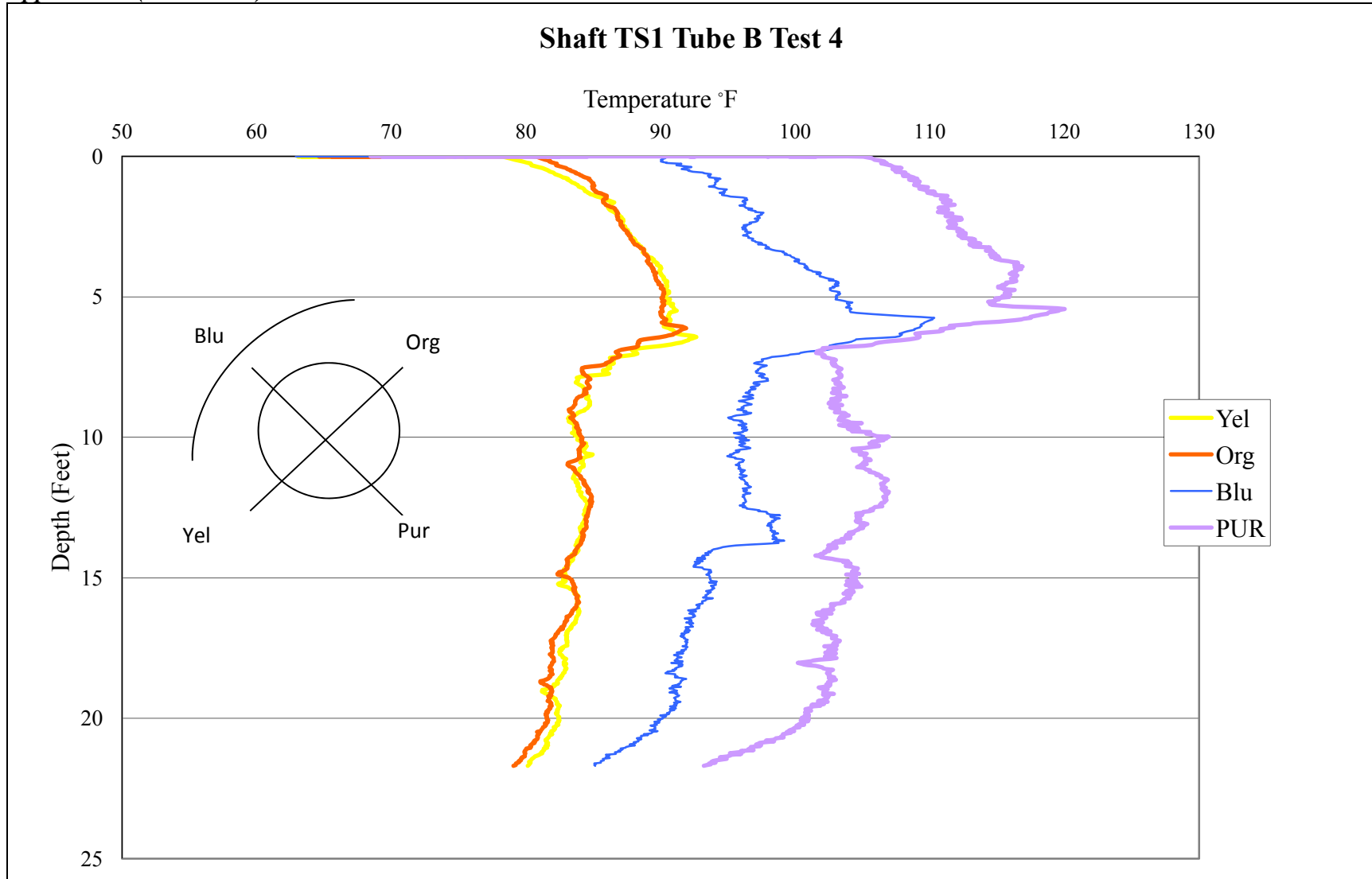


Figure C53 - Auburn test site TIP test results TS1 Tube B Test 4

Appendix C (Continued)

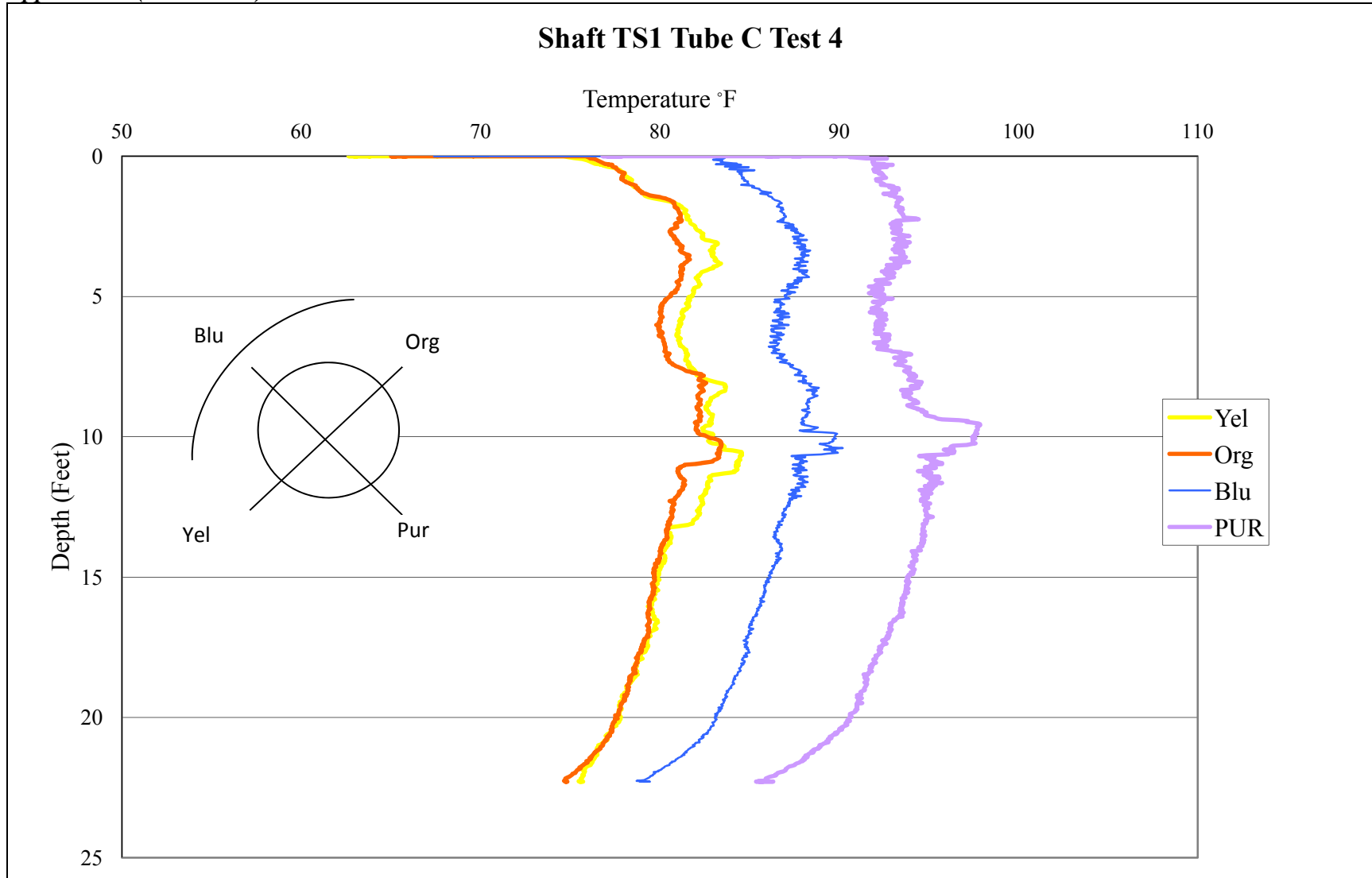


Figure C54 - Auburn test site TIP test results TS1 Tube C Test 4

Appendix C (Continued)

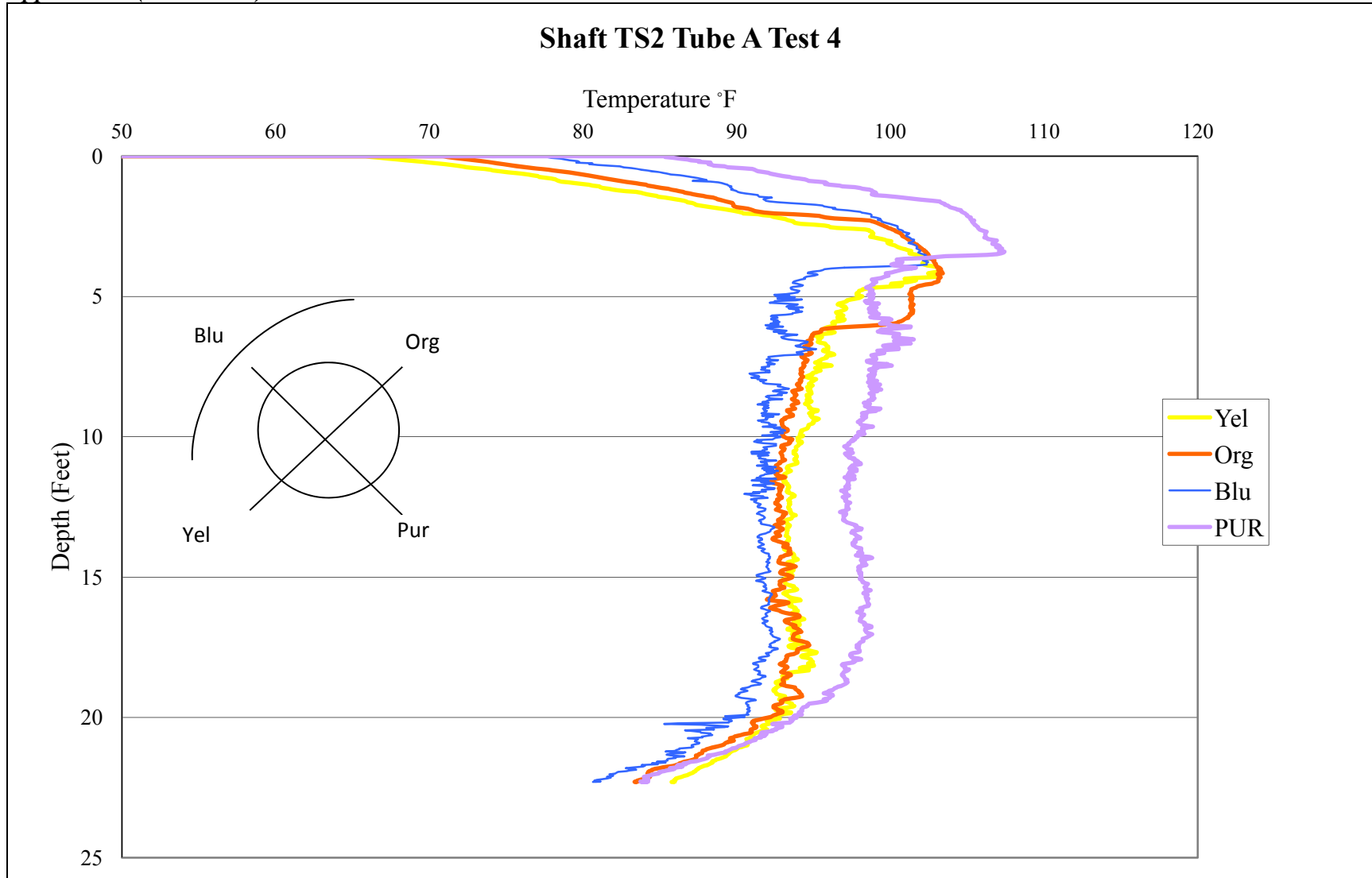


Figure C55 - Auburn test site TIP test results TS2 Tube A Test 4

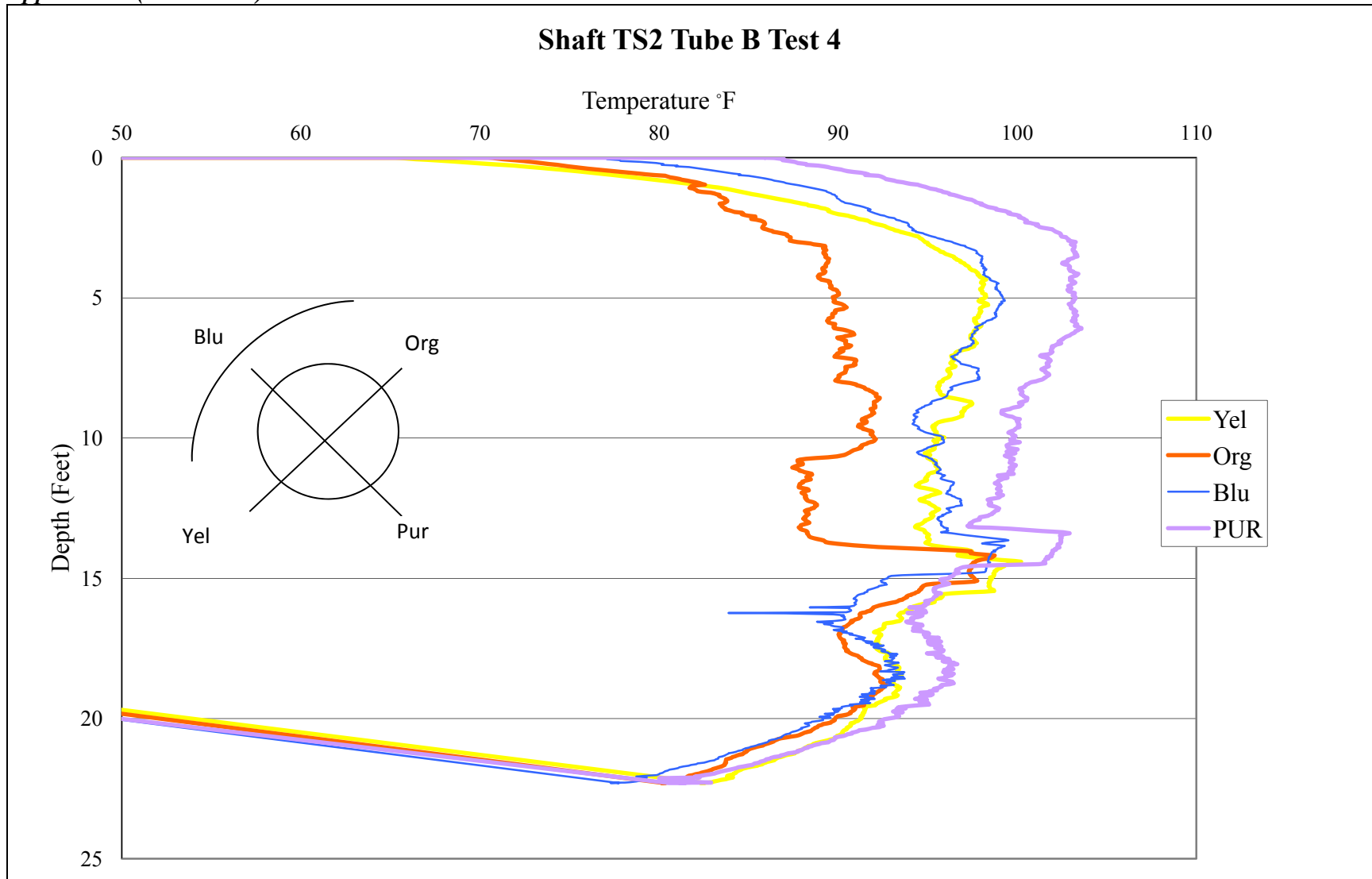


Figure C56 - Auburn test site TIP test results TS2 Tube B Test 4

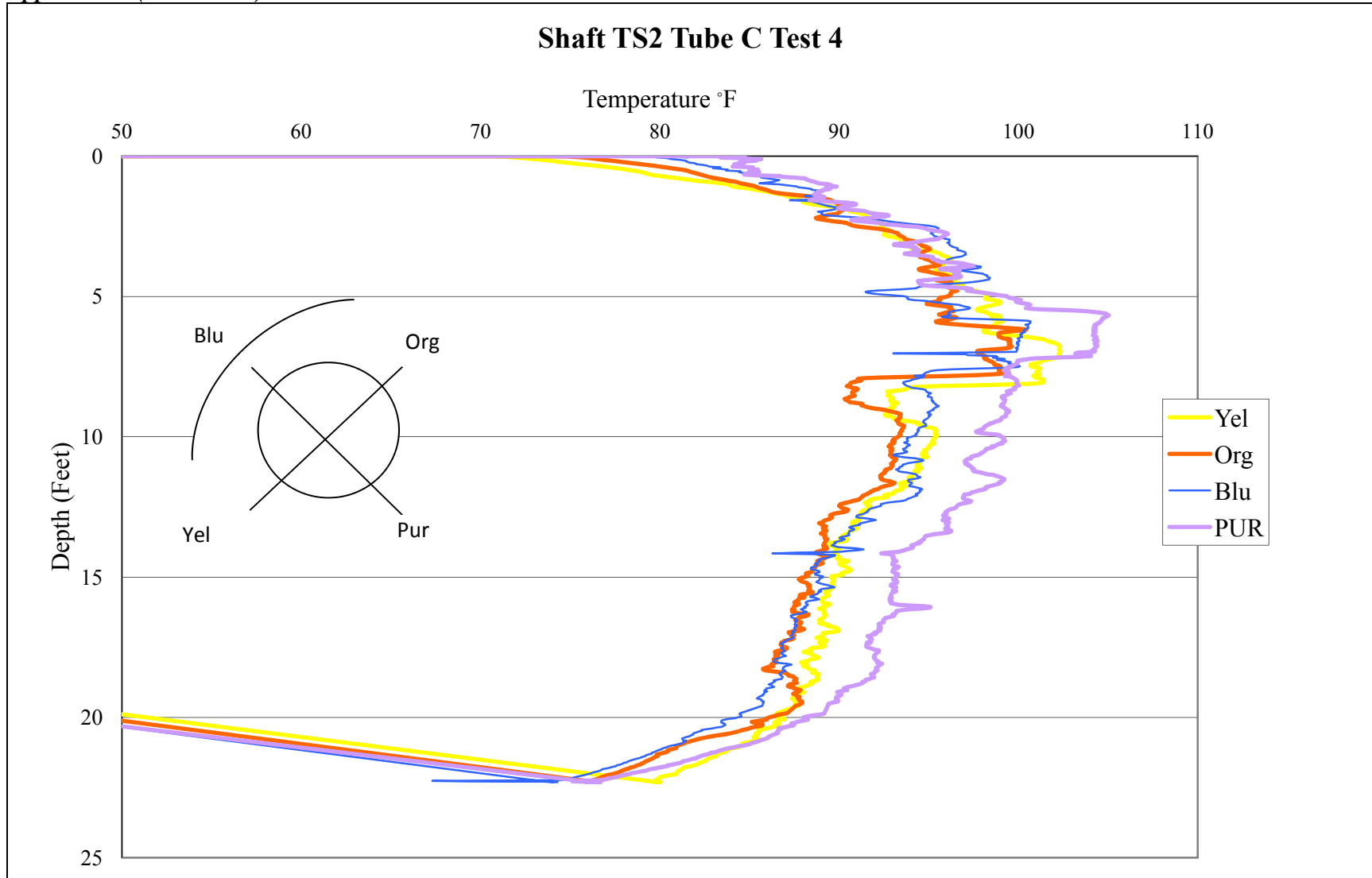


Figure C57 - Auburn test site TIP test results TS2 Tube C Test 4

Appendix C (Continued)

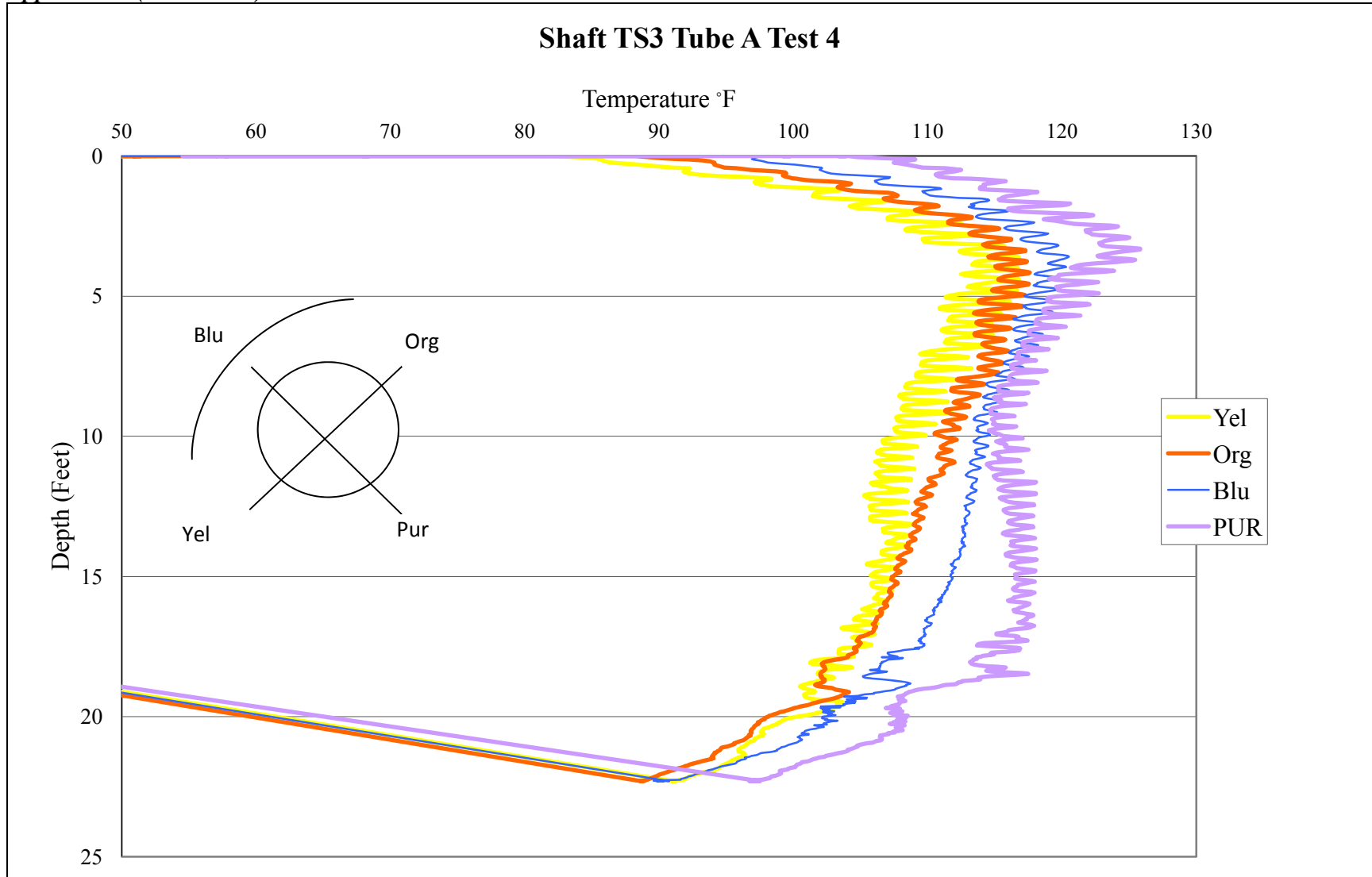


Figure C58 - Auburn test site TIP test results TS3 Tube A Test 4

Appendix C (Continued)

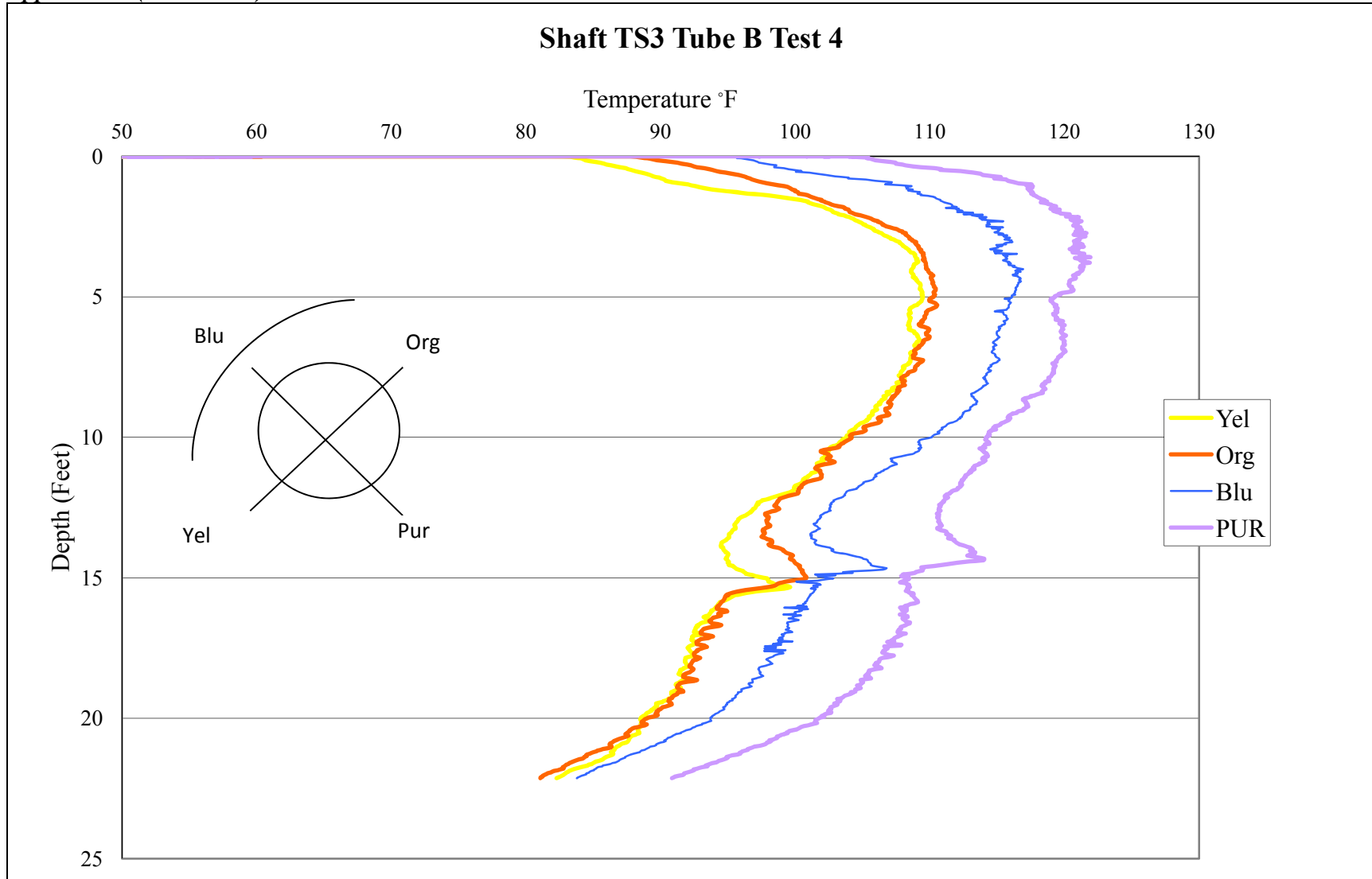


Figure C59 - Auburn test site TIP test results TS3 Tube B Test 4

Appendix C (Continued)

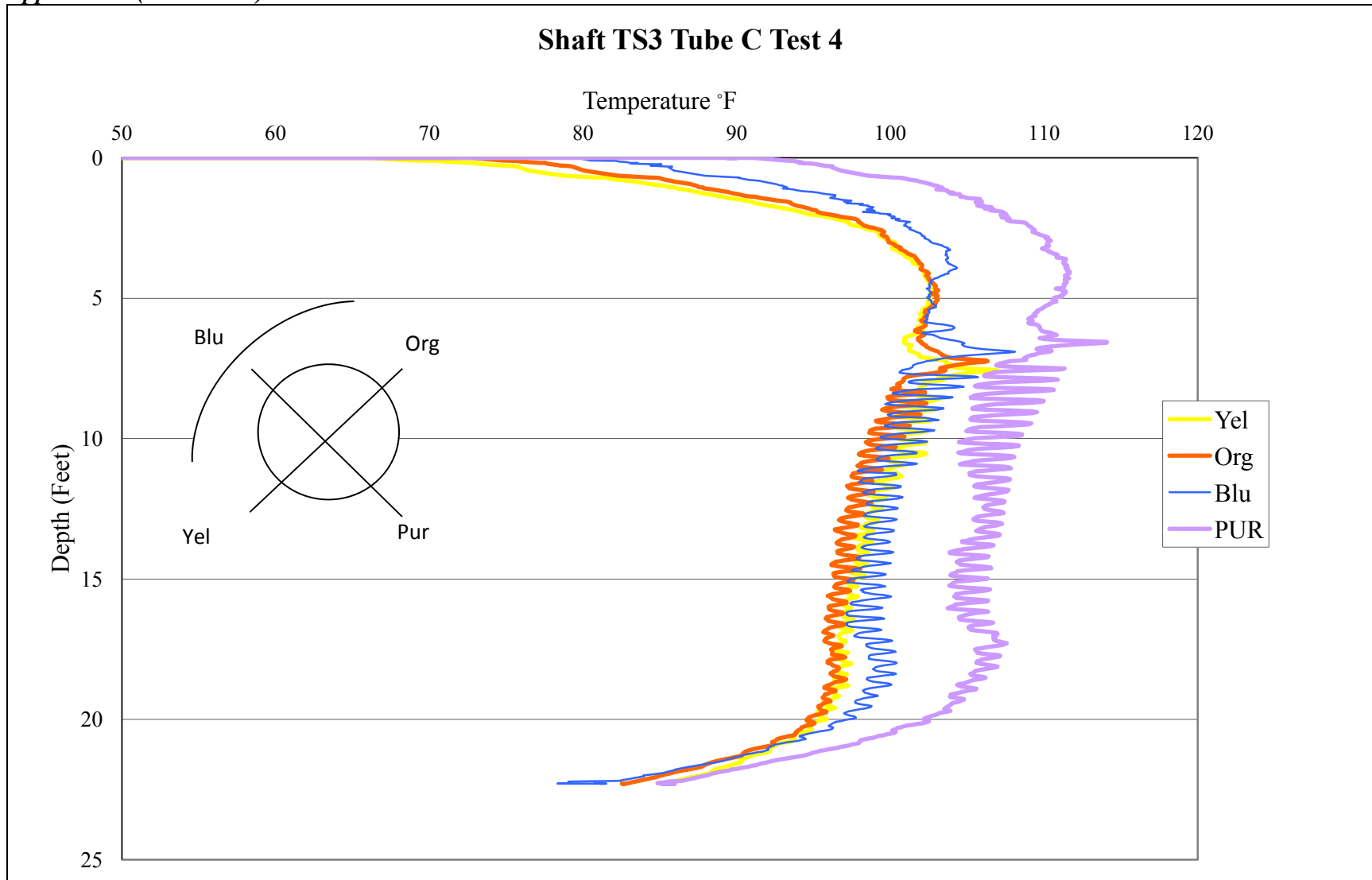


Figure C60 - Auburn test site TIP test results TS3 Tube C Test 4

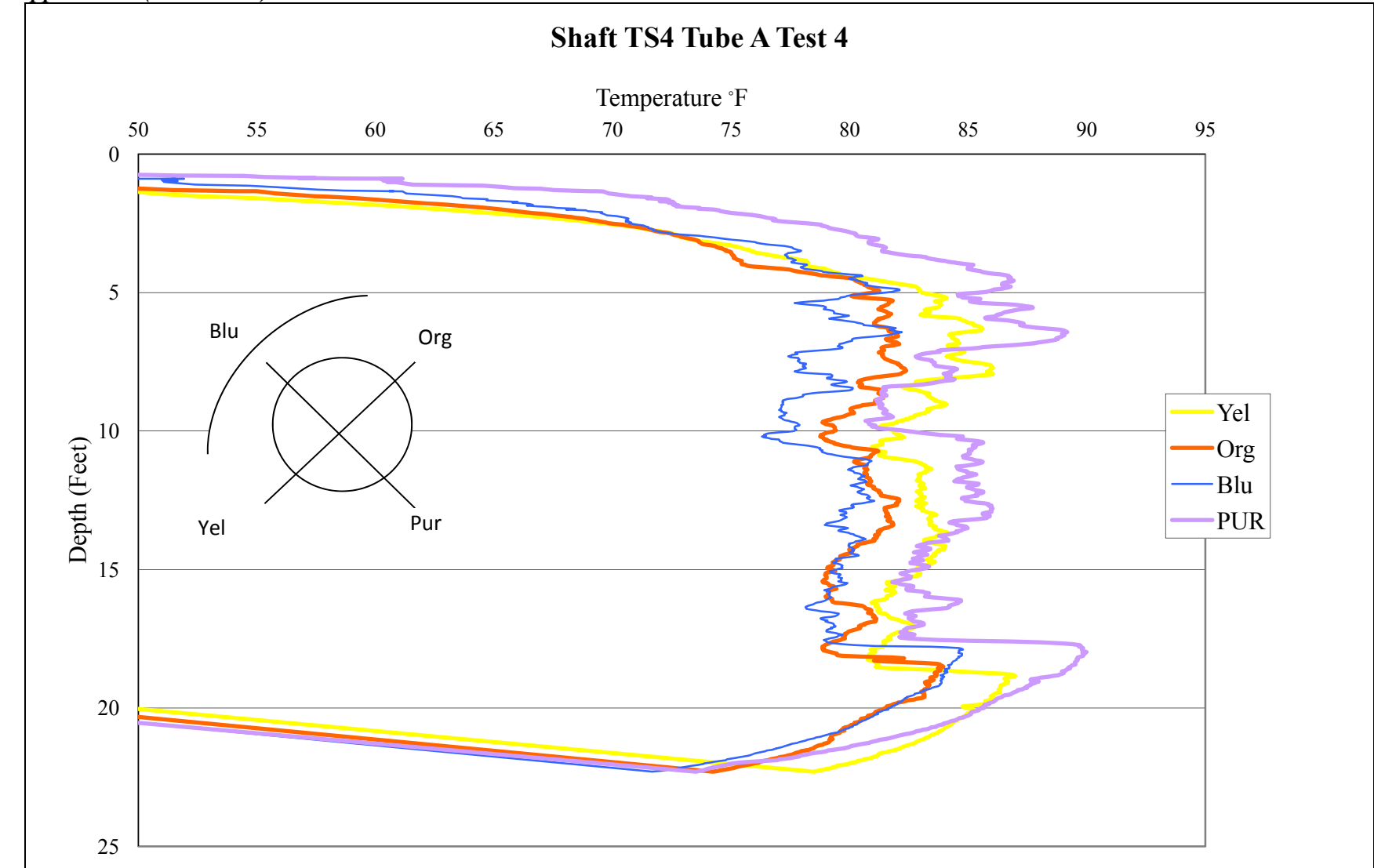


Figure C61 - Auburn test site TIP test results TS4 Tube A Test 4

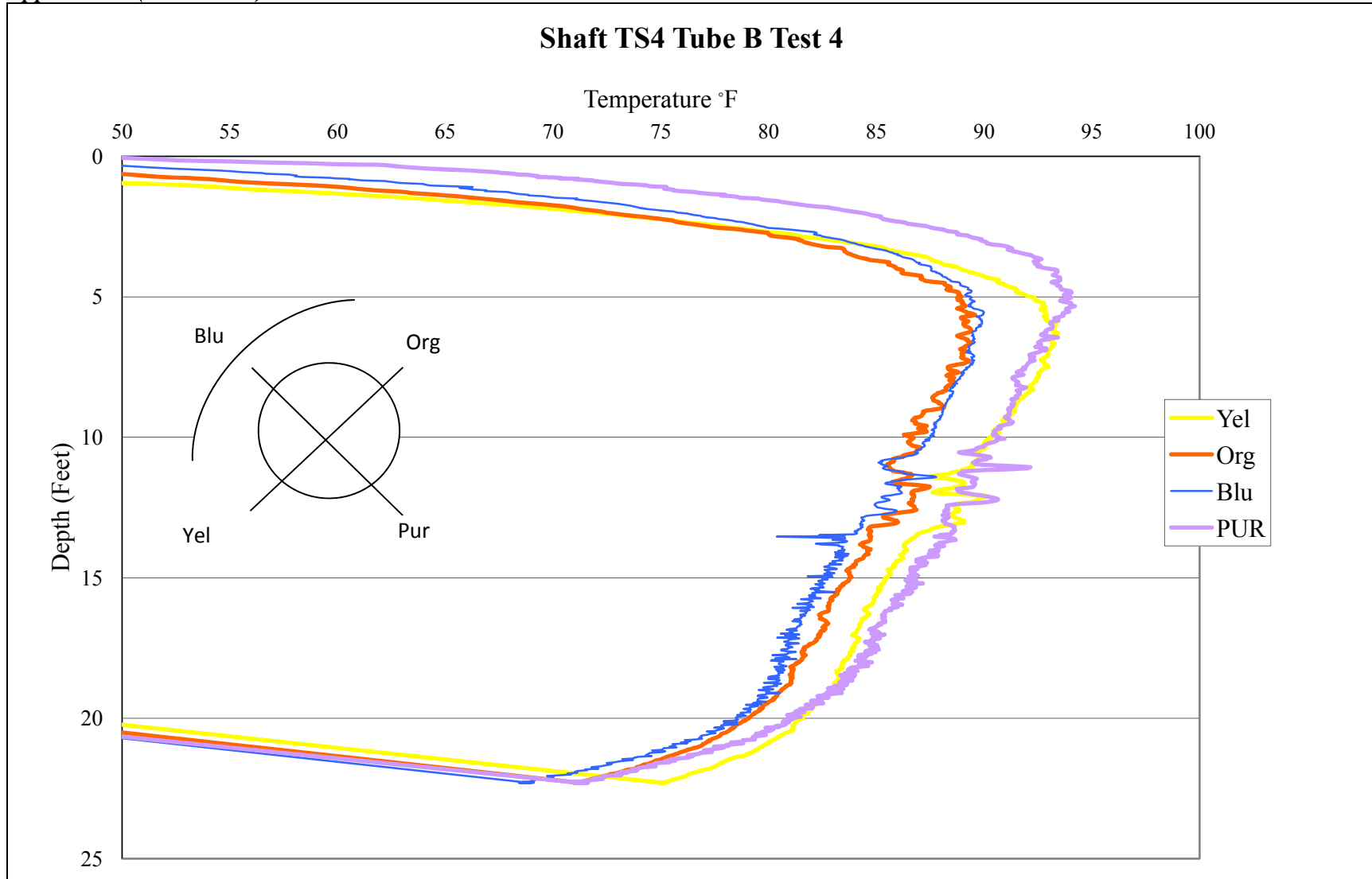


Figure C62 - Auburn test site TIP test results TS4 Tube B Test 4

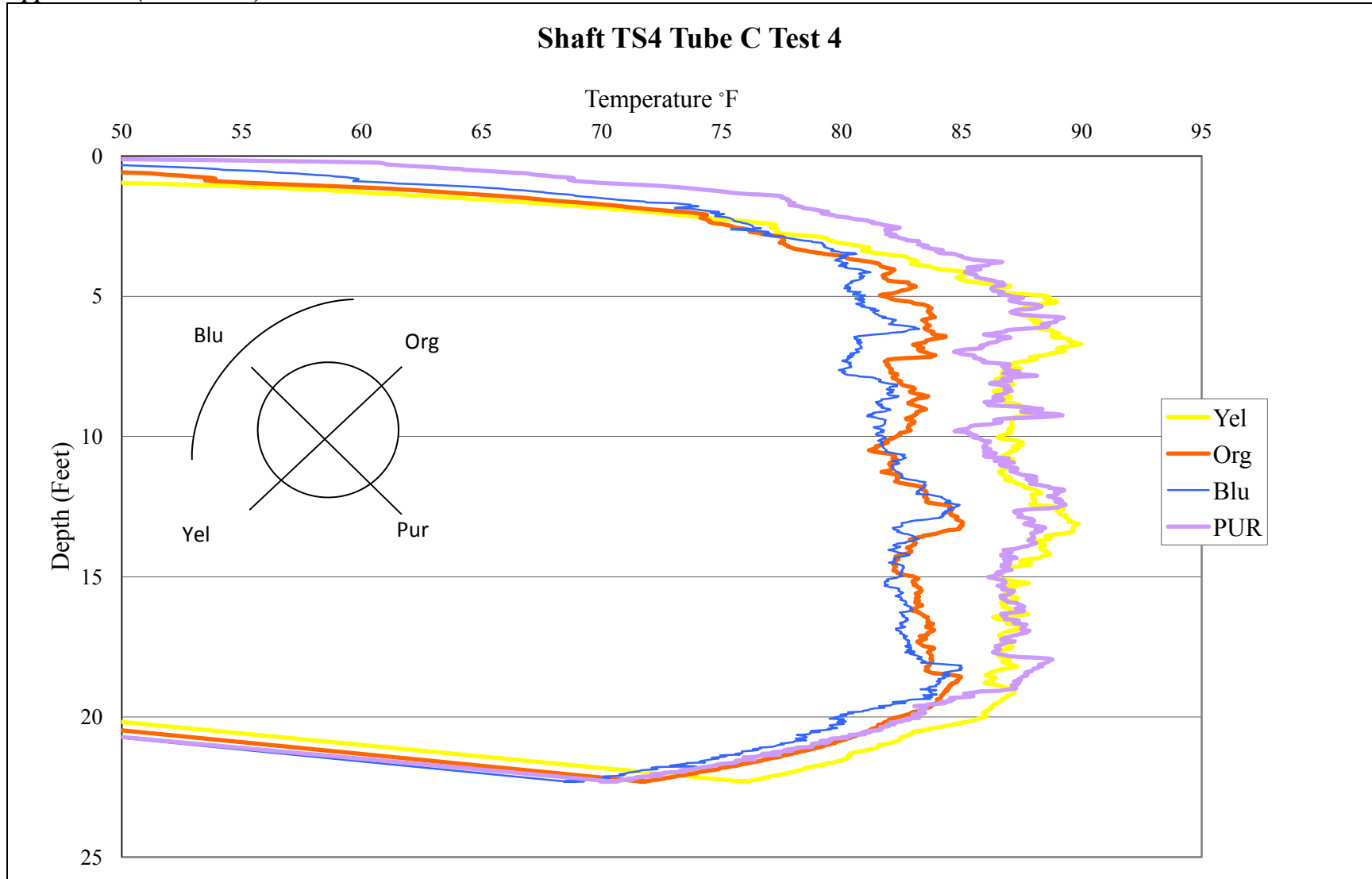


Figure C63 - Auburn test site TIP test results TS4 Tube C Test 4

Appendix C (Continued)

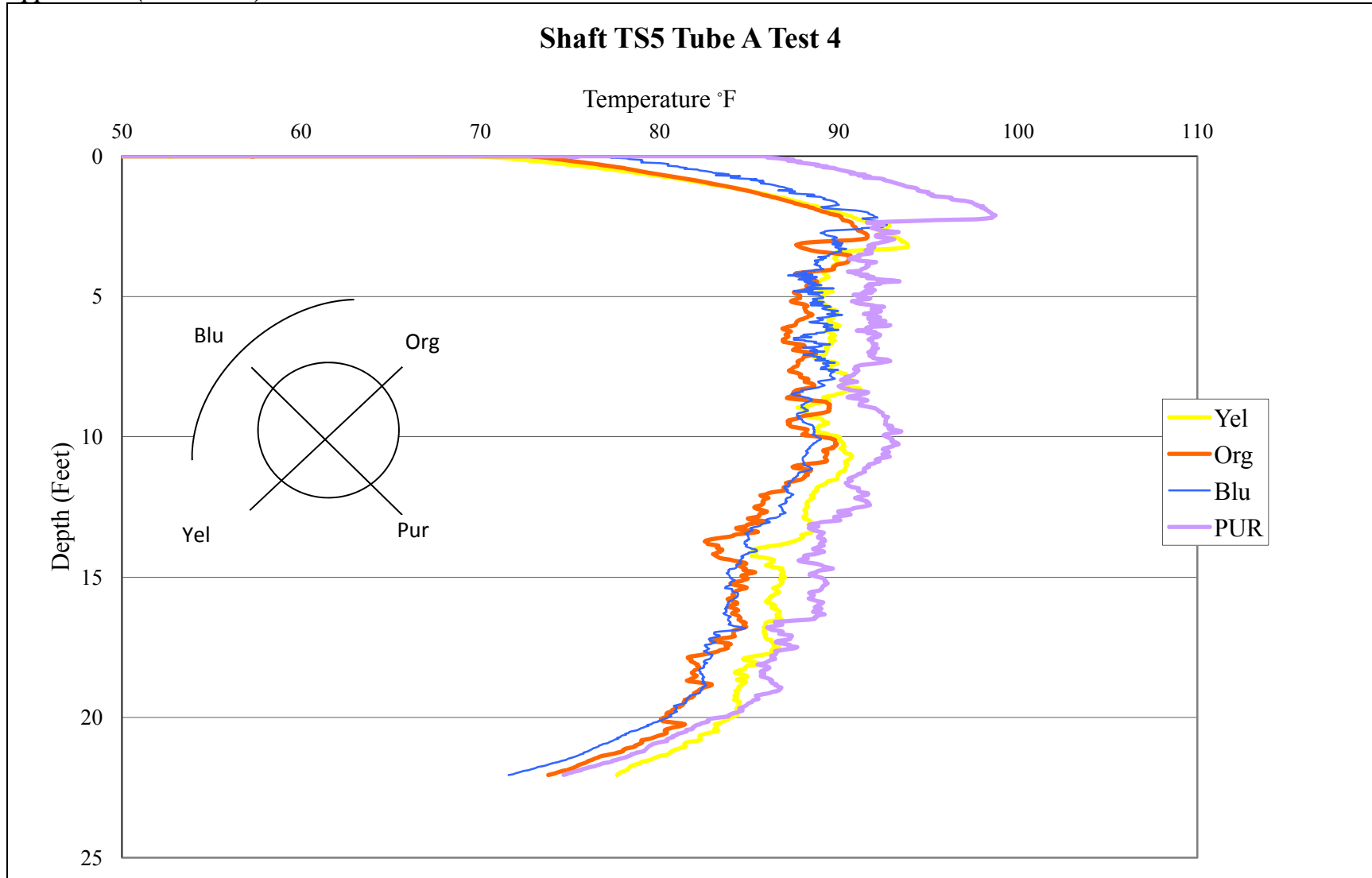


Figure C64 - Auburn test site TIP test results TS5 Tube A Test 4

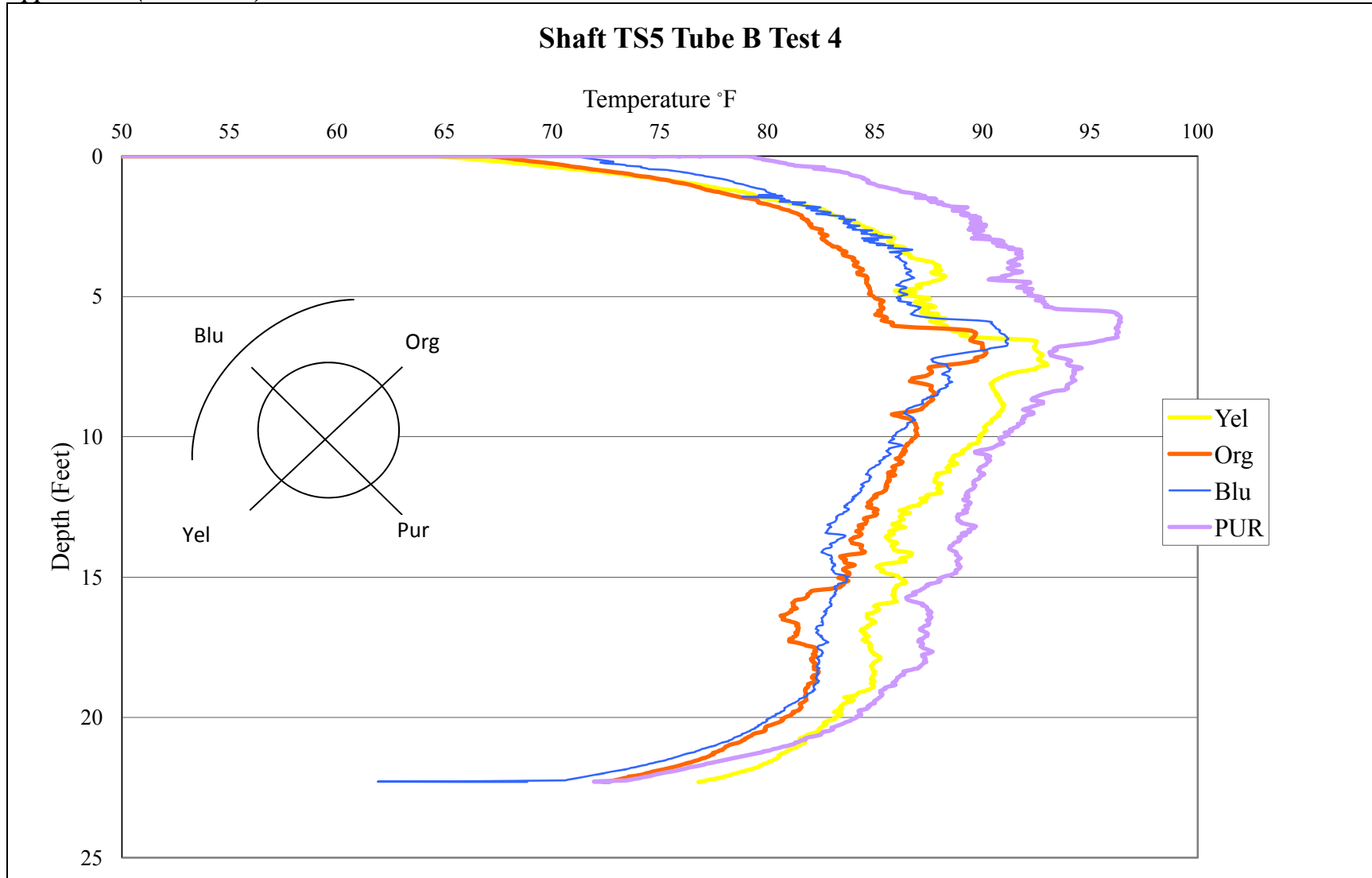


Figure C65 - Auburn test site TIP test results TS5 Tube B Test 4

Appendix C (Continued)

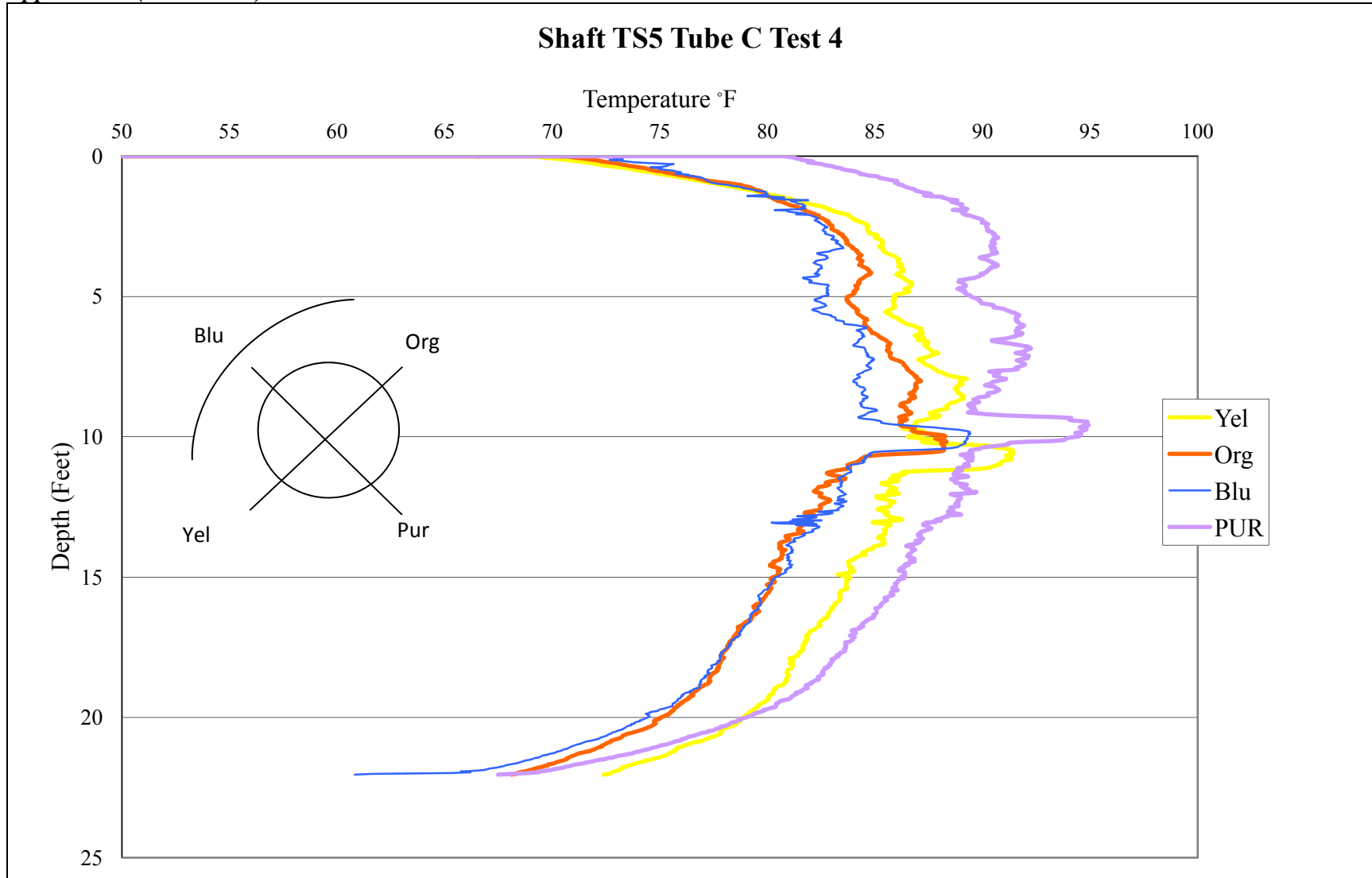


Figure C66 - Auburn test site TIP test results TS5 Tube C Test 4

Appendix C (Continued)

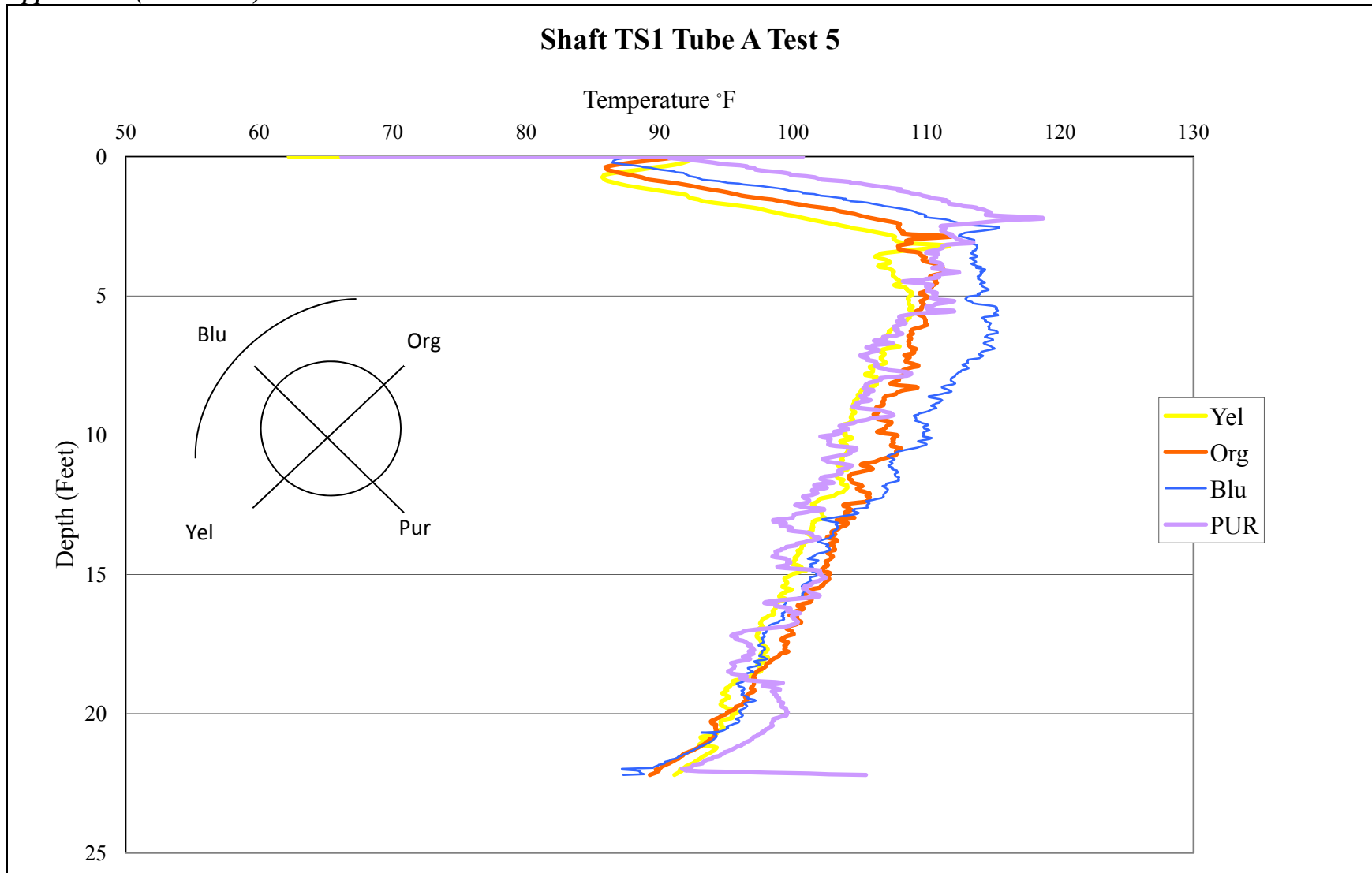


Figure C67 - Auburn test site TIP test results TS1 Tube A Test 5

Appendix C (Continued)

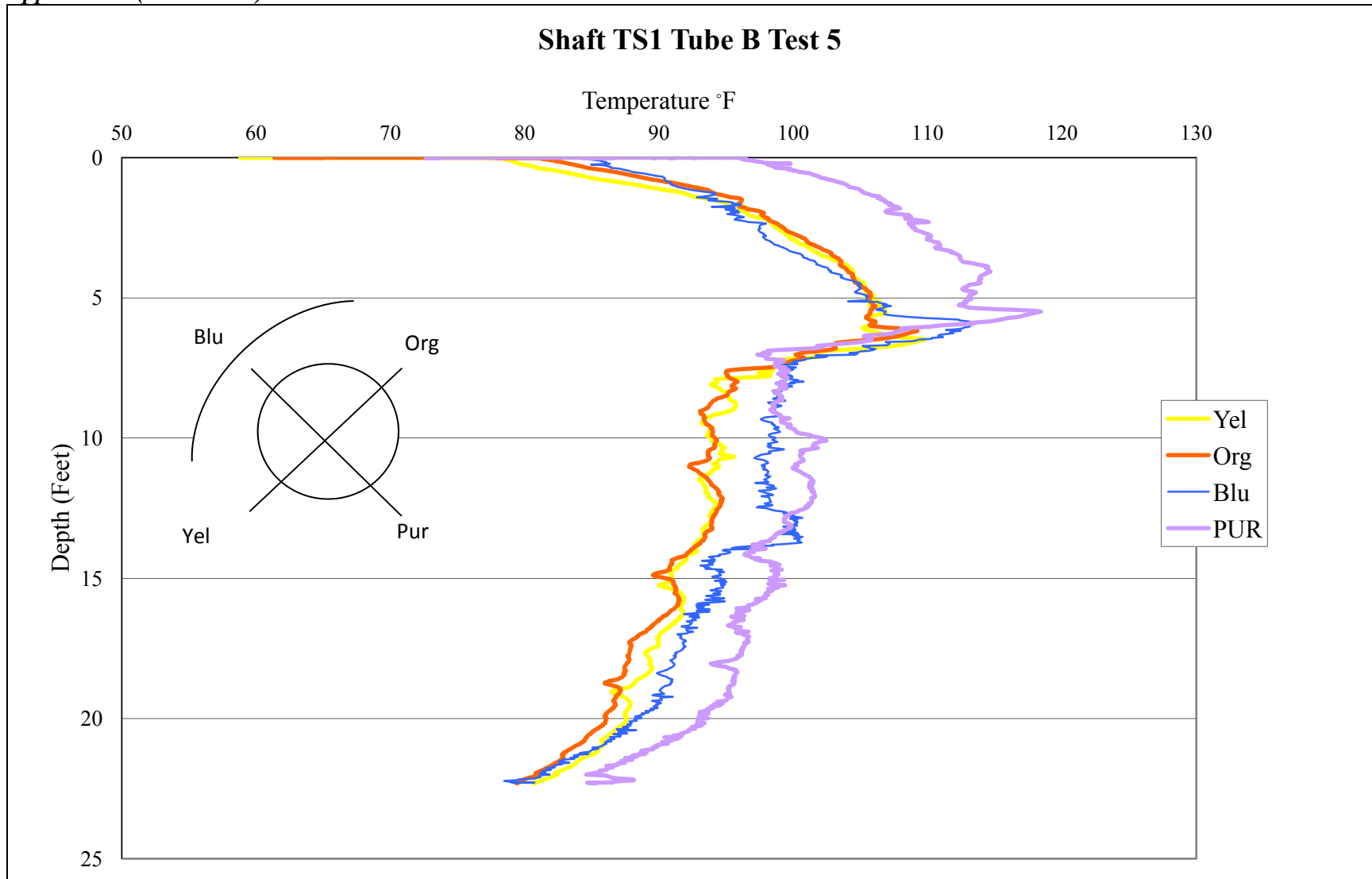
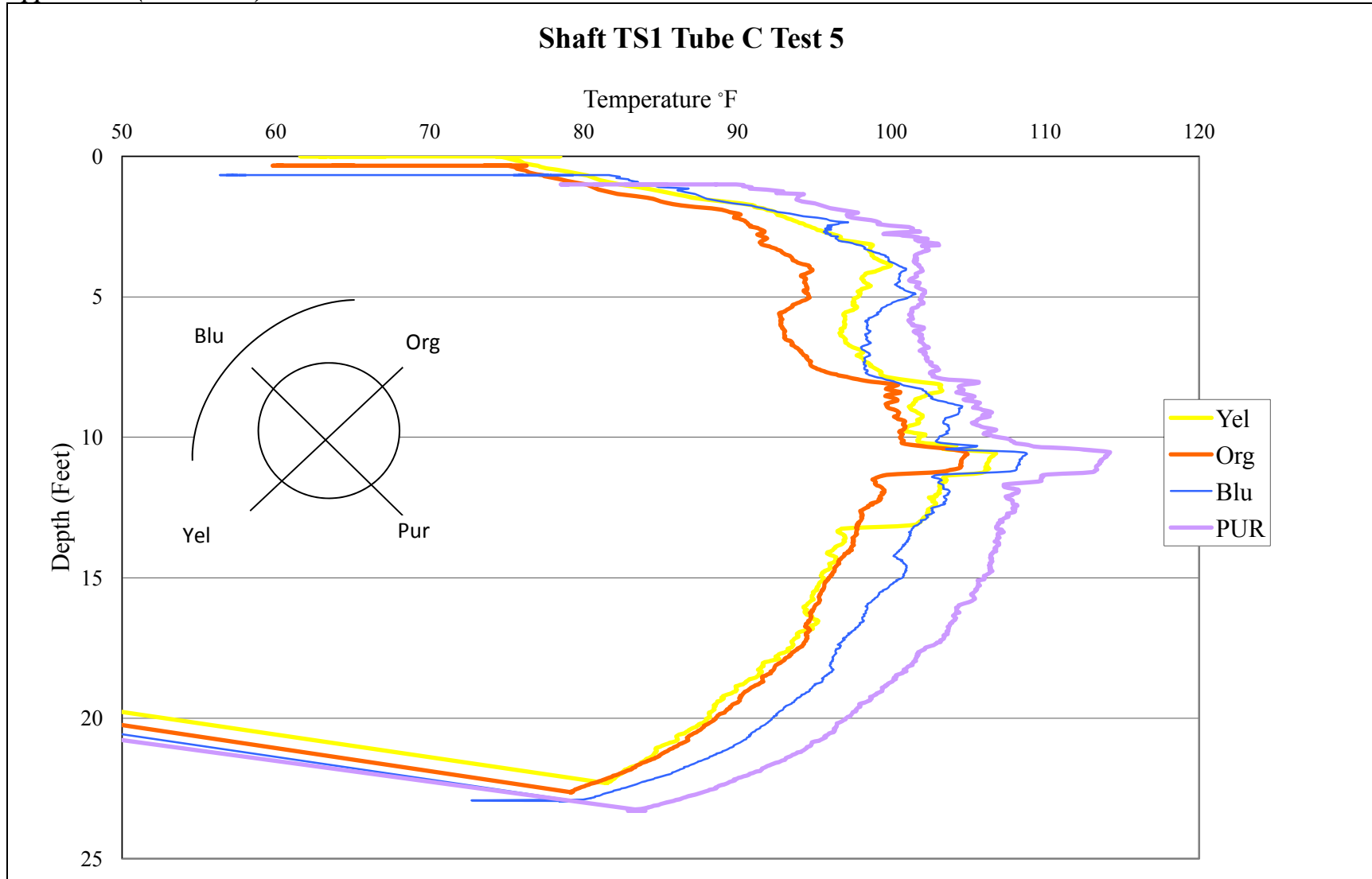


Figure C68 - Auburn test site TIP test results TS1 Tube B Test 5



Appendix C (Continued)

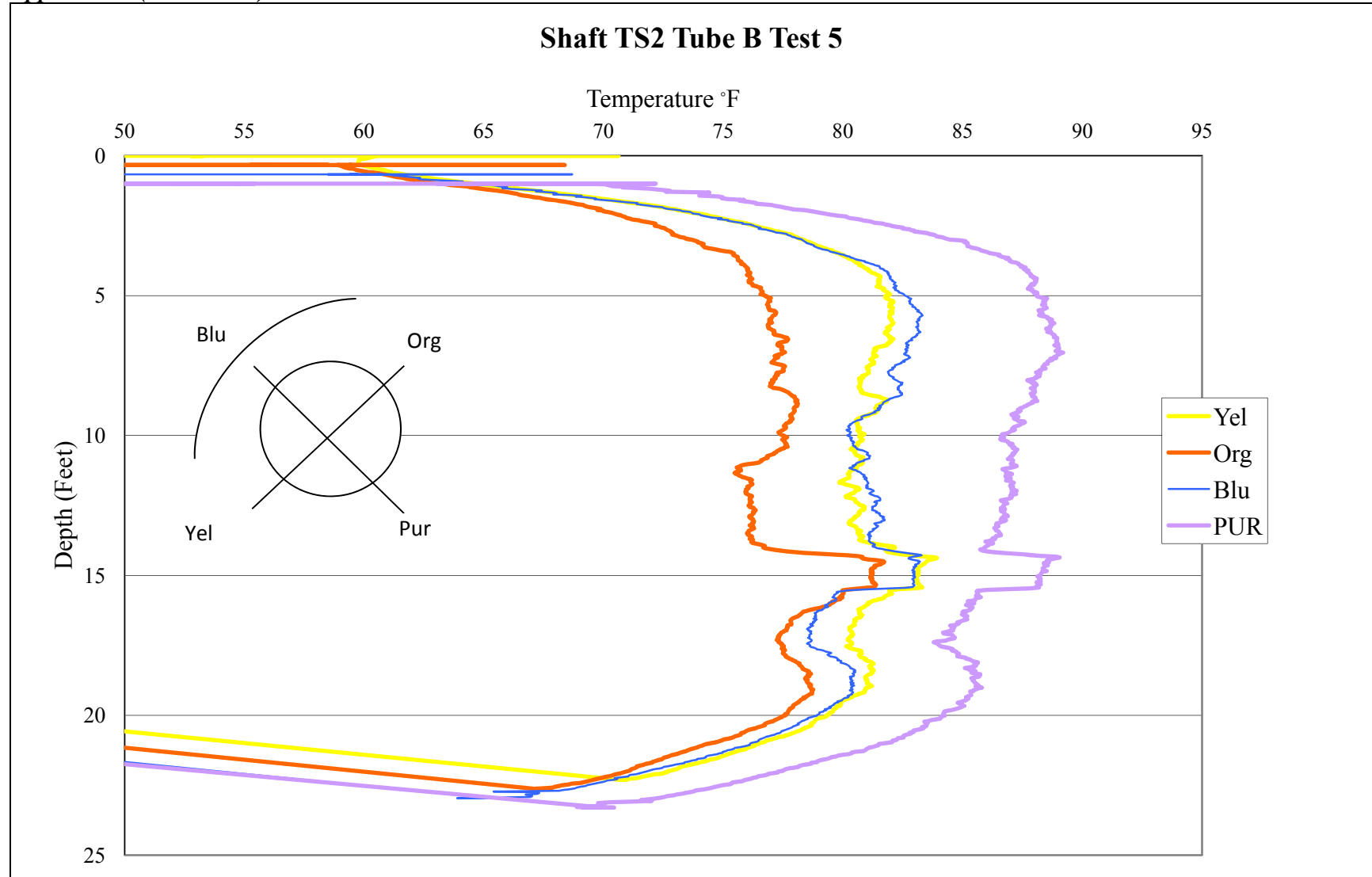


Figure C70 - Auburn test site TIP test results TS2 Tube B Test 5

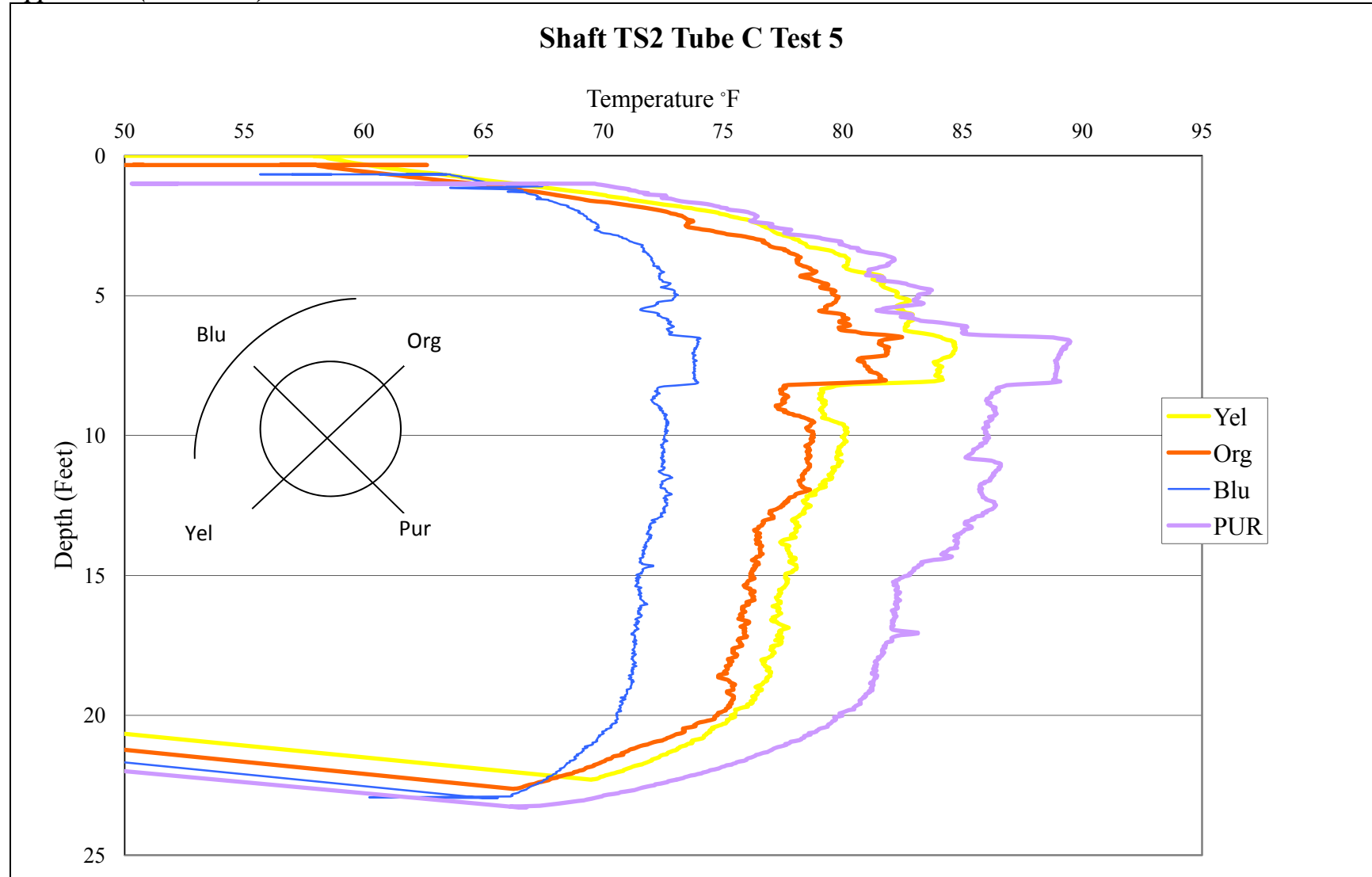


Figure C71 - Auburn test site TIP test results TS2 Tube C Test 5

Appendix C (Continued)

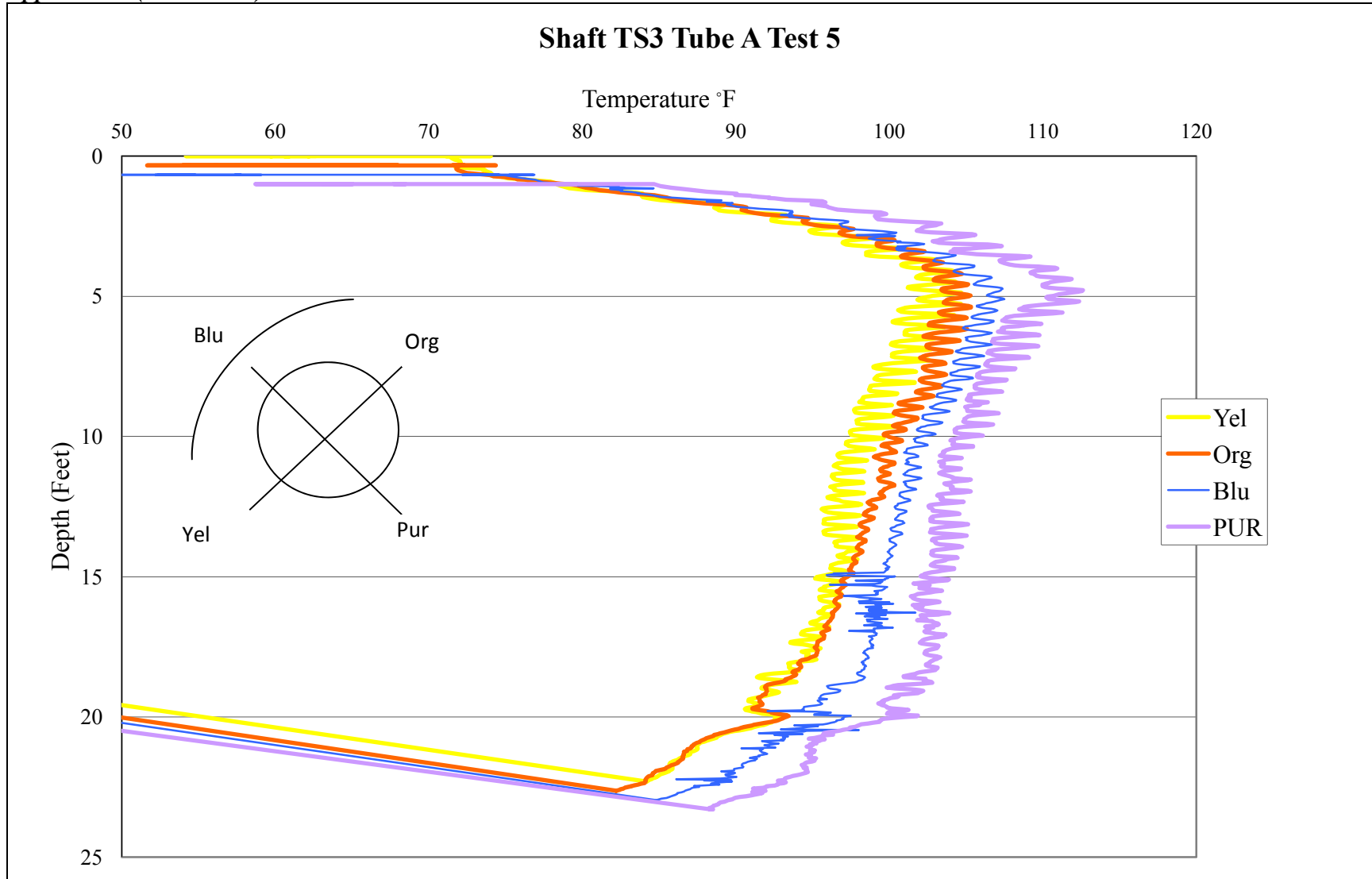


Figure C72 - Auburn test site TIP test results TS3 Tube A Test 5

Appendix C (Continued)

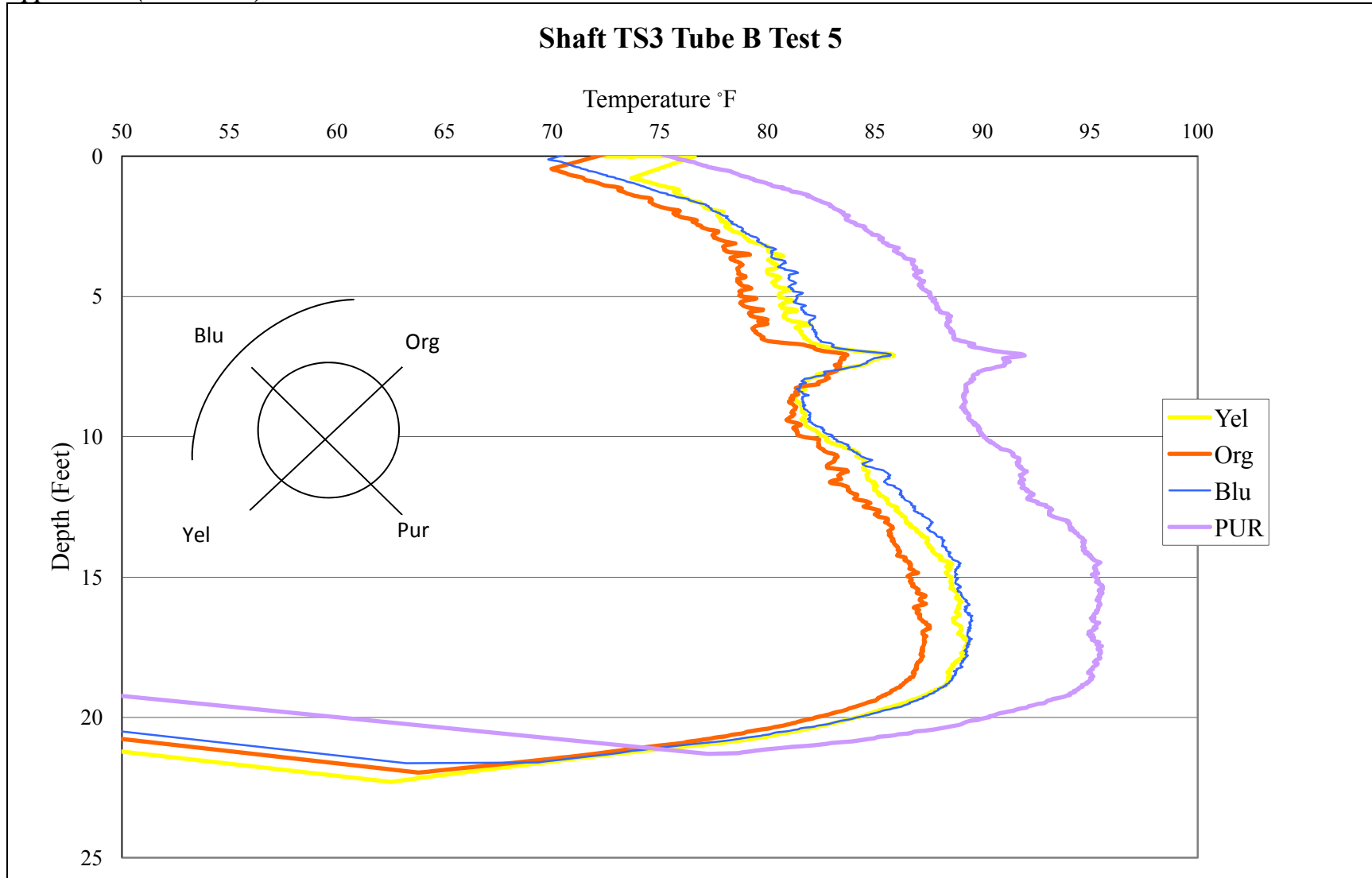


Figure C73 - Auburn test site TIP test results TS3 Tube B Test 5

Appendix C (Continued)

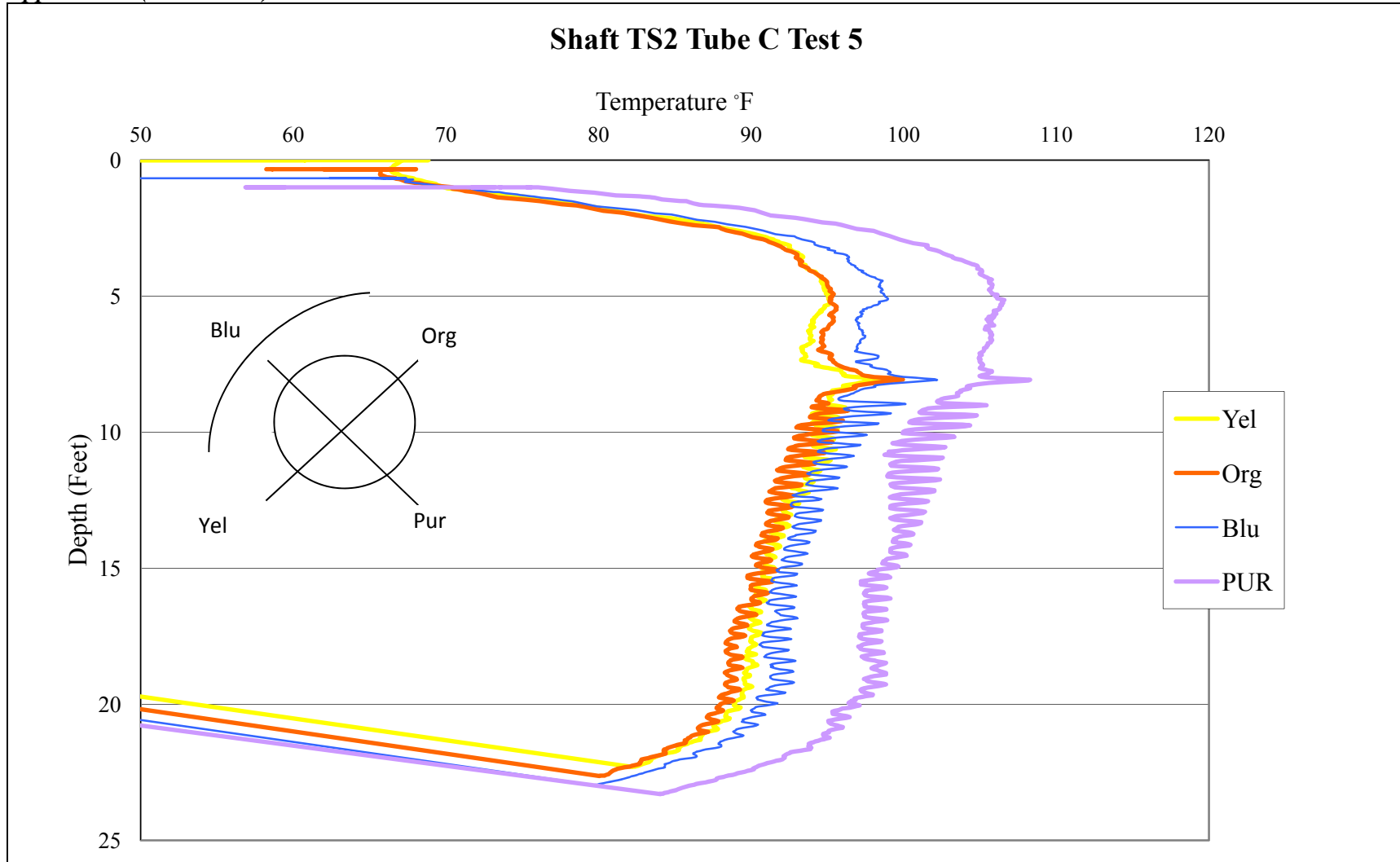


Figure C74 - Auburn test site TIP test results TS3 Tube C Test 5